BEHAVIOR AND ANALYSIS OF A HORIZONTALLY CURVED AND SKEWED I-GIRDER BRIDGE

A Thesis
Presented to
The Academic Faculty

by

Cagri Ozgur

In Partial Fulfillment
of the Requirements for the Degree
Master of Science in the
School of Civil and Environmental Engineering

Georgia Institute of Technology
May 2007

BEHAVIOR AND ANALYSIS OF A HORIZONTALLY CURVED AND SKEWED I-GIRDER BRIDGE

Approved by:

Dr. Donald W. White, Advisor
School of Civil and Environmental Engineering
Georgia Institute of Technology

Dr. Roberto T. Leon
School of Civil and Environmental Engineering
Georgia Institute of Technology

Dr. Kenneth M.Will
School of Civil and Environmental Engineering
Georgia Institute of Technology

Date Approved: April 6, 2007

For my parents Huri and Guner Kemal Ozgur

ACKNOWLEDGEMENTS

The author would like to express his appreciation his advisor, Dr. Donald W. White, for his guidance, patience and encouragement during the course of this study. Heartfelt appreciation is also extended to the committee members, Dr. Roberto T. Leon, Dr. Kenneth M. Will for their valuable comments and revisions.

Financial support provided by the Federal Highway Administration (FHWA) and the Professional Service Industries (PSI), Inc. is gratefully acknowledged. In addition, the author would like to thank the following personnel at BSDI, Inc. for their help through the research study: Dann Hall, Michael Grubb. Also, thanks to Fassil Beshah, Bill Wright and the staff at the Turner Fairbank Highway Research Center for their collaboration on this curved steel bridge research.

Special thanks to author's colleagues, Se-Kwon Jung, Ching-Jen Chang, Yoon Duk Kim and Murat Efe Guney for their help, advice and support. In addition, author would like to thank to Can Canbolat for his help with the programming issues.

Greatest thanks to the authors' parents, Huri and Guner Kemal Ozgur, for their unconditional love and support that they provided throughout the study.

TABLE OF CONTENTS

LIST OF TABLES

LIST OF FIGURES

SUMMARY

This thesis investigates the strength behavior of a representative highly skewed and horizontally curved bridge as well as analysis and design procedures for these types of structures. The bridge responses at and above a number of limits in the AASHTO (2007) Specifications are considered. The study includes the evaluation of various attributes of the elastic analysis of the subject bridge. These attributes include: (1) the accuracy of 3-D grid versus 3-D FEA models, (2) first-order versus second-order effects during the construction, (3) the ability to predict layover at bearing lines using simplified equations and (4) the benefit of combining the maximum and concurrent major-axis and flange lateral bending values due to live load compared to combining the maximums due to different live loads when checking the section resistances. The study also addresses the ability of different AASHTO 2007 resistance equations to capture the ultimate strength behavior. This is accomplished by comparing the results from full nonlinear 3-D FEA studies to the elastic design and analysis results. Specifically the use of the 2007 AASHTO moment based one-third rule equations is evaluated for composite sections in positive bending.

CHAPTER 1

INTRODUCTION

Tight geometric requirements are often placed on highway structures due to right-of-way restrictions in congested urban areas. Skewed horizontally curved steel I-girder bridges are one of the most economical options for satisfying these demands. Increasingly strict and complex site constraints are leading to bridge projects with longer spans, more severe curvature and more complex geometries. These characteristics exacerbate the inherent three-dimensional (3-D) response of curved and skewed bridge structures. As a result, the behavior of these types of bridges needs to be better understood. The ability of various levels of analysis to capture (or account for) the 3-D bridge responses needs to be studied in more depth, and the implications of various analysis and design approximations on the safety, constructability and economy of curved and skewed bridges need to be defined more clearly.

Recent extensive research efforts have led to unified provisions for the design of general straight and curved I- and box-girder bridges now contained in the 4th Edition of the AASHTO LRFD Specifications (AASHTO 2007). Nevertheless, there still are areas where further design economy can be realized by improved characterization of the maximum resistances. One of these areas is the characterization of the resistance of curved composite I-girders in positive bending. Prior research studies indicate that the true strength of curved composite I-girders in positive bending is often close to the full plastic moment capacity of the cross-section (M_p) with some minor reduction for flange lateral bending effects (White et al. 2001; White 2002; White and Grubb 2005; Jung 2006). However, the research and development teams involved with the creation of

the unified AASHTO provisions opted to restrict the design of all curved composite I-section members to a yield moment (M_y) or flange yield stress (F_y) based resistance with some reduction for flange lateral bending effects. This restriction was implemented because of limited information about the effect of girder inelastic deformations on the overall behavior of horizontally curved I-girder bridge systems. The primary concerns involved the influence of inelastic redistribution from more heavily loaded curved I-girders on the validity of elastic analysis results. Of particular concern was the potential underestimation of the axial forces in cross-frame members, since these members serve an essential role in curved bridge construction but may not respond in as ductile of a fashion as the I-girders if subjected to larger than predicted loads.

Jung (2006) developed a refined inelastic shell-beam finite element analysis (FEA) modeling approach and demonstrated its ability to closely predict the experimental response of a full-scale bridge constructed and tested at the Federal Highway Administration (FHWA) Turner-Fairbank Highway Research Center. In addition, Jung applied his inelastic FEA modeling approach to 10 parametric variations on the FHWA test bridge. Jung's studies showed that the influence of the girder inelastic deformations on the deviation from the predicted elastic responses was minor up to a flexural resistance characterized by the equation

$$M_u + \frac{1}{3} f_\ell S_x \le \phi_f M_n \tag{1.1}$$

where:

f_ℓ = flange lateral bending stress,

M_u = member major-axis bending moment,

S_x = elastic section modulus about the major-axis of the section to the flange under consideration taken as M_{yf}/F_{yf}, and

$\phi_f M_n$ = factored flexural resistance in terms of member major-axis bending moment.

Although Jung's studies considered a wide range of bridge parameters, detailed studies of other I-girder bridge systems of various complexity can be helpful to provide further scrutiny of the potential effects of inelastic deformations with respect to concerns about allowing more liberal plastic moment-based flexural strengths.

In addition, the AASHTO (2007) Specifications and Commentary provide some guidance regarding the analysis of horizontally curved and skewed I-girder bridges. However, there are many analysis considerations and therefore the guidance is somewhat limited. In particular, the following aspects deserve further study in the context of the above types of bridges:

- The accuracy of various simplified models based on beam theory relative to refined 3-D FEA.
- The importance of considering geometric nonlinear (second-order) effects during construction.
- The use of envelope values for separate maximum values of the quantities M_u and f_ℓ in design using Eq. 1.1 versus the use of concurrent M_u and f_ℓ values.

3-D FEA methods generally are accepted as providing the most rigorous and theoretically the most accurate solutions. As noted above, Jung (2006) demonstrated highly accurate predictions of the experimental responses from the FHWA bridge test using these types of solutions. However, the sophistication of 3-D FEA models can make them potentially more prone to inadvertent errors in design. Furthermore, there are

numerous approximating assumptions that can influence the accuracy of the sophisticated analysis models. Simpler methods of analysis often can exhibit fewer of these analysis difficulties, although the simpler methods can require special considerations of their own. Chang (2006) and Krzmarzick and Hajjar (2006) have developed and demonstrated 3-D grid analysis capabilities that also provide highly accurate predictions of curved I-girder bridge elastic responses. These capabilities use the typical 3-D beam displacement and rotational degrees of freedom plus a seventh warping degree of freedom at the beam element nodes. It is desirable to compare the results from these more sophisticated types of grid analysis to refined 3-D FEA solutions using the types of modeling approaches developed by Jung (2006). Carefully presented results from both of these approaches also can serve as useful benchmark data for various other more simplified analysis solutions. For instance, simplified equations are provided by NHI (2007) for the twist rotation and layover of I-girders at skewed bearing lines. It is useful to check these equations against the results from refined analysis solutions.

Composite I-girder bridge systems generally tend to be significantly more flexible in their noncomposite construction condition compared to their final composite condition. These flexibilities can make the systems sensitive to second-order effects during construction. It is desirable to understand the significance of these potential sensitivities on representative curved and skewed I-girder bridges.

One bridge attribute that can be important in the context of both of the above considerations is the influence of the method of detailing of the cross-frames on the bridge response and the prediction of this influence by the analysis. One of the types of detailing that is often preferred is called no-load fit detailing, or detailing for the girder

webs to be plumb in the theoretical no-load condition (AASHTO 2007; Chang 2006). With this type of detailing, the cross-frames are fabricated to connect perfectly to the girders with the webs plumb in their theoretical cambered no-load geometry. As a result, no additional stresses are "locked into" the system due to lack of fit. However, due to the torsional deformations of the bridge system under its self weight, the girder webs will not be plumb in the final constructed geometry neither after erection of the steel nor after placement of the deck slab. Generally, for curved and/or skewed I-girder bridge systems, the prediction of these system displacements is important. Girder rotations must be checked against maximums that can be tolerated by the bearings, including additional rotations due to the subsequent bridge live loads. Also, the deflected slab positions must be checked against roadway alignment tolerances. Furthermore, engineers and owners have often questioned whether web out-of-plumbness can have any adverse effect on the strength limit states, e.g., due to the associated second-order effects.

Finally, the impact of using maximum envelope values versus concurrent values in design interaction expressions such as Eq. 1.1 needs to be better understood. Checking of Eq. 1.1 using the maximum M_u and the maximum f_ℓ envelope values is generally conservative since the different maximum values can be associated with different live load conditions. In horizontally curved I-girder bridges with minor or no skew, it is expected that the maximum M_u and the maximum f_ℓ often may be concurrent, or the concurrent values may differ from the maximum values by only a small percentage. However, when a substantial part of the I-girder flange lateral bending is due to effects other than the horizontal curvature, such as skew, eccentric loads from overhang brackets on facia girders, or wind, it is possible that the concurrent values may differ substantially

from the maximum values. Therefore, it is desirable to check whether the use of the maximum M_u with its concurrent f_ℓ along with the maximum f_ℓ with its concurrent M_u results in any significant differences in the I-girder limit state checks relative to the simpler combination of the maximum M_u and f_ℓ envelope values for a bridge with characteristics where these subtleties may be more important.

1.1 Objectives and Scope

The objectives of this research are as follows:

1. Evaluate the implications of the AASHTO (2007) moment-based one-third rule flexural resistance equations for compact composite sections in positive bending.
2. Scrutinize the capability of 3-D grid models for capturing the responses predicted by refined 3-D FEA solutions using the modeling approach validated by Jung (2006). Present the 3-D FEA results in a manner such that they also can serve as potential benchmark solutions for checking of other types of simplified analysis.
3. Assess the potential importance of geometric nonlinear (second-order) effects during construction.
4. Compare refined elastic-analysis results with simplified equations used for estimating the layover of I-girders at the bearing lines.
5. Investigate the benefit of using the maximum and concurrent major-axis and flange lateral bending values due to live load when checking the section resistances, compared to using the maximums due to different live loads.

These objectives are achieved by conducting a thorough analysis and design study of a representative simply-supported I-girder bridge containing both horizontal curvature and substantial skew of its bearing lines.

1.2 Description of the Composite Bridge

The bridge shown in Figs. 1.5.1 and 1.5.2 was recommended by Mr. Dann Hall of BSDI Inc. as an important example to consider the validation of the unified AASHTO (2007) flexural resistance equations and various types of analysis. This bridge has the following key attributes:

- One simply-supported span.
- Six horizontally curved I-girders with 8.5 ft girder spacing.
- Deck slab thickness of 7.5 inches, resulting in tributary widths larger than the slab effective widths based on the AASHTO (2007) rules.
- Staggered cross-frames.
- Significant skew angles with maximum values of 60.46° at the left bearing and 64.64° at the right bearing on the inside girder G6.
- Section transitions in the bottom flanges of Girder 1 (G1) and Girder 2 (G2) but otherwise all the girders are prismatic.
- Cross-frames detailed for the no-load fit condition.
- Yield stress of 50 ksi for all steel members and 4 ksi for the concrete deck slab.

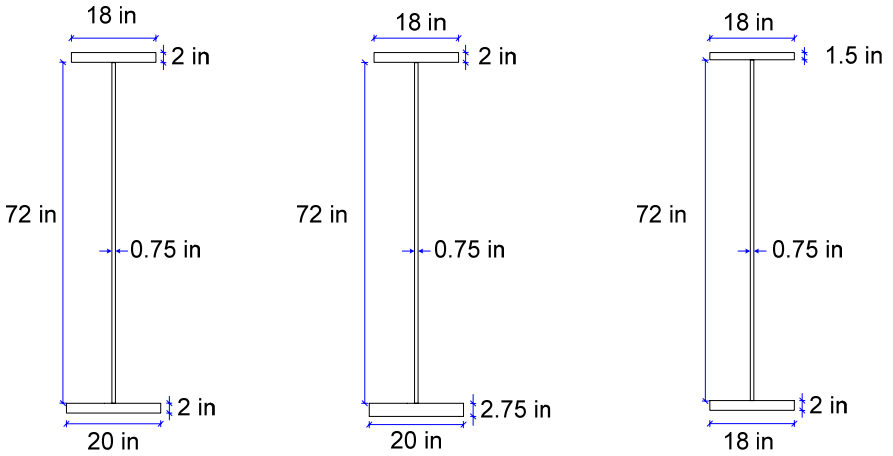

(a)
G1-cross-section 1(G1-1)
G2-cross-section 1(G2-1)

(b)
G1-cross-section 2 (G1-2)
G2-cross-section 2 (G2-2)

(c)
Girder 3 cross-section (G3)
Girder 4 cross-section (G4)
Girder 5 cross-section (G5)
Girder 6 cross-section (G6)

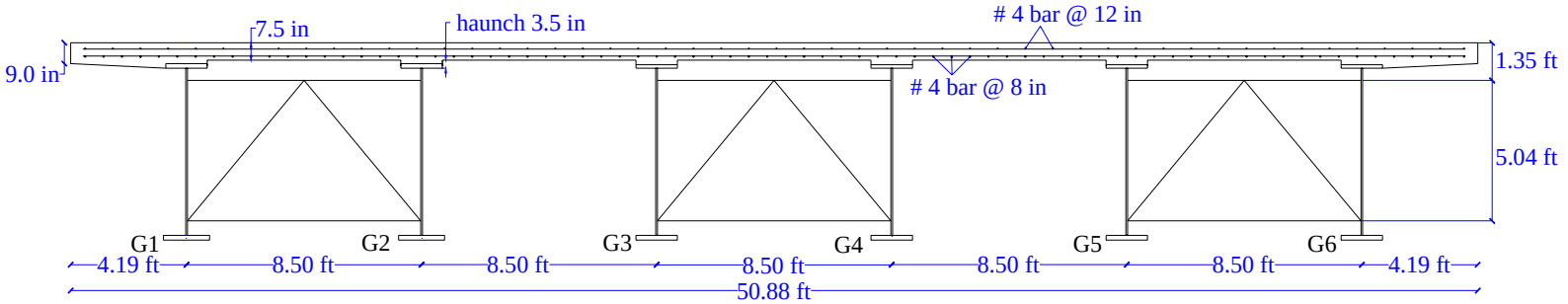

(d) Typical bridge cross section

Figure 1.5.1. Composite bridge geometry

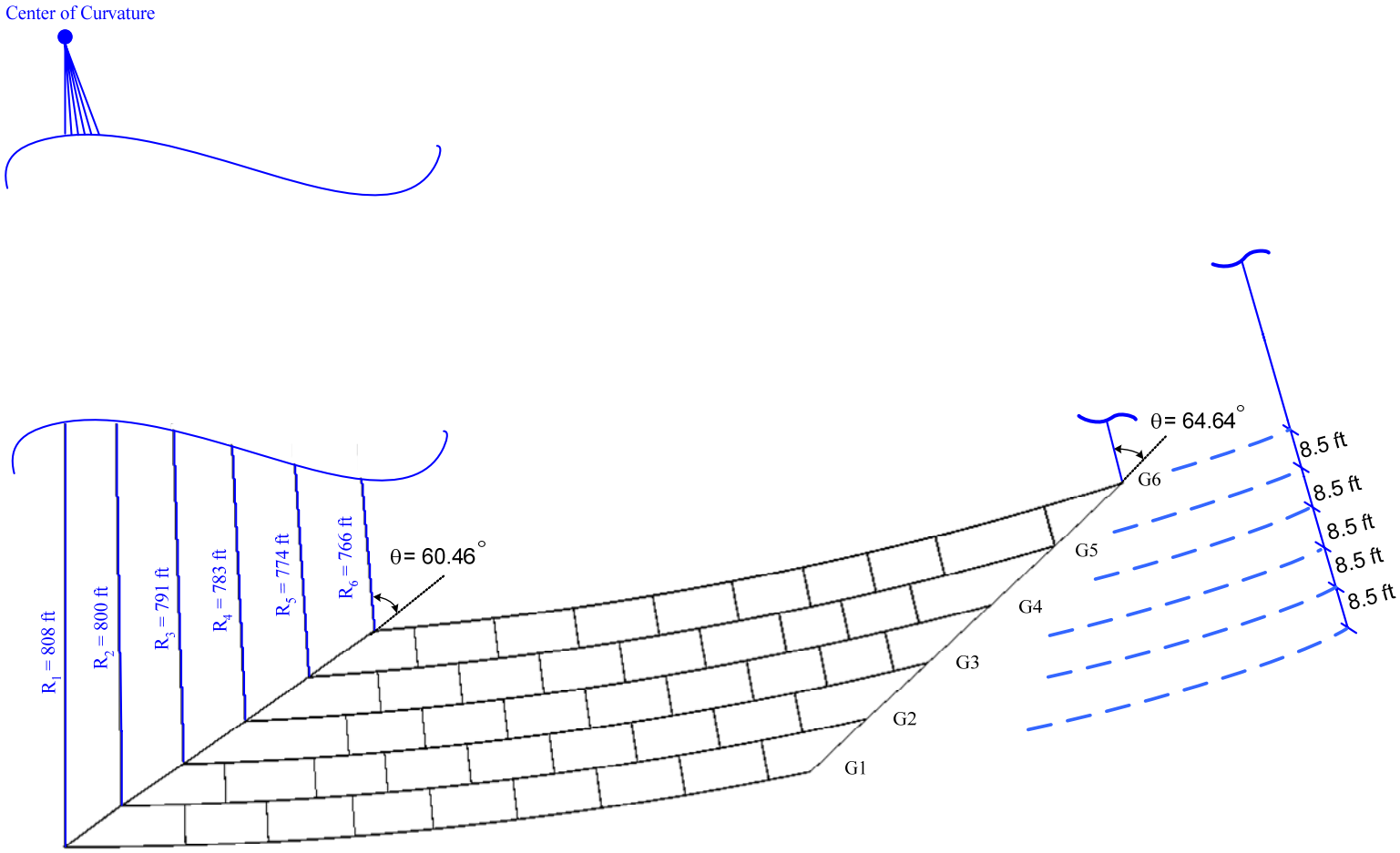

Figure 1.5.2. Plan view of steel superstructure

Girder 1 changes from Section G1-1 to G1-2 at 39.76 ft from the left bearing line and it changes back to section G1-1 at 128.32 ft from the left bearing line. Additionally, Girder 2 changes from Section G2-1 to G2-2 at 39.62 ft from the left bearing line and it changes back to section G2-1 at 79.68 ft from the left bearing line. The detailed information about the flange and web dimensions is shown in Fig. 1.5.1 a through c. The girder dimensions and important non-dimensional ratios are tabulated in Table 1.5.1. Furthermore, the radius of curvature of the girders is provided in Fig. 1.5.2. The arc span length is 159.88 ft for G1, 159.93 ft for G2, 160.29 ft for G3, 160.78 ft for G4, 161.52 ft for G5 and 162.48 ft for G6. Moreover, the unsupported lengths and subtended angles of the cross-frames starting from the left bearing line and progressing to the right bearing line of each girder are listed in Table 1.5.2. The maximum subtended angle is 0.03 which satisfies the AASHTO (2007) limit of $L_b / R \leq 0.1$.

The slab is cast in place with a thickness of 7.5 inches except for the haunch over each of the girder flanges and the slab overhangs. Wood forms are used during the concrete casting. The haunch thickness is 3.5 inches from the bottom surface of the slab to the bottom face of the top flanges. As shown in Fig. 1.5.1, the total width of the deck is 50.88 ft. The roadway is composed of 3 lanes and has a width of 46 ft. The overhang width is 4.19 ft.

Also, future wearing surface and parapet loads are considered. The parapets are 2.440 ft high with a width of 1.583 ft.

Table 1.5.1. Summary of girder cross-section dimensions and non-dimensional ratios

GIRDER	CROSS-SECTION	b_{fc} (in)	t_{fc} (in)	$b_{fc}/2t_{fc}$	b_{ft} (in)	t_{ft} (in)	$b_{ft}/2t_{ft}$	D (in)	t_w (in)	D/ t_w	A_g (in^2)	L (ft)	R (ft)
1	G1-1	18	2	4.5	20	2	5	72	0.75	96	130	159.86	808
	G1-2	18	2	4.5	20	2.75	3.64	72	0.75	96	145		
2	G2-1	18	2	4.5	20	2	5	72	0.75	96	130	159.93	800
	G2-2	18	2	4.5	20	2.75	3.64	72	0.75	96	145		
3	G3	18	1.5	6	18	2	4.5	72	0.75	96	117	160.29	791
4	G4	18	1.5	6	18	2	4.5	72	0.75	96	117	160.78	783
5	G5	18	1.5	6	18	2	4.5	72	0.75	96	117	161.52	774
6	G6	18	1.5	6	18	2	4.5	72	0.75	96	117	162.48	766

Table 1.5.2. Important girder dimensional properties

GIRDER	CROSS-SECTION	L_b (ft)	L_b / R	L_b / b_{fc}	L_b / b_{ft}
1	G1-1	25.87	0.03	17.25	15.52
	G1-1, G1-2	17.65	0.02	11.77	10.59
	G1-2	18.48	0.02	12.32	11.09
	G1-2	16.75	0.02	11.17	10.05
	G1-2	18.02	0.02	12.02	10.81
	G1-2	18.02	0.02	12.02	10.81
	G1-1, G1-2	18.02	0.02	12.02	10.81
	G1-1	18.02	0.02	12.02	10.81
	G1-1	9.01	0.01	6.01	5.41
2	G2-1	13.47	0.02	8.98	8.98
	G2-1	8.90	0.01	5.93	5.93
	G2-1	8.57	0.01	5.71	5.71
	G2-1 , G2-2	10.71	0.01	7.14	7.14
	G2-2	7.58	0.01	5.05	5.05
	G2-2	7.66	0.01	5.11	5.11
	G2-2	8.92	0.01	5.95	5.95
	G2-2	8.92	0.01	5.95	5.95
	G2-2	8.92	0.01	5.95	5.95
	G2-2	8.92	0.01	5.95	5.95
	G2-2	8.92	0.01	5.95	5.95
	G2-2	8.92	0.01	5.95	5.95
	G2-2	8.92	0.01	5.95	5.95
	G2-1 , G2-2	8.92	0.01	5.95	5.95
	G2-1	8.92	0.01	5.95	5.95
	G2-1	8.92	0.01	5.95	5.95
	G2-1	8.92	0.01	5.95	5.95
	G2-1	13.89	0.02	9.26	9.26
3	G3	8.80	0.01	5.87	5.87
	G3	19.07	0.02	12.71	12.71
	G3	7.50	0.01	5.00	5.00
	G3	7.58	0.01	5.05	5.05
	G3	8.82	0.01	5.88	5.88
	G3	8.82	0.01	5.88	5.88
	G3	8.82	0.01	5.88	5.88
	G3	8.82	0.01	5.88	5.88
	G3	8.82	0.01	5.88	5.88
	G3	8.82	0.01	5.88	5.88
	G3	8.82	0.01	5.88	5.88
	G3	8.82	0.01	5.88	5.88
	G3	8.82	0.01	5.88	5.88
	G3	8.82	0.01	5.88	5.88
	G3	8.82	0.01	5.88	5.88
	G3	8.82	0.01	5.88	5.88
	G3	7.08	0.01	4.72	4.72
	G3	14.52	0.02	9.68	9.68
	G3	7.52	0.01	5.01	5.01

Table 1.5.2. Important girder dimensional properties (continued)

GIRDER	CROSS-SECTION	L_b (ft)	L_b / R	L_b / b_{fc}	L_b / b_{ft}
4	G4	21.55	0.03	14.36	14.36
	G4	7.50	0.01	5.00	5.00
	G4	8.73	0.01	5.82	5.82
	G4	8.73	0.01	5.82	5.82
	G4	8.73	0.01	5.82	5.82
	G4	8.73	0.01	5.82	5.82
	G4	8.73	0.01	5.82	5.82
	G4	8.73	0.01	5.82	5.82
	G4	8.73	0.01	5.82	5.82
	G4	8.73	0.01	5.82	5.82
	G4	8.73	0.01	5.82	5.82
	G4	8.73	0.01	5.82	5.82
	G4	8.73	0.01	5.82	5.82
	G4	7.01	0.01	4.67	4.67
	G4	6.59	0.01	4.39	4.39
	G4	7.78	0.01	5.19	5.19
	G4	7.44	0.01	4.96	4.96
	G4	15.66	0.02	10.44	10.44
5	G5	14.75	0.02	9.83	9.83
	G5	8.63	0.01	5.75	5.75
	G5	8.63	0.01	5.75	5.75
	G5	8.63	0.01	5.75	5.75
	G5	8.63	0.01	5.75	5.75
	G5	8.63	0.01	5.75	5.75
	G5	8.63	0.01	5.75	5.75
	G5	8.63	0.01	5.75	5.75
	G5	8.63	0.01	5.75	5.75
	G5	8.63	0.01	5.75	5.75
	G5	8.63	0.01	5.75	5.75
	G5	8.63	0.01	5.75	5.75
	G5	6.93	0.01	4.62	4.62
	G5	6.51	0.01	4.34	4.34
	G5	7.69	0.01	5.13	5.13
	G5	7.36	0.01	4.90	4.90
	G5	7.70	0.01	5.14	5.14
	G5	24.24	0.03	16.16	16.16
6	G6	8.54	0.01	5.69	5.69
	G6	17.08	0.02	11.38	11.38
	G6	17.08	0.02	11.38	11.38
	G6	17.08	0.02	11.38	11.38
	G6	17.08	0.02	11.38	11.38
	G6	15.39	0.02	10.26	10.26
	G6	14.05	0.02	9.37	9.37
	G6	14.89	0.02	9.93	9.93
	G6	23.98	0.03	15.99	15.99
	G6	17.33	0.02	11.55	11.55

There are 41 intermediate cross-frames and 10 end cross-frames in the bridge. Since the skew angles at both bearing lines are much greater than 20°, the intermediate cross-frames are oriented normal to the girders. The cross-frames are placed in a staggered pattern in order to reduce the magnitude of the cross-frame forces at the expense of increased lateral bending stresses in the girder flanges. The top chord centroids of the intermediate cross-frames are located 1.35 ft below the top surface of the slab. These cross-frames have a depth of 5.04 ft. The top chord centroids of the bearing cross-frames are located 1.42 ft below the top surface of the concrete deck and they have a depth of 4.90 ft. The cross-frame sections and areas are shown in Table 1.5.3. In addition, the dimensions for the bearing stiffeners, intermediate stiffeners and connection plates are tabulated in Table 1.5.4.

Table 1.5.3. Cross-frame sections and areas

CROSS FRAMES	SECTION	AREA (in^2)
BEARING		
Top chord	WT 7x49.5	14.60
Bottom chord	RECTANGULAR	14.60
Diagonals	RECTANGULAR	4.22
INTERMEDIATE		
Top chord	L 5x3x1/2	3.75
Bottom chord	RECTANGULAR	3.75
Diagonals	RECTANGULAR	3.75

Table 1.5.4. Stiffener dimensions

STIFFENER		Height (in)	Width (in)	Thickness(in)
Bearing Stiffeners	Outside web panel	72	6.25	0.625
	Inside web panel	72	6.25	0.625
Intermediate	Stiffeners	72	6.25	0.625
Connection Plates	Outside web panel	72	6.25	0.625
	Inside web panel	72	6.25	0.625

1.3 Organization

Chapter 2 addresses the elastic design behavior of the bridge predicted by 3-D beam-shell FEA and 3-D grid models. A brief explanation of the unified AASHTO (2007) flexural resistance equations is presented first. Then, the elastic FEA modeling approaches used in this study are outlined. Next, the elastic FEA analysis results are discussed. This is followed by detailed discussions of the bridge component designs. Finally, the elastic 3-D FEA results are compared with the results of 3-D grid models.

Chapter 3 presents the additional considerations for the full nonlinear FEA of the bridge. Loading schemes, material properties and full nonlinear FEA procedures are the major topics discussed in this chapter.

Chapter 4 shows the findings from extensive nonlinear finite element analyses. The sections that have maximum unity checks are evaluated for G1, G3 and G6 at different load levels. Finally, these results are discussed to understand the implications of using Eq. 1.1 with $M_n = M_p$ for compact composite sections in positive bending.

Chapter 5 provides a summary of the research with key observations. This is followed by conclusion. Finally, recommendations are suggested for further research.

Appendix A presents the detailed girder flexural design checks for the outside girder (G1) based on the AASHTO (2007) Specifications. Also, key checks for critical cross-frame members using the procedures from the AISC (2005) Specification are illustrated.

CHAPTER 2

ELASTIC ANALYSIS AND DESIGN

2.1 Overview

Bridges are designed predominantly based on elastic analysis. Curved and skewed steel girder bridges can experience significant elastic three-dimensional deflections and rotations. In this research, numerous approximating assumptions that can influence the accuracy of 3-D analysis models are considered. A detailed 3-D beam-shell FEA model of a highly skewed and horizontally curved bridge is prepared to illustrate and investigate analysis and design considerations using the 4th edition of the AASHTO LRFD Specifications (AASHTO 2007). The finite element software ABAQUS 6.5.1 is used to conduct the elastic analyses for the 3-D beam-shell model. First, Section 2.2 provides information about the AASHTO (2007) flexural resistance equations and a number of other design considerations. Then Section 2.3 introduces the detailed 3-D beam-shell finite element modeling approaches used for elastic analysis. Next, Section 2.4 presents elastic analysis results from the 3-D beam-shell model of the bridge. This section includes linear (first-order) and geometric nonlinear (second-order) analysis results of the noncomposite structure under construction loadings and linear results of the composite structure under dead and live loads. Section 2.5 focuses on the design of the girders using AASHTO (2007). It also focuses on the design of the single-angle cross-frame compression members using the AISC (2005) procedures as discussed by White (2007). Finally, the 3-D beam-shell model results are compared with 3-D grid model results in Section 2.6. The structural analysis program GT-SABRE is used for the 3-D grid analysis.

2.2 AASHTO (2007) Flexural Resistance Equations

The AASHTO (2007) flexural resistance equations that address the combined effects of major-axis bending and flange lateral bending are

$$f_{\text{bu}} + \frac{1}{3} f_\ell \le \phi_f F_n \tag{2.1}$$

for members in which the flexural resistance is expressed in terms of stresses and

$$M_u + \frac{1}{3} f_\ell S_x \le \phi_f M_n \tag{2.2}$$

for members in which the flexural resistance is expressed in terms of moments, where:

f_{bu} = flange major-axis bending stress,

f_ℓ = flange lateral bending stress,

$\phi_f F_n$ = factored flexural resistance in terms of the major-axis bending stress,

M_u = member major-axis bending moment,

S_x = elastic section modulus about the major-axis of the section to the flange under consideration taken as M_{yf}/F_{yf}, and

$\phi_f M_n$ = factored flexural resistance in terms of member major-axis bending moment.

Equation 2.1 is derived by considering the isolated flanges of an I-girder subjected to combined major-axis bending and lateral bending. The idealized fully-plastic stress distribution shown in Fig. 2.2.1 can be assumed for the flange in the absence of local or lateral buckling.

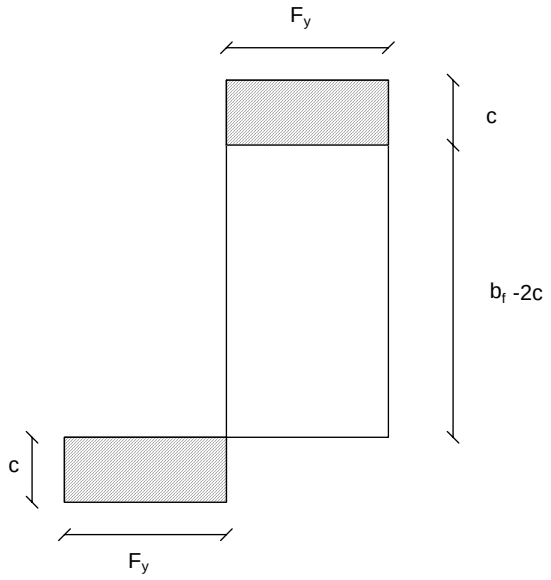

Figure 2.2.1. Idealized fully plastic stress distribution in an isolated flange due to combined effects of major-axis and lateral bending

Within this idealized stress distribution the lateral moment is produced by the strips of width c at the tips of the flange, and the remaining width (b_f -2c) generates forces related to major-axis bending. The elastically-computed major-axis bending stress associated with the flange plastic strength can be expressed by equating elastic flange force due to major-axis bending ($f_{bu}\, b_f\, t_f$) to the fully-plastic flange force ($F_y\, (b_f - 2c) t_f$).

$$f_{bu} = F_y \frac{b_f - 2c}{b_f} \tag{2.3}$$

The lateral bending moment can be written in terms of the flange lateral bending stress as

$$M_t = \frac{f_t b_f^2 t_f}{6} \tag{2.4}$$

and in a similar fashion this lateral bending moment also can be calculated from Fig. 2.2.1 and equated with the Eq. 2.4:

$$\frac{f_t b_f^2 t_f}{6} = F_y c\, t_f (b_f - c) \tag{2.5}$$

Equation 2.5 is solved for the width c and the expression for c is substituted into Eq. 2.3 to obtain the elastically-computed major-axis bending stress associated with the flange fully-plastic strength as a function of the elastically-computed lateral bending stress.

$$c = \frac{b_f}{2}\left(1 - \sqrt{1 - \frac{2}{3}\frac{f_l}{F_y}}\right) \tag{2.6}$$

$$f_{bu} = F_y\sqrt{1 - \frac{2}{3}\frac{f_t}{F_y}} \tag{2.7}$$

Since in practical design of bridge I girders flange lateral bending stress is much smaller than the yield stress, Eq. 2.7 is accurately approximated by the following linear equation:

$$f_{bu} = F_y - \frac{1}{3}f_t \tag{2.8}$$

On the other hand, Eq. 2.2 is derived by considering a doubly-symmetric I-section subjected to combined major-axis bending and lateral bending including the contribution of the web to the fully-plastic strength of the section. For example, the idealized fully-plastic stress distribution shown in Fig. 2.2.2 for a doubly symmetric noncomposite I-section, may be considered with equal and opposite lateral bending in each of its equal size flanges (Mozer et al. 1971).

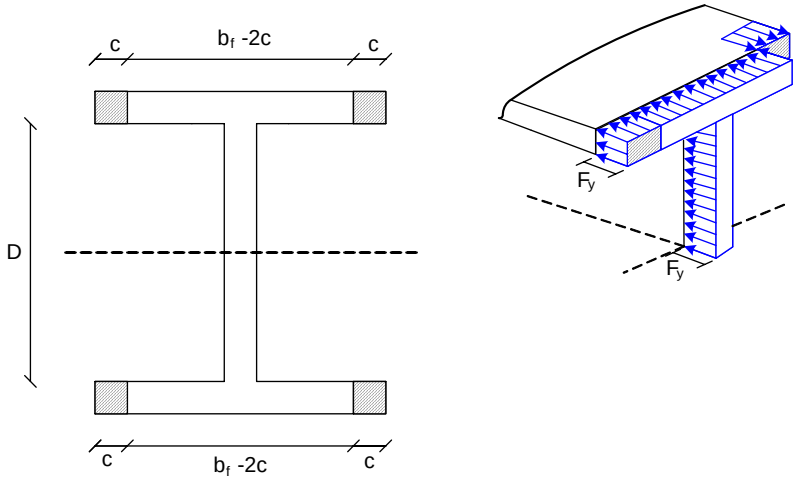

Figure 2.2.2. Stress distribution on a fully plastified compact doubly-symmetric I–section defined at Mozer et al.

The major-axis bending moment capacity, reduced due to the flange lateral bending, can be determined by taking the net moment of the fully-plastic forces including the web contribution about the section centroidal axis. For a doubly symmetric noncomposite cross-section it is expressed as

$$M_p^* = (b_f - 2c)\, t_f F_y \frac{h}{2}(2) + \frac{D^2 t_w F_y}{4} \tag{2.9}$$

where c corresponds to the width of the plastic stress distribution in the flanges related to the flange lateral bending. If the web depth is assumed equal to the distance between the flange centroids ($D = h$) Eq. 2.9 becomes,

$$M_p^* = \left[\left(1 - \frac{2c}{b_f}\right) + \frac{1}{4}\frac{A_w}{A_f}\right] A_f h F_y \tag{2.10}$$

where, $A_w\,(= D\,t_w)$ is the area of the web and $A_f\,(= b_f\ t_f)$ is the area of the flange. When the expression for c, which is the same as that defined previously in Eq. 2.6, is substituted in Eq. 2.10 and a finite A_w / A_f ratio is assumed, a closed form expression for the

elastically-computed major-axis bending moment associated with the flange fully-plastic strength is obtained as a function of elastically-computed lateral bending stress. This moment capacity can be approximated conservatively as

$$M_p^* = M_p - \frac{1}{3} f_\ell S_x \tag{2.11}$$

In the case of typical horizontally curved bridges, lateral torsional buckling or flange local buckling may govern the flexural strength limit state during the construction stage where the bridge is noncomposite. Therefore, the flexural capacity is generally equal to or less than the specified minimum yield strength of a flange in these cases. On the other hand, lateral torsional buckling or flange local buckling limit states do not govern in positive bending when the bridge becomes composite. As a result, the flexural capacity can be as high as the plastic capacity of the section. White et al. (2001) and White (2002) develop and demonstrate the extension from Eqs. 2.8 and 2.11 to Eqs. 2.1 and 2.2 to address the influence of the lateral torsional buckling and flange local buckling for noncomposite sections and composite sections in negative bending. This extension entails the simple substitution of $\phi_f F_n$ for F_y and $\phi_f M_n$ for M_p.

Equation 2.1 is a stress-based flexural resistance equation targeted mainly for checking slender-web noncomposite members, slender-web composite members in negative bending and noncompact composite members in positive bending. This is mainly because in these situations, the maximum resistance tends to be less than or equal to the yielding strength in major-axis bending due to slender-web bend buckling and/or hybrid-web yielding effects, or due to compression flange lateral torsional or local buckling limit states. On the other hand, the moment-based flexural resistance equation (Eq. 2.2) is aimed at checking the strength of noncomposite members or composite

members in negative bending that have compact or noncompact webs and compact composite sections in positive bending since the maximum resistance can be as large as the plastic resistance. This is because significant yielding within these cross-sections results in moments larger than the yield moment of the section.

At the time of the implementation of 3rd edition of the AASHTO LRFD provisions (AASHTO 2004), there was insufficient information about the influence of inelastic girder deformations at the strength level on the distribution of internal forces and moments in horizontally curved steel bridges. Therefore, the development team decided to restrict the design all I-section members to Eq. 2.1. White and Grubb (2005) summarize the background, usage and validation of the AASHTO (2007) one-third rule flexural resistance equations (Eqs. 2.1 & 2.2) in a more detailed fashion. The bridge described in Section 1.5 is studied to provide further information toward potentially allowing the use of the moment-based flexural resistance equation (Eq. 2.2) with $\phi_f M_n$ up to $\phi_f M_p$ where applicable in horizontally curved I-girder bridges.

Software packages may calculate simplified estimates of the flange lateral bending values based on the maximum major-axis bending moments. Generally first-order lateral flange bending stresses are amplified to account for the second-order effects by the following equation given in AASHTO (2007):

$$f_\ell = \left(\frac{0.85}{1 - \frac{f_{bu}}{F_{cr}}} \right) f_{\ell 1} \geq f_{\ell 1} \tag{2.12}$$

where $f_{\ell 1}$ is the first-order compression flange lateral bending stress at the section under consideration, f_{bu} is the largest value of the compressive major-axis bending stress in the

unbraced segment under consideration and F_{cr} is the elastic lateral torsional buckling stress for the flange under consideration. Equation 2.12 is derived from the behavior of an isolated unbraced length. Therefore it can only capture local effects associated with that unbraced length. The bridge described in Section 1.5 is studied to investigate the validity of Eq. 2.12 under overall system effects such as combination of horizontal curvature and skew.

Major-axis bending and flange lateral bending values are used in the resistance checks of Eq. 2.1 or Eq. 2.2. There are two ways of combining the major-axis bending and flange lateral bending values from the analysis software for these checks:

(1) Combine the maximums. However, this may introduce some unwanted conservatism into the design.

(2) Determine a critical combination of concurrent values that maximizes the resistance check. This may be accomplished approximately by: (a) combining the maximum major-axis bending envelope values (M_b or f_b) with concurrent flange lateral bending stresses (f_f) and (b) combining the maximum flange lateral bending envelope values (f_f) with concurrent major-axis bending values (M_b *or* f_b). This approach is approximate because theoretically, intermediate concurrent values of the major-axis bending and flange lateral bending may lead to the largest interaction check.

In this work, both approaches (1) and (2) are considered.

2.3 Elastic FEA Modeling of the Subject Bridge

In this section, the overall FEA model of the subject bridge is discussed first. Second, the displacement boundary conditions are considered in detail. Next, the elastic material

properties are described, and finally detailed information about the calculation of loads is presented.

2.3.1 FEA Discretization

The finite element model of the bridge is constructed by using ABAQUS 6.5.1 (HKS 2004). Figure 2.3.1 shows a perspective view illustrating the overall geometry of the bridge and the specified boundary conditions of the FEA model used throughout this research.

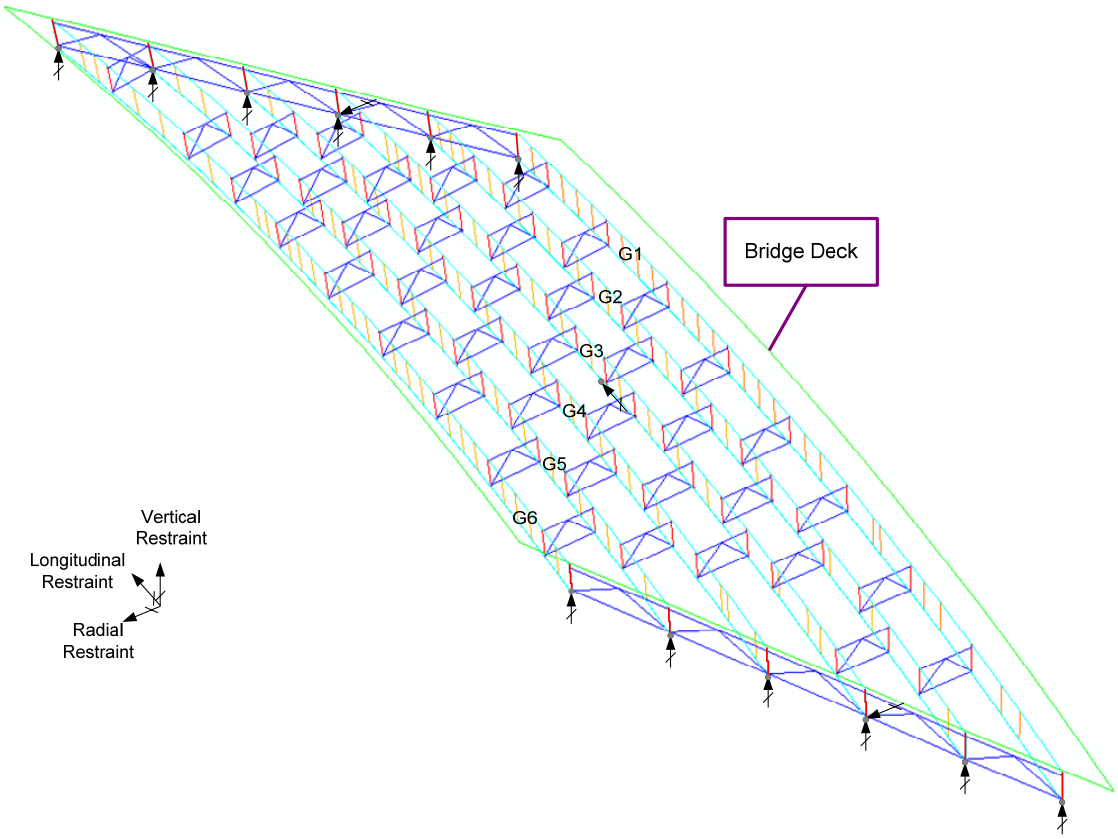

Figure 2.3.1. Perspective view of the bridge FEA model and its boundary conditions.

Twelve elements are used through the depth of the web in all girders. The number of elements along the girder length is selected such that each shell element has an aspect

ratio close to one. The girder webs and concrete deck are modeled with the S4R element, which is 4-node quadrilateral displacement-based shell element with reduced integration and a large-strain formulation, and the S3R element, which is a compatible 3-node triangular shell element used for modeling some parts of the deck. The S3R is a degenerated version of S4R. Figure 2.3.2 shows the mesh through the depth of the webs at an example location within the bridge. All elements are created based on a cylindrical coordinate system.

Five integration points for the webs of the steel I-girders and nine integration points for the concrete deck are used through the thickness of the shell elements. The number of integration points is increased in the concrete deck in order to capture the progressive failure of the concrete deck more effectively in the subsequent nonlinear analysis (HKS 2004).

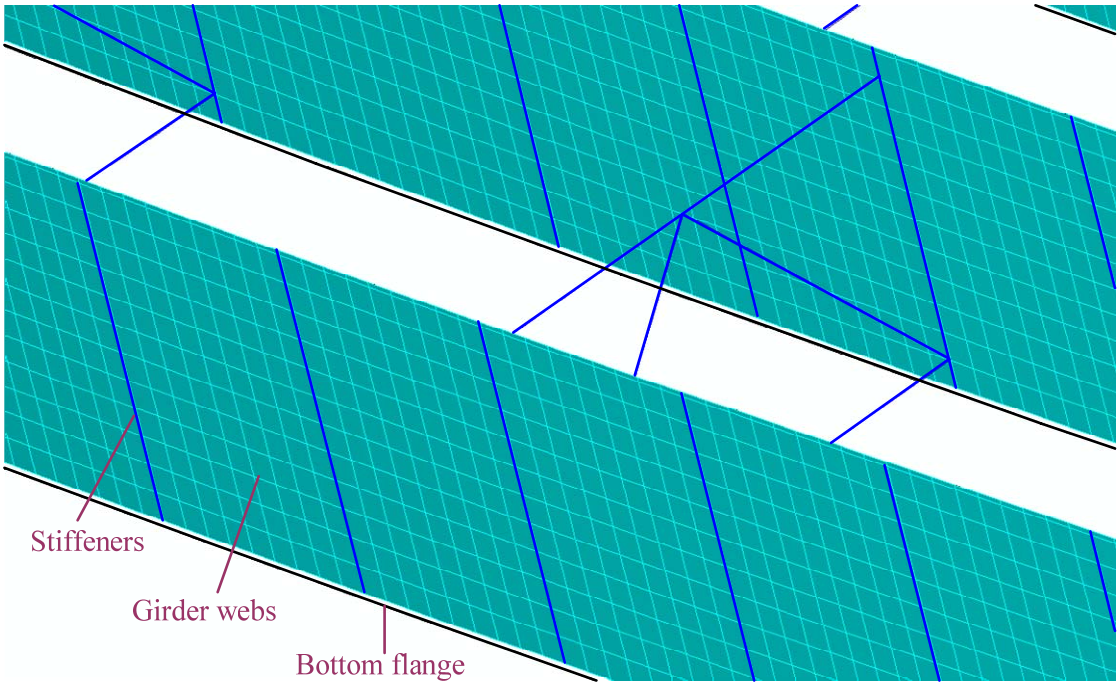

Figure 2.3.2. Mesh through the depth of the web

Figure 2.3.3 shows a cross-section schematic of the bridge FEA model. To begin with the deck of the bridge, it is represented by rectangular sections along the width. The slab thickness is 7.5 in. with the exception of the haunch over each of the girder flanges and the slab overhangs. The haunch thickness is 3.5 inches from the bottom surface of the slab to the bottom face of the top flanges. The tapered overhangs (See Fig. 1.5.1) are represented with rectangular sections with an average slab thickness of 10 inches. The shell element reference surface for the slab is chosen as the intersection of the web and the top flange. The slab is positioned 6.25 inches over the reference point and the nodal offset option is used within the shell element definitions to offset the element nodes from the centroidal axis of each rectangular section of the slab elements. Moreover, 53 shell elements are used along the width and approximately 161 shell elements are used along the length of the deck. Since the bearing lines are skewed, the number of the shell elements varies along the length of the deck. The 3-node triangular shell elements are used in the regions close to the bearing lines to maintain a nearly rectangular geometry of the 4-node shell elements throughout the slab. Figure 2.3.4 shows the mesh of the concrete deck. A coarser grid is used for modeling the concrete deck compared to grid of the webs. The mesh density of the slab in the length direction is one half of the girder web mesh density. The ABAQUS linear-type multi-point constraint is used for mesh refinement. This command constrains each degree of freedom at middle node to be interpolated linearly from the corresponding degrees of freedom at the adjacent web nodes.

Also, the EQUATION command is used to model the ideal full composite action between the top flanges and the concrete deck. Specifically, the EQUATION command is

used to implement a constraint that is similar to the ABAQUS beam-type multi-point constraint. The EQUATION command lets the user introduce a dummy node that is not attached to any element in the model. The composite slab can be introduced without inducing any deformations and internal stresses due to the noncomposite system displacements by creating dummy nodes at the slab nodes just above the top flanges. As a result, the displacements at the slab nodes just above the top flanges are expressed in terms of displacements at the top flange nodes and dummy nodes. This constraint makes the rotational degrees of freedom equal at all three of these nodes whereas the three translational degrees of freedom at the dummy nodes and slab nodes just above the top flanges are expressed as a function of the translational displacements at the top flange nodes and the translational contributions from the nodal rotations of the top flange nodes. The boundary conditions of the dummy nodes and slab nodes just above the top flanges are changed during the analysis of the different kinds of loadings to satisfy the compatibility between the top flanges and slab. The slab nodes just above the top flanges are fixed during the analysis of the noncomposite loadings whereas the dummy nodes move freely. The slab displacements are equal to zero during the noncomposite structure analysis due to this constraint. The boundary conditions and multi-point constraint are changed for the analysis of the composite structure. The dummy nodes are fixed and the slab nodes just above the top flanges move freely during the analysis of the composite structure. As a result, the slab can be introduced at its ideal position without inducing any deformations and internal stresses due to the noncomposite system displacements.

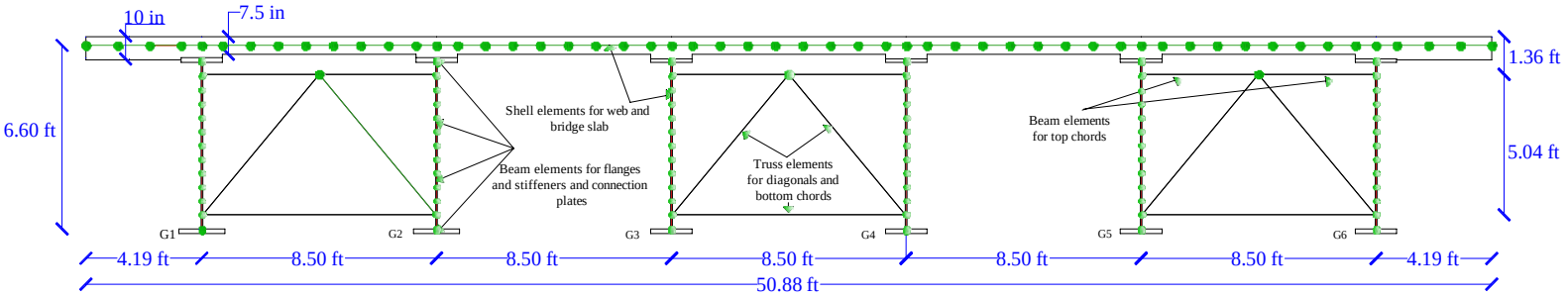

Figure 2.3.3. Cross section schematic of FEA model

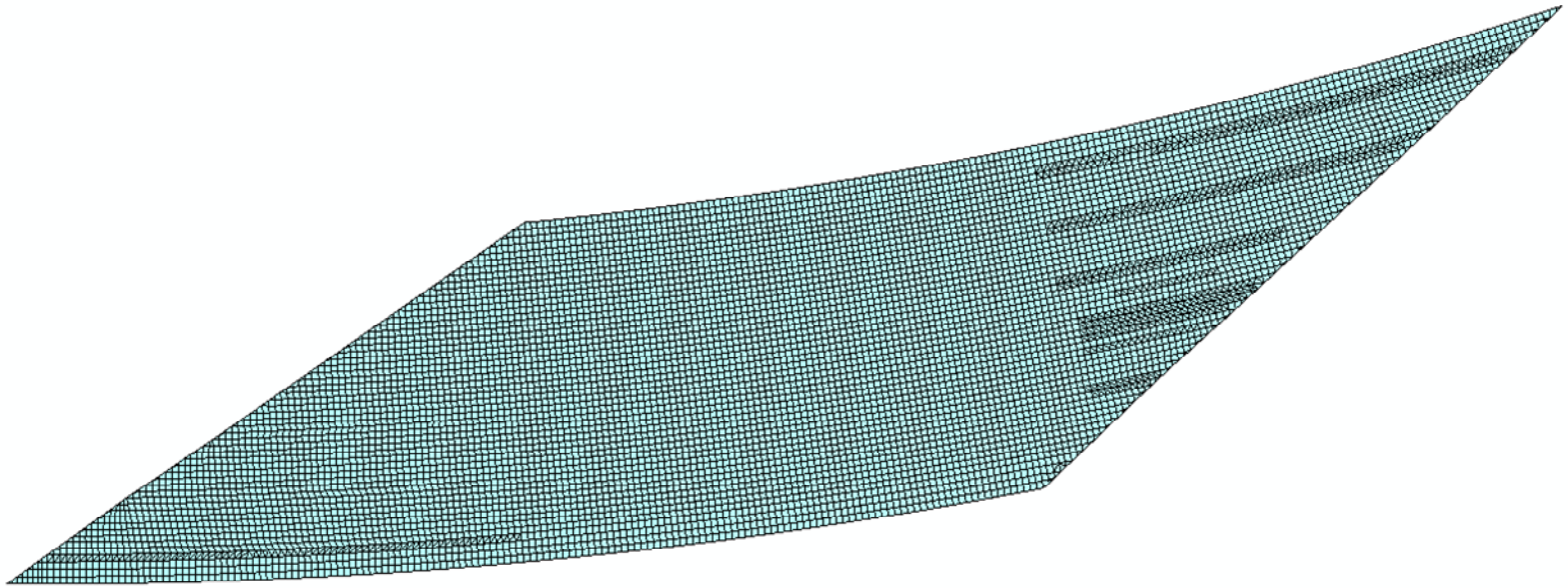

Figure 2.3.4. Plan view of FEA model of the bridge deck.

The flanges of the girders and the transverse stiffeners (bearing stiffeners, intermediate transverse stiffeners and cross-frame connection plates) are modeled using the B31 element, which is a two-node beam element compatible with the S4R and S3R shell elements. Since the bottom flanges of G1 and G2 have section transitions along their length. These flanges are modeled with their reference axes at the flange centroids and the flange elements are connected to the bottom of the web plate finite element discretizations using the ABAQUS beam-type multi-point constraint. Figure 2.3.5 shows a representative model of the section transition on the bottom flanges of G1 and G2. At the transition points, prismatic beam elements with a thickness equal to the average of the flange thickness on each side of the transition are used for two elements lengths along the flanges.

The bottom and diagonal members of the cross-frames are modeled with T31 truss elements and the top chords are represented by B31 beam elements to maintain the stability of the cross-frames in the direction normal to the plane of the cross-frames.

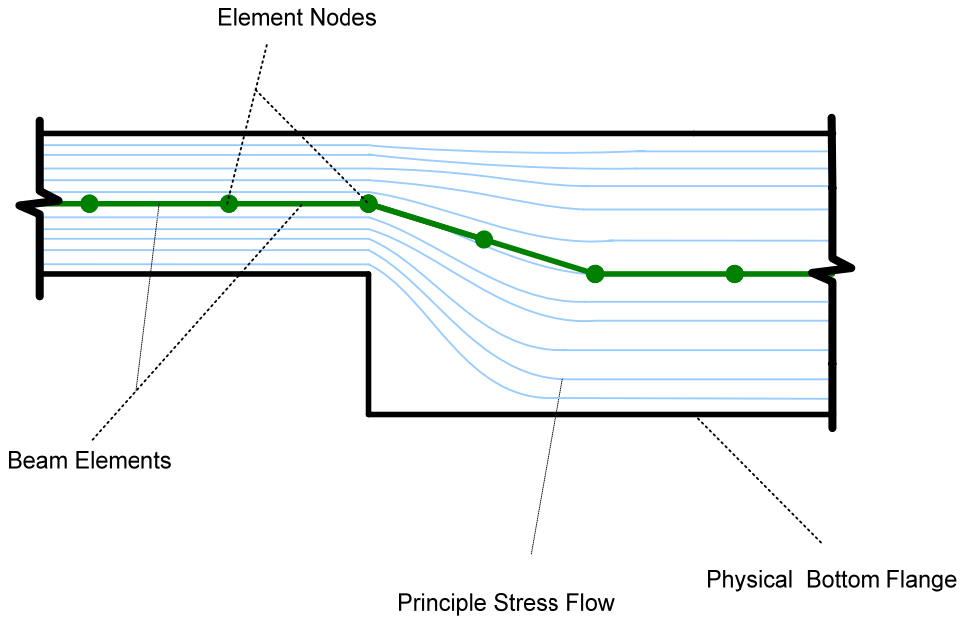

Figure 2.3.5. Representative model of the section transition on the bottom flanges of G1 and G2

2.3.2 Displacement Boundary Conditions

The bridge considered throughout this research is a simply-supported single-span bridge. The bearings are arranged to provide the minimum amount of horizontal restraint to the bridge while still maintaining equilibrium. Since the system is curved, a global cylindrical coordinate system is used to describe the boundary conditions. Also, the bearings at the ends of girders G1, G2, G4, G5, and G6 provide vertical support only. Therefore, they are modeled as ideal roller supports by restraining the displacements in the vertical direction and allowing the bearings to move freely along the longitudinal and tangential directions and rotate in all directions (See Fig. 2.3.1). In addition to the vertical

displacement constraints, radial displacement constraints are used for the bearings at the ends of G3. Finally, a tangential (circumferential) restraint at the mid-span of the bottom flange of G3 is used. This restraint prevents rigid body motion in the longitudinal direction in the model (See Fig. 2.3.1). The reactions are negligible in all cases at this node (the largest reaction obtained in any of the analyses is 0.0001 kips). A more appropriate location for the longitudinal constraint would be a single fixed bearing location at one of the ends of girder G3. The effect of moving the longitudinal constraint to one of the ends of G3 is that a rigid body translation of the bridge is induced due to the girder rotations at the fixed point.

2.3.3 Material Properties

The material properties for the elastic bridge FEA and design checks are tabulated in Table 2.3.1.

Table 2.3.1. Material properties used for the response from the elastic bridge FEA and design checks

Member	Material	Properties
Steel members	E_s (ksi)	F_y (ksi)
Steel	29000	50
Reinforcement bars	29000	60
Concrete	E_c (ksi)	f'_c (ksi)
Concrete	3644	4

2.3.4 Loads

The bridge is analyzed for the dead load due to the self-weight of the steel, the concrete deck and other loads acting on the noncomposite bridge (DC1), and for the dead load from the parapets (DC2), the dead load for the future wearing surface (DW) and the

vehicular live load (LL) acting on the composite bridge. The loads are based on the 4th edition of AASHTO LRFD Bridge Design Specifications (AASHTO 2007). In order to understand their separate effects, DW and DC2 are analyzed separately in this work. Finally, LL is assumed to consist of vehicular live loads (The AASHTO Design Vehicles and Design Lane Loads), including a multiple presence factor, a dynamic load allowance and centrifugal forces as applicable.

2.3.4.1 Noncomposite Dead and Construction Loads (DC1)

The steel section alone must resist the permanent component loads applied before the concrete deck is hardened. These permanent component loads include the weight of the steel components, wet concrete, slab reinforcing steel, forms and construction equipment. The GRAV command is used in the FEA model to calculate the steel self weight. The steel density is taken as 490 pcf. Table 2.3.2 presents the weight of the steel components. The stiffener weights are included in the girder weights.

Table 2.3.2. Weight of the steel components

Member	Weight (kips)
Girder 1	76.60
Girder 2	75.77
Girder 3	65.10
Girder 4	65.29
Girder 5	65.52
Girder 6	66.54
Cross-Frames	50.25

The weight of the formwork, slab reinforcing steel, wet concrete and construction equipment is applied to the top flanges as uniformly distributed line loads based on the tributary width of each girder across the cross-section of the bridge. G1 and G6 have a

tributary width of 8.44 ft whereas G2, G3, G4 and G5 have a tributary width of 8.5 ft. In addition, the overhang brackets used for resisting the weight of wet concrete and formwork at the exterior girders are considered in the model. The overhang brackets are assumed to frame into the webs at a location 4 ft below the top flanges. Typical overhang brackets can be seen in Fig. 2.3.6. The exterior girders are subjected to torsion from the overhang brackets. In order to simulate this loading, the overhang bracket loads are modeled as two equal and opposite radial forces that create a uniformly distributed torque on the exterior girders. The exterior girder flange lateral bending responses tend to increase because of the additional torque due to overhang bracket loads. The calculations of the distributed line loads and uniformly distributed torque for the noncomposite permanent component loads are shown in Table 2.3.3. The weight of the construction equipment is neglected as the effects of the equipment on the bridge responses are assumed to be small. Generally, the weight of the formwork is removed from the bridge after the slab has sufficiently hardened, unless stay-in-place metal deck forms are used. As a simplification, this weight is not removed from the bridge in this study. To sum up, the total applied vertical load due to the weight of steel components is 465.07 kips and the total applied vertical load from the wet concrete, slab reinforcing steel and formwork is 939.56 kips.

Figure 2.3.6. Overhang brackets attached to the exterior girders prior to concrete casting operation (Jung 2006).

Table 2.3.3. Distributed line loads and facia girder uniformly distributed torque for noncomposite permanent component loads

Interior Deck ***(Between girder top flanges)***

Density (lbs/ft^3)	Density (lbs/in^3)	Thickness (in)	Concrete weight per area (density / thickness)
150	0.08681	7.5	0.6510

Girder	Width (ft)	Weight per length (lbs/in)	Haunch weight (lbs/in)	Total Force (kips/in)
1	4.25	33.203	4.833	0.038
2	8.5	66.406	4.833	0.071
3	8.5	66.406	4.833	0.071
4	8.5	66.406	4.833	0.071
5	8.5	66.406	4.833	0.071
6	4.25	33.203	4.833	0.038

Overhangs

Density (lbs/ft^3)	Density (lbs/in^3)	Thickness (in)	Concrete weight per area (density / thickness)
150	0.08681	10	0.8681

Width (ft)	Weight per length (lbs/in)	Total Vertical Force (kips/in)	Torque (in x lbs / in)	Torque Arm (ft)	Radial load (lbs/in)	Total Radial Force (kips/in)
4.19	43.646	0.04365	1097.256	4	22.860	0.023

Table 2.3.3. Distributed line loads and facia girder uniformly distributed torque for noncomposite permanent component loads (continued).

Formwork

Dead load Assumed (psf)	Girder	Dead load (kips)	Width (ft)	Load (kips/in)
7	1	0.007	6.94	0.00405
	2	0.007	7	0.00408
	3	0.007	7	0.00408
	4	0.007	7	0.00408
	5	0.007	7	0.00408
	6	0.007	6.94	0.00405

Steel Reinforcement

Reinforment used in deck	Unit weight (psf)	Girder	Number of longitudinal bars		Load (kips/in)	Width (ft)	Length (ft)	Number of bars along width		Load (kips/in)	Total Load (kips/in)
			Bottom	Top				Bottom	Top		
#4	0.668	1	13	9	0.00122	8.44	159.86	240	160	0.0012	0.0024
		2	13	9	0.00122	8.5	159.93	240	160	0.0012	0.0024
		3	13	9	0.00122	8.5	160.29	240	160	0.0012	0.0024
		4	13	9	0.00122	8.5	160.78	240	160	0.0012	0.0024
		5	13	9	0.00122	8.5	161.52	240	160	0.0012	0.0024
		6	13	9	0.00122	8.44	162.48	240	160	0.0012	0.0024

Summary of Construction Loads

Load Direction	Vertical Direction					Radial Direction
Girder	Interior Deck (kips/in)	Formwork (kips/in)	Reinforcement (kips/in)	Overhang (kips/in)	Total (kips/in)	Overhang Brackets (kips/in)
1	0.03804	0.00405	0.00240	0.04365	0.08813	0.023
2	0.07124	0.00408	0.00241		0.07773	
3	0.07124	0.00408	0.00241		0.07773	
4	0.07124	0.00408	0.00240		0.07772	
5	0.07124	0.00408	0.00240		0.07772	
6	0.03804	0.00405	0.00239	0.04365	0.08812	0.023

2.3.4.2 Composite Dead Loads

The composite dead loads are applied after the slab is hardened. In this section the composite dead loads and their calculations are presented. First the calculations for the weight of the parapets are shown and then the future wearing surface load calculations are presented.

2.3.4.2.1 Weight of Parapets (DC2)

DC2 consists of the dead weight of the parapets. The parapets are 2.440 ft high and 1.583 ft wide. The parapets have a weight of 1150 lbs per ft. In the model, DC2 is applied as an uniform distributed load over the width of the parapets which is their actual location. The total applied vertical load due to DC2 is 191 kips. Moreover, it is assumed that the parapets do not make any contribution to the stiffness of the bridge.

2.3.4.2.2 Wearing Surface Dead Load (DW)

The load DW (weight of the wearing surface) is applied to the deck along the roadway, which is 46 ft wide, as a distributed load. The weight of the wearing surface is 25 lbs per ft^2. Furthermore, the total applied vertical load due to DW is 184.49 kips.

2.3.4.3 Design Live loads for Flexure (LL)

The live loads of interest in this research are the AASHTO (2007) design vehicular live loads with the appropriate dynamic load allowance, multiple presence factors and centrifugal forces evaluated in this work. Braking forces and vehicular collision forces are neglected due to their anticipated small effect on the bridge responses. Additionally,

according to the provisions of Guide Specifications for Horizontally Curved Bridges (2003) the effect of superelevation can be neglected for superelevation angles between 0 and 10 percent. Therefore, the effect of superelevation is neglected. Since the bridge is horizontally curved, the effects of centrifugal force must be considered. Centrifugal force is a radial force, applied above the deck, which is transferred through the wheels of the vehicle to deck. Since centrifugal force is applied above the deck, it creates an overturning moment. As a result, the overturning moment tends to increase the vertical wheel forces toward the outside of the bridge and decrease them toward the inside of the bridge. The design speed is calculated as 45 mph for the subject bridge from the document *A Policy on Geometric Design of Highways and Streets* (AASHTO 2004). The radial centrifugal force as a percentage of the total vehicle weight is given in AASHTO (2007) as

$$C = \frac{6.68(S)}{R} \tag{2.3.4.1}$$

where, S is the design speed and R is the radius of curvature. The design vehicular live loads are discussed in grater detail in the following sections.

2.3.4.3.1 Design Vehicular Live Loads

Based on AASHTO (2007), the design live loads are designated as HS-93 and are composed of a design truck (DT) and a design lane load (DL). The bridge has a 46 ft roadway which consists of three 12 ft traffic lanes. Design vehicular live loads are arranged to maximize the force effects. Additionally, the traffic lanes are oriented to maximize these effects. For instance, traffic lanes are shifted as close as possible to the outside girder along the roadway to obtain the maximum responses for the outside girder.

The dynamic load allowance increases the percentage of static effects of the design truck. However, this is applicable only to the design truck; it is not applied to the lane load discussed subsequently. Additionally, multiple presence factors are applied as function of the number of side-by-side lanes and trucks from the design live loads.

Figure 2.3.7 shows typical design truck properties. One design truck is placed transversely within a given lane and it is positioned no closer than 2 ft from the edge of the middle lanes and 1 ft from the edge of the exterior traffic lanes. In addition, the axle loads are applied as point loads to the composite deck including the dynamic load allowance.

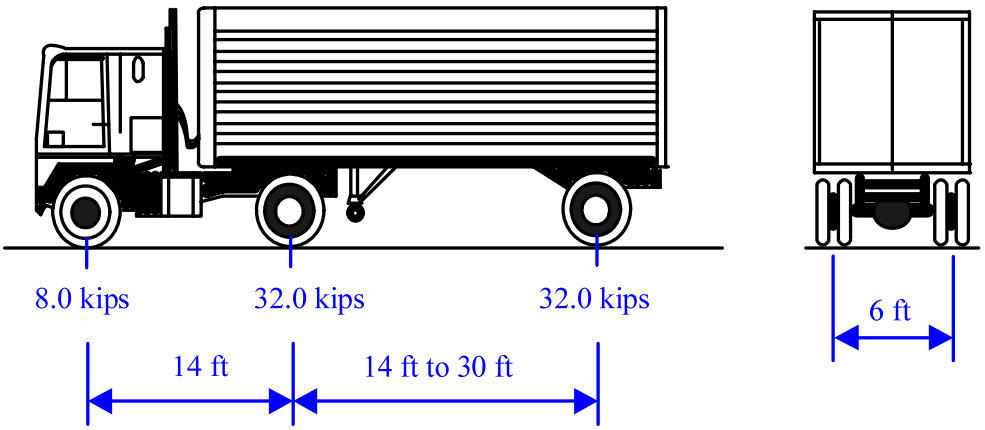

Figure 2.3.7. Design Truck Specified in AASHTO (2007).

To continue with the design lane load, a load of 0.064 kip/ft^2 is applied as a distributed load over a 10 ft width of each traffic lane where applicable. Moreover, multiple presence factors are considered to account for the probability of simultaneous lane occupation by design vehicular live loads.

The placement of the design vehicular loads is determined by using the influence surfaces. Major-axis bending and flange lateral bending envelopes are generated for the

specific girders and maximum tension and compression force values are generated for the cross-frame members. Generation of influence surfaces, envelopes and maximum force values is discussed further in the subsequent sections.

2.3.4.3.1.1 Influence Surfaces

Influence surfaces are needed for complex bridges to determine the placement of the design vehicular loads. In this study, unit loads are applied at 156 points on the slab of the composite bridge to generate the influence surfaces for various responses. Points through the width of the deck are chosen such that they are directly above the girders, at the mid-spacing between the girders and are close to the edges of the roadway. In a similar fashion, points along the length of the deck are selected to create equal arc lengths. Figures 2.3.8 and 2.3.9 show the locations of the points on the deck used to generate influence surfaces.

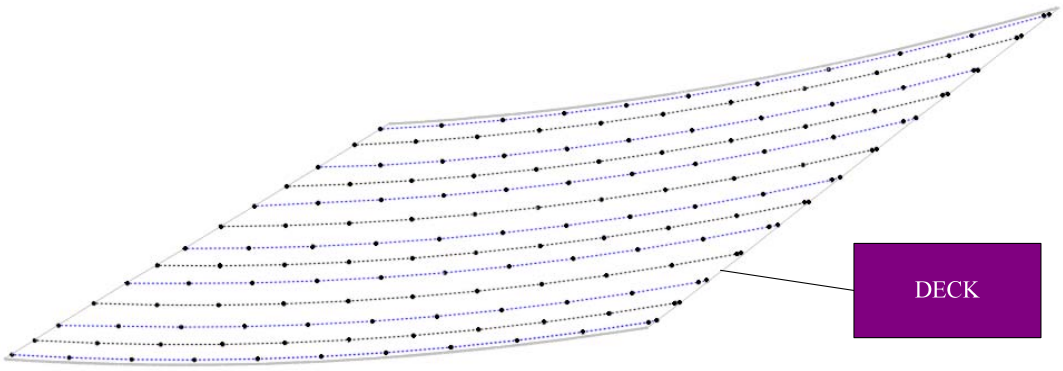

Figure 2.3.8. Locations where the unit load is applied on the concrete deck to determine the influence surfaces (156 points)

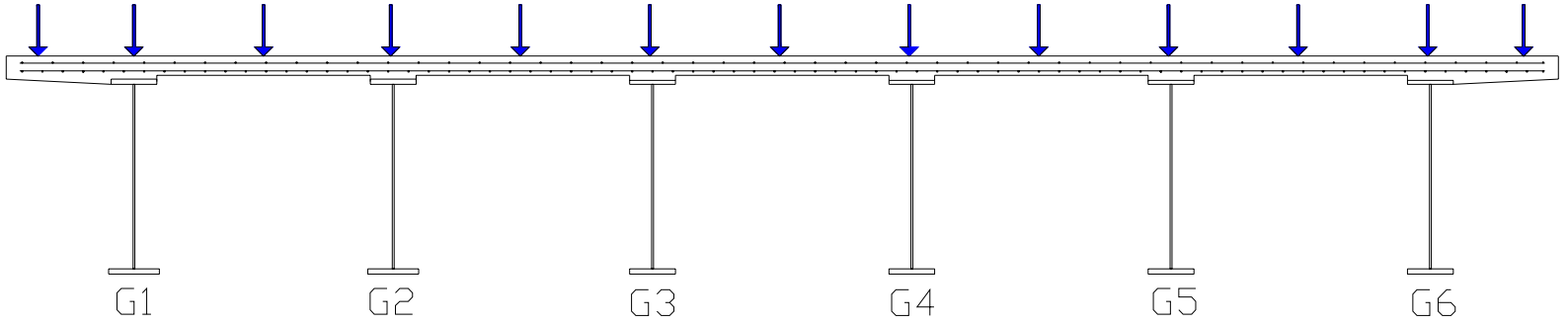

Figure 2.3.9. Locations where the unit load is applied along the width (13 points).

This study focuses on the behavior of G1, G3 and G6 to simplify the interpretation and presentation of the results. Therefore, discrete locations are selected along these girder lengths to monitor the bridge behavior. Since the flange lateral bending responses tend to have a local maximum approximately at the middle of the unbraced lengths as well as at the cross-frame locations, these locations on G1, G3, and G6 are chosen. Influence surfaces are created for the responses at these locations. Then these influence surface responses are used to generate the major-axis bending and flange lateral bending live load envelopes. Live load envelopes give the maximum response quantities at the various locations along the girder lengths caused by the design vehicular loads. Additionally, influence surfaces for the cross-frame members are developed to construct maximum axial force values for the cross frames.

As an illustration, Fig. 2.3.10 shows the major-axis bending moment influence surface for the location on G1 where the maximum total major-axis bending moment is subsequently computed. Figure 2.3.11 shows the bottom flange lateral bending moment influence surface for the location on G3 found to have the largest flange lateral bending stress of all the girders.

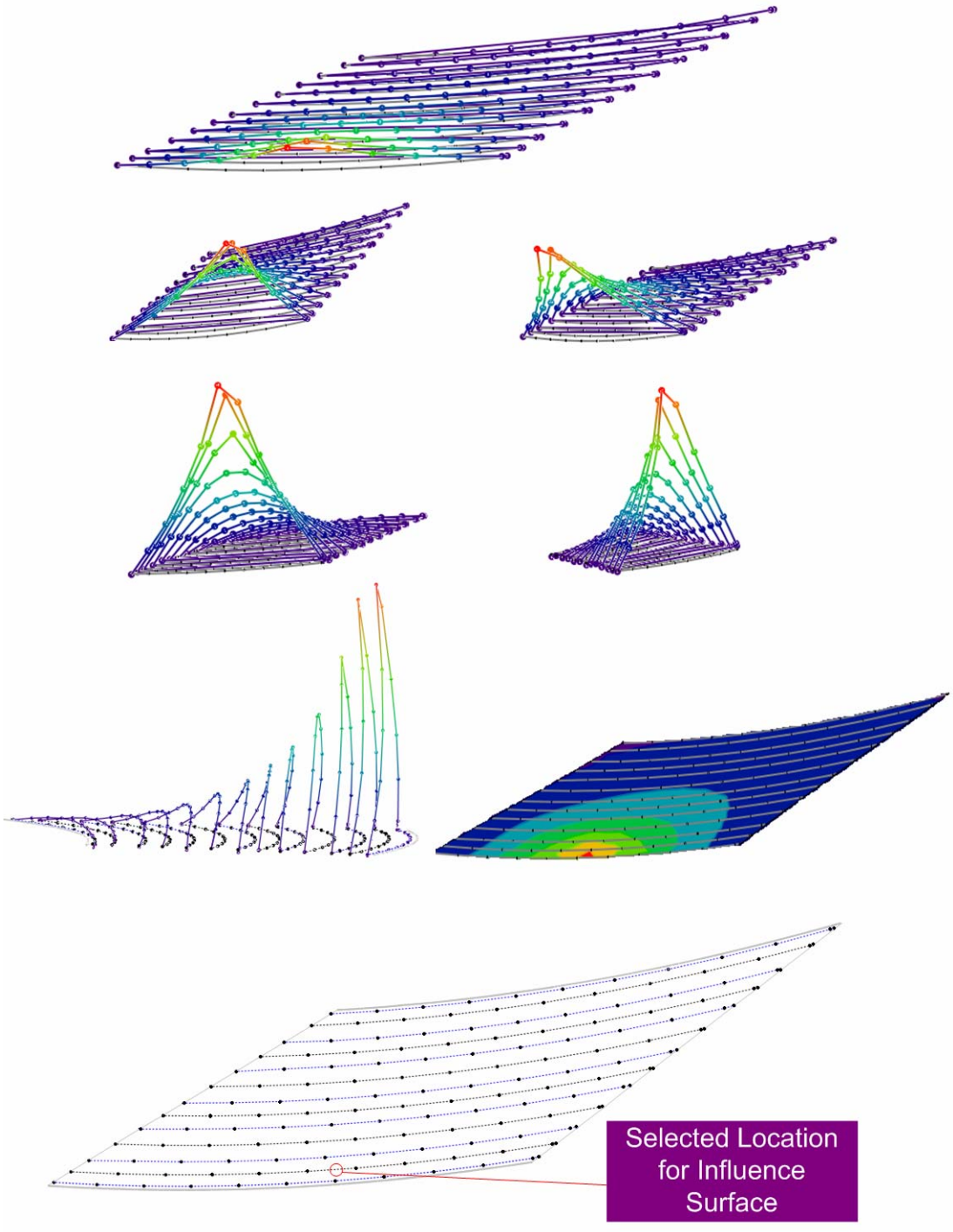

Figure 2.3.10. Major-axis bending moment influence surface for the location on G1 where the maximum total major-axis bending moment is subsequently computed

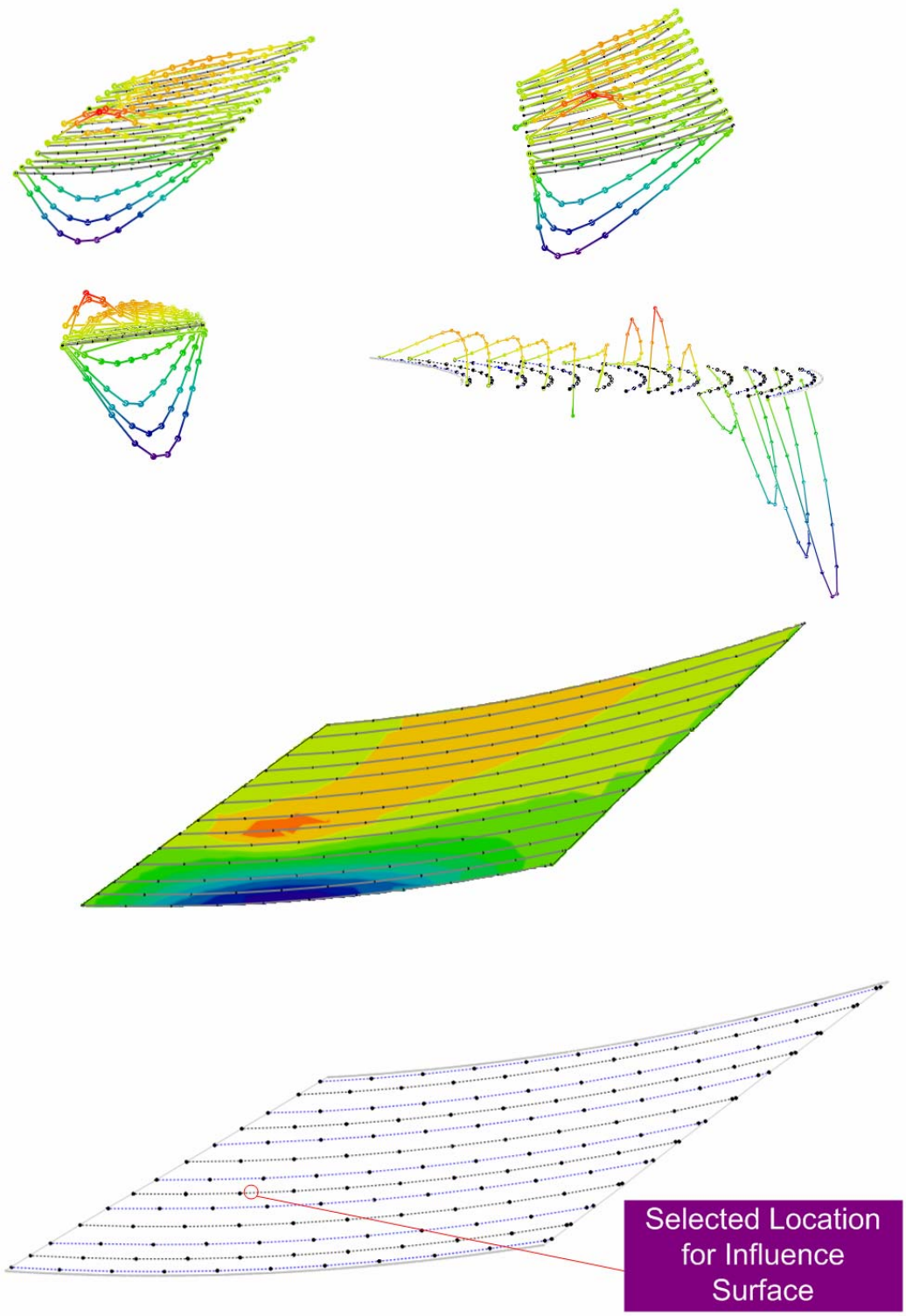

Figure 2.3.11. Bottom flange lateral bending stress influence surface for the location on G3 found to have the largest flange lateral bending stress of all the girders.

2.3.4.3.1.2 Live Load Envelopes

Live load envelopes are essential to bridge design as they represent the overall maximum live load response along the length of the corresponding member. As mentioned before, the mid-point of the unbraced lengths and the cross-frame locations of bottom flanges of G1, G3, and G6 are chosen for developing the major-axis bending and flange lateral bending envelopes for girders. Additionally, maximum axial force values are obtained for selected cross-frames. These cross-frames are selected based on preliminary analyses.

Since the vehicular loading positions do not necessarily coincide with the applied unit load locations, influence surface values are determined at desired points by using a bilinear quadrilateral (Q4) isoparametric finite element approach. Figure 2.3.12 shows a bilinear quadrilateral (Q4) element.

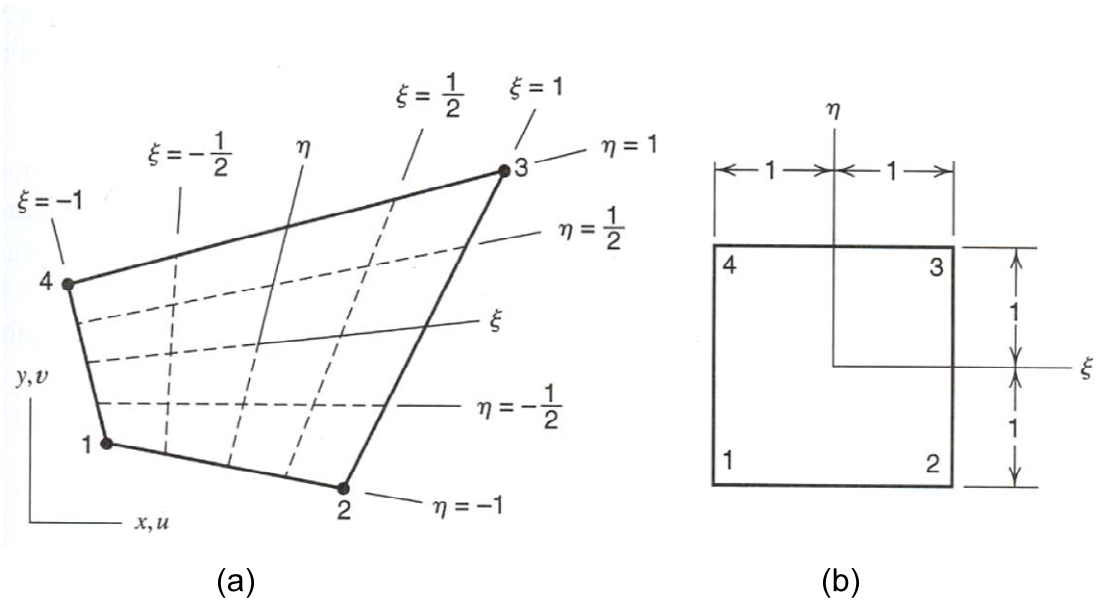

Figure 2.3.12. (a) Four-node plane element in physical space. (b) The same element mapped into ξ η space (Cook et al 2001).

If the response due to a point load with given global coordinates (*x, y*) is needed, such as a design truck wheel load, the influence surface values are interpolated from the unit load locations to the desired points by using the following bilinear quadrilateral (Q4) isoparametric element equations.

$$N_1 = \frac{1}{4}(1-\xi)(1-\eta) \quad N_2 = \frac{1}{4}(1+\xi)(1-\eta)$$
$$N_3 = \frac{1}{4}(1+\xi)(1+\eta) \quad N_4 = \frac{1}{4}(1-\xi)(1+\eta) \tag{2.3.4.2}$$

Since the elements are created based on the cylindrical coordinate system, the η coordinate of each wheel can be calculated directly from the wheel load position in the radial direction across the slab width. All elements have the same center of curvature. Therefore, the radial distance of a wheel position with respect to the center of curvature can be obtained easily. Similarly, the radial distance between the center of the element and the center of curvature can be obtained. The η coordinate can be estimated by dividing the difference between those distances which are defined above to the radius of the element. Once the η coordinate is determined, the ξ coordinate can be calculated by using the geometry interpolation along with the (*x, y*) coordinates of the wheel.

$$\begin{Bmatrix} x \\ y \end{Bmatrix} = \begin{bmatrix} \Sigma N_i x_i \\ \Sigma N_i y_i \end{bmatrix} \tag{2.3.4.3}$$

Since an isoparametric element approach is employed, shape functions are used to interpolate both the coordinates (Eq. 2.3.4.3) and the influence surface intensities.

$$\{I_c\} = \left[\Sigma N_i I_i\right] \tag{2.3.4.4}$$

As a result, the response due to the specified wheel load can be calculated using

$$R = P \times \{I_c\} = P \times \left[\sum N_i I_i\right] \tag{2.3.4.5}$$

where I_c is the computed intensity at a specific location, P is the wheel load of the design truck and R is the response due to P.

Also, if the response due to a distributed loading is needed, such as a design lane loading, Gauss quadrature is used to evaluate the surface values over the element area. A 2*x*2 Gauss quadrature is used. The basic equation for the response due to a given design lane load of w applied over a given isoparametric element area is

$$R = \int_A w\, I_c\, dA \tag{2.3.4.6}$$

When the Eq. 2.3.4.4 is substituted into Eq. 2.3.4.6 it becomes,

$$R = \int_A w \sum N_i I_i\, dA \tag{2.3.4.7}$$

and the integral is evaluated by using Gauss quadrature as

$$R = \int_{-1}^{1} \int_{-1}^{1} w \sum N_i I_i\, J\, d\xi\, d\eta \tag{2.3.4.8}$$

$$R = \sum_j \sum_k w \sum N_i I_i\, J\, w_j w_k \tag{2.3.4.9}$$

$$J = det[J] = J_{11}J_{22} - J_{21}J_{12} \tag{2.3.4.10}$$

$$[J] = \frac{1}{4}\begin{bmatrix} -(1-\eta) & (1-\eta) & (1+\eta) & -(1+\eta) \\ -(1-\xi) & -(1+\xi) & (1+\xi) & (1-\xi) \end{bmatrix} \begin{bmatrix} x_1 & y_1 \\ x_2 & y_2 \\ x_3 & y_3 \\ x_4 & y_4 \end{bmatrix} = \begin{bmatrix} J_{11} & J_{12} \\ J_{21} & J_{22} \end{bmatrix} \tag{2.3.4.11}$$

where; w_j and w_k are the integration weight factors, which are equal to unity for 2*x*2 Gauss integration, R is the response due to the design lane load and $[\mathrm{J}]$ is the Jacobian matrix. The term J is the determinant of the Jacobian matrix referred to as the Jacobian. The Jacobian is a scale factor that multiplies $d\xi\, d\eta$ to produce the physical area *dx dy*.

The desired maximum response for each mid-point of the unbraced lengths and each cross-frame location along the bottom flanges of G1, G3, and G6 are obtained by applying the corresponding critical live load configuration on the bridge deck. Later these responses are combined to create the desired envelopes for the member responses. Maximum major-axis bending stress and moment and concurrent flange lateral bending stress envelopes and maximum flange lateral bending stress and concurrent major-axis bending stress and moment envelopes are developed for G1, G3 and G6. Figures 2.3.13 through 2.3.16 show the live load envelopes for G1. The cross-frame locations are denoted by the lighter color vertical lines in the plots.

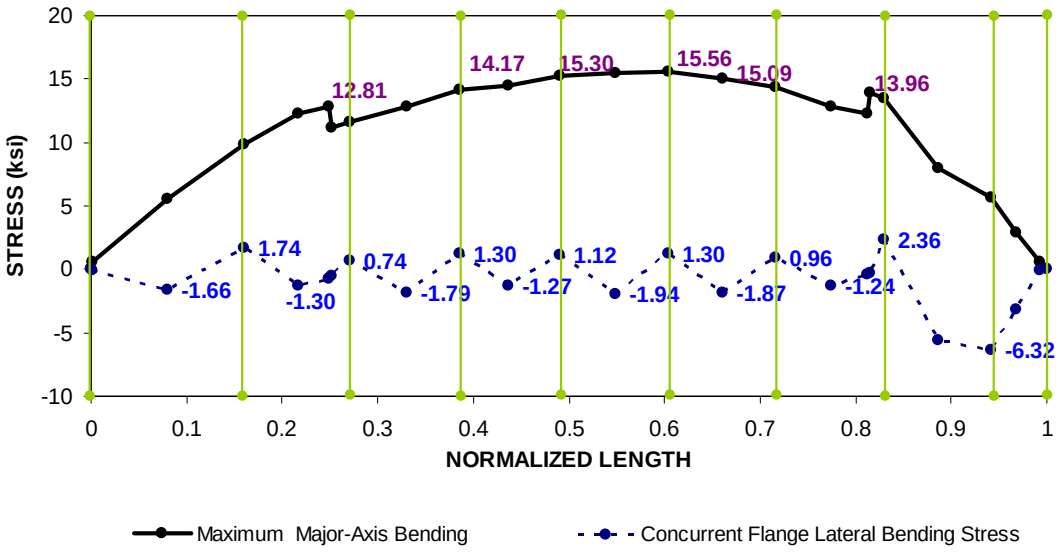

Figure 2.3.13. G1 bottom flange maximum major-axis bending and concurrent lateral bending live load stress envelopes.

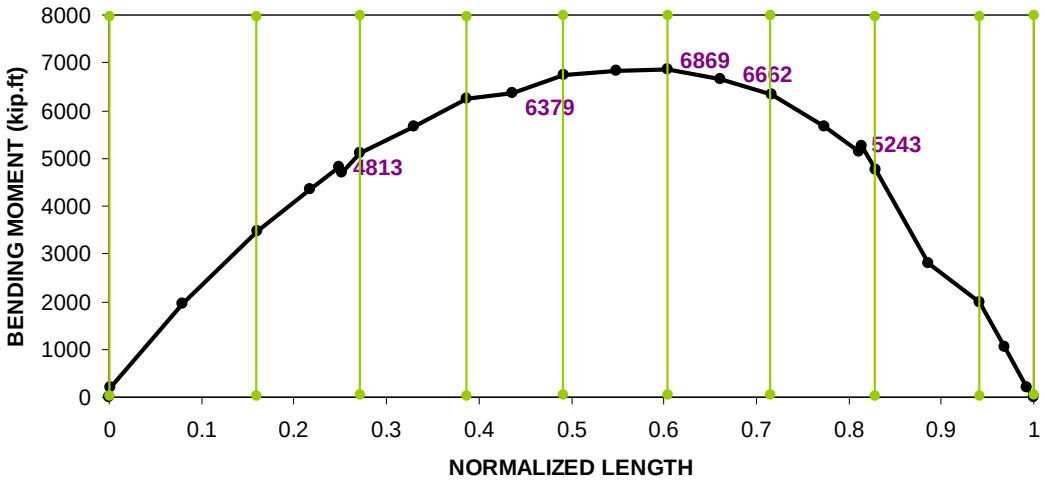

Figure 2.3.14. G1 maximum major-axis bending live load moment envelope.

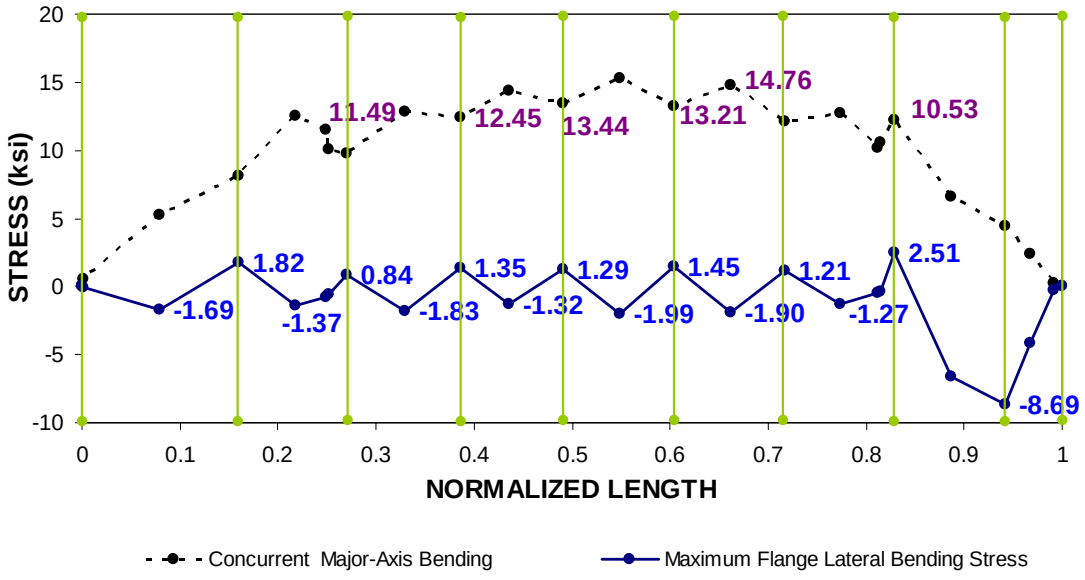

Figure 2.3.15. G1 bottom flange maximum flange lateral bending and concurrent major-axis bending live load stress envelopes.

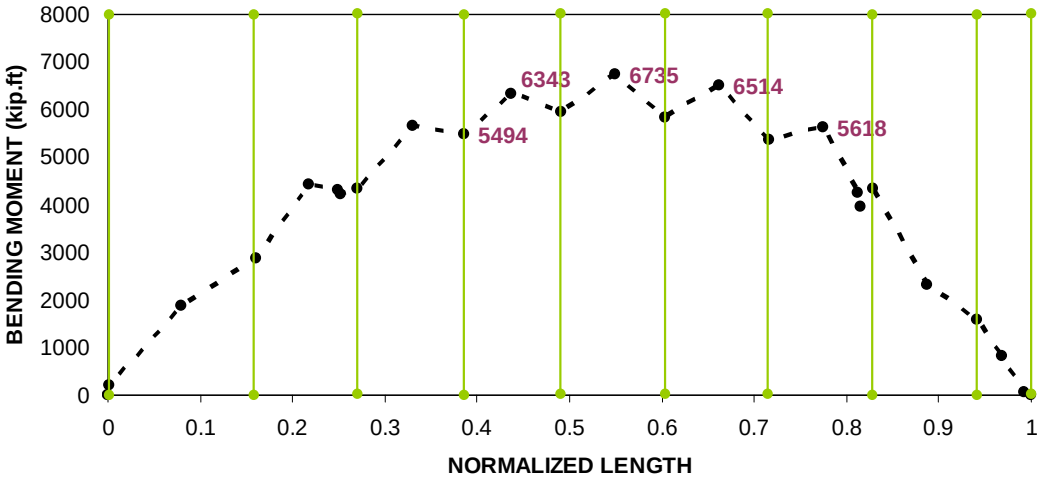

Figure 2.3.16. G1 concurrent major-axis bending live load moment envelope.

2.4 Elastic Analysis of the Bridge

The elastic analysis of the bridge is conducted to assess the constructability, strength and service limits states defined in AASHTO (2007). Although other limit states may control the design they are not considered in this work. This study focuses on the STRENGTH IV, STRENGTH I and SERVICE II load combinations. These load combinations are as follows:

$$STRENGTH\quad IV: \qquad 1.5DC1+1.5DC2+1.5DW$$

$$STRENGTH\quad I: \qquad 1.25DC1+1.25DC2+1.5DW+1.75LL$$

$$SERVICE\quad II: \qquad 1.0DC1+1.0DC2+1.0DW+1.33LL$$

Where:

DC1 = Noncomposite dead and construction loads

DC2 = Weight of parapets acting on the composite structure.

DW = Weight of future wearing surface.

LL = Vehicular live loads.

Based on the assumption that the system is elastic and that the response under composite loadings is geometrically linear, superposition is valid. Therefore, separate analyses are conducted for DC1, DC2, DW and LL and the resulting stresses and deflections are superimposed. For the stress results, bottom flange and top flange responses at the flange mid-thickness are calculated and the flange major-axis bending stresses are extrapolated to the extreme fiber. These results are converted to internal

moments by using the corresponding girder section properties. Noncomposite section properties are used for computing moments from the stresses obtained from noncomposite dead and construction load analysis. Furthermore, long term composite section properties are used for converting the composite dead load stresses to moments. On the other hand, short term section properties of the bridge are used for converting the live load stresses to moments. The full tributary width of the deck is used in determining the composite cross-section properties.

The above internal moments are verified by making radial cuts in the FEA model at several locations of interest along the girder lengths and calculating the internal moments by obtaining the nodal forces from the FEA model and summing them up over the undeformed cross-sections at the radial cuts. The maximum difference between those two internal moments is 4 percent.

Linear elastic (first-order) and geometrically nonlinear (second-order) analyses are conducted for DC1. After a preliminary study, it is found that when the deck is hardened the system is much stiffer and the influence of geometric nonlinearity can be neglected for the composite loadings. The influence of geometric nonlinearity for the noncomposite loadings is discussed subsequently. Therefore, linear elastic analyses are conducted for the composite loadings (DC2, DW and LL).

2.4.1 Results of the Noncomposite Dead and Construction Load Analysis (DC1)

Since the STRENGTH IV load combination is more critical then the STRENGTH I load combination for the constructability checks, first the top flange and bottom flange responses and deflected geometries are shown under the STRENGTH IV load

combination (1.5 DC1) for the noncomposite dead and construction loads. Figures 2.4.1 through 2.4.8 show the bottom and top flange stresses obtained from geometrically nonlinear (second-order) and linear elastic (first-order) analyses under 1.5 DC1 for G1, G3 and G6. The cross-frame locations are denoted by the lighter-color vertical lines in the plots. It is observed that all of the factored noncomposite responses are below the yielding stress of the members. Also, it is noted that the flange lateral bending stresses are largest at the cross frame locations and close to the mid-span of the unbraced lengths as expected. Additionally, the major-axis bending stresses are not affected significantly by the geometric nonlinearity whereas the influence of geometric nonlinearity is noticeably high for the flange lateral bending stresses. The maximum deflection at G1 is 13.11 inches when the influence of geometric nonlinearity is considered and 12.56 inches when linear elastic analysis is conducted, an increase of 4 percent. Figure 2.4.9 presents the vertical deflections obtained from geometrically nonlinear and linear elastic analyses of the outside girder (G1) under the STRENGTH IV load combination. Since the influence of geometric nonlinearity is obviously important for the noncomposite dead and construction loadings, the responses from geometric nonlinear (second-order) analysis are combined with the responses from the subsequent geometrically linear (first-order) analysis for the composite loadings in the subsequent design checks.

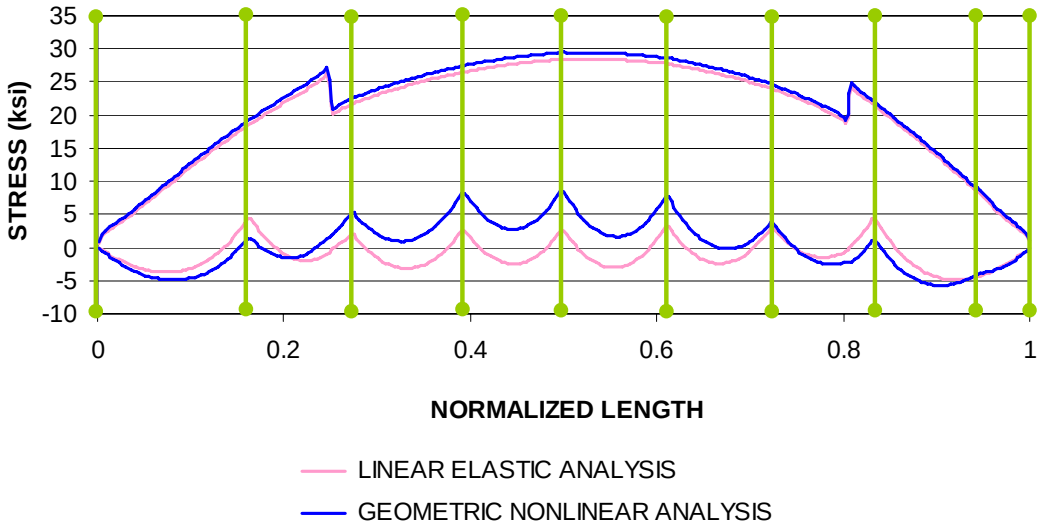

Figure 2.4.1. Bottom flange major-axis bending and flange lateral bending stresses along the length of G1under DC1, comparison of linear elastic analysis and geometric nonlinear analysis (Load factor = 1.5).

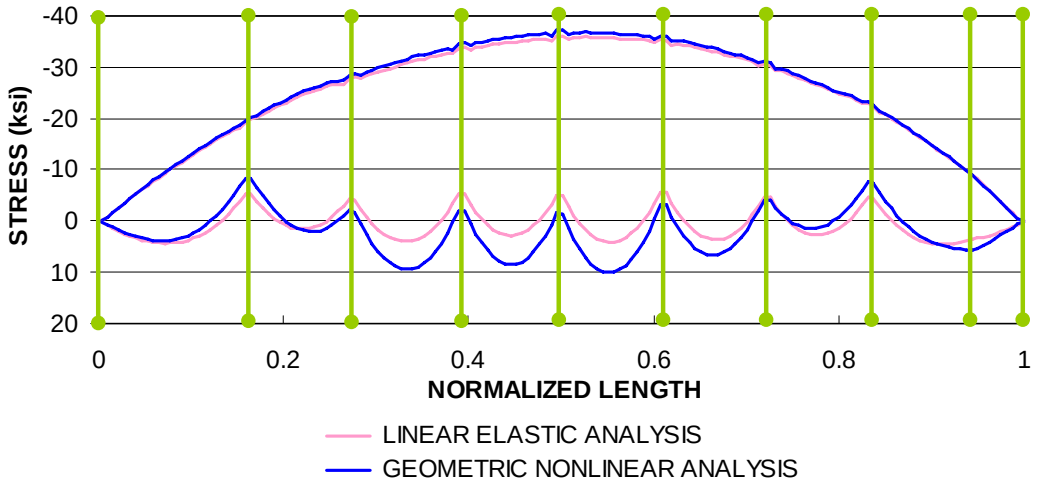

Figure 2.4.2. Top lange major-axis bending and flange lateral bending stresses along the length of G1under DC1, comparison of linear elastic analysis and geometric nonlinear analysis (Load factor = 1.5).

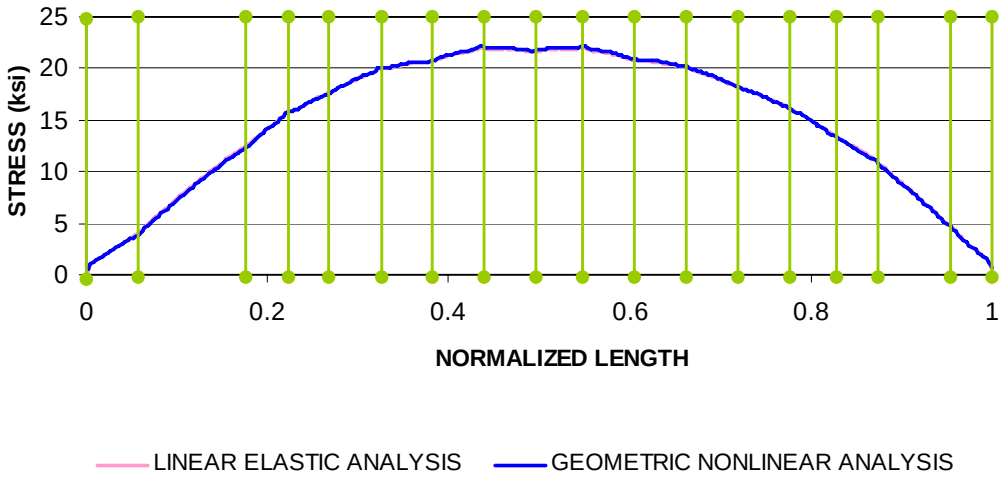

Figure 2.4.3. Bottom flange major-axis bending stresses along the length of G3 under DC1, comparison of linear elastic analysis and geometric nonlinear analysis (Load factor = 1.5).

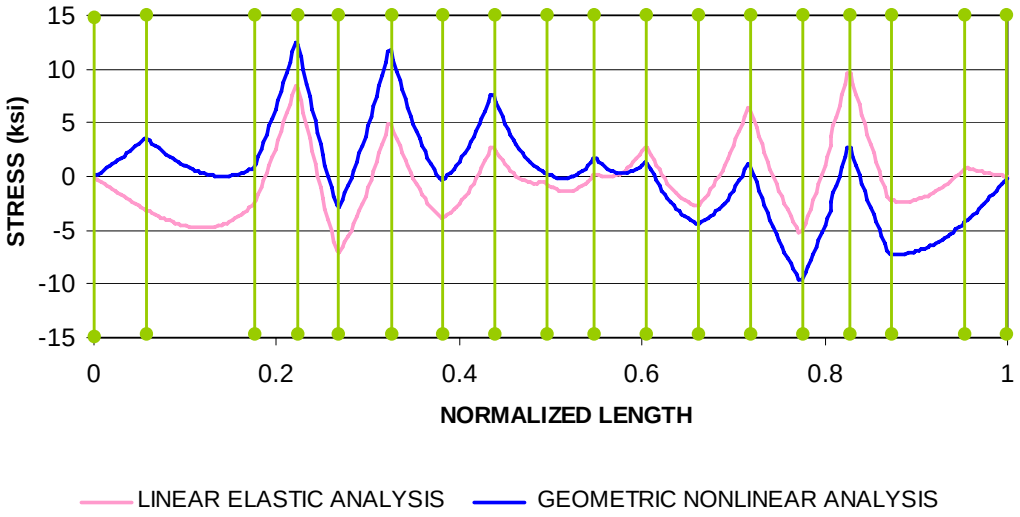

Figure 2.4.4. Bottom flange lateral bending stresses under DC1 along the length of G3 under DC1, comparison of linear elastic analysis and geometric nonlinear analysis (Load factor = 1.5).

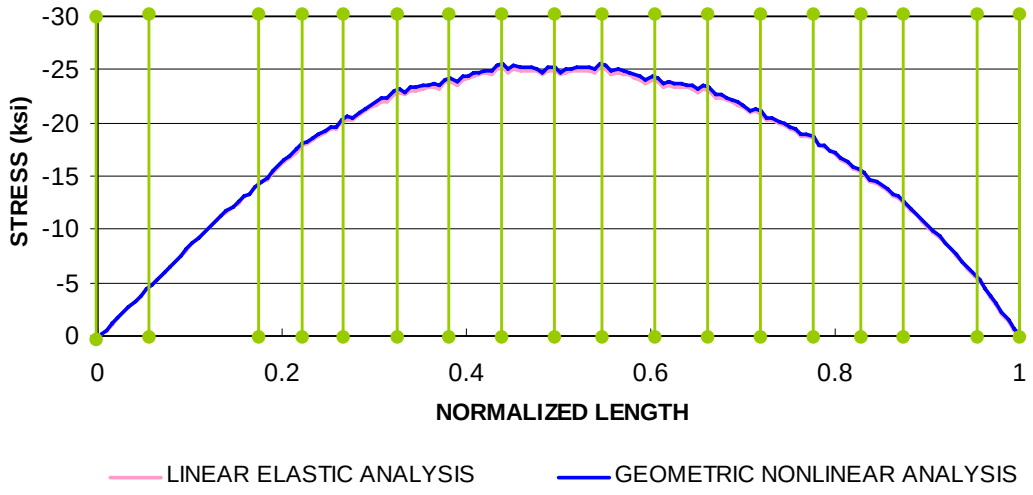

Figure 2.4.5. Top flange major-axis bending stresses along the length of G3 under DC1, comparison of linear elastic analysis and geometric nonlinear analysis (Load factor = 1.5).

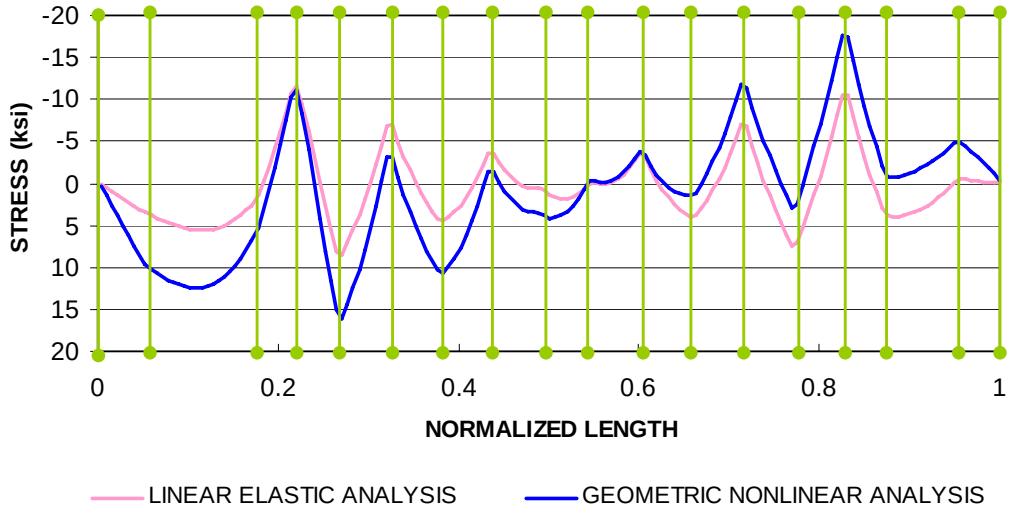

Figure 2.4.6. Top flange lateral bending stresses along the length of G3 under DC1, comparison of linear elastic analysis and geometric nonlinear analysis (Load factor = 1.5).

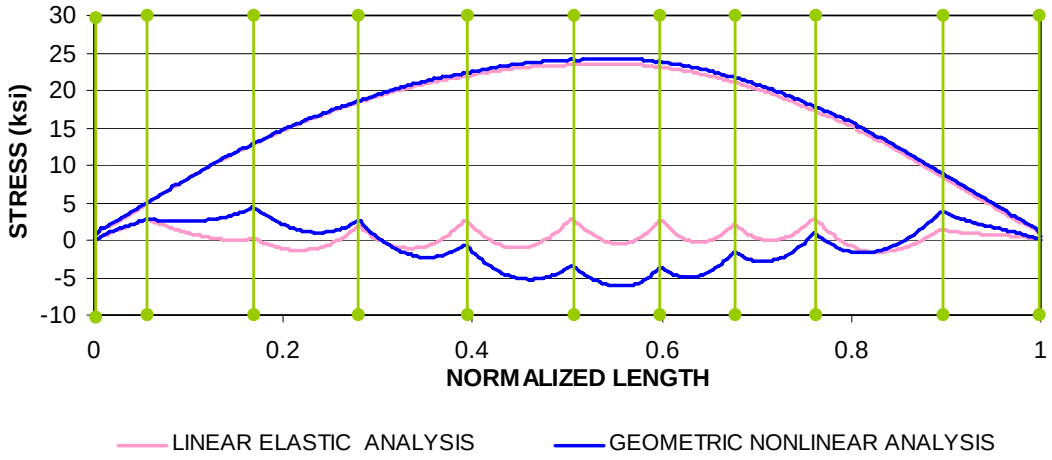

Figure 2.4.7. Bottom flange major-axis bending and flange lateral bending stresses along the length of G6 under DC1, comparison of linear elastic analysis and geometric nonlinear analysis (Load factor = 1.5).

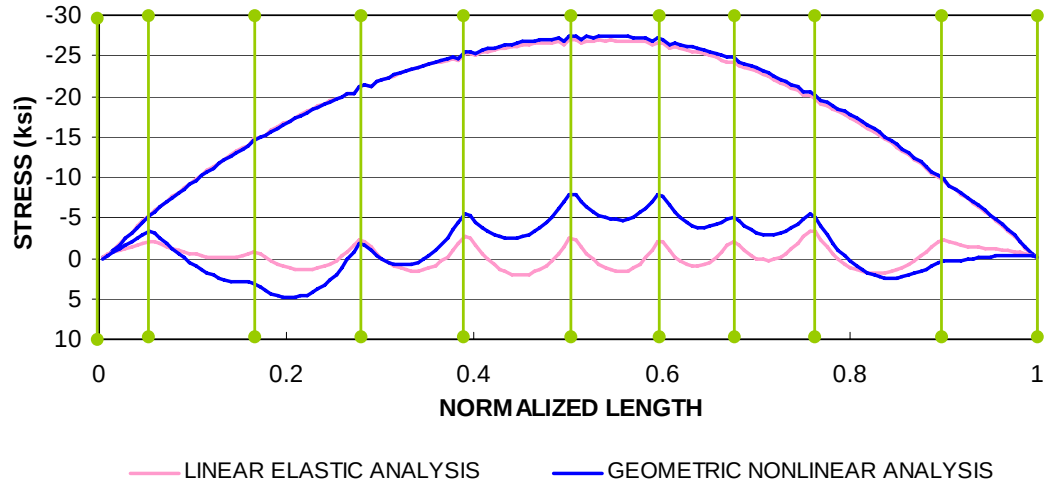

Figure 2.4.8. Top flange major-axis bending and flange lateral bending stresses along the length of G6 under DC1, comparison of linear elastic analysis and geometric nonlinear analysis (Load factor = 1.5).

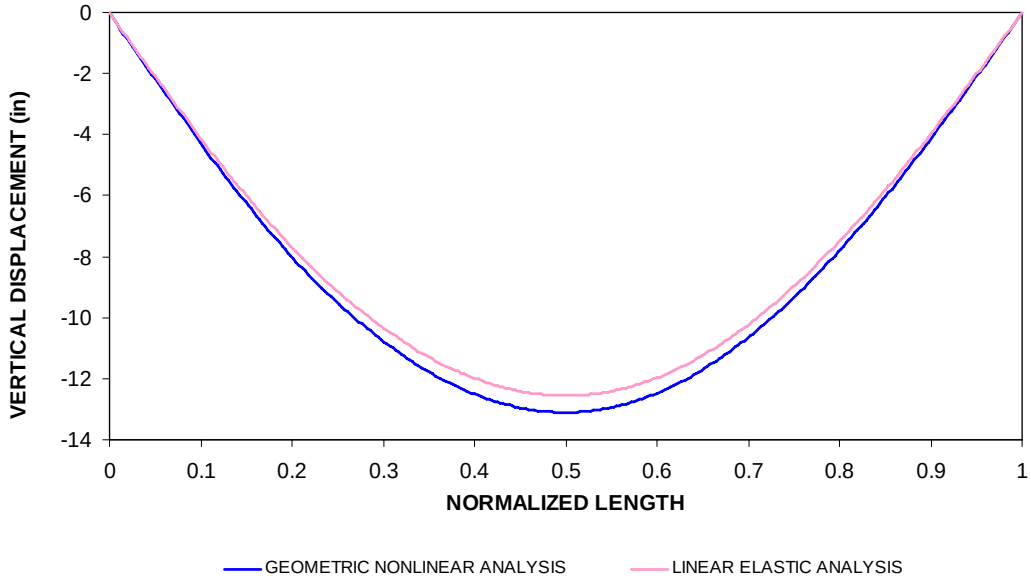

Figure 2.4.9. Vertical displacement along G1 obtained from geometric nonlinear and linear elastic analyses under DC1 (Load factor = 1.5).

The STRENGTH I load combination for the bridge in the final composite configuration governs the strength limit state checks for the bottom flanges of the girders. Therefore, the geometrically nonlinear analysis responses for the bottom flanges are shown under 1.25 DC1 in Figs. 2.4.10 through 2.4.15. As mentioned above, only the geometric nonlinear DC1 results are considered for the subsequent strength checks since the second-order analysis results differ significantly from the linear elastic analysis results.

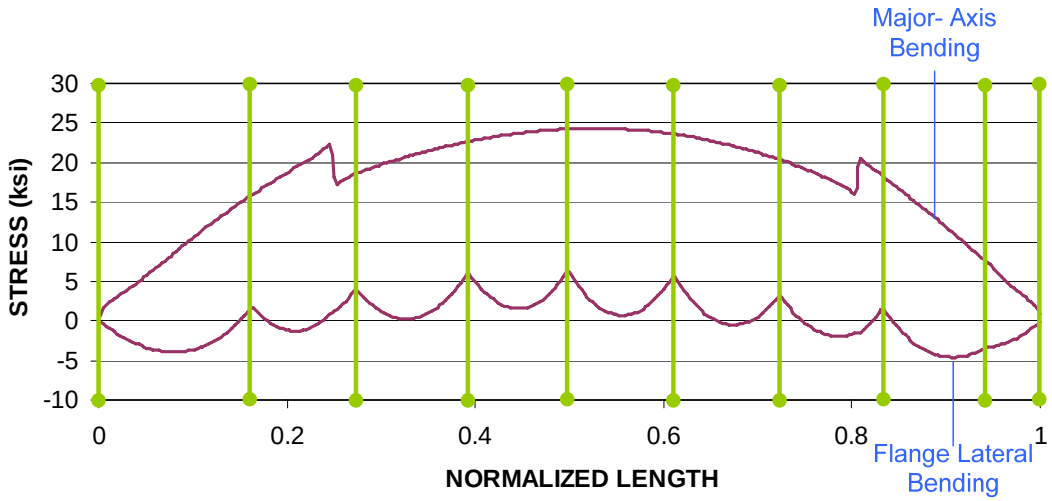

Figure 2.4.10. Bottom flange major-axis bending and flange lateral bending stresses along the length of G1due to DC1 from geometric nonlinear analysis (Load factor=1.25).

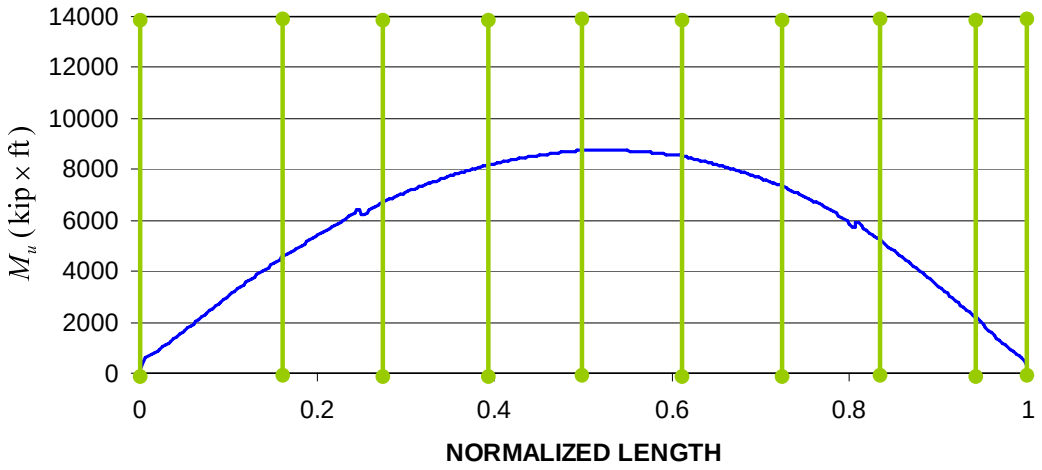

Figure 2.4.11. Major-axis bending moments along the length of G1from geometric nonlinear analysis due to DC1 (Load factor = 1.25).

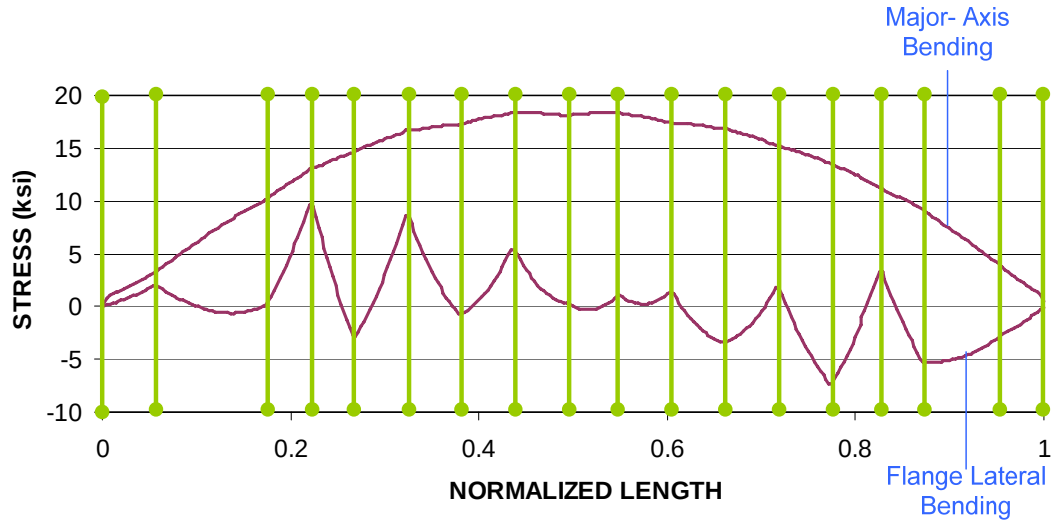

Figure 2.4.12. Bottom flange major-axis bending and flange lateral bending stresses along the length of G3 due to DC1 from geometric nonlinear analysis (Load factor =1.25).

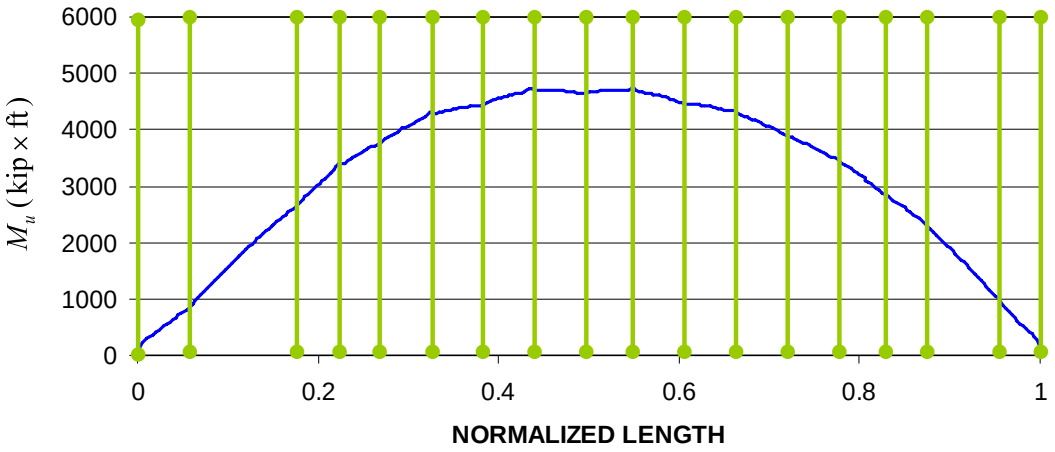

Figure 2.4.13. Major-axis bending moments along the length of G3 from geometric nonlinear analysis due to DC1 (Load factor = 1.25).

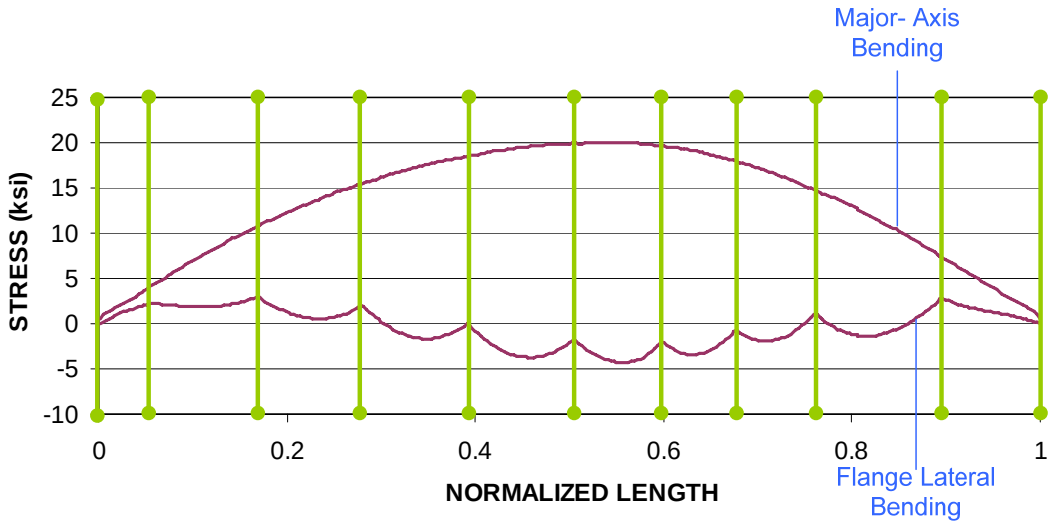

Figure 2.4.14. Bottom flange major-axis bending and flange lateral bending stresses along the length of G6 due to DC1 from geometric nonlinear analysis (Load factor =1.25).

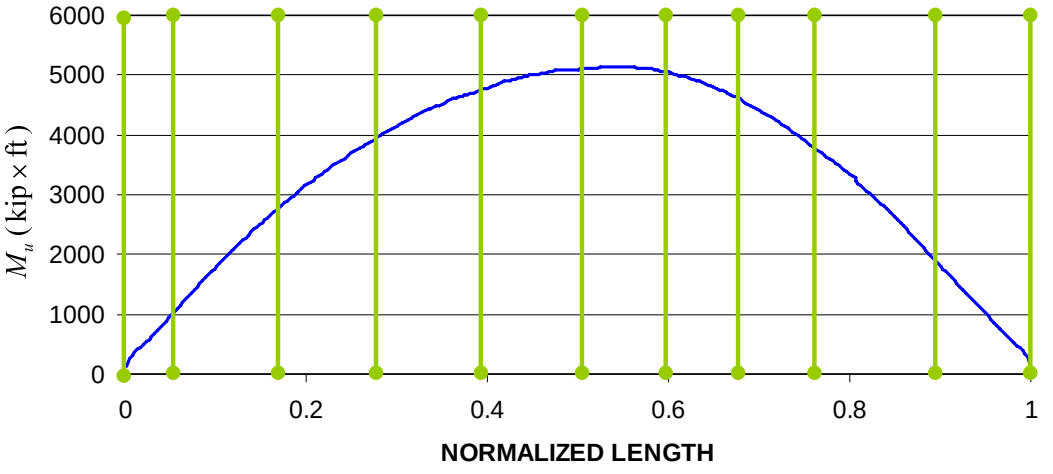

Figure 2.4.15. Major-axis bending moments along the length of G6 from geometric nonlinear analysis due to DC1 (Load factor = 1.25).

Also, in this work, the noncomposite structure is analyzed under 1.25 DC1 to predict the initial camber so that the girder top flanges are perfectly situated in a horizontal plane under this loading. This allows the slab to be instantiated in the finite element model in an initially flat position for the subsequent full nonlinear analysis studies. Furthermore, this exaggerates the influence of any girder twists from the initially-plumb no-load fit condition due to the noncomposite dead load (since the factored dead load 1.25 DC1 is used rather than the actual 1.0 DC1). Figure 2.4.16 shows the noncomposite structure perspective view of the deformed shape obtained from the second order analysis under 1.25 DC1. Furthermore, Fig. 2.4.17 shows a plot of the vertical deflection of the outside girder.

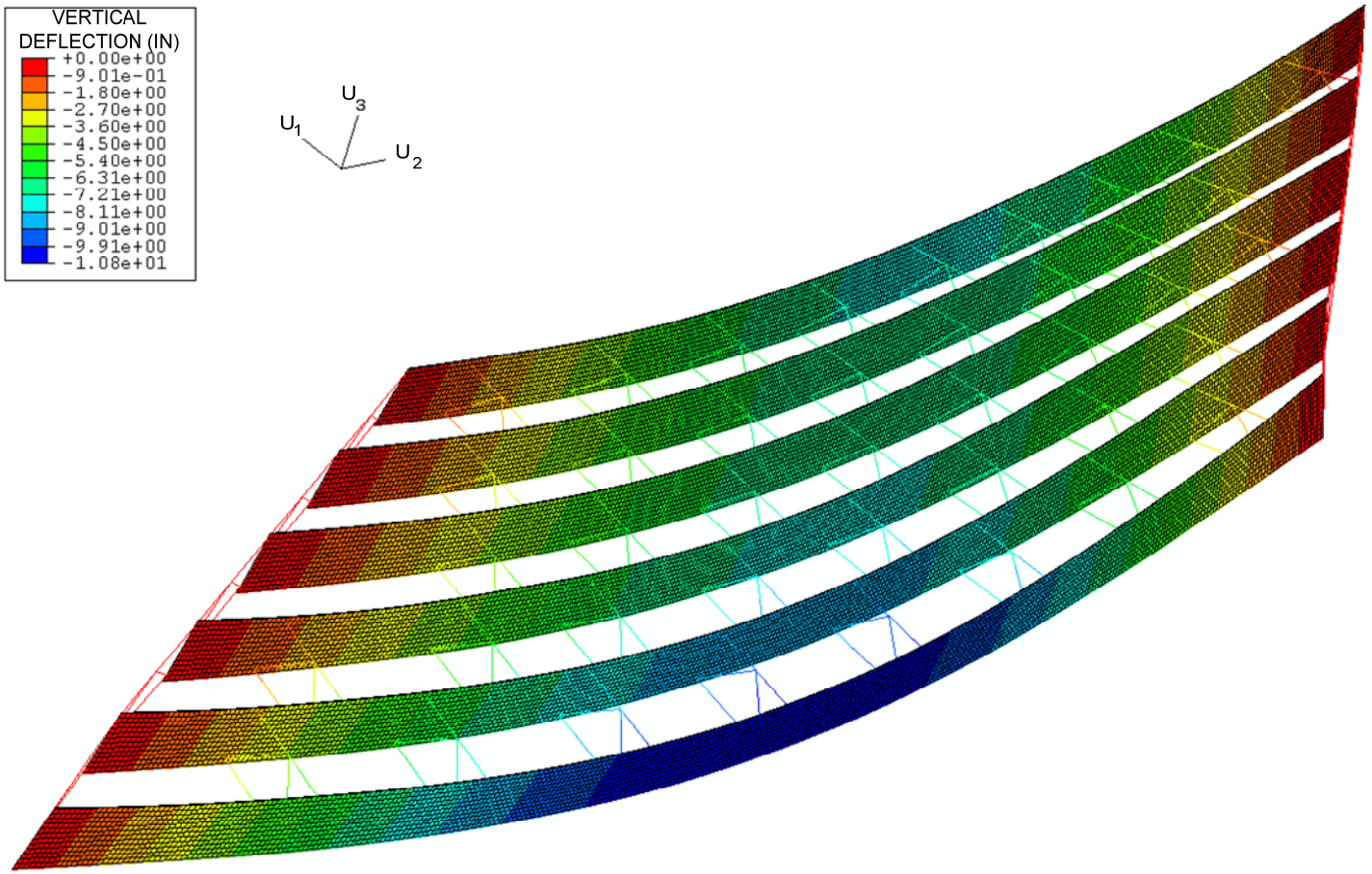

Figure 2.4.16. Noncomposite structure perspective view of deformed shape from geometric nonlinear analysis with load factor of 1.25 due to DC1 (displacements are amplified 10 times).

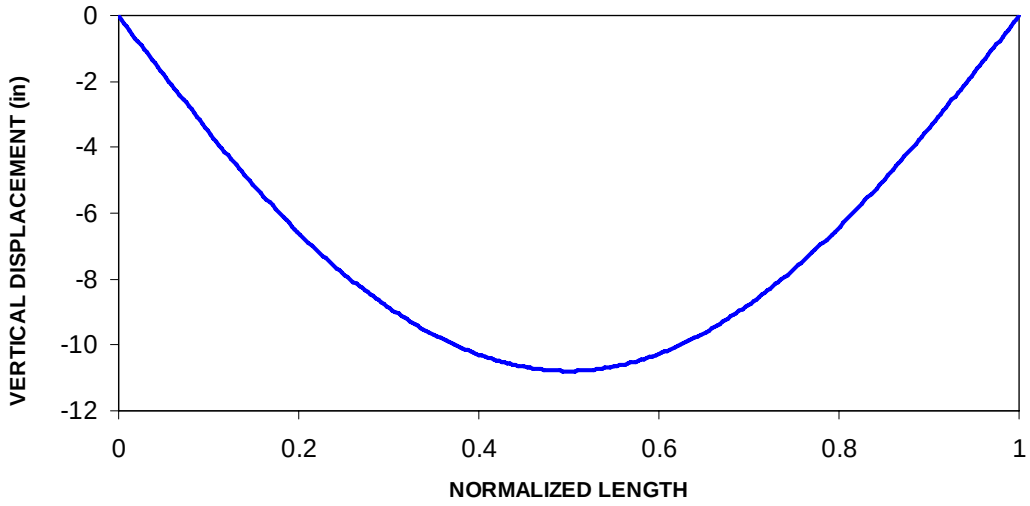

Figure 2.4.17. Vertical displacement along G1 from geometric nonlinear analysis due to DC1 (Load Factor =1.25).

Moreover, the web out-of-plumbness along the length of G1, G3 and G6 under 1.25 DC1 is shown in Figs. 2.4.18 through 2.4.20. These movements are caused by the skewed bearing lines and the horizontal curvature of the bridge. The cross-frames at the skewed bearing lines tend to rotate about their own skewed axis and warp (twist) out of their plane due to the girder rotations. Representative deflections at the top connection points of a skewed cross-frame to a bridge girder at a fixed bearing location are illustrated in Fig. 2.4.21. The skewed cross-frame forces a coupling between the major-axis bending rotation and the torsional rotation, since the in-plane cross-frame deformations tend to be small relative to the other displacements. The deflection at the bearing due to the major-axis bending rotation can be written from the geometry as

$$\Delta_z = d \times \phi_x \tag{2.4.1}$$

where, Δ_z is the deflection of the top flange at the bearing due to the major-axis bending rotation, ϕ_x is the girder major-axis bending end rotation in radians and d is the girder depth. Moreover, the layover of the girders at the skewed bearings can be calculated from the compatibility between the girder and cross-frames, assuming negligible cross-frame in-plane deformations, as

$$\Delta_x = \Delta_z \times Tan(\theta) \tag{2.4.2}$$

where, Δ_x is the layover, Δ_z is the deflection of the top flange at the bearing due to the major-axis bending rotation and θ is the skew angle of the considered bearing. Similarly, the twist angle or out-of-plumbness of the member at the cross-frame location can be obtained as

$$\phi_z = \phi_x \times Tan(\theta) \tag{2.4.3}$$

where, ϕ_x is the girder major-axis bending end rotation in radians, ϕ_z is the girder major-axis bending end rotation in radians.

In the case of non-fixed bearing, Eq. 2.4.2 gives the relative displacement of the top and bottom flanges. Similarly, Eq. 2.4.3 gives the relative angle of twist angle for top and bottom flanges.

Table 2.4.1 compares the twist angle and the layover of the outside girder from the above equations and the refined FEA under 1.25 DC1. It should be noted that the layover and twist angle predictions of the outside girder from Eqs. 2.4.2 and 2.4.3 are very close to the FEA results. The difference between results of the equations and FEA predictions is 1.27 % for the left bearing and 5.96 % for the right bearing. This difference is due to the cross-frame in-plane deflections.

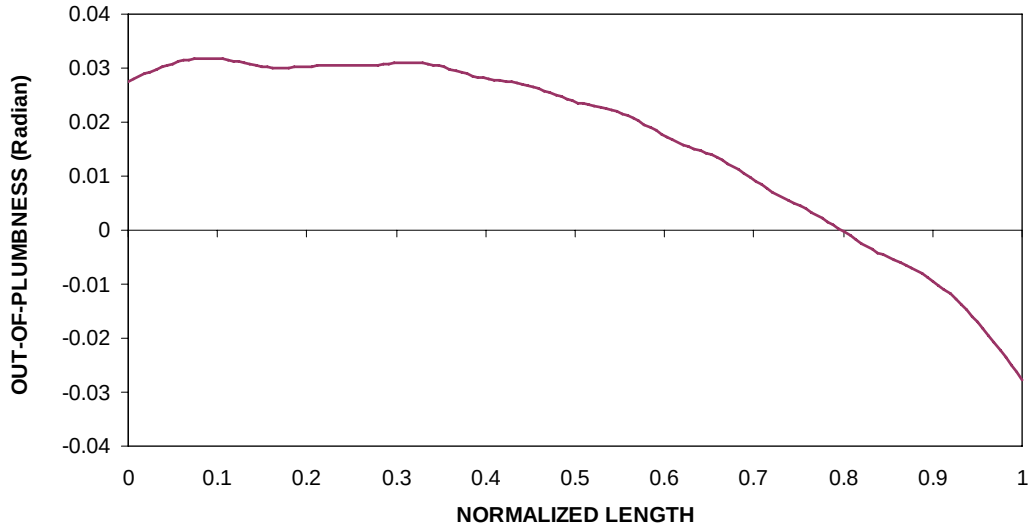

Figure 2.4.18. Web out-of-plumbness along the length of G1 from geometric nonlinear analysis due to DC1 (Load Factor =1.25).

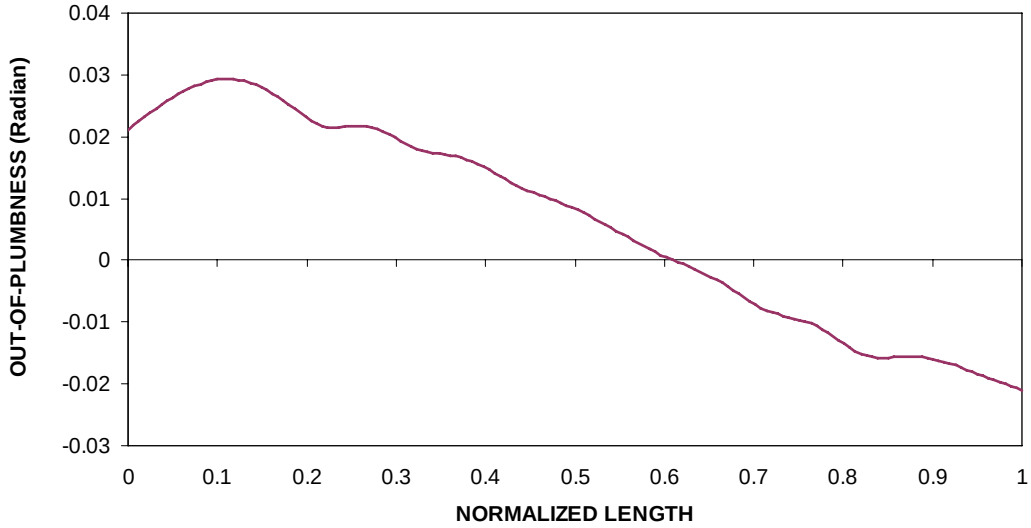

Figure 2.4.19. Web out-of-plumbness along the length of G3 from geometric nonlinear analysis due to DC1 (Load Factor =1.25).

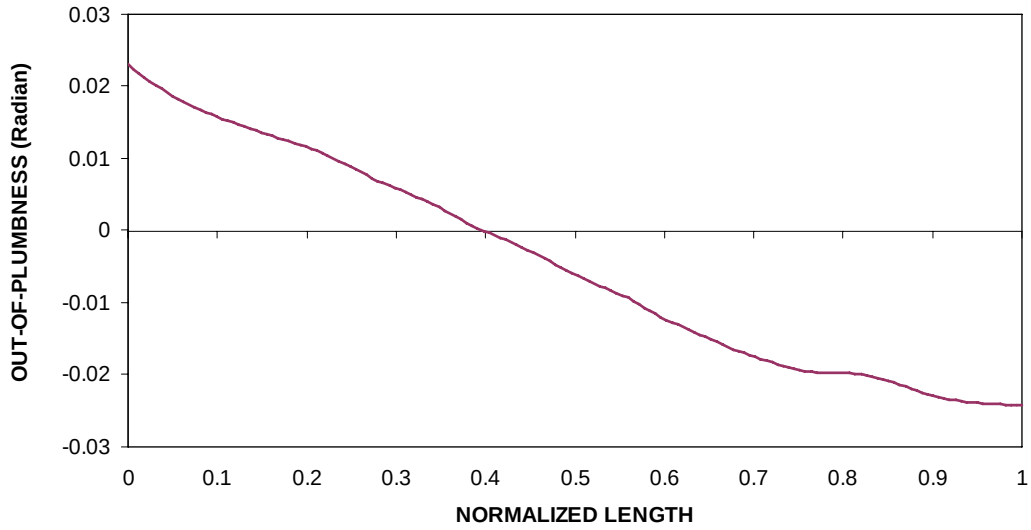

Figure 2.4.20. Web out-of-plumbness along the length of G6 from geometric nonlinear due to DC1 (Load Factor =1.25).

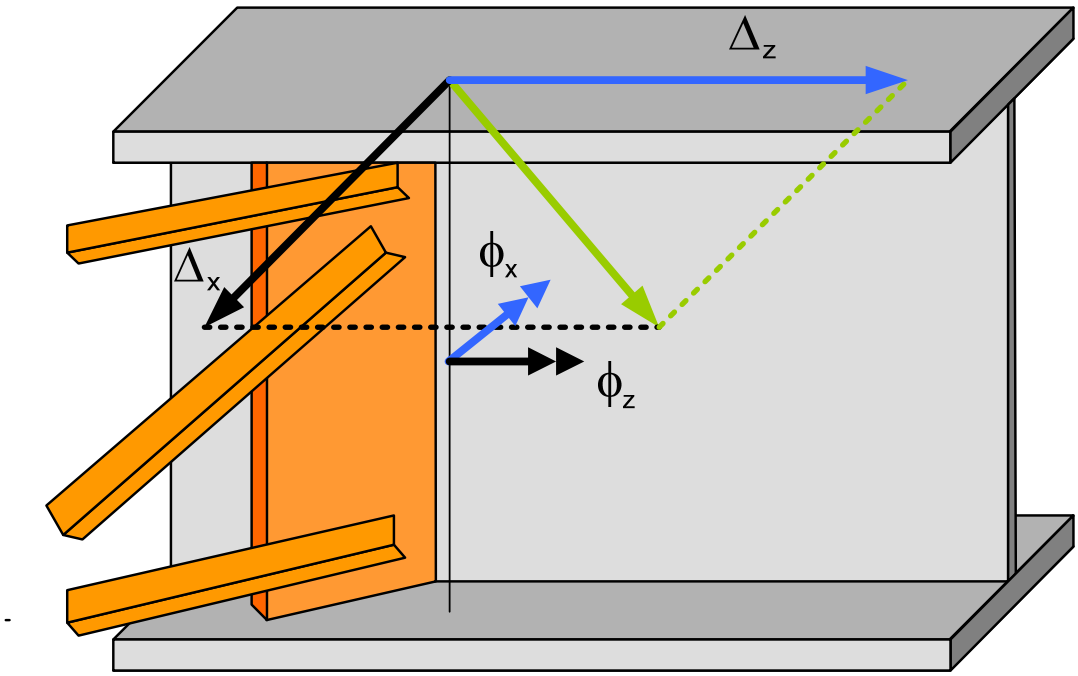

Figure 2.4.21. Deflections at the top connection points of a skewed cross-frame and a fixed bearing bridge girder, forcing a coupling between the major-axis bending and torsional rotation of the girders.

Table 2.4.1. Comparison of the web out-of-plumbness (ϕ_z) and the layover of the outside girder from the approximated equations and the refined FEA under 1.25DC1

	θ	ϕ_x	$\phi_{z\ (Approx.)}$	$\phi_{z\ (FEA)}$	% Diff.
Left Bearing	54.7	0.01917	0.0271	0.0274	-1.27
Right Bearing	58.2	-0.01825	-0.0294	-0.0277	5.96

	d_{FEA} (in)	$Layover_{(Approx.)}$	$Layover_{(FEA)}$	% Diff.
Left Bearing	74	2.003	2.029	-1.27
Right Bearing	74	-2.175	-2.053	5.96

2.4.2 Results of the Composite Dead Load Analysis (DC2 & DW)

Only the linear elastic analysis results are shown in this section since the influence of the geometric nonlinearity is insignificant after the bridge becomes composite. Figures 2.4.22 through 2.4.29 show the bottom flange stresses for G1, G3 and G6 due to DC2 under the STRENGTH I load combination. Additionally, Figs. 2.4.30 through 2.4.36 show the bottom flange stresses for G1, G3 and G6 due to DW under the STRENGTH I load combination. Also, the long term material properties are used in the elastic composite dead load analysis model.

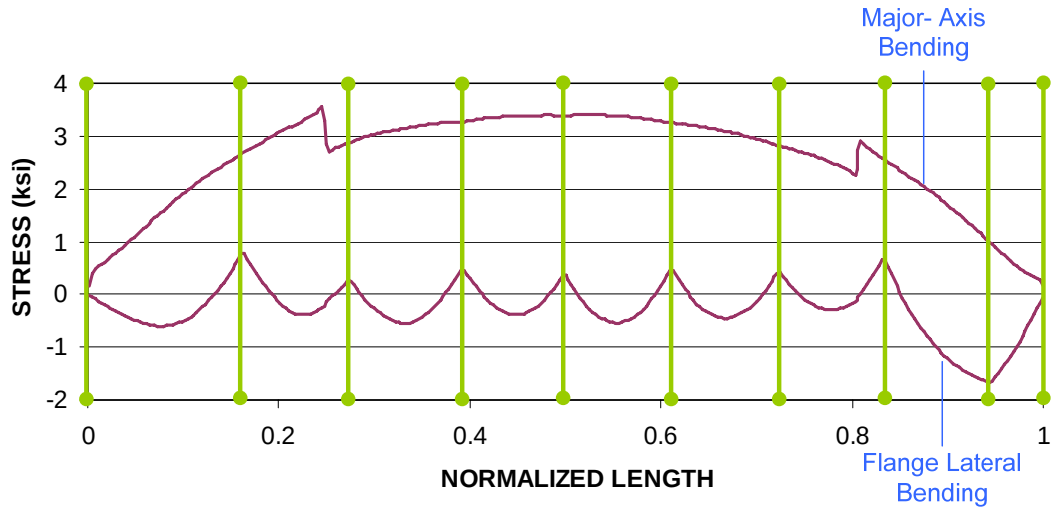

Figure 2.4.22. Bottom flange major-axis bending and flange lateral bending stresses along the length of G1 from linear elastic analysis due to DC2 (Load factor = 1.25).

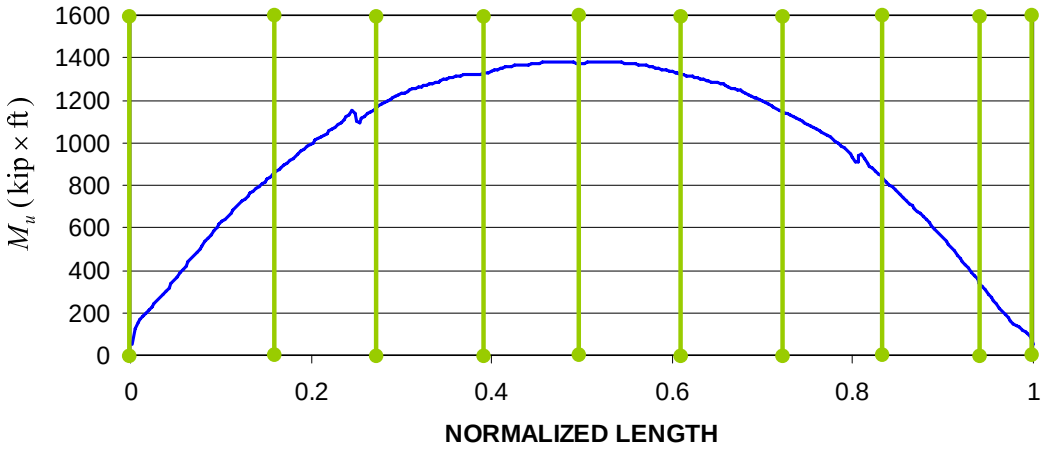

Figure 2.4.23. Major-axis bending moments along the length of G1 from linear elastic analysis due to DC2 (Load factor = 1.25).

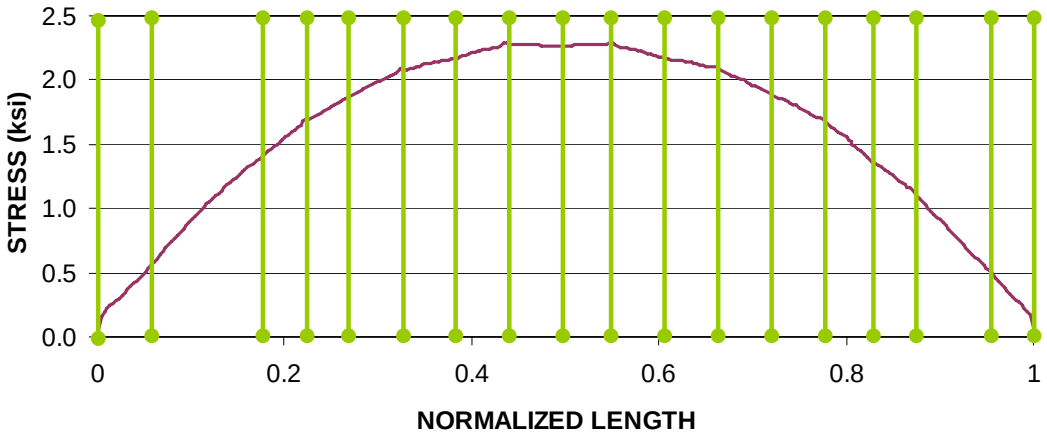

Figure 2.4.24. Bottom flange major-axis bending stresses along the length of G3 from linear elastic analysis due to DC2 (Load factor = 1.25).

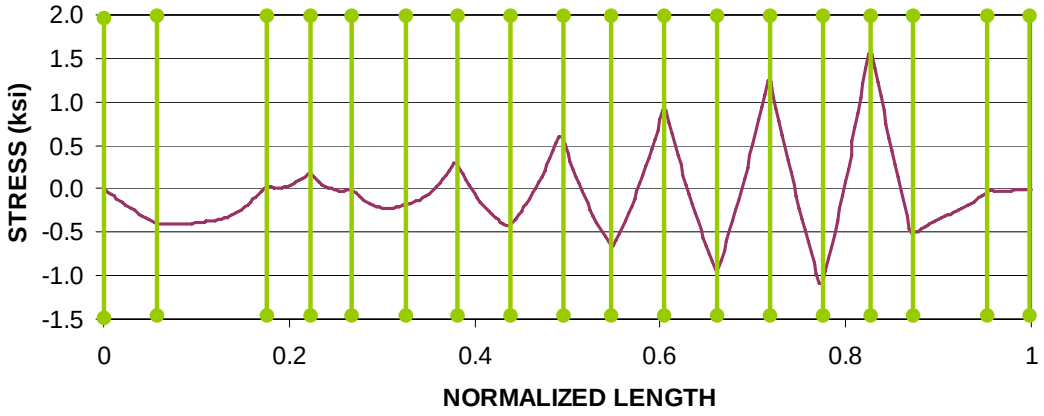

Figure 2.4.25. Bottom flange lateral bending stresses along the length of G3 from linear elastic analysis due to DC2 (Load factor = 1.25).

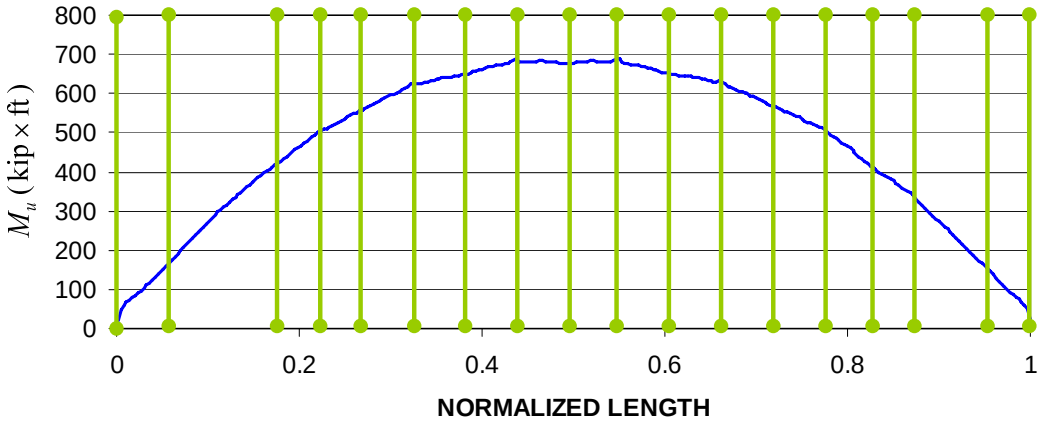

Figure 2.4.26. Major-axis bending moments along the length of G3 from linear elastic analysis due to DC2 (Load factor = 1.25).

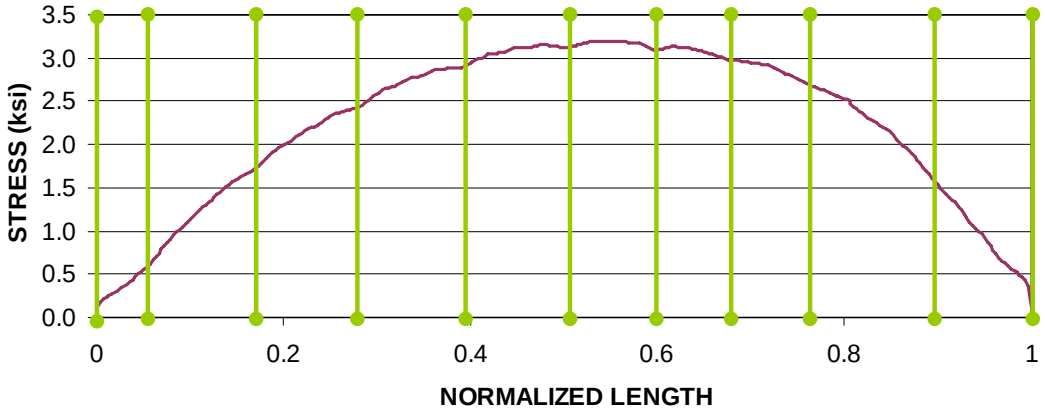

Figure 2.4.27. Bottom flange major-axis bending stresses along the length of G6 from linear elastic analysis due to DC2 (Load factor = 1.25).

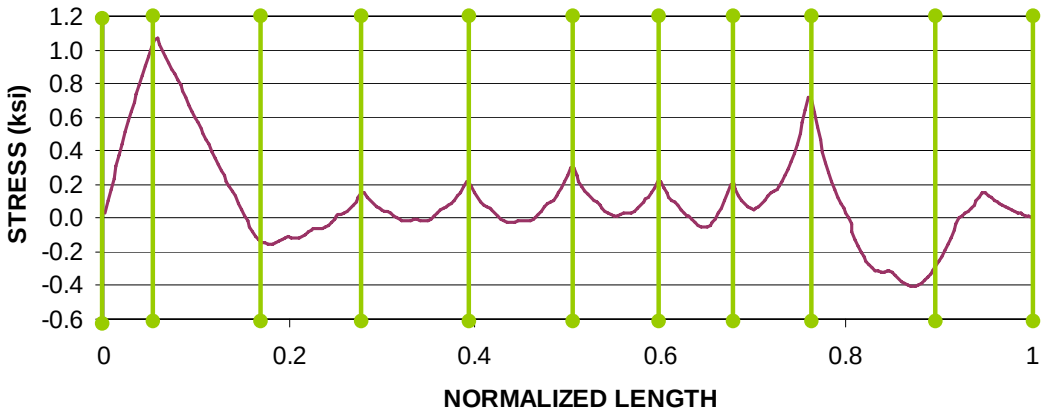

Figure 2.4.28. Bottom flange lateral bending stresses along the length of G6 from linear elastic analysis due to DC2 (Load factor = 1.25).

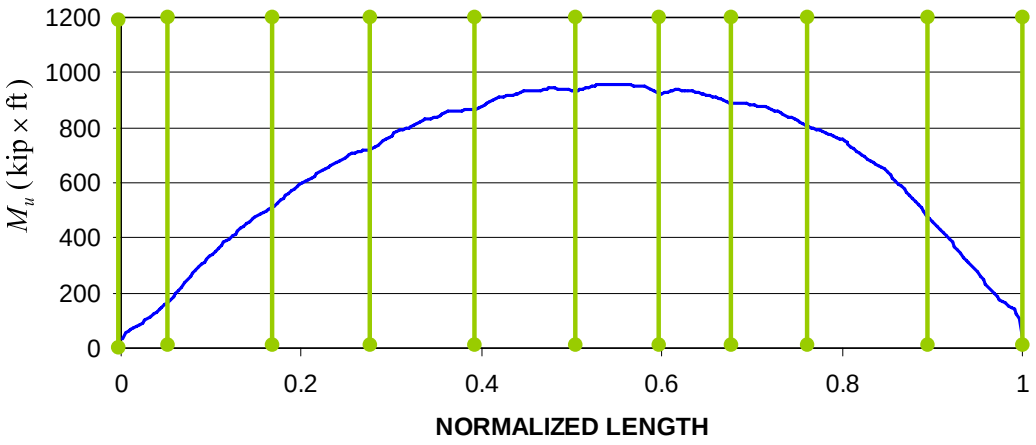

Figure 2.4.29. Major-axis bending moments along the length of G6 from linear elastic analysis due to DC2 (Load factor = 1.25).

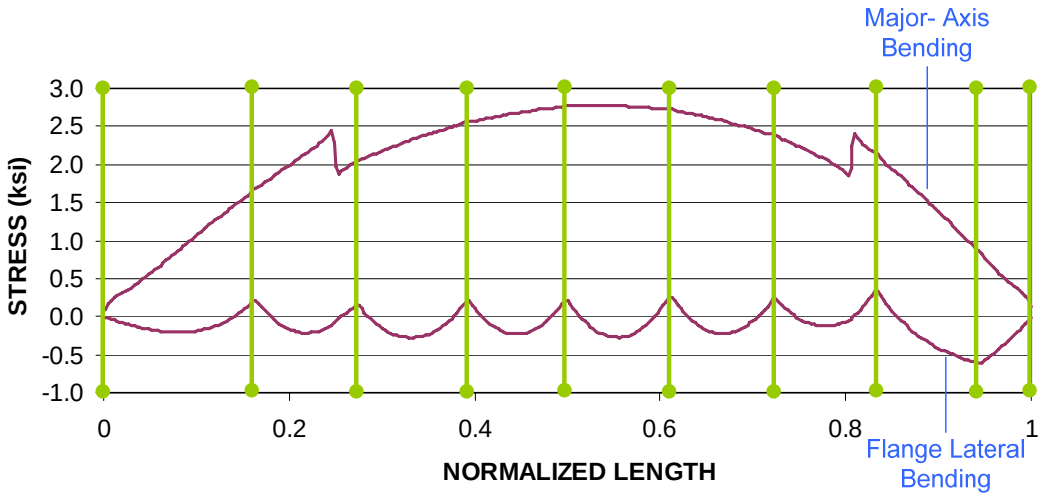

Figure 2.4.30. Bottom flange major-axis bending and flange lateral bending stresses along the length of G1from linear elastic analysis due to DW (Load factor = 1.5).

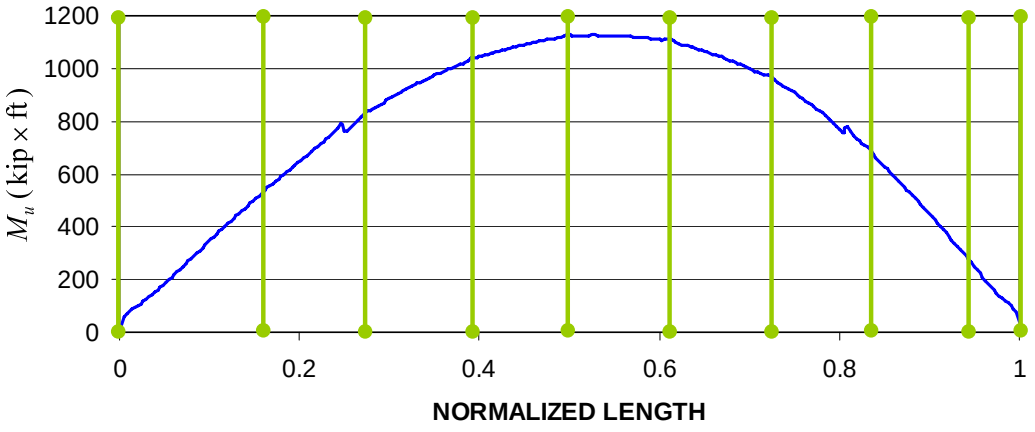

Figure 2.4.31. Major-axis bending moments along the length of G1 from linear elastic analysis due to DW (Load factor = 1.5).

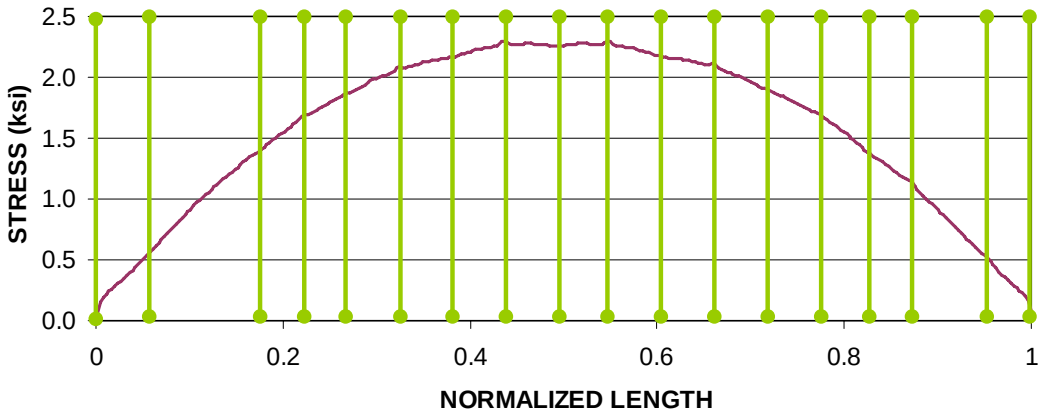

Figure 2.4.32. Bottom flange major-axis bending stresses along the length of G3 from linear elastic analysis due to DW (Load factor = 1.5).

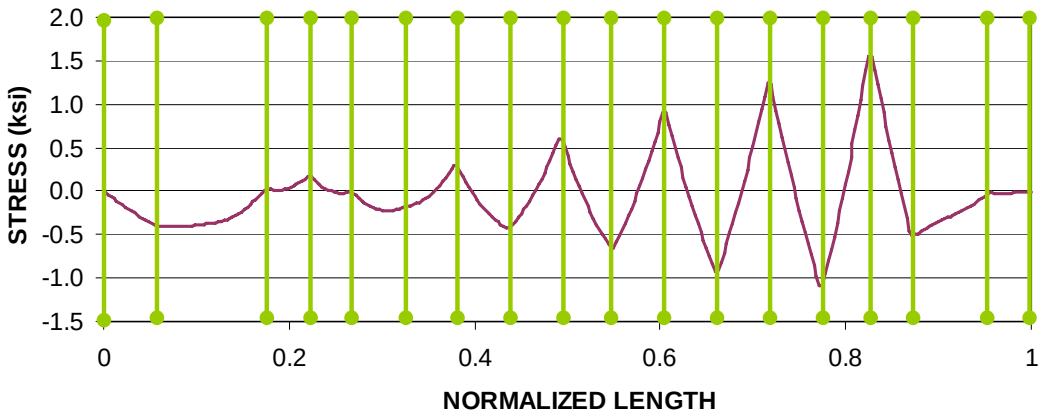

Figure 2.4.33. Bottom flange lateral bending stresses along the length of G3 from linear elastic analysis due to DW (Load factor = 1.5).

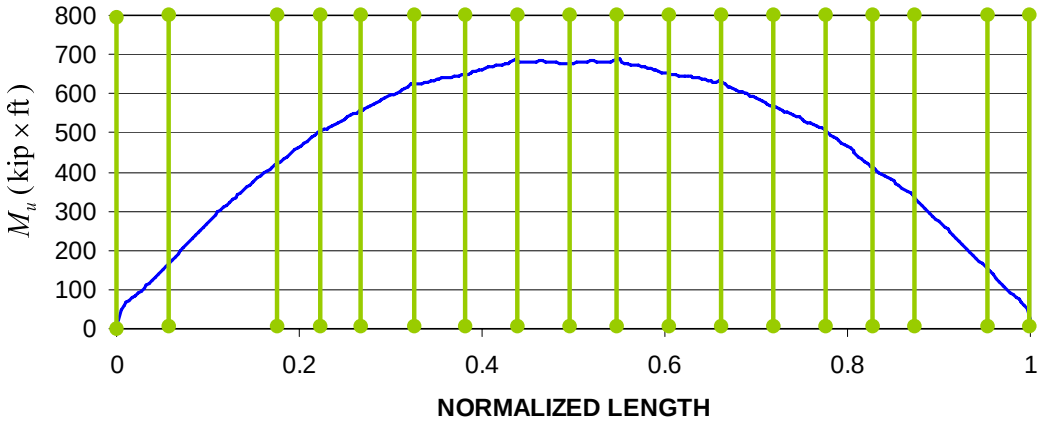

Figure 2.4.34. Major-axis bending moments along the length of G3 from linear elastic analysis due to DW (Load factor = 1.5).

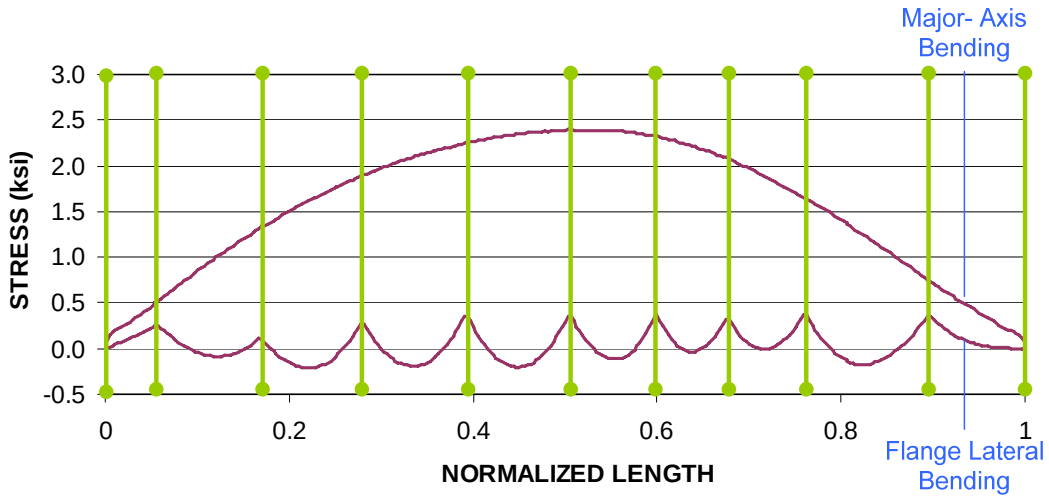

Figure 2.4.35. Bottom flange major-axis bending and flange lateral bending stresses along the length of G6 from linear elastic analysis due to DW (Load factor = 1.5).

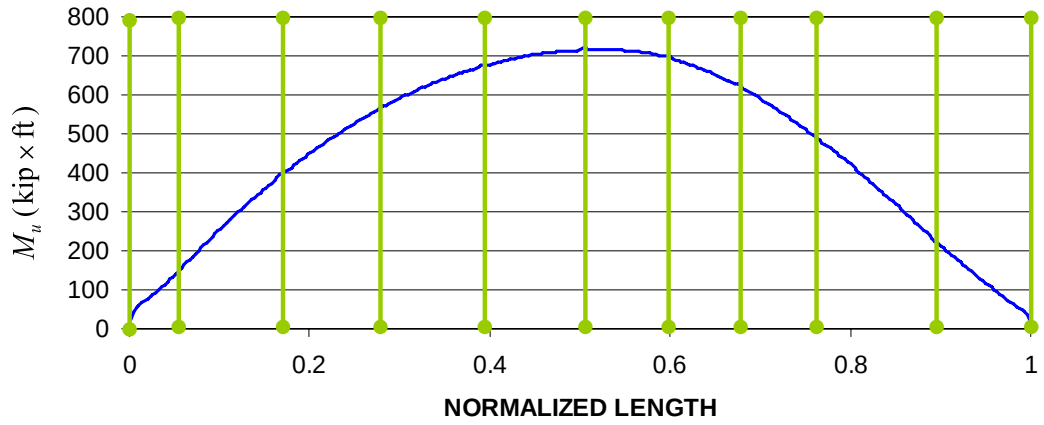

Figure 2.4.36. Major-axis bending moments along the length of G6 from linear elastic analysis due to DW (Load factor = 1.5).

2.4.3 Identification of the Critical Sections and LL Positions

Critical sections are determined by comparing the unity checks at various sections for the constructability, strength and service limit states under the STRENGTH IV and STRENGTH I load combinations defined in AASHTO (2007). Unity checks are the ratios of the demand computed from the analysis to the capacity for any given limit state. Two critical sections for each of G1, G3 and G6 are identified for the constructability limit states under 1.5 DC1. One has the maximum strength unity check and other has the maximum lateral bending stress. The critical sections for the constructability under the STRENGTH IV load combination are presented and labeled in Fig. 2.4.37. Section G1-S2 on G1, G3-S2 on G3 and G6-S2 on G6 have the maximum strength unity check on these girders under the STRENGTH IV load combination. Separated critical sections are

identified as G1-S1 on G1, G6-S1 on G6 for strength limit state check on the completed structure. Also, section G1-S3 on G1, G3-S1 on G3 and G6-S3 on G6 have the maximum lateral bending stress on these girders under the STRENGTH IV load combination.

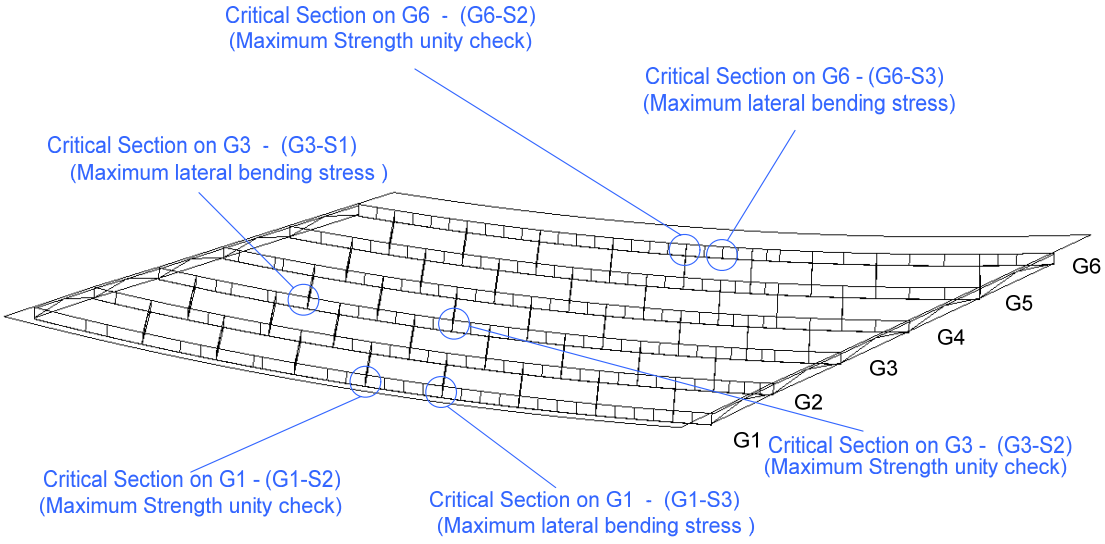

Figure 2.4.37. Critical sections for checking constructability limit states under STRENGTH IV load combination (1.5 DC1).

Furthermore, one critical section for each of G1, G3 and G6 is identified for the strength limit state under the STRENGTH I load combination on the completed structure. For G1 and G6, these critical sections correspond to the maximum strength unity checks. The vehicular live load configurations are determined to maximize these unity checks. However, for G3, the critical section is defined as the location that has the largest flange lateral bending stress (f_ℓ) under the STRENGTH I load combination. In this case, the vehicular live loads are configured to maximize this largest f_ℓ value. This section is selected for G3 because the above f_ℓ is the largest flange lateral bending stress throughout

the bridge. The critical sections for the strength limit state under the STRENGTH I load combination are presented and labeled in Fig. 2.4.38.

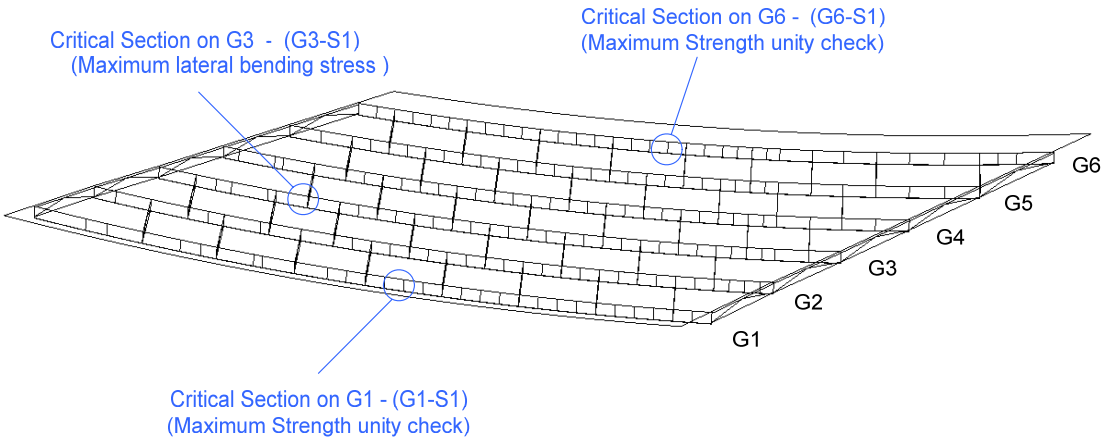

Figure 2.4.38. Considered critical sections and their notations (STRENGTH I load level)

Key parameters for describing the location of a representative applied design truck loading positioned in the i^{th} lane are illustrated in Fig. 2.4.39.The term d_{1i} represents the radial distance between the first wheel of the design truck and the outside edge of the lane. The first wheel is the one closest the outside edge of the lane that is also closest to the left bearing line. The distance d_{2i} is the radial distance of the first wheel on the outside edge of the lane measured from the left bearing line.

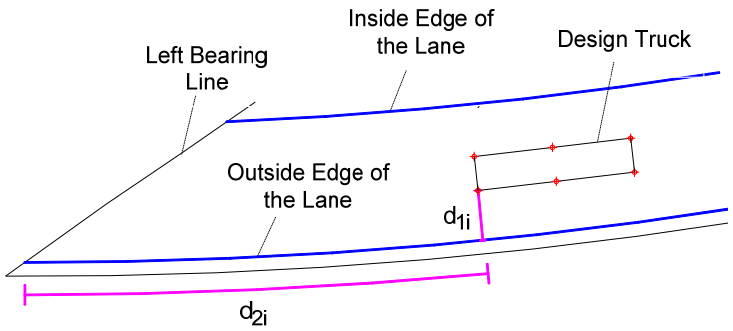

Figure 2.4.39. Key parameters for describing the location of the applied design truck loading

Figures 2.4.40 and 2.4.41 show the applied vehicular design load configuration that gives the maximum strength unity check on G1 at G1-S1 under the STRENGTH I load combination. Figures 2.4.42 and 2.4.43 show the applied vehicular design load configuration that gives the maximum flange lateral bending stress on G3 at G3-S1 under the STRENGTH I load combination. Figures 2.4.44 and 2.4.45 show the applied vehicular design load configuration that gives the maximum strength unity check on G6 at G6-S1 under the STRENGTH I load combination.

One aim of this study is to investigate the influence of combining the maximum values of the major-axis bending or flange lateral bending with the corresponding concurrent ones or combining the maximums when designing the girders. Therefore, different vehicular live load positions are also determined to obtain the maximum flange lateral bending values for G1 at G1-S1 and for G6 at G6-S1 and the maximum major-axis bending values for G3 at G3-S1.

Moreover, after preliminary study of the maximum axial forces of the cross-frames, several cross-frames are chosen for understanding the overall behavior of the bridge. These cross-frames are shown and labeled in Fig. 2.4.46. After further study with the maximum axial load values of the cross-frames under the STRENGTH I load

combination, CF-107 was found to have the largest diagonal force and CF-203 was found to have the largest force in the bottom chord among the selected cross-frames for the STRENGTH I load combination. Thus, CF-107 and CF-203 are selected for illustration of the cross-frame member design checks and strength behavior. The maximum axial load values for the selected cross-frames under the STRENGTH I load combination can be seen in Figs. 2.4.47 and 2.4.48. Figures 2.4.49 and 2.4.50 show the applied vehicular design load configuration that causes the largest axial force on the critical diagonal of CF-107. Figures 2.4.51 and 2.4.52 show the applied vehicular design load configuration that produces the largest axial force on the critical bottom chord of CF-203.

In summary, different live load configurations are identified to obtain the maximum with concurrent or both maximums of the major-axis bending and flange lateral bending values under the STRENGTH I load combination for G1, G3 and G6 at sections G1-S1, G3-S1 and G6-S1. Moreover, different live load configurations are identified to obtain the maximum axial force effects on the diagonal of CF107 and bottom chord of CF-203. Again, only linear elastic analyses results are considered for the composite bridge since the influence of the geometric nonlinearity is insignificant on the composite structure. Figures 2.4.53 through 2.4.55 show contour plots of the vertical deflections on the bridge due to live load for obtaining the maximum strength unity check on G1 and G6, and the maximum flange lateral bending stress limit unity check on G3 under the STRENGTH I load combination. Detailed stress and moment results for the critical sections are tabulated in the next section.

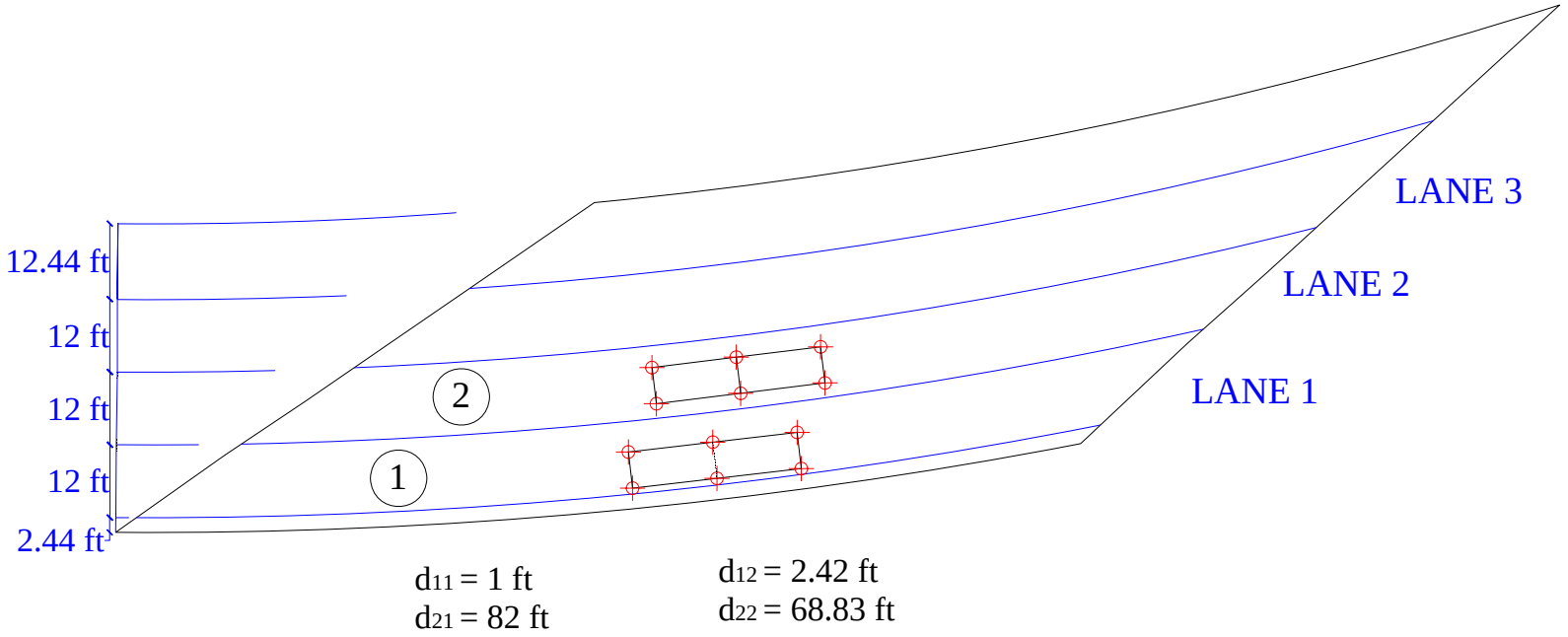

Figure 2.4.40. Critical design truck loading to obtain the maximum strength unity check on G1 at G1-S1.

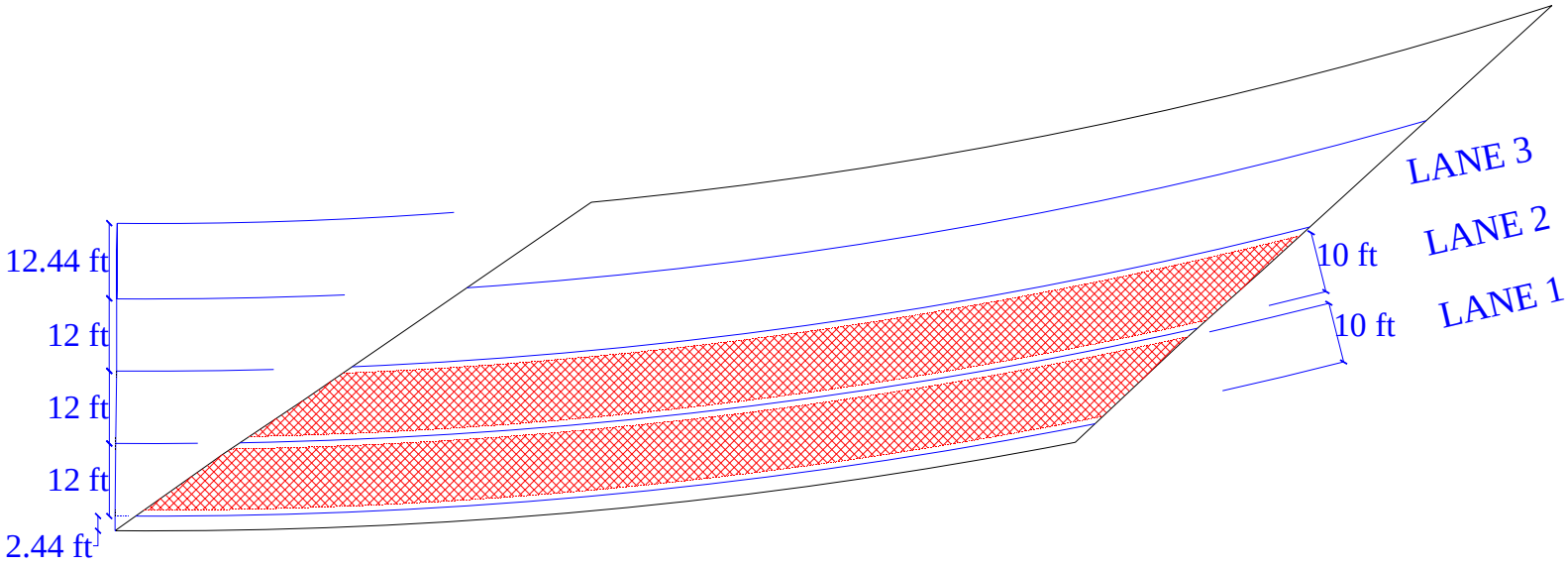

Figure 2.4.41. Critical design lane loading to obtain the maximum strength unity check on G1 at G1-S1

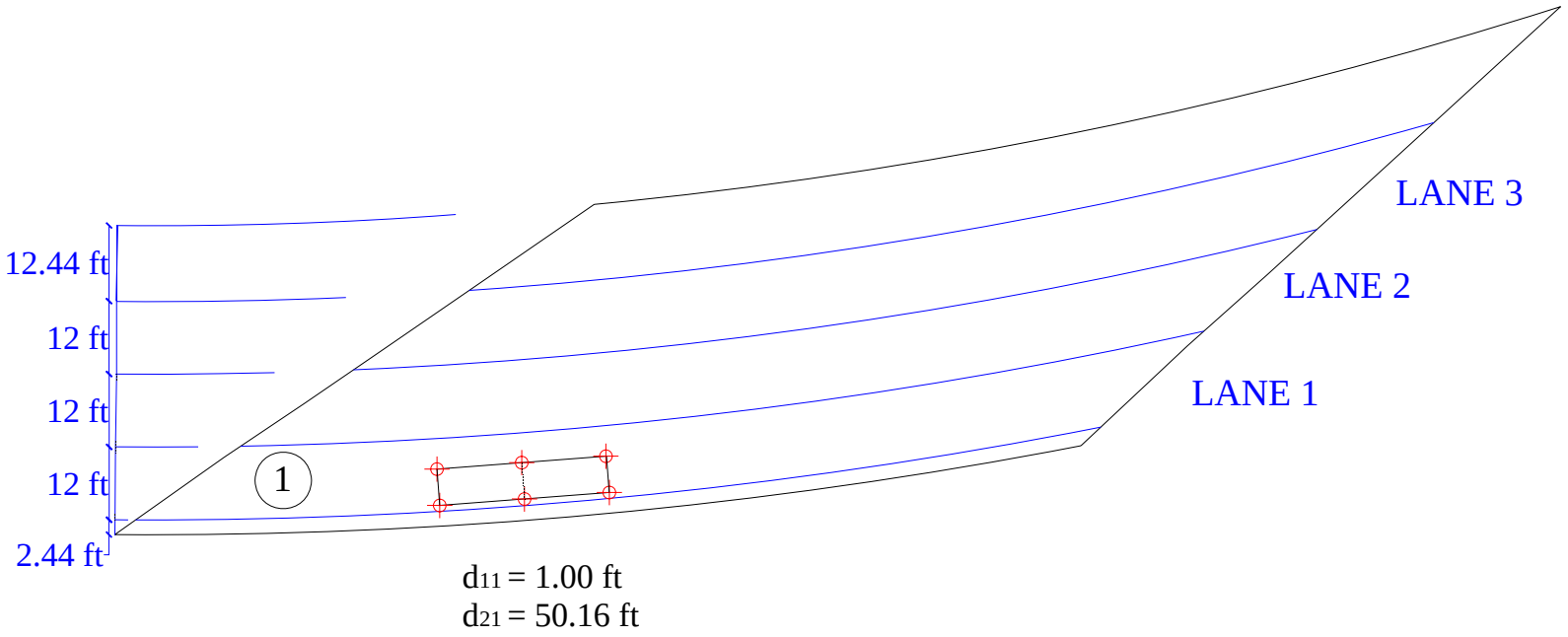

Figure 2.4.42. Critical design truck loading to obtain the maximum flange lateral bending stress limit unity check on G3 at G3-S1.

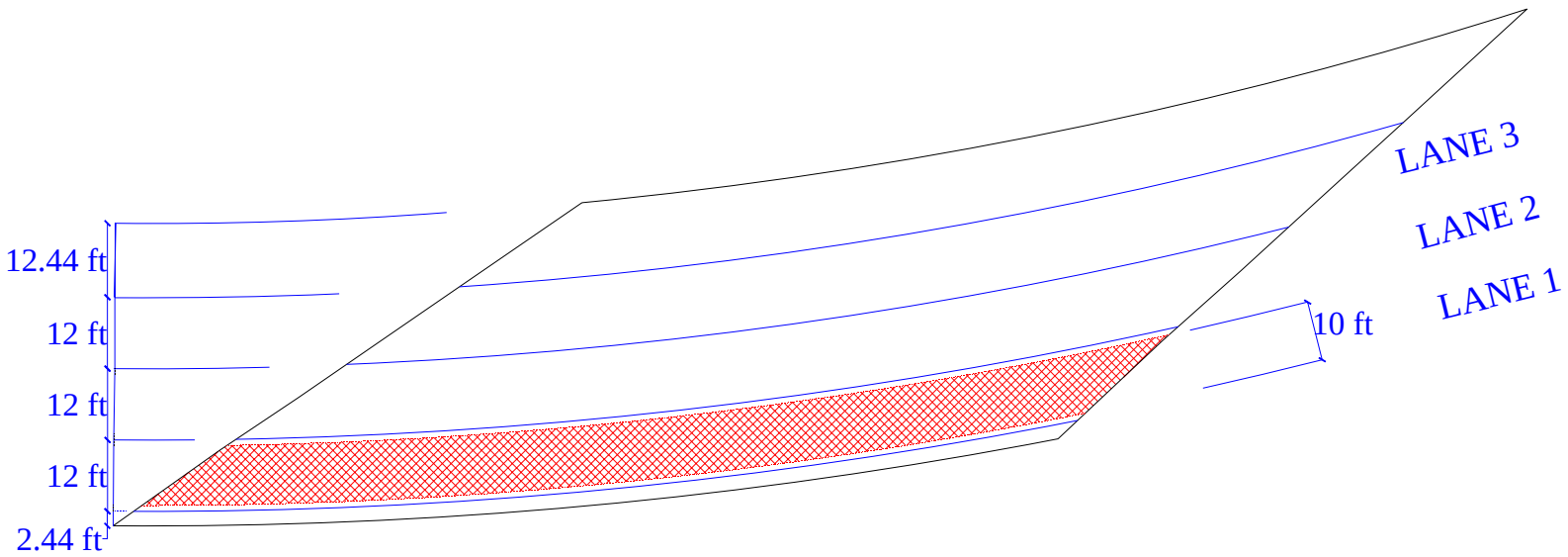

Figure 2.4.43. Critical design lane loading to obtain the maximum flange lateral bending stress limit unity check on G3 at G3-S1.

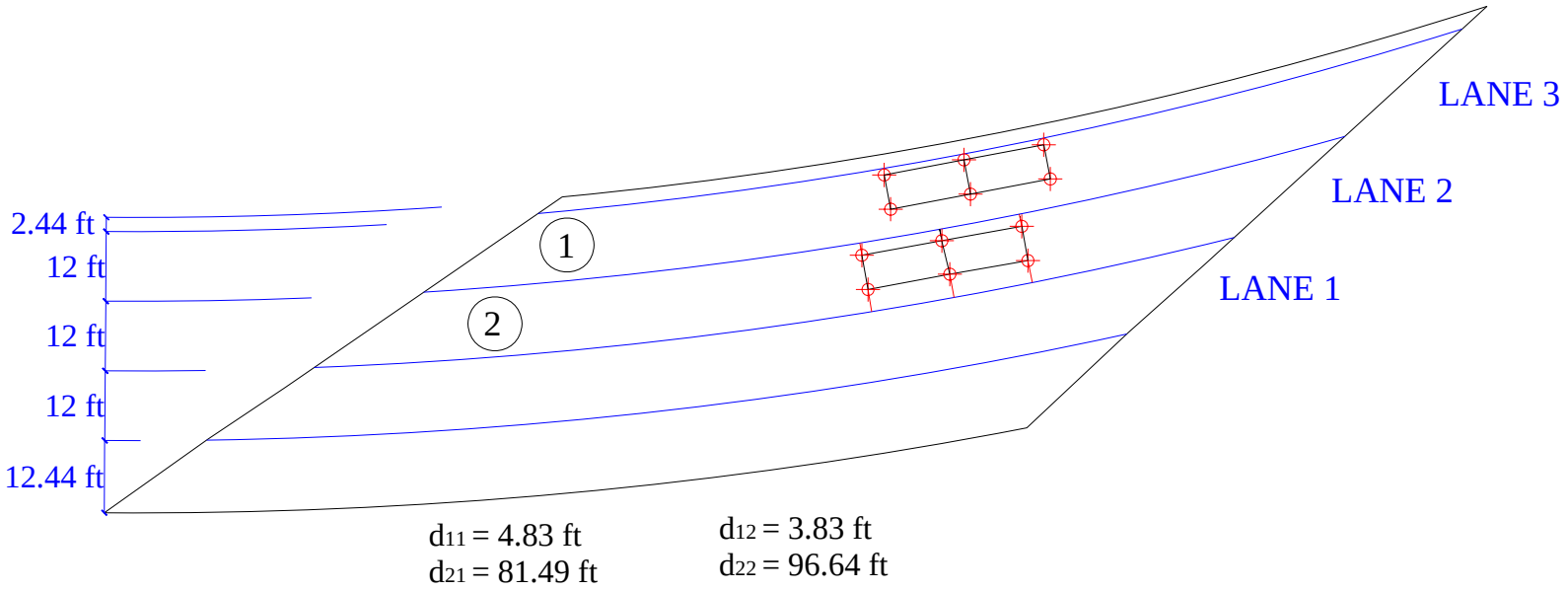

Figure 2.4.44. Critical design truck loading to obtain the maximum strength unity check on G6 at G6-S1.

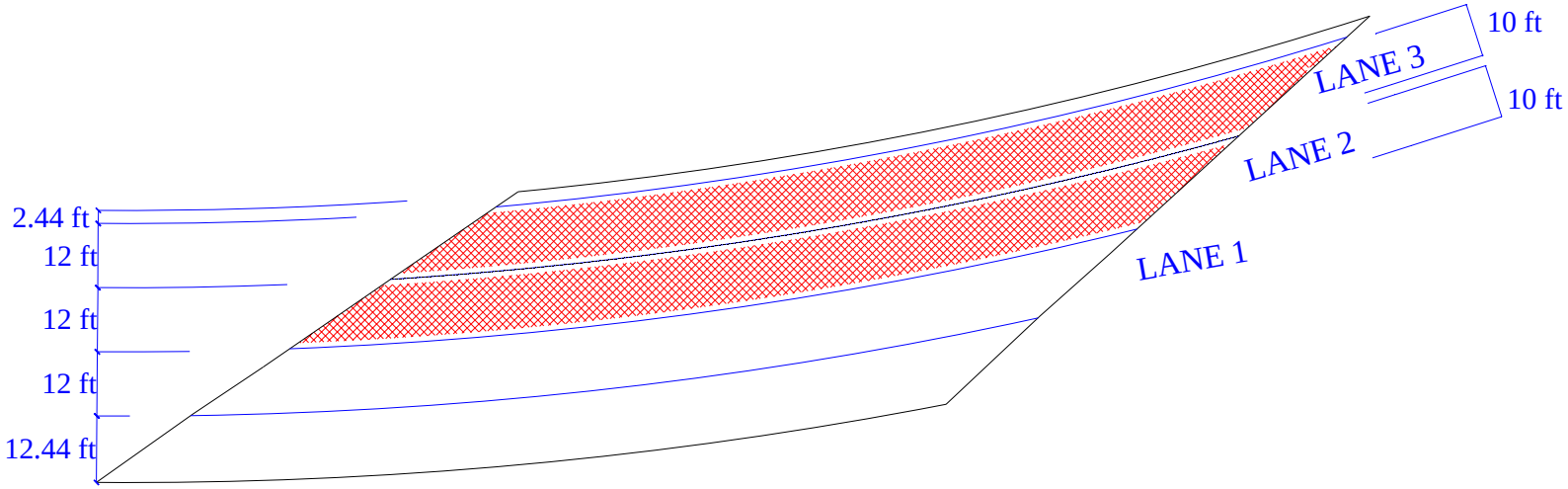

Figure 2.4.45. Critical design lane loading to obtain the maximum strength unity check on G6 at G6-S1.

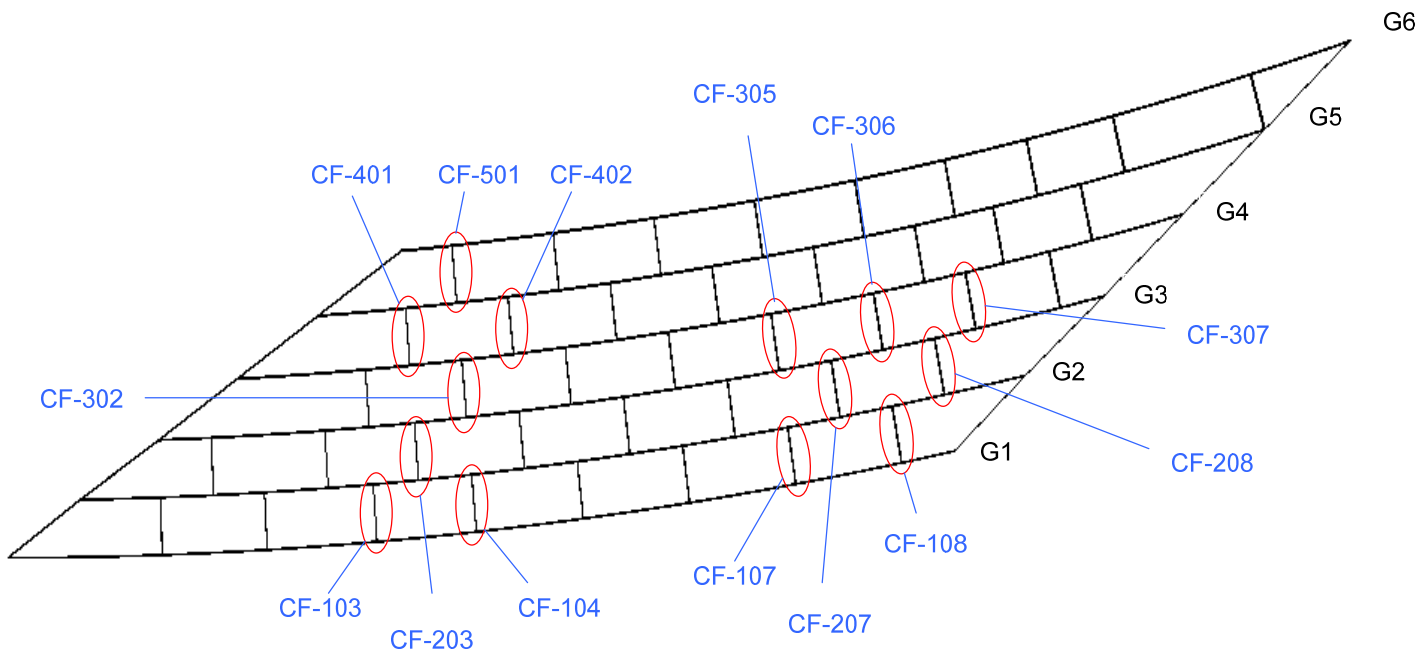

Figure 2.4.46. Selected cross-frames and their notations.

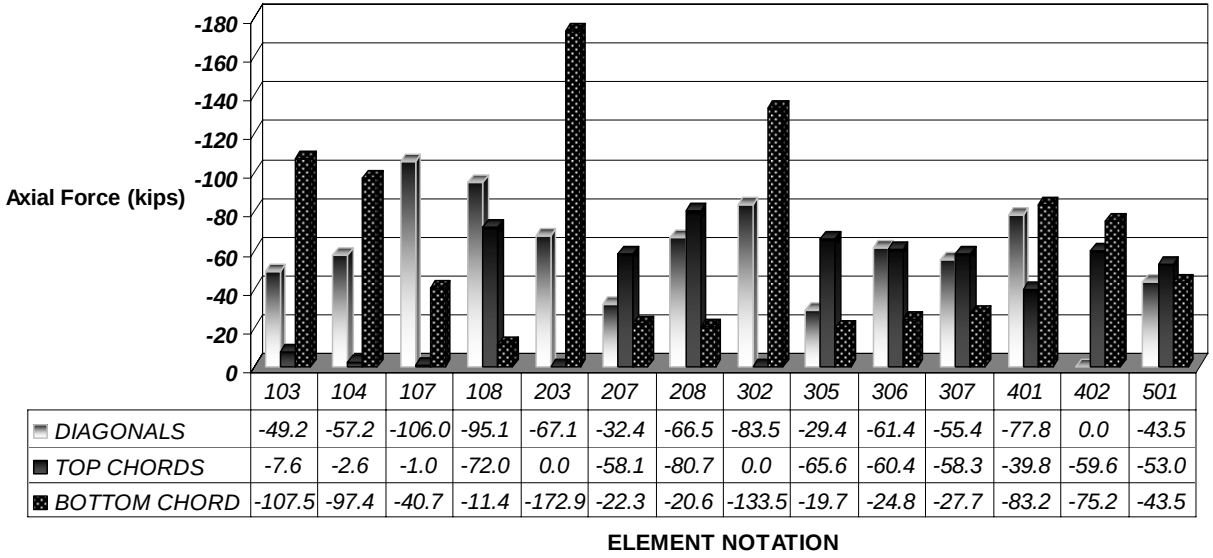

	103	104	107	108	203	207	208	302	305	306	307	401	402	501
DIAGONALS	-49.2	-57.2	-106.0	-95.1	-67.1	-32.4	-66.5	-83.5	-29.4	-61.4	-55.4	-77.8	0.0	-43.5
TOP CHORDS	-7.6	-2.6	-1.0	-72.0	0.0	-58.1	-80.7	0.0	-65.6	-60.4	-58.3	-39.8	-59.6	-53.0
BOTTOM CHORD	-107.5	-97.4	-40.7	-11.4	-172.9	-22.3	-20.6	-133.5	-19.7	-24.8	-27.7	-83.2	-75.2	-43.5

Figure 2.4.47. Maximum compression axial load values for selected cross-frames under the STRENGTH I load combination.

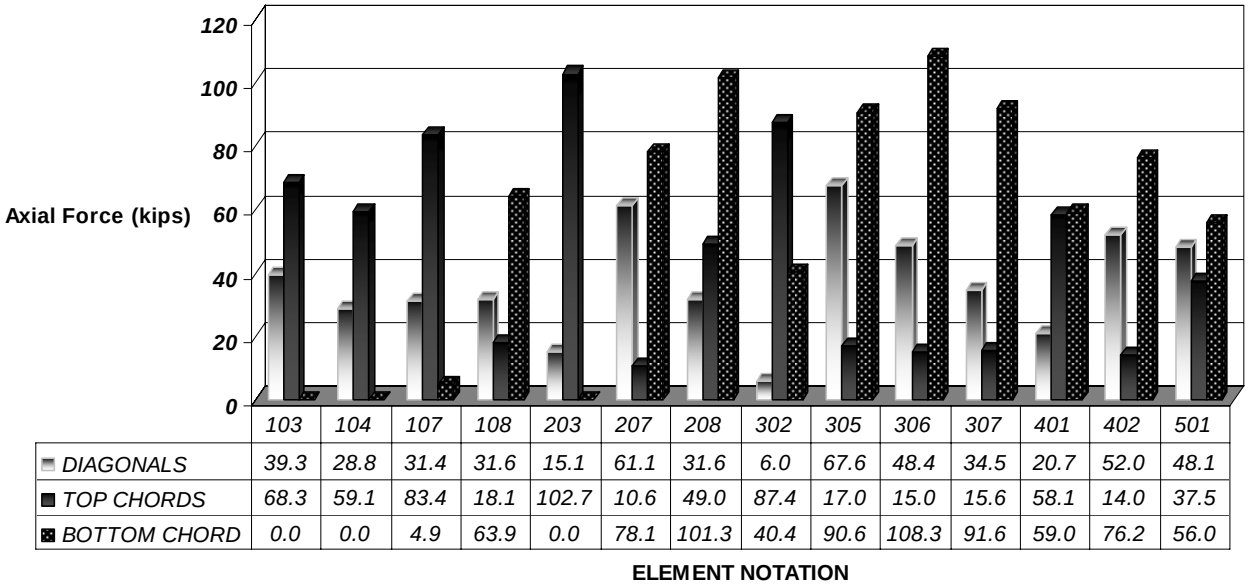

	103	104	107	108	203	207	208	302	305	306	307	401	402	501
DIAGONALS	39.3	28.8	31.4	31.6	15.1	61.1	31.6	6.0	67.6	48.4	34.5	20.7	52.0	48.1
TOP CHORDS	68.3	59.1	83.4	18.1	102.7	10.6	49.0	87.4	17.0	15.0	15.6	58.1	14.0	37.5
BOTTOM CHORD	0.0	0.0	4.9	63.9	0.0	78.1	101.3	40.4	90.6	108.3	91.6	59.0	76.2	56.0

Figure 2.4.48. Maximum tension axial load values for selected cross-frames under the STRENGTH I load combination.

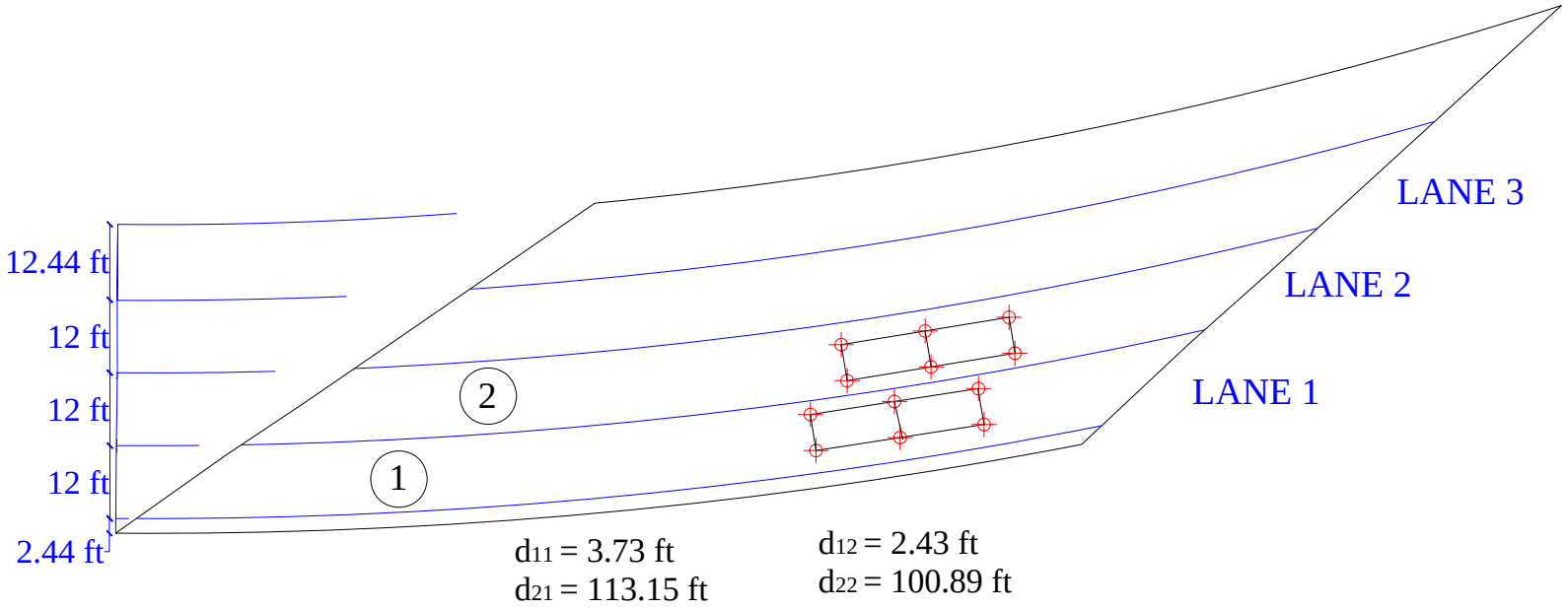

Figure 2.4.49. Critical design truck loading for critical diagonal member of CF107.

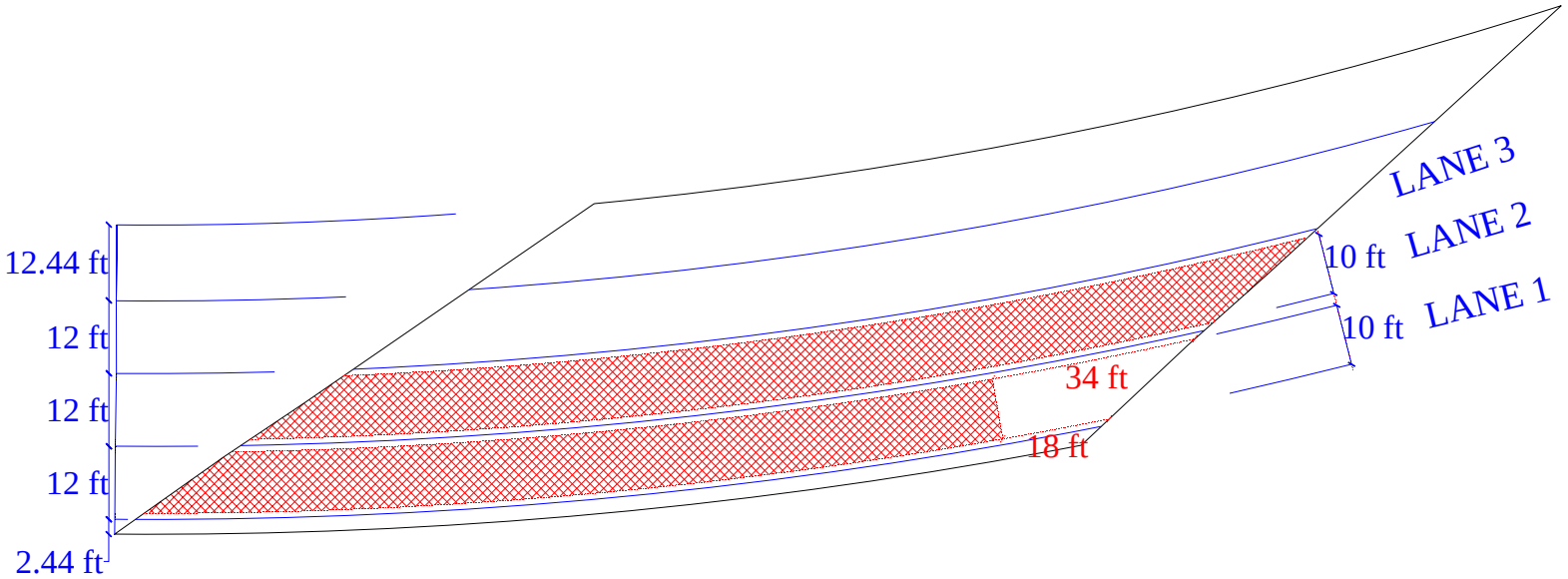

Figure 2.4.50. Critical design lane loading for critical diagonal member of CF107.

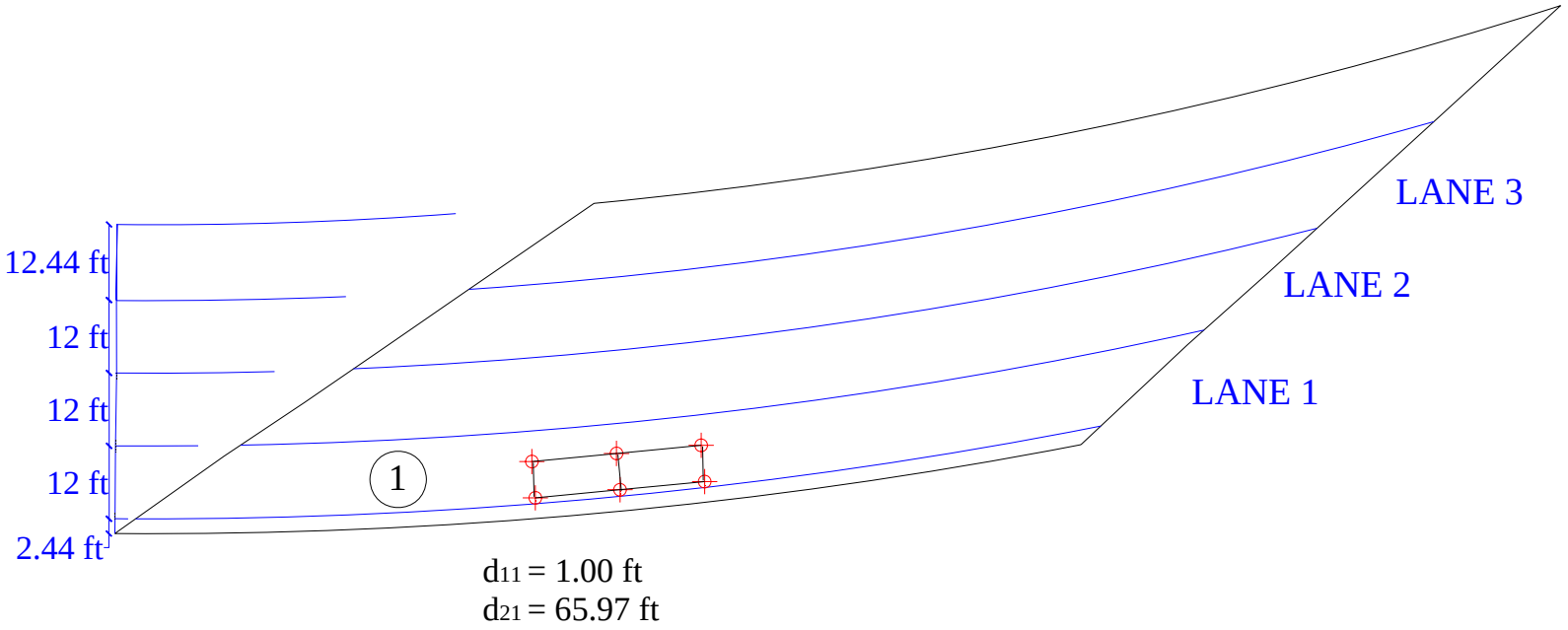

Figure 2.4.51. Critical design truck loading for critical bottom chord of CF203.

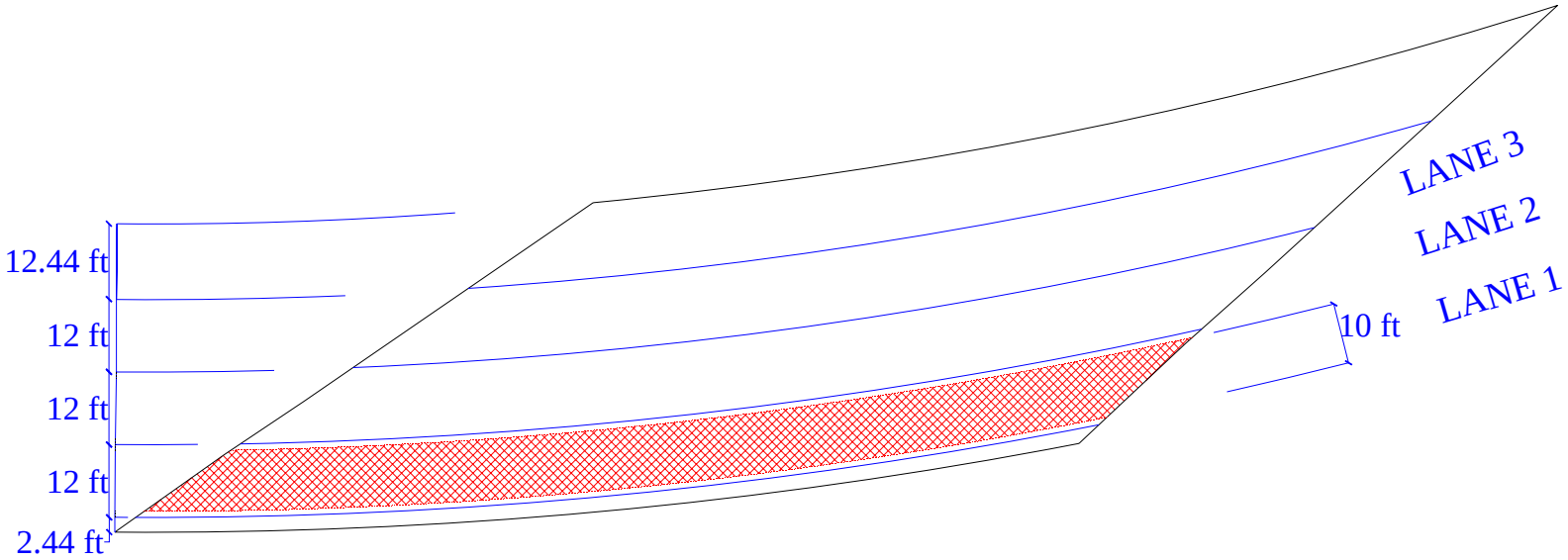

Figure 2.4.52. Critical design lane loading for critical bottom chord of CF203.

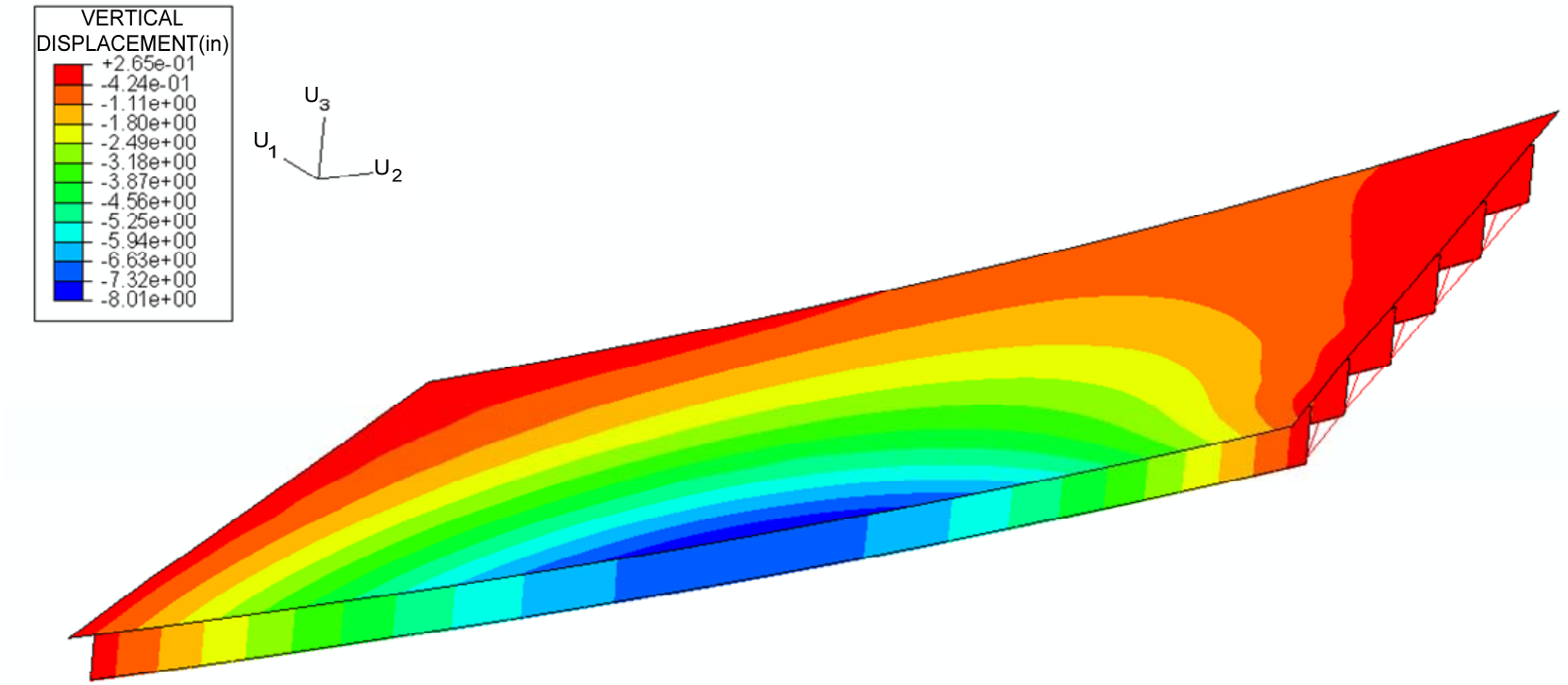

Figure 2.4.53. Perspective view of contour plot of vertical deflections due to live load causing the maximum strength unity check on G1 (Load factor =1.75).

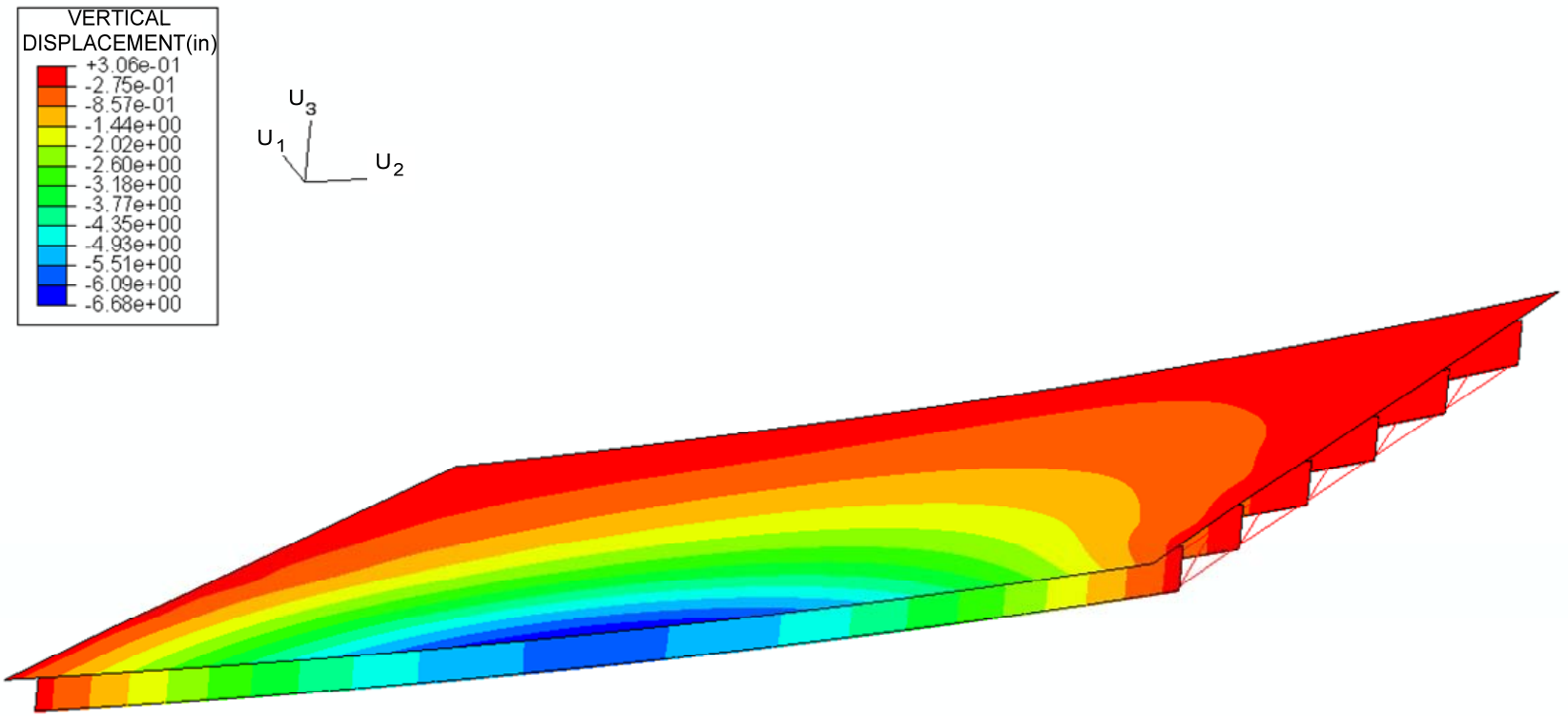

Figure 2.4.54. Perspective view of contour plot of vertical deflections due to live load causing the maximum flange lateral bending stress limit unity check on G3 (Load factor =1.75).

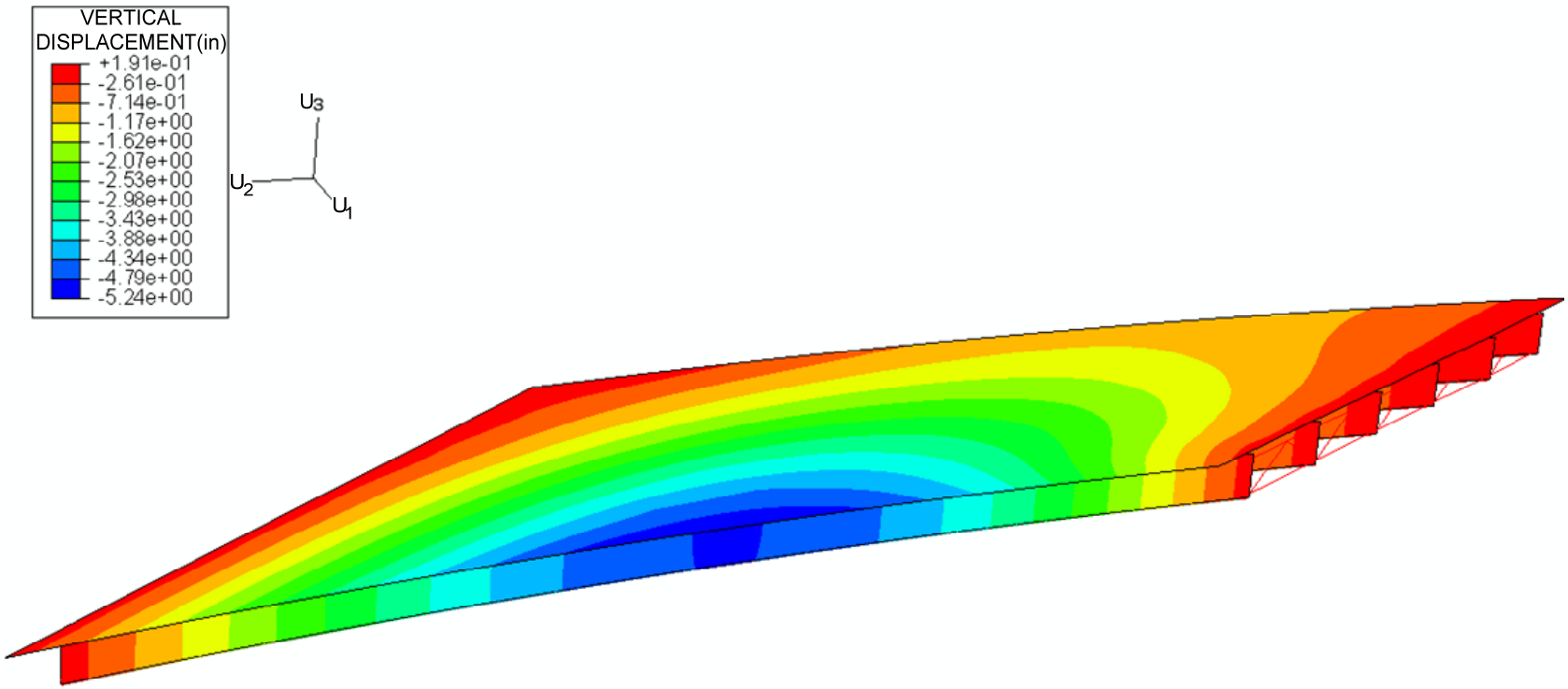

Figure 2.4.55. Perspective view of contour plot of vertical deflections due to live load causing the maximum strength unity check on G6 (Load factor =1.75).

2.4.4 Summary of Elastic Analysis Results

The factored noncomposite construction load analysis results used for checking the constructability are listed in Table 2.4.2 for sections G1-S2, G1-S3, G3-S1, G3-S2, G6-S2 and G6-S3. Both the top and bottom flange stress results are tabulated under STRENGTH VI load combination (1.5 DC1). Also, Table 2.4.3 presents the elastic analysis results used for checking the strength limit state at sections G1-S1, G3-S1 and G6-S1 under STRENGTH I load combination. It should be noted that the long term material properties are used in the elastic composite dead load analysis model whereas the short term material properties are used in the elastic live load analysis model. The results in Table 2.4.3 include only the maximum bottom flange stresses and the corresponding section moments. Furthermore, the live load results include the maximum major-axis bending with concurrent flange lateral bending values as well as both maximums for the critical sections on G1 and G6. In addition, the maximum flange lateral bending with the concurrent major-axis bending response and with both maximums are reported for the critical section on G3. Table 2.4.4 summarizes the axial force results due to the STRENGTH I load combination for CF-107 and CF-203.

To sum up, the results from Table 2.4.2 illustrate the results for the constructability limit states under the STRENGTH IV load combination. Table 2.4.3 illustrates the results for the strength limit states under the STRENGTH I load combination. Table 2.4.4 illustrates the results for the cross-frame members.

Table 2.4.2. Factored noncomposite construction load analysis results for checking constructability limit states under STRENGTH IV load combination (1.5 DC1).

Load Case & Analysis Type	Top Flange	Section	f_b (ksi)	f_ℓ (ksi)	L_b (ft)	Maximum f_ℓ within L_b
1.5 DC1 - Linear Elastic	G1	G1-S2	-36.15	-4.91	18.02	-5.56
		G1-S3	-35.34	-5.56	18.02	-5.56
	G3	G3-S2	-25.18	-3.63	8.82	3.63
		G3-S3	-17.92	-11.52	7.58	11.52
		G6-S2	-27.03	-2.36	15.39	-2.36
	G6	G6-S3	-26.87	1.71	15.39	-2.36
1.5 DC1 - Geometric Nonlinear	G1	G1-S2	-37.16	-1.26	18.02	10.03
		G1-S3	-36.18	-3.13	18.02	10.03
	G3	G3-S2	-25.53	-1.48	8.82	3.5
		G3-S1	-18.14	-11.07	7.58	15.11
		G6-S2	-27.5	-7.77	15.39	-7.85
	G6	G6-S3	-27.38	-4.73	15.39	-7.85
Load Case & Analysis Type	Bottom Flange	Section	f_b (ksi)	f_ℓ (ksi)		
1.5 DC1 - Geometric Nonlinear	G1	G1-S2	29.51	8.48		
		G1-S3	28.74	7.65		
	G3	G3-S2	22.04	6.85		
		G3-S1	15.66	12.52		
		G6-S2	24.12	-3.47		
	G6	G6-S3	24.19	-6.14		

** *Positive sign of f_ℓ indicates bending in the opposite direction of the horizontal curvature of the girders.*

Table 2.4.3. Elastic analysis results for checking strength limit state under STRENGTH I load combination.

Load Case & Anlaysis Type	Section	f_b (ksi)	f_ℓ (ksi)	M_u (kip x ft)
1.25 DC1 - Geometric Nonlinear	G1-S1	24.27	0.85	8739
	G3-S1	13.05	9.66	3350
	G6-S1	19.80	-3.36	5084
DC2 - Linear Elastic	G1-S1	1.85	-0.18	750
	G3-S1	1.12	0.11	335
	G6-S1	1.58	-0.03	474
DW - Linear Elastic	G1-S1	2.71	-0.41	1101
	G3-S1	1.18	3.28	354
	G6-S1	2.53	0.07	757
LL - Linear Elastic	G1-S1-1	15.46	-1.94	6823
	G1-S1-2	15.46	-1.99	6823
	G3-S1-1	4.89	15.91	1610
	G3-S1-2	8.69	15.91	2861
	G6-S1-1	13.53	2.47	4455
	G6-S1-2	13.53	2.58	4455

*** *G1-S1-1, G6-S1-1 indicates results for maximum major axis bending with concurrent lateral bending*
G1-S1-2, G6-S1-2 indicates results for maximum major axis bending with maximum lateral bending
G3-S1-1 indicates results for maximum lateral bending with concurrent major axis bending
G3-S1-2 indicates results for maximum lateral bending with maximum major axis bending

Table 2.4.4. Member axial forces resulting from factored loadings for CF-107 and CF-203 under STRENGTH I load combination.

		AXIAL FORCE (KIPS)			
Cross-Frame	Member	1.25DC1 - 2nd ORDER	1.25DC2 - 1st ORDER	1.5DW - 1st ORDER	1.75LL - 1st ORDER
CF-107	Bottom Chord	-9.2	-8.4	0.5	16.5
	Diagonal	-34.1	3.0	-5.2	-69.7
	Top Chord	33.0	-6.1	3.9	52.6
CF-203	Bottom Chord	-42.8	-21.1	-1.0	-108.1
	Diagonal	23.4	1.4	2.9	-20.0
	Top Chord	59.5	-2.8	2.2	-32.6

Cross-Frame	Member	Σ Axial Force (kips)
CF-107	Bottom Chord	-0.6
	Diagonal	-106
	Top Chord	83.4
CF-203	Bottom Chord	-172.9
	Diagonal	7.7
	Top Chord	26.3

2.5 Bridge Component Design

As mentioned earlier, the bridge is checked for the constructability, strength and service limit states. AASHTO (2007) is used for checking these limit states. In this section, the unity check results are discussed for the critical sections on G1, G3 and G6 and for the critical cross-frame members in CF-107 and CF-203. Detailed flexural design check calculations for G1 including the determination of the lateral torsional buckling capacity based on the buckling of the overall structural system and special handling of the critical cross-frame compression members are illustrated at Appendix A. The top flanges are the most critical part of the girders for the constructability checks under the STRENGTH IV load combination. In addition the bottom flanges are the most critical part of the girders for the strength limit state checks under the STRENGTH I load combination. Therefore, only the top flange design checks for the constructability and the bottom flange design check results for the strength limit state are summarized in the following sections. Additionally, the influence of combining the maximum major-axis bending with concurrent lateral bending results and with maximums of both are considered in the strength and service limit state checks for G1 and G6. Similarly, the influence of combining the maximum lateral bending with concurrent major-axis bending results and maximums of both are considered for G3 in the strength and service limit state checks.

2.5.1 Girder Flexural Design

Table 2.5.1 summarizes the results for the constructability limit states under the STRENGTH IV load combination. Since the deck is not considered in the noncomposite structure, the top flanges of the girders are critical. As can be seen from the table, all the critical sections satisfy the design requirements for the constructability limit states. Additionally, Table 2.5.1 presents the ratio of the second-order to first-order stress values determined from the FEA solutions. Table 2.5.1 also includes the second-order amplifiers defined in AASHTO (2007). It is clear that the AASHTO amplification factors are not capturing the system behavior. This is due to the complex interactions between the girders in the three-dimensional bridge structural system. The AASHTO amplification factors are based only on the characteristics of the unbraced lengths between the cross-frame locations. Therefore, only the second-order analysis results are used for the noncomposite structure stresses in the subsequent checks.

Table 2.5.2 presents the unity checks for the strength limit state under the STRENGTH I load combination. Unity checks are conducted for the bottom flanges of G1-S1, G3-S1 and G6-S1. Both Eqs. 2.1 and 2.2 are considered. In addition, the change in the strength ratio is calculated to assess the effect of using Eq. 2.2 for the subject bridge. Moreover, unity checks are conducted for G1-S1 and G6-S1 to address the influence of combining the maximum major-axis bending with concurrent flange lateral bending values and combining both maximums. Likewise, unity checks are done for G3-S1 to investigate the influence of combining the maximum flange lateral bending with concurrent bending values and combining both maximums. It is observed that there is little penalty associated with combining both maximums for this bridge. However,

section G3-S1 does not have the maximum strength unity check on G3. Therefore, further observations on the sections that has the maximum strength unity check on G3 show that combining both maximums make small difference with respect to combining the maximum flange lateral bending values with concurrent maximum major-axis bending value in the unity checks. As a result, no extra effort is needed, other than bookkeeping, to determine the maximum with their concurrent value for each of the major-axis bending and flange lateral bending from different live load positions for the considered section.

The strength ratio for outside girder (G1-S1) is 1.17 when the stress-based flexural resistance equations are considered. It is close to unity when the moment-based flexural resistance equations are used. Although the strength ratio is satisfied, the flange lateral bending stress limit is exceeded by approximately 40 % at G3-S1. Table 2.5.3 summarizes the unity checks for service limit state under the SERVICE II load combination. Sections G1-S1, G3-S1 and G6-S1 are checked for the service limit state under SERVICE II load combination. SERVICE II in all cases are smaller than the STRENGTH unity checks.

Table 2.5.1. Unity checks for constructability under STRENGTH IV load combination.

Load Combination	Section		AASHTO (2004) 2nd Order Amplifier	Actual 2nd Order Amplifier (2nd/1st)	Design Unity Checks: Stress Limit (f_ℓ / 0.6F_y)	Design Unity Checks: Yielding (f_b+f_ℓ) / $\phi_f F_y$	Design Unity Checks: Strength (f_b+(1/3) f_ℓ) / $\phi_f F_n$
STRENGTH IV	G1-S2	Top Flange	1.158	0.257	0.042	0.768	0.891
	G1-S3		1.149	0.563	0.104	0.786	0.870
	G3-S1		1	0.961	0.369	0.584	0.464
	G3-S2		1	0.408	0.049	0.540	0.534
	G6-S2		1.007	3.292	0.259	0.705	0.647
	G6-S3		1.006	2.766	0.158	0.642	0.645

Table 2.5.2. Unity checks for strength limit state under STRENGTH I load combination.

Load Combination	Section		Design Unity Checks: Stress Limit (f_ℓ / 0.6F_y)	Design Unity Checks: Strength [f_b+(1/3) f_ℓ] / $\phi_f F_n$	Design Unity Checks: Strength [M_u+(1/3) f_ℓ S_{xt}] / $\phi_f M_n$	Ratio of Strengths
STRENGTH I	G1-S1-1	Bottom Flange	0.111	1.172	1.038	1.149
	G1-S1-2		0.114	1.172	1.038	1.150
	G3-S1-1		1.392	0.774	0.596	1.335
	G3-S1-2		1.392	0.907	0.710	1.335
	G6-S1-1		0.033	0.987	0.767	1.288
	G6-S1-2		0.040	0.988	0.768	1.288

*** *G1-S1-1, G6-S1-1 indicates results for maximum major axis bending with concurrent lateral bending*
G1-S1-2, G6-S1-2 indicates results for maximum major axis bending with maximum lateral bending
G3-S1-1 indicates results for maximum lateral bending with concurrent major axis bending
G3-S1-2 indicates results for maximum lateral bending with maximum major axis bending

$$**Ratio\ of\ Strengths = \left[\frac{M_n - \frac{f_\ell S_{xt}}{3}}{\left(F_y - \frac{f_\ell}{3}\right) S_{xt}} \right]$$

Table 2.5.3. SERVICE II unity checks

Load Combination	Section		Design Unity Checks: Permanent deformation $[f_b+(1/2)\,f_\ell] / 0.95\,R_h\,F_{yt}$
SERVICE II	G1-S1-1	Bottom Flange	0.966
	G1-S1-2		0.967
	G3-S1-1		0.739
	G3-S1-2		0.846
	G6-S1-1		0.810
	G6-S1-2		0.812

2.5.2 Cross-Frame Member Design

The cross-frames are main load carrying members in skewed and curved bridges. The cross-frames are assumed to remain elastic throughout this study. The compressive axial capacity of the diagonal of CF-107 and the bottom chord of CF-203 are checked under the STRENGTH I load combination using the procedures from the AISC (2005) Specification as discussed in White (2007). L 5*x*3*x*1/2 cross-frame members are used for both cross-frames. The results of the unity checks are shown in Table 2.5.4.

Table 2.5.4. Unity checks for axial load capacity of CF-107 and CF-203 under STRENGTH I load combination.

Load Combination	Section		Axial Force N (kips)	Design Unity Checks: Axial Load Capacity $N / \phi\, N_n$
STRENGTH I	CF-107	Diagonal (L 5x3x1/2)	106	2.889
	CF-203	Bottom Chord (L 5x3x1/2)	176	7.121

As can be seen from Table 2.5.4, both members are insufficient to support the axial load acting on them. The axial load on the diagonals of CF-107 is 2.9 times larger than its axial capacity. The axial load on the bottom chord of CF-203 is 7.1 times larger than the axial capacity of those members. As a result, the cross-frames are redesigned. Recommended dimensions and their unity checks are provided in Table 2.5.5.

L 5*x*5*x*5/8 members are required for the diagonals and L 8*x*8*x*9/16 members are required for the bottom chords of the interior cross-frames. The details of these solutions are shown in Appendix A. These cross-frame members appear to be adequate throughout the bridge.

Table 2.5.5. Unity checks for axial load capacity of required CF-107 and CF-203 under STRENGTH I load combination.

				Design Unity Checks
Load Combination	Required Section		Axial Force N (kips)	Axial Load Capacity $N / \phi N_n$
STRENGTH I	CF-107	Diagonal (L 5x5x5/8)	106	0.99
	CF-203	Bottom Chord (L 8x8x9/16)	176	0.958

The critical loading for G1-S1 under the STRENGTH I load combination is re-applied to the bridge using the recommended cross-frame member sizes for the interior cross-frames. On the other hand, end cross-frame dimensions are kept same. Figure 2.5.1 compares the stress distribution along G1 before and after the change in the cross-frame member sizes. The change of area of the interior cross-frames has a negligible effect on the flange stresses for this bridge. On the other hand, the bottom chord axial force in CF-203 increases by 8.4%. Figure 2.5.2 shows the maximum axial forces for CF-203 before and after the change in the cross-frame member sizes. The above cross-frame member forces correspond to the critical loading for G1-S1. If the critical live load position under the STRENGTH I load combination for the bottom chord of CF-203 is employed, the increase in the axial force is 8.1% for this member. Figure 2.5.3 shows the axial force in the bottom chord of CF-203 before and after the change in the cross-frame member sizes, using the critical live load configuration for this member. The sensitivity of the cross-frame member forces and the girder responses to the cross-frame member area changes are small. Therefore, the initial cross-frame areas are retained in the subsequent full nonlinear studies.

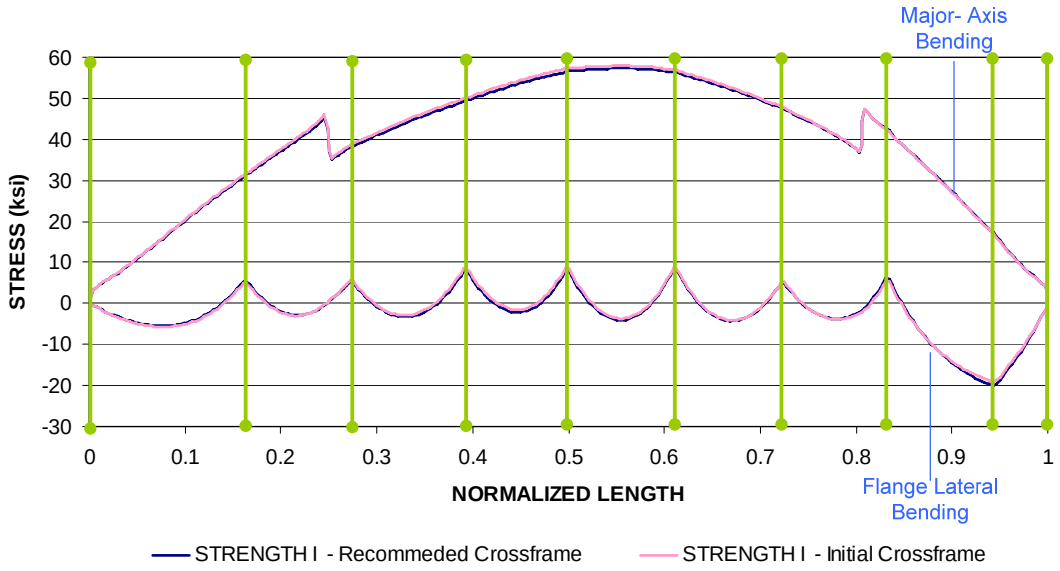

Figure 2.5.1. G1 bottom flange stress variation by using different interior cross-frame areas, LL position causing the maximum STRENGTH I unity check at G1-S1.

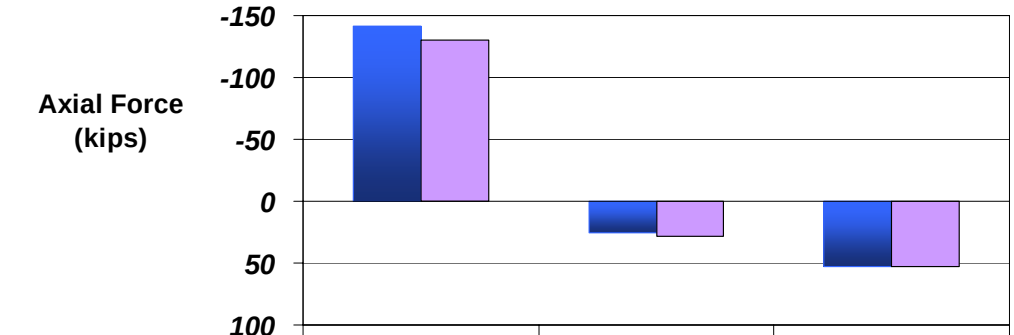

	Bottom Chord	Diagonal	Top Chord
Recommended Cross-frames	-141	26	52
Initial Cross-frames	-130	28	53

Figure 2.5.2. Axial load variations for CF-203, LL position causing the maximum STRENGTH I unity check at G1-S1.

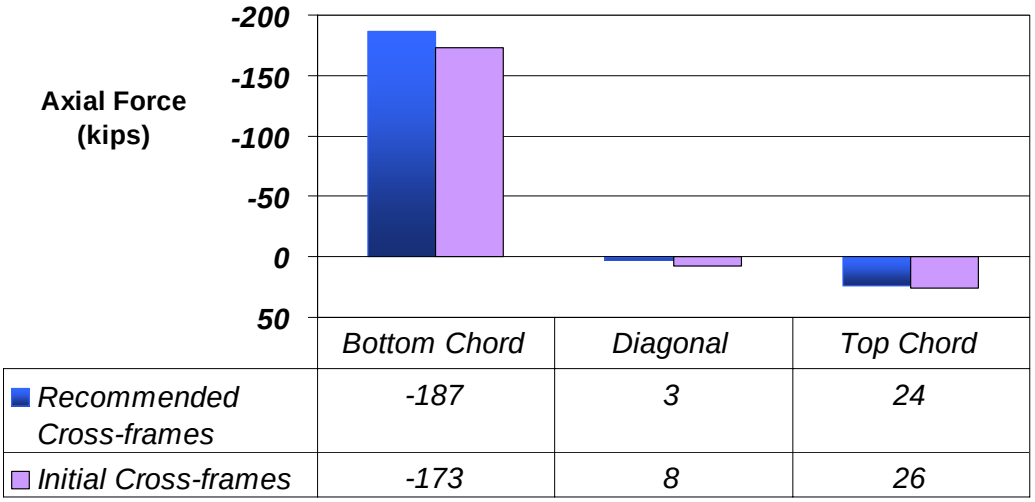

Figure 2.5.3. Axial load variations for CF-203, LL position causing the maximum STRENGTH I axial force in the bottom chord.

2.6 Comparison of 3-D Beam-Shell and 3-D Grid Results

Responses gathered from the 3-D beam-shell FEA model are shown in the previous sections. In this section these 3-D beam-shell model results are compared with 3-D grid results in order to observe the variation of the responses. Figure 2.6.1 shows the 3-D grid model view of the study bridge in the GT-SABRE Viewer. The 3-D grid model is created and analyzed using the structural analysis program GT-SABRE (Chang 2006). All the girders are modeled with the B14DGLW element which is a displacement-based element based on thin-walled open-section beam theory. The B14DGLW element has seven degrees of freedom per node to capture the warping effects on the member. Moreover, the diagonals of the cross-frames are modeled using T6 truss elements, which have three degrees of freedom per node. The top and bottom chords of the cross-frames are modeled with B12CW beam elements, which have 6 degrees of freedom per node. Furthermore,

the slab is modeled explicitly by using conventional beam elements. A grid system is created by using beam elements with 6 dofs per node. Each girder and the corresponding effective width of the slab is represented by a longitudinal grid member, and the transverse actions of the cross-frames and the slab are represented by transverse grid members solely at the cross-frame locations. The open-section thin-walled beam element model of the girder and the slab model are connected by rigid offsets with idealized hinges at the girder top flange. The torsional and lateral bending rotations are released at the top flange nodes. The rotation about the vertical axis at the top flange, due to lateral bending and warping, is compatible with the rotation of the slab throughout the girder length. Further information about GT-SABRE can be found in (Chang 2006).

The steel dead weight is applied to the girders as uniformly distributed loads in GT-SABRE. Although, the stiffeners are not considered in the 3-D grid model, the total steel dead load is increased 2.13 % so that the 3-D beam-shell model and the beam theory model are supporting the same dead load. The weight of formwork, reinforcement, wet concrete are applied to the top face of the top flanges of the girders as uniformly distributed line loads based on the tributary width of each girder across the cross-section of the bridge. Also, the weights of the cross-frames are applied to girders as point loads. Furthermore, eccentric overhang bracket loadings and parapet loadings are treated as the vertical loads on the two exterior girders and uniform concentrated torsion at the joints of the girder. Similarly, the lever rule is used to distribute the design truck wheel load to the near girder nodes with respect to the distance ratio between the position of the wheel and the girders.

Responses from both models are compared under the STRENGTH I load combination. The critical live load position used for creating maximum flexural effects on G1-S1 is used while comparing the results. Figure 2.6.2 shows the vertical deflections of the noncomposite structure along the outside girder under 1.25 DC1. Also, the web out-of-plumbness for the noncomposite structure under 1.25 DC1 is illustrated in Fig. 2.6.3. Moreover, the top and bottom flange stress distribution for the noncomposite structure under 1.25 DC1 is presented in Figs. 2.6.4 and 2.6.5. Furthermore, Fig. 2.6.6 shows the bottom flange stresses under the STRENGTH I load combination. Additionally, Fig. 2.6.7 shows the axial forces for CF-203.

Figures 2.6.2 through 2.6.6 clearly show that the variation in the girder responses between the 3-D FEA and the 3D grid models is very small. However, the 3-D beam-shell model predicts the bottom chord axial force on CF-203 as -130 kips whereas the 3-D grid model predicts it as -160 kips. This difference is believed to be due to the web distortional flexibility in the beam-shell FEA model.

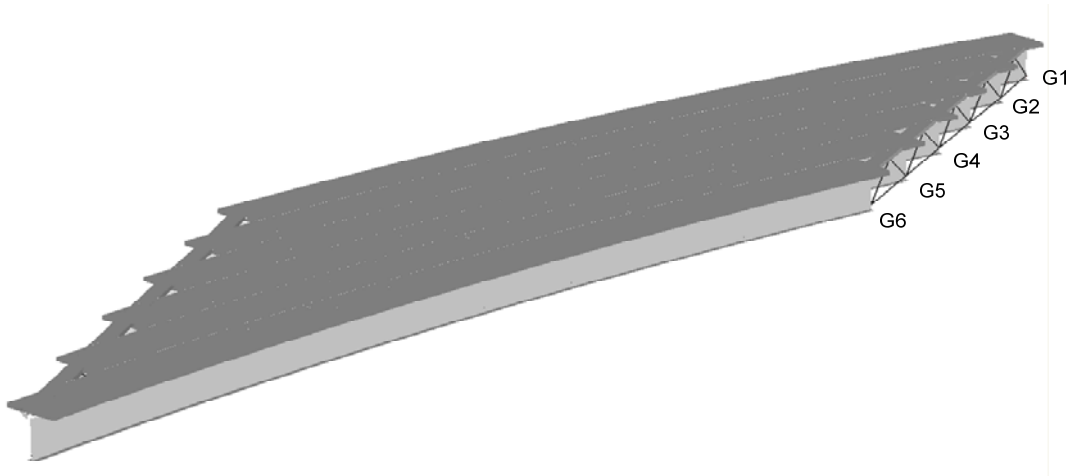

Figure 2.6.1. 3-D grid model view of the study bridge in the GT-SABRE Viewer

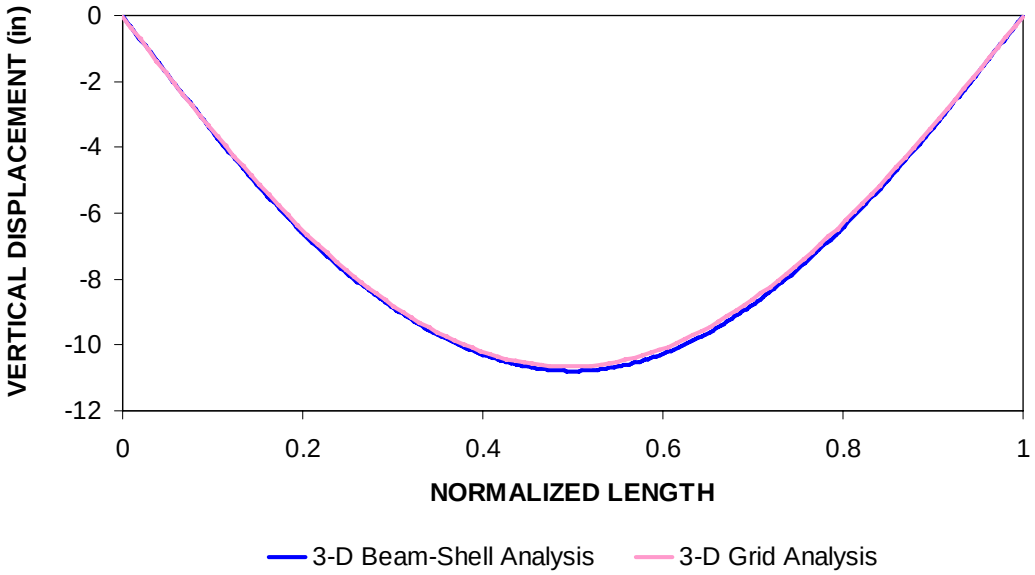

Figure 2.6.2. Vertical displacement along G1 which is obtained from different models. (Load factor = 1.25).

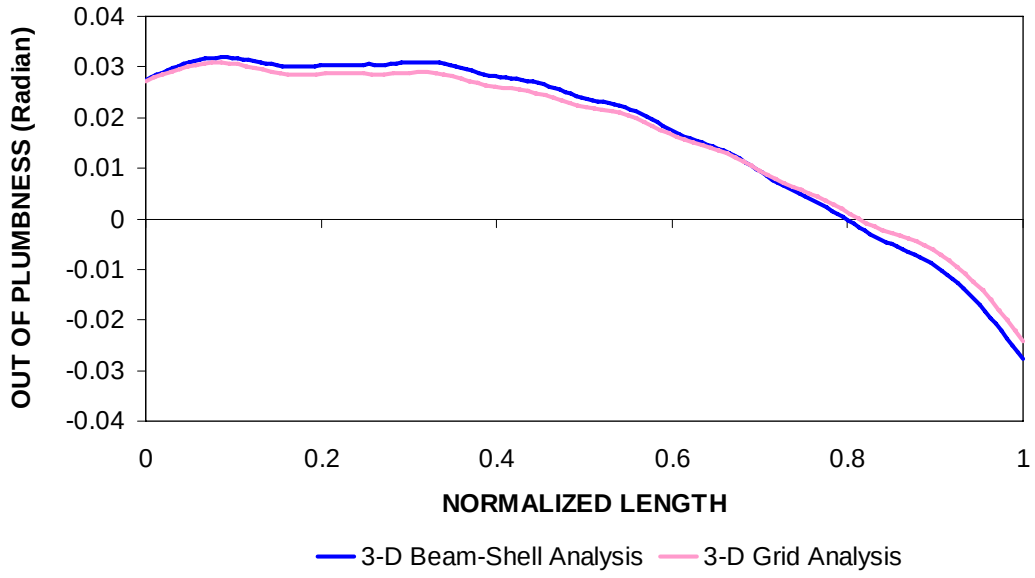

Figure 2.6.3. Web plumbness along the length of G1 due to DC1 (Load Factor =1.25).

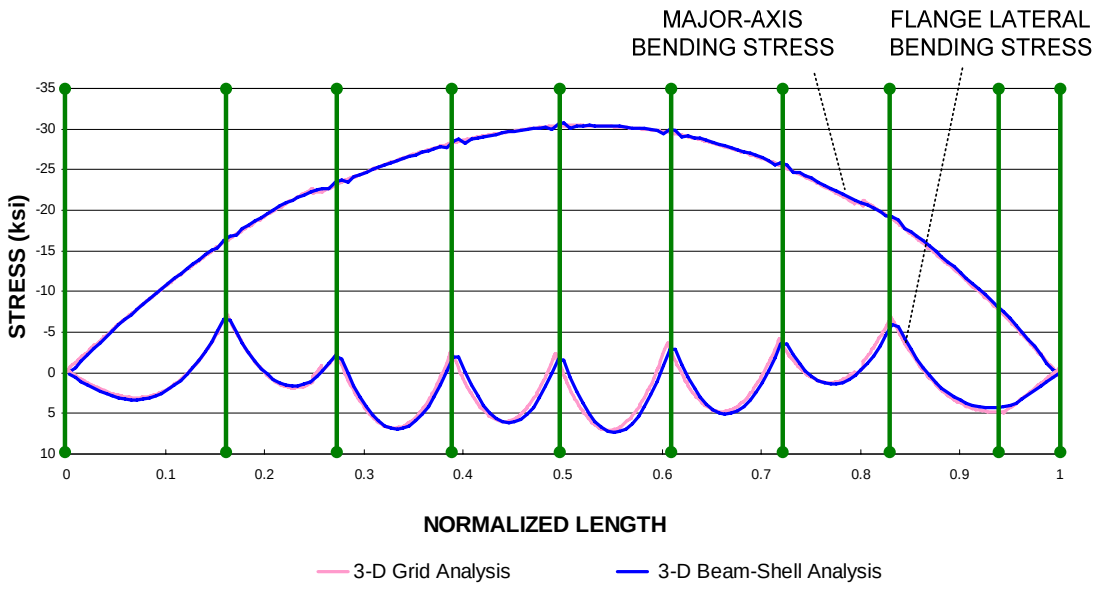

Figure 2.6.4. Top flange major-axis bending and flange lateral bending stresses along G1 due to DC1 from both models (Load factor=1.25).

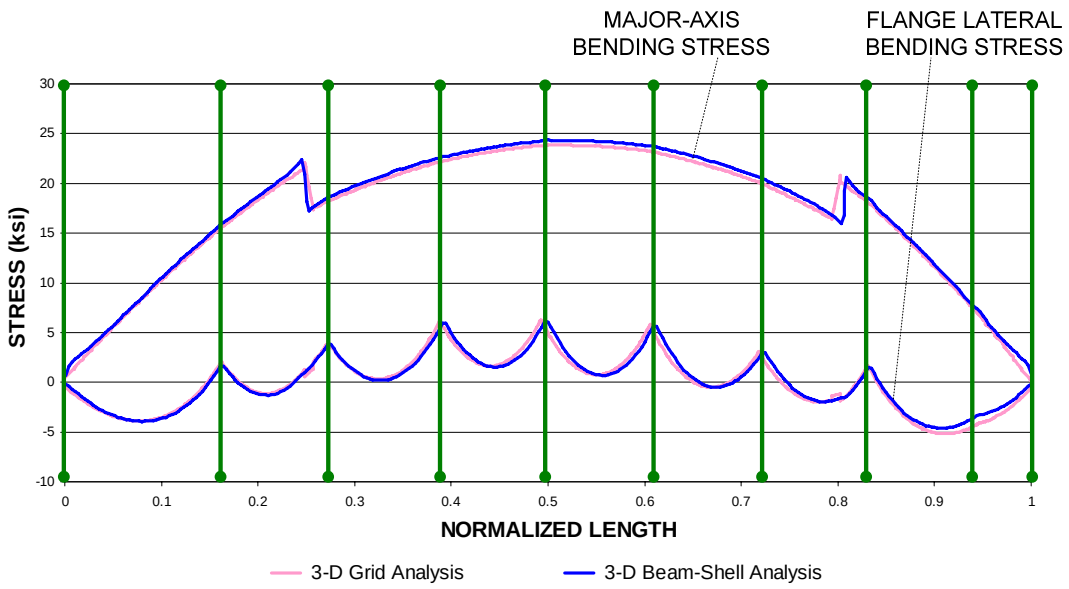

Figure 2.6.5. Bottom flange major-axis bending and flange lateral bending stresses along G1 due to DC1 from both models (Load factor=1.25).

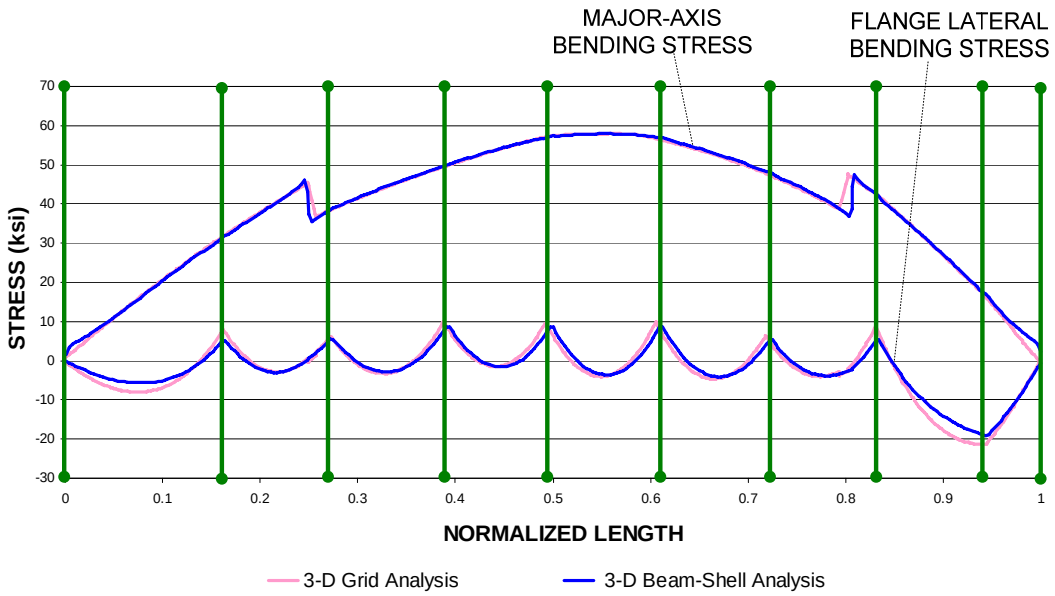

Figure 2.6.6. Bottom flange major-axis bending and flange lateral bending stresses along G1 due to DC1 from both models (STRENGTH I).

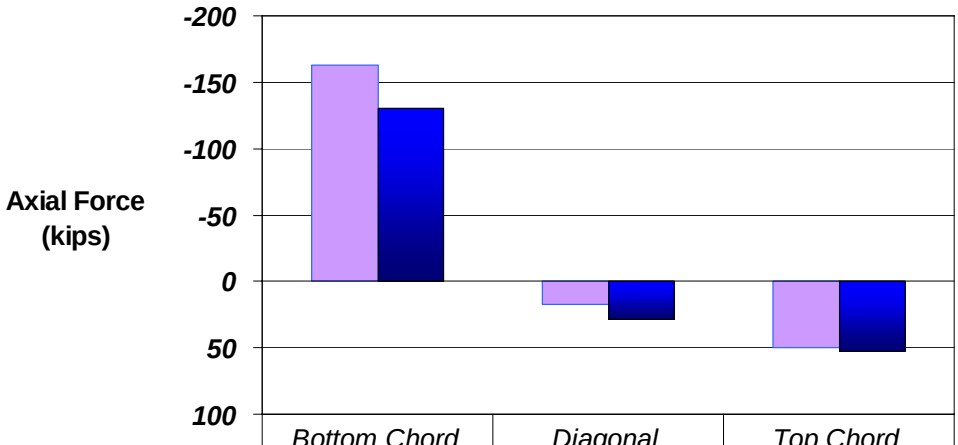

	Bottom Chord	Diagonal	Top Chord
3-D Grid Analysis	-162	17	50
3-D Beam-Shell Analysis	-130	28	53

Figure 2.6.7. Axial load variation for CF-203 LL position causing the maximum STRENGTH I unity check at G1-S1.

CHAPTER 3

FULL NONLINEAR FEA MODELING

3.1 Overview

In this work, the same finite element discretization and boundary conditions are used for both the full nonlinear and the elastic FEA solutions. However, a number of changes in the material properties and in the application of the loads are employed for the full nonlinear analysis. With respect to the material properties, J2-plasticity (von Mises yield criteria) and multi-linear isotropic hardening are assumed for the steel in the full nonlinear analysis. Also, for the concrete constitutive description, the concrete damaged plasticity model formulated by Lee at al. (1999) is selected. This model is based on damage theory and the corresponding stiffness degradation. Tensile and compressive damage variables are established separately to account for different damage states.

Although residual stresses can have a significant effect on the stability, strength and load deflection response of the steel structures in general, they are not considered in this research. This is because the subject bridge is a simply-supported span. Prior studies have shown that the influence of residual stresses on the load-deflection response of horizontally-curved bridges is rather inconsequential with respect to positive bending behavior (Jung 2006). The noncomposite dead load and the composite dead and live loads are applied sequentially in the full nonlinear analysis. Conversely, separate analyses are conducted for the noncomposite and composite loadings in the linear analysis and design studies and the results are combined using superposition. The bridge has an approximate span length of 160 ft so the deck is assumed to be cast in one step.

Therefore, staged casting operations and their influence on the behavior are not a consideration. Since the final responses under strength loading conditions are targeted, the steel erection sequence is not modeled explicitly in this study. It is assumed that zero yielding occurs within the structure during the erection process and that all the structural components connect ideally in the no-load configuration without any lack of fit. Based on these assumptions, the final state of the bridge at the end of the construction is unique and independent of the construction sequence.

In the following sections additional modeling considerations for full nonlinear analysis are described. The loading schemes for the full nonlinear analysis are illustrated in Section 3.2, the nonlinear material properties are explained in Section 3.3, and finally the full nonlinear FEA procedures are described in Section 3.4.

3.2 Loading Schemes

Since determining the strength behavior of the bridge is the primary objective of this study, the AASHTO STRENGTH I load combination is applied to the bridge. Specifically, the factored live load is increased incrementally to investigate the influence of material nonlinearity on bridge responses at the F_y and M_p based one-third rule load levels.

In Chapter 2, critical cross-sections under the STRENGTH I loadings are identified on girders G1, G3 and G6. These are labeled as G1-S1, G3-S1 and G6-S1. Sections G1-S1 and G6-S1 are selected as they exhibit the maximum strength unity check on these girders whereas G3-S1 is selected because it has the maximum flange lateral bending stress limit unity check on G3. Different truck and lane load arrangements are applied for

each of these cases to obtain the maximum of the above unity checks at these locations. These live loads are applied directly to the bridge for the full nonlinear FEA studies in the subsequent chapters. Figures 2.4.40 and 2.4.41 show the applied vehicular design load configuration that gives the maximum strength unity check on G1 at G1-S1 under the STRENGTH I load combination. Figures 2.4.42 and 2.4.43 show the applied vehicular design load configuration that gives the maximum flange lateral bending stress on G3 at G3-S1 under the STRENGTH I load combination. Figures 2.4.44 and 2.4.45 show the applied vehicular design load configuration that gives the maximum strength unity check on G6 at G6-S1 under the STRENGTH I load combination. The design live load calculations are discussed in detail in Chapter 2.

3.3 Material Properties

3.3.1 Steel Stress-Strain Responses

Grade 50 material is used for all the structural steel in the subject bridge. A representative stress-strain curve for AASHTO M270 Grade 50W steel and a multilinear fit to averaged results from a suite of coupon tests are shown in Fig. 3.3.1. Results of the stress-strain data from tension coupon tests obtained from Beshah (2006) are used as a base for the description of the material yield and strain hardening characteristics in this work. The test results are summarized in Table 3.3.1 in terms of the average engineering stress and strain. Since the finite elements used in this research are formulated for large strain, the true stress and true strain must be used when defining the material stress-strain response. The static yield of the test result is scaled such that the yield is exactly equal to

50 ksi for this research. Therefore, stress-strain data is converted to true stress-strain data using the following formulas (HKS 2004):

$$\sigma = \sigma_{nom}\left(1+\varepsilon_{nom}\right) \tag{3.1}$$

$$\varepsilon = \ln\left(1+\varepsilon_{nom}\right) \tag{3.2}$$

where,

σ = True stress

σ_{nom} = Engineering stress

ε = True strain

ε_{nom} = Engineering strain.

A multi-linear stress-strain curve is fit to the above true stress-strain results by defining four anchor points (Zureick et al. 2002). The first anchor point is the initial yield point of the material where the plastic strain is zero. The second point is defined at the onset of strain hardening (e_{st}, F_y). The third point is arbitrarily selected at a total engineering stress of $F_y + 2/3\ (F_u - F_y)$. The engineering strain corresponding to this point is determined as $e_{st} + 2/3\ (F_u - F_y) / E_{st}$. The fourth point is defined at the ultimate tensile stress on the engineering stress-strain curve. Lastly, the true stress is assumed to be constant for strains larger than those associated with the fourth point. Figure 3.3.2 shows the resulting multi-linear stress-strain curve. Table 3.3.2 gives the specific stress-strain data. For the slab reinforcing steel, an elastic-perfectly plastic stress-strain response with a nominal yield strength of 60 ksi is assumed.

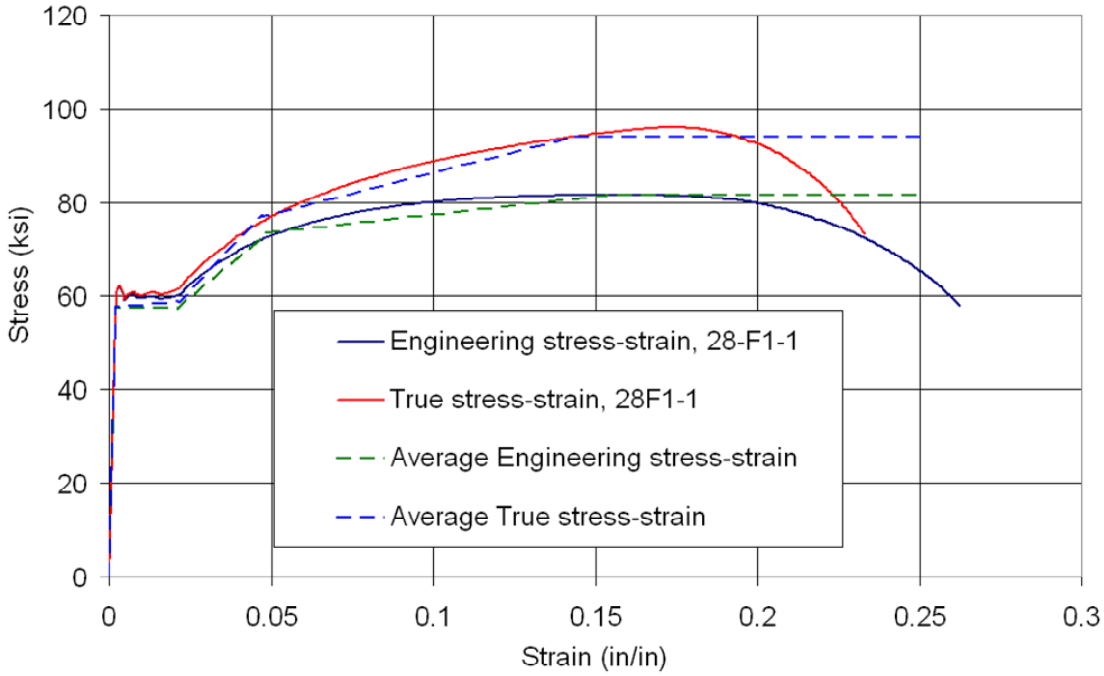

Figure 3.3.1. Representative stress-strain curve for AASHTO M270 Grade 50W steel

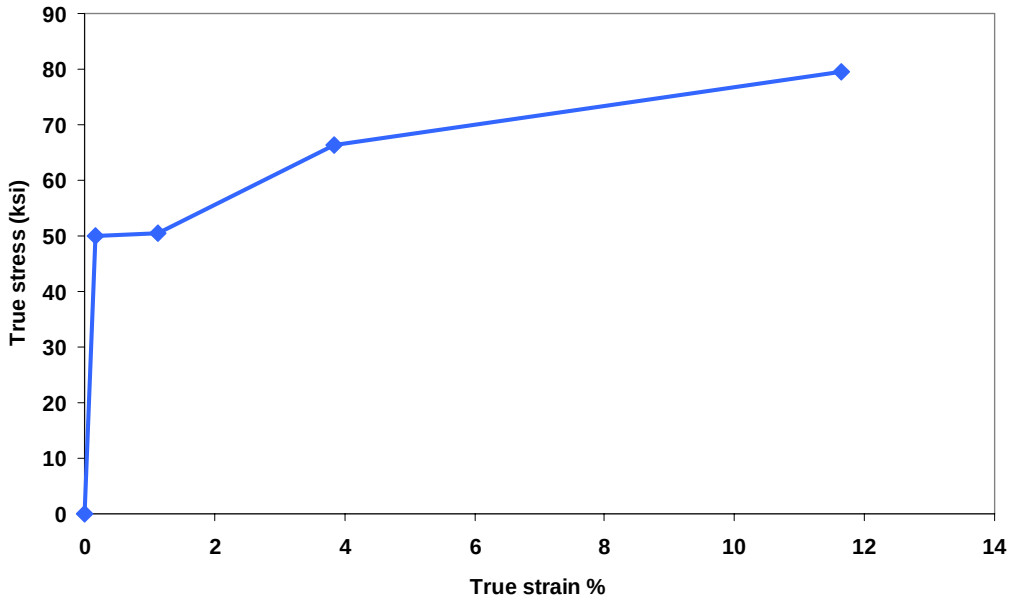

Figure 3.3.2. True stress-strain responses for the structural steel (Grade50).

Table 3.3.1. Average engineering stress-strain data from the tension coupon tests (Beshah 2006)

N	E (ksi)	Static F_y (ksi)	E_{st} (ksi)	ε_{st} (%)	F_u (ksi)	ε_u (%)
6	29650	57.56	592	1.18	81.85	12.3

Table 3.3.2. Data points for multi-linear stress-strain response for steel members

Point	True Strain (%)	True Stress (ksi)
Yielding	0.17	50
Onset of strain Hardening	1.12	50.38
Intermediate strain hardening	3.84	66.31
Ultimate Strength	11.65	79.56

3.3.2 Concrete Stress-Strain Responses

3.3.2.1 Compressive Strength

Figure 3.3.3 shows a multi-linear representation of the average measured concrete compression stress-strain response used by Jung (2006) in his studies of the FHWA composite bridge test. The concrete strength in this test was $f_c^{'} = 4.870$ ksi, which is similar to the strength of the concrete specified for the bridge considered in this research. Therefore, Jung's concrete constitutive properties are also used in this work.

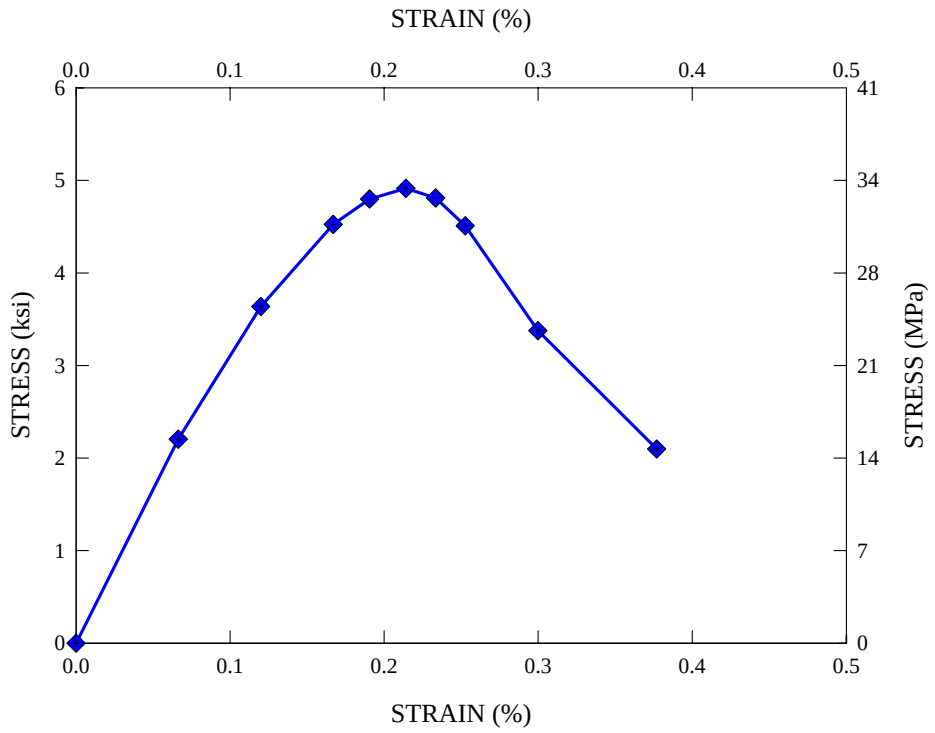

Figure 3.3.3. Multi-linear representation of measured average concrete compression stress-strain response (Jung 2006).

Jung (2006) derives a multi-linear representation of measured average concrete compression stress-strain response from measured concrete compressive stress-strain curves based on six 298 day cylinder tests (Beshah 2006). Nine points are obtained on the multi-linear curves as follows. The first point is the elastic limit of the material taken as $0.45f_c'$ as described at commentary for Section 8.5 of the ACI 318-02. The second point is arbitrarily defined at a total engineering stress of $(0.45f_c' + f_c')/2$. The third to seventh points are defined around the peak stress. The fifth point is defined at the ultimate compressive stress on the engineering stress-strain curve. The third and fourth points are arbitrary points selected before the peak compressive stress whereas the sixth and seventh points are defined after the peak compressive stress. These four data points near the peak stress are intended to better represent a smooth transition from loading branch to strain

softening branch. The eighth point is selected at the point where there is a slight slope change in the descending branch. Lastly, the ninth point is defined at the end of the measured stress-strain curve.

3.3.2.2 Tensile Strength

Since the slab of the bridge is expected to experience predominantly a state of plane stress, the split-cylinder test is considered for determining the tensile strength of the concrete. A multi-linear representation of the average concrete tension stress-strain response is derived from six 298 day concrete split-cylinder strength tests (Beshah 2006). Figure 3.3.4 shows the multi-linear representation of the concrete tension stress-strain response.

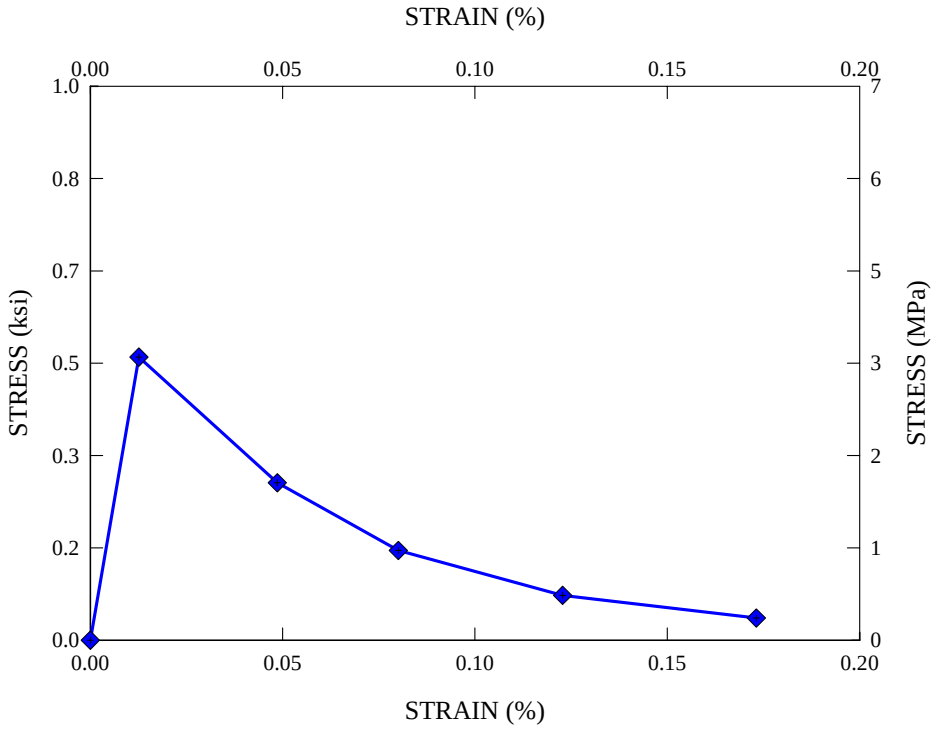

Figure 3.3.4. Multi-linear representation of concrete tension stress-strain response used for the full nonlinear FEA of the test bridge, based on six 298-day split-cylinder tests (Beshah 2006).

3.4 Full Nonlinear FEA Procedures

The composite bridge behavior is assumed to be geometrically linear and elastic in Chapter 2. Therefore, the results of separate analyses for DC1, DC2, DW and LL may be superposed. However, superposition is not possible for the full nonlinear analysis since the system experiences both material and geometric nonlinearity. Consequently, application of the noncomposite dead load is followed by sequential application of the DC2, DW and LL in the full nonlinear FEA. This sequential application for the full nonlinear analysis simulation is addressed by Jung 2006. The girders are cambered for 1.25 DC1 so that the girder top flanges are perfectly situated in a horizontal plane under this loading. This allows the slab to be instantiated in the finite element model in an initially flat position for the subsequent full nonlinear analysis studies. Also, this exaggerates the influence of any girder twists from the initially-plumb no-load fit condition due to the noncomposite dead load (since the factored dead load 1.25 DC1 is used rather than the actual 1.0 DC1).

The sequence of application of the loads to the FEA model of the bridge is summarized as follows:

1) Generation of the Complete Model

FEA model of the composite bridge is generated assuming that the girder webs are plumb in the initial no-load configuration. An initial camber of the girders is applied by using the IMPERFECTION command. The girder cambers are set so that the slab is ideally flat under the total noncomposite dead load. Superelevation of the bridge deck is neglected in this research to simplify the modeling and the behavior

2) Applying the Steel Dead Load

The deck of the FEA model is removed by using CHANGE MODEL command (See Fig. 3.4.1). The self weight of the steel members is applied to the bridge by turning on the GRAVITY command.

3) Application of the Weight of the Forms and the Concrete Dead Weight

The steel section alone must resist the dead and construction loads that are applied before the concrete deck is hardened. Therefore, the dead load from the wet concrete and forms is assumed to be carried by the noncomposite FEA model alone. Also, eccentric bracket loads on G1 and G6 are modeled as two equal and opposite radial forces which create a uniformly distributed torque on the exterior girders. The dead load from the forms is not removed from the model to be consistent with the elastic analysis and design checks.

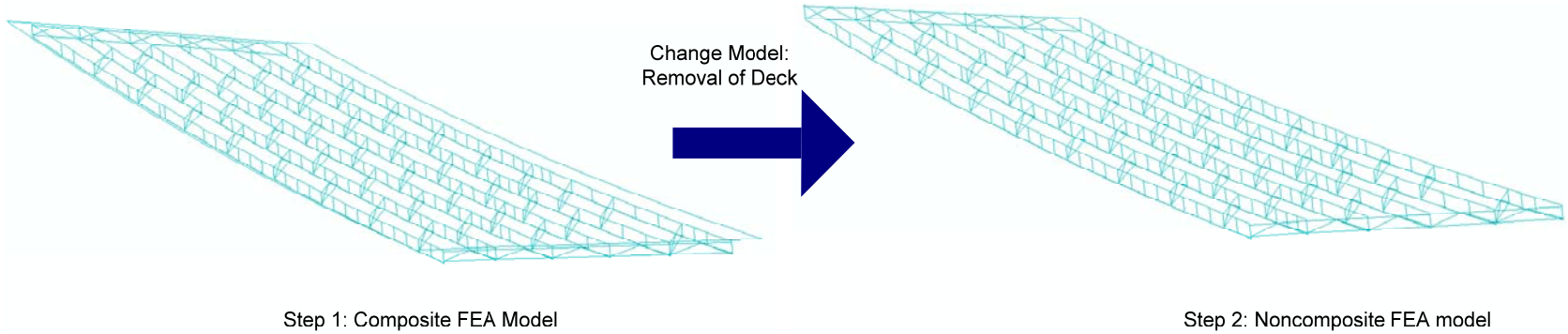

Figure 3.4.1. Removal of the deck for Step 2.

4) Strength and Stiffness Gain of the Slab for Composite Action

The slab is activated by using the CHANGE MODEL command to simulate the onset of composite action in the ABAQUS FEA model. Since the girders and cross-frames are adjusted with initial camber for the no-load fit condition, they are out of plumb in the final erected dead load position (DC1). Figure 3.4.2 shows a cross-section profile of the girders and cross-frames at the right bearing line after 1.25DC1. The top flanges are tied to the slab nodes with the EQUATION command in ABAQUS.. The usage of the EQUATION command is discussed in Section 2.3.1.

5) Application of of Future Wearing Surface Load

The future wearing surface load (DW) is applied on the composite bridge along the roadway as a distributed load.

6) Placement of Parapets

The parapet loads (DC2) are applied as uniform distributed loadings over the width of the parapets. It is assumed that the parapets do not make any contribution to the structural resistance.

7) Application of Live Loads

The live loads are applied on the composite bridge at the locations shown in Figs. 2.4.40 through 2.4.45 depending on the critical section being considered.

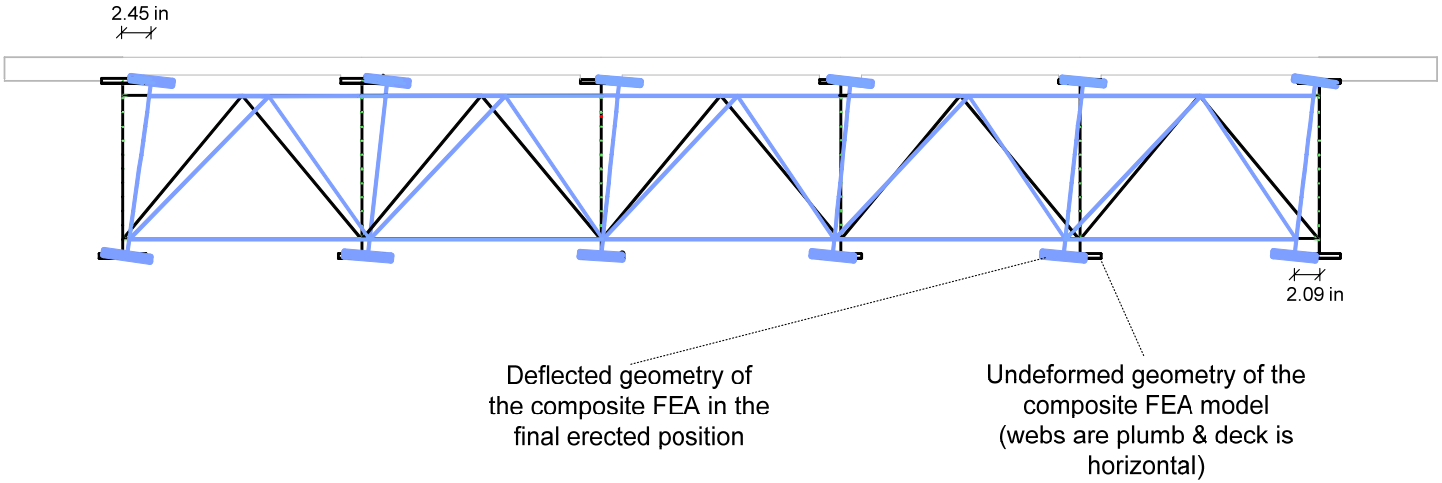

Figure 3.4.2. Cross-section profile view of the right bearing in the final constructed dead load position under 1.25 DC1. (Displacements are amplified 5 times).

CHAPTER 4

FULL NONLINEAR FEA RESULTS

4.1 Overview

The strength behavior of the subject bridge is investigated in this chapter by conducting full nonlinear analyses. Several critical cross-sections defined in Chapter 3 are monitored while loads are applied corresponding to their critical STRENGTH I load combination. Initial camber of the girders is provided in Section 4.2. The significant load levels are shown in Section 4.3. Moreover, in Sections 4.4 through 4.6 full nonlinear results for G1-S1 on G1, G3-S1 on G3 and G6-S1 on G6 are presented and compared with the elastic analysis responses at different load levels. Furthermore, in Section 4-7 the critical STRENGTH I load combinations for cross-frames CF-107 and CF-203 (See Figs. 2.4.49 through 2.4.52) are applied in the full nonlinear analyses and the cross-frame member forces are compared with the elastic analysis results. Finally, Section 4.8 provides a synthesis of the full nonlinear analysis results.

4.2 Girder Camber

Girder cambers are not considered in the elastic analysis and design as the separate analyses for each of the different loadings are superposed. However, the appropriate deflected geometry in the full nonlinear analysis simulation is desired. Therefore, the girder camber is considered in the full nonlinear analyses so that the girder top flanges are perfectly situated in a horizontal plane under the total dead load. This allows the slab

to be instantiated in the finite element model in an initially flat position for the subsequent full nonlinear analysis studies. As a result, the girders are cambered for 1.25 DC1, obtained from the geometrically nonlinear analysis under 1.25 DC1. Figure 4.2.1 shows the cambers specified for each of the bridge girders.

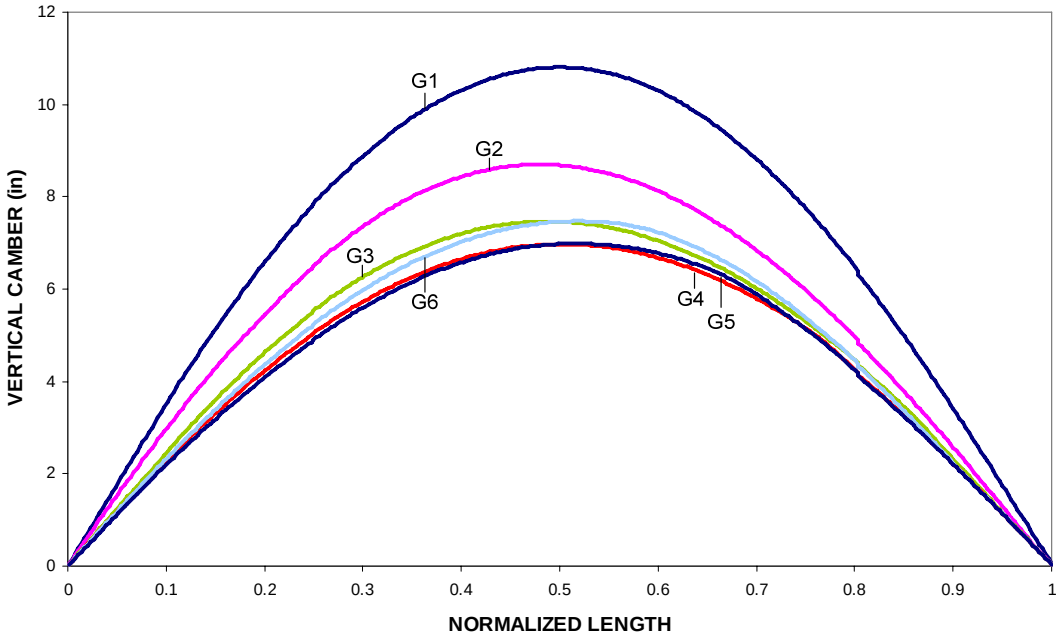

Figure 4.2.1. Initial cambers of the bridge girders along the normalized length (1.25 DC1)

4.3 Significant Load Levels

Several load levels are of potential interest in investigating the strength behavior of the bridge. One way of defining these significant load levels is to consider the following combinations of the girder stresses or moments from elastic analyses that correspond to the AASHTO or other potential strength limit states:

$$STRENGTH\ \ I\ \ condition:\ \ f_b + f_\ell/3 = R_h F_{yt} \tag{4.1}$$

$$Plastic\ \ moment\ \ capacity\ \ with\ \ 1/3\ \ reduction:\ M_u + f_\ell S_{xt}/3 = M_p \tag{4.2}$$

where;

f_b = Tension flange major-axis bending stress.

f_ℓ = Tension flange lateral bending stress.

S_{xt} = Elastic section modulus about the major-axis of the section to the bottom tension flange, taken generally as $M_y/F_{yt.}$

M_p = Plastic moment capacity in the absence of any flange lateral bending.

F_{yt} = Specified minimum yield strength of the tension flange.

R_h = Hybrid Factor

Table 4.3.1 shows the elastic section modulus to the bottom tension flange (S_{xt}) for G1-S1, G3-S1 and G6-S1. AASHTO (2007) defines the elastic section modulus in major-axis bending in general as M_{yf}/F_{yf}, where M_{yf} is the moment causing first yield in the cross-section at the flange under consideration if the flange lateral bending stresses are taken equal to zero, and F_{yf} is the specified minimum yield strength of the flange. Composite bridge girders are assumed to resist moment based on the three different cross-section models: the noncomposite section, the long-term composite section and the short term composite section. The elastic section moduli correspond to each of the cross-section models are denoted by S_{NC}, S_{LT} and S_{ST} respectively. The noncomposite section resists the moment due to dead loads before the concrete reaches its compressive strength (M_{D1}). The long term composite section resists the moment due to the remainder

of the dead loads (wearing surface, concrete barriers, etc.) (M_{D2}). The long term section modulus is calculated using the modular ratio *3n*, where $n = E_c/E$ is the modular ratio of the section corresponding to short term loadings. This accounts approximately for the long-term effects of creep deformations in the concrete slab. The short term composite section resists the additional moment required to cause yielding in the flange under consideration (M_{AD}). The moment M_{AD} can be determined from the equation

$$F_{yf} = \frac{M_{D1}}{S_{NC}} + \frac{M_{D2}}{S_{LT}} + \frac{M_{AD}}{S_{ST}} \tag{4.3}$$

and the yield moment M_{yf} is then can be calculated as

$$M_{yf} = M_{D1} + M_{D2} + M_{AD} \tag{4.4}$$

Table 4.3.1. Elastic section modulus values for critical cross-sections

	S_{xt} (in^3)
G1-S1	4767
G3-S1	3702
G6-S1	3564

Wittry (1993) introduced an additional margin of safety to the AASHTO LRFD Design Specifications which is applied to the theoretical nominal flexural resistance of compact composite sections in positive flexure when the distance from the top of the concrete deck to the plastic neutral axis D_p exceeds a certain value. This additional margin of safety is intended to protect the concrete deck from premature crushing and ensures adequate ductility of the composite section. It is applied to the subject bridge in the strength limit state checks since $D_p/D_t > 0.1$ where D_t is the total depth of the composite section. Therefore, the moment capacity of the section is reduced by

$1.07 - 0.7(D_p/D_t)$ in the design checks. Different load levels are determined as follows:

$$F_y \, based \, 1/3 \, rule = \left(F_y - \frac{f_\ell}{3} \right) S_{xt} \tag{4.5}$$

$$M_p \, based \, 1/3 \, rule = M_p - \frac{f_\ell S_{xt}}{3} \tag{4.6}$$

$$M_n \, based \, 1/3 \, rule = M_n - \frac{f_\ell S_{xt}}{3} \tag{4.7}$$

Table 4.3.2 compares and presents the strength unity checks based on F_y based one-third rule, M_n based one-third rule and M_p based one-third rule. This reduction is neglected in this chapter and the behavior is considered at the plastic moment capacity based 1/3 rule load level to provide a more critical assessment of the strength behavior of the bridge system.

Table 4.3.2. Comparison of the strength unity checks based on F_y based one-third rule, M_n based one-third rule and M_p based one-third rule

Load Combination	Section		Design Unity Checks: Strength $[f_b+(1/3)\ f_\ell] / \phi_f F_n$	Strength $[M_u+(1/3)\ f_\ell\ S_{xt}] / \phi_f M_n$	Strength $[M_u+(1/3)\ f_\ell\ S_{xt}] / \phi_f M_p$	Ratio of Strengths with reduction	Ratio of Strengths without reduction
STRENGTH I	G1-S1-1	Bottom Flange	1.172	1.038	0.912	1.149	1.312
	G1-S1-2		1.172	1.038	0.912	1.150	1.312
	G3-S1-1		0.774	0.596	0.556	1.335	1.457
	G3-S1-2		0.907	0.710	0.663	1.335	1.457
	G6-S1-1		0.987	0.767	0.714	1.288	1.383
	G6-S1-2		0.988	0.768	0.715	1.288	1.383

*** *G1-S1-1, G6-S1-1 indicates results for maximum major axis bending with concurrent lateral bending*
G1-S1-2, G6-S1-2 indicates results for maximum major axis bending with maximum lateral bending
G3-S1-1 indicates results for maximum lateral bending with concurrent major axis bending
G3-S1-2 indicates results for maximum lateral bending with maximum major axis bending

$$**Ratio\ of\ Strengths\ with\ reduction = \left[\frac{M_n - \frac{f_\ell S_{xt}}{3}}{\left(F_y - \frac{f_\ell}{3}\right)S_{xt}}\right]$$

$$**Ratio\ of\ Strengths\ without\ reduction = \left[\frac{M_p - \frac{f_\ell S_{xt}}{3}}{\left(F_y - \frac{f_\ell}{3}\right)S_{xt}}\right]$$

4.4 Evaluation of G1

The strength behavior of G1 is investigated at section G1-S1 where the maximum strength unity check is observed under its critical STRENGTH I load combination. Different load levels are obtained by increasing the factored applied live load while keeping the loads $1.25(DC1+DC2)+1.5DW$ constant at their STRENGTH I values. Figure 4.4.1 shows the vertical deflections and Fig. 4.4.2 shows the radial displacements versus the fraction of factored live load at G1-S1 at the different load levels. The vertical deflection of G1-S1 at the M_p based 1/3 rule load level is 22.2 inches when the full nonlinear analysis is considered whereas it is 20.4 inches based on the elastic analysis.

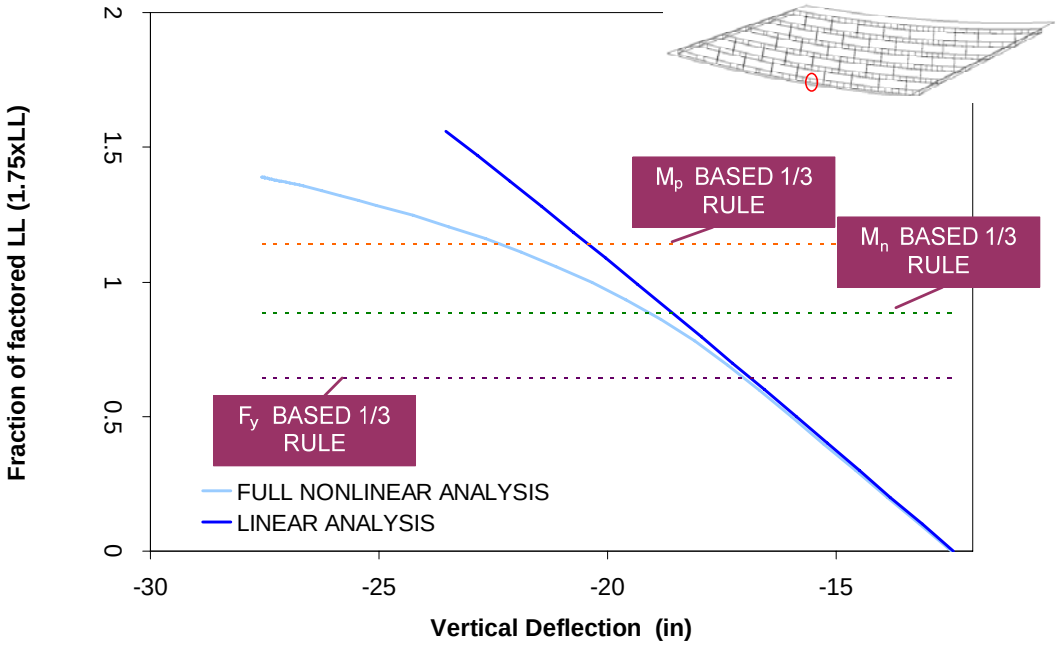

Figure 4.4.1. Vertical deflection at G1-S1 under different fractions of factored live load

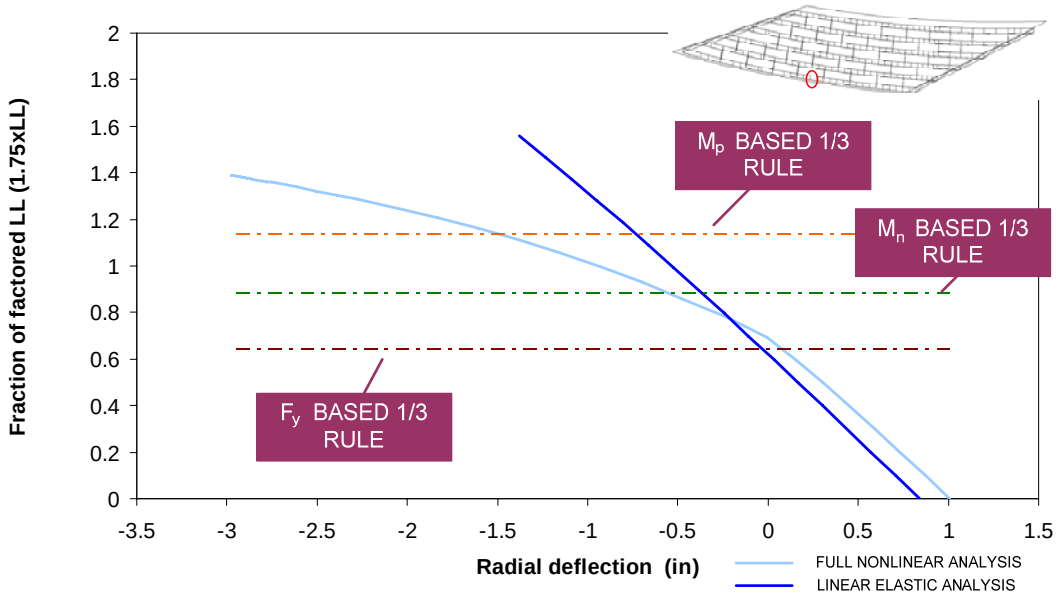

Figure 4.4.2. Radial deflection at G1-S1 under different fractions of factored live load.

The internal moment at the critical section is determined by obtaining the nodal forces in the deformed FEA model and summing their contributions to the cross-section moment using the undeformed orientation of the cross-section. The full tributary slab width is used for these sections. Jung (2006) showed that the error associated summing the nodal forces over the undeformed cross sections was negligible in his studies. Figure 4.4.3 illustrates the internal moments at G1-S1 for the different load levels.

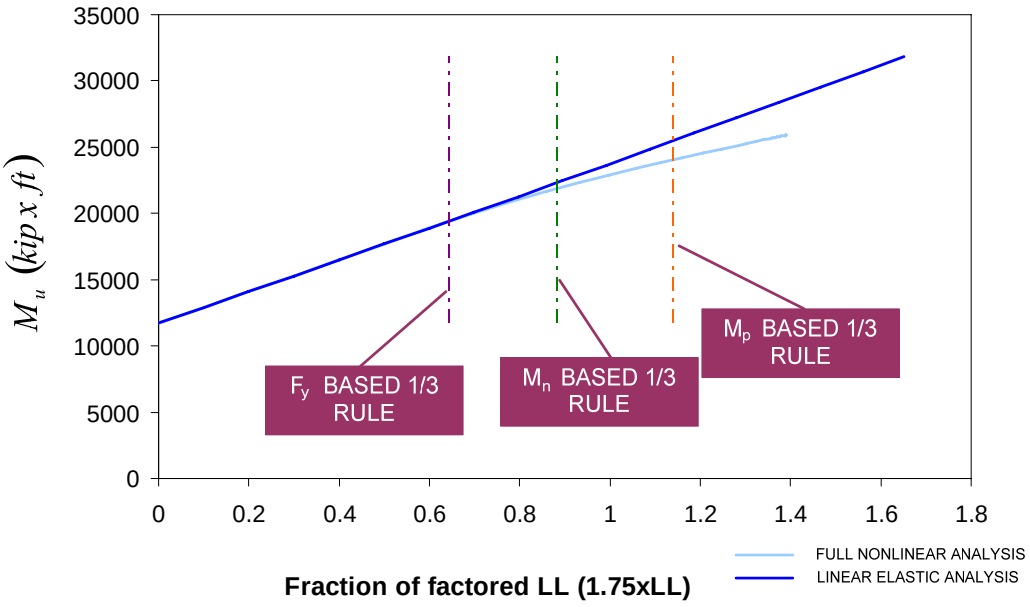

Figure 4.4.3. Internal moments at G1-S1 under different fractions of factored live load.

Figures 4.4.4 and 4.4.5 present the normalized bottom flange major axis bending and flange lateral bending strains along the length of G1 at the M_p based 1/3 rule load level. Since the bottom flanges of G1 are yielded, the strain results are shown for the bottom flanges. The maximum bottom flange major-axis bending strain is 2.6 times the yield strain. The maximum flange lateral bending strain is 1.8 times the yield strain. Figures 4.4.6 through 4.4.8 show the web out-of-plumbness of G1, G3 and G6 under the critical G1-S1 live load at the M_p based 1/3 rule load level on G1. The skewed bearing lines and horizontally curved girders introduce torsional deflections and differential displacements in the girders. Figures 4.4.6 through 4.4.8 illustrate these 3-D effects on the girders. Also, the slab top surface strains are plotted along the radial line across the width of the bridge at G1-S1 at the M_p based 1/3 rule load level in Fig. 4.4.9.

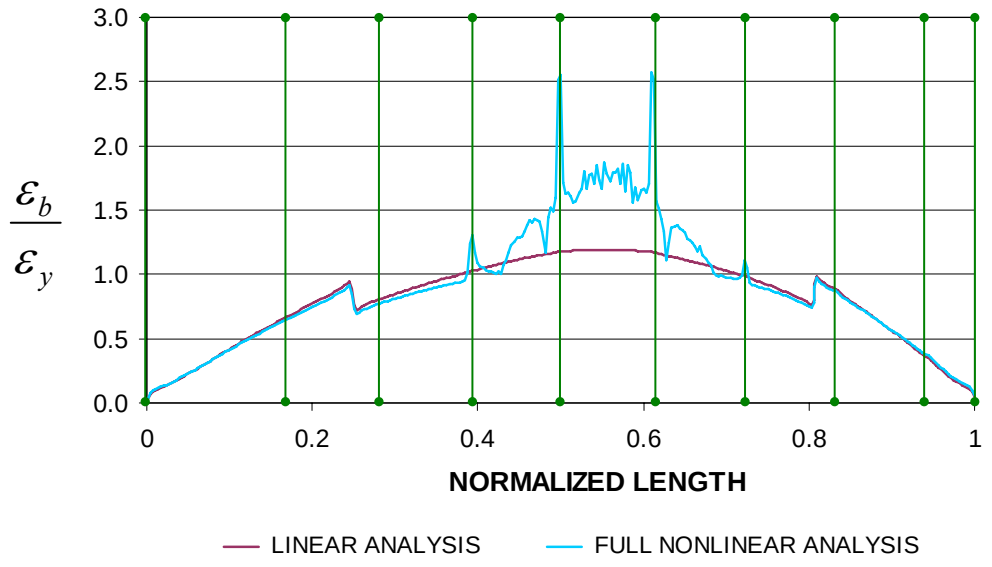

Figure 4.4.4. Normalized major-axis bending strain along G1 bottom flange at M_p based 1/3 rule load level.

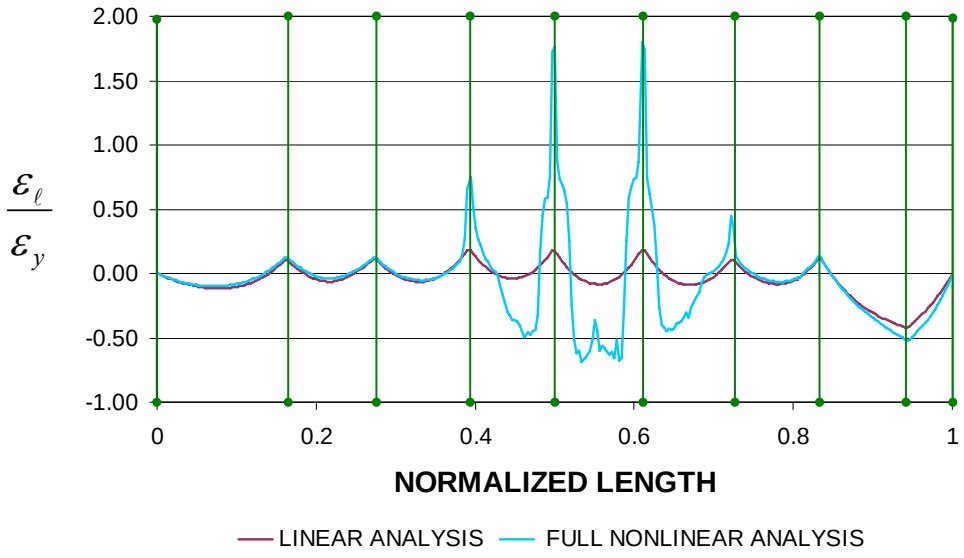

Figure 4.4.5. Normalized flange lateral bending strain along G1 at M_p based 1/3 rule load level.

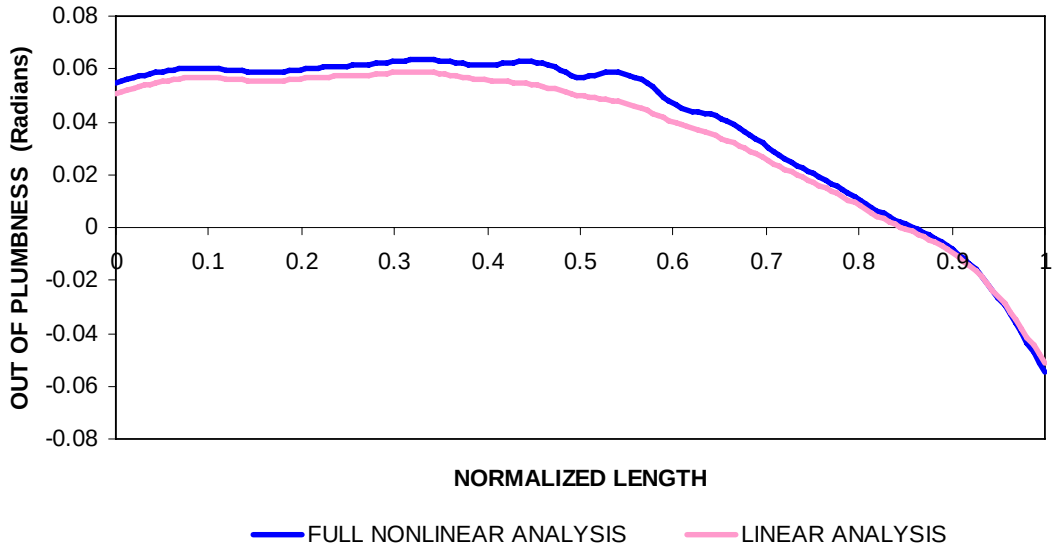

Figure 4.4.6. Out-of-plumbness along G1at M_p based 1/3 rule load level.

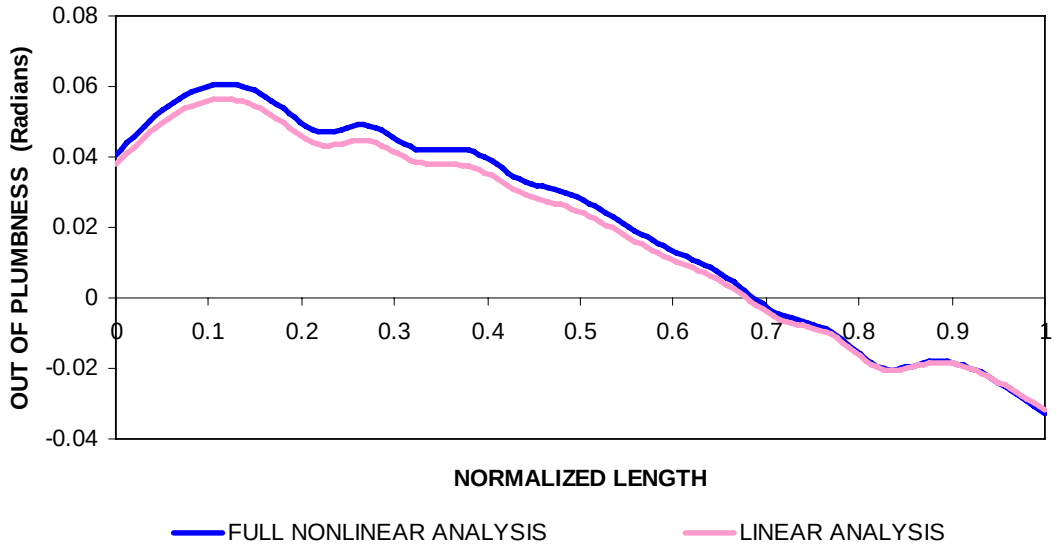

Figure 4.4.7. Out-of-plumbness along G3 at M_p based 1/3 rule load level.

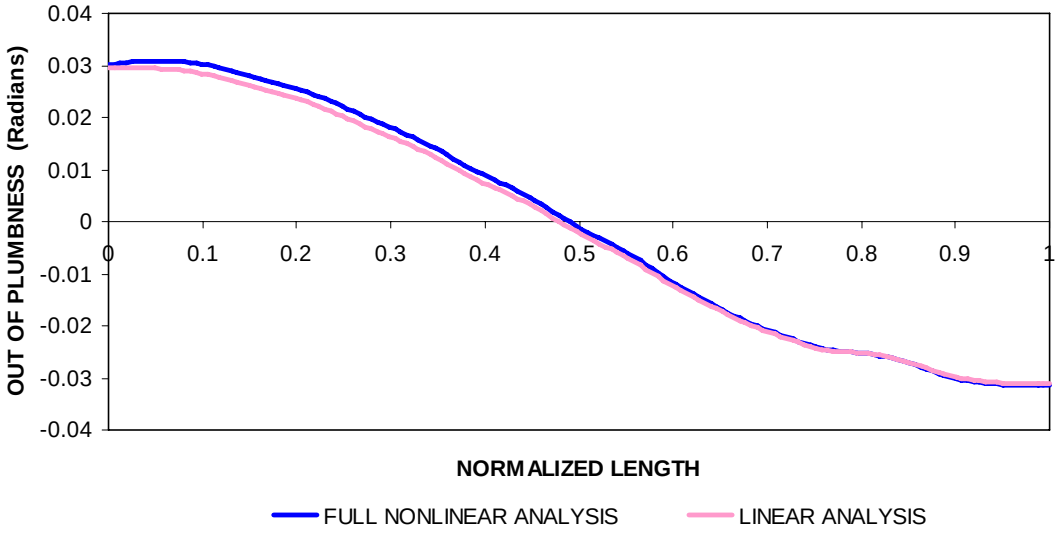

Figure 4.4.8. Out-of-plumbness along G6 at M_p based 1/3 rule load level.

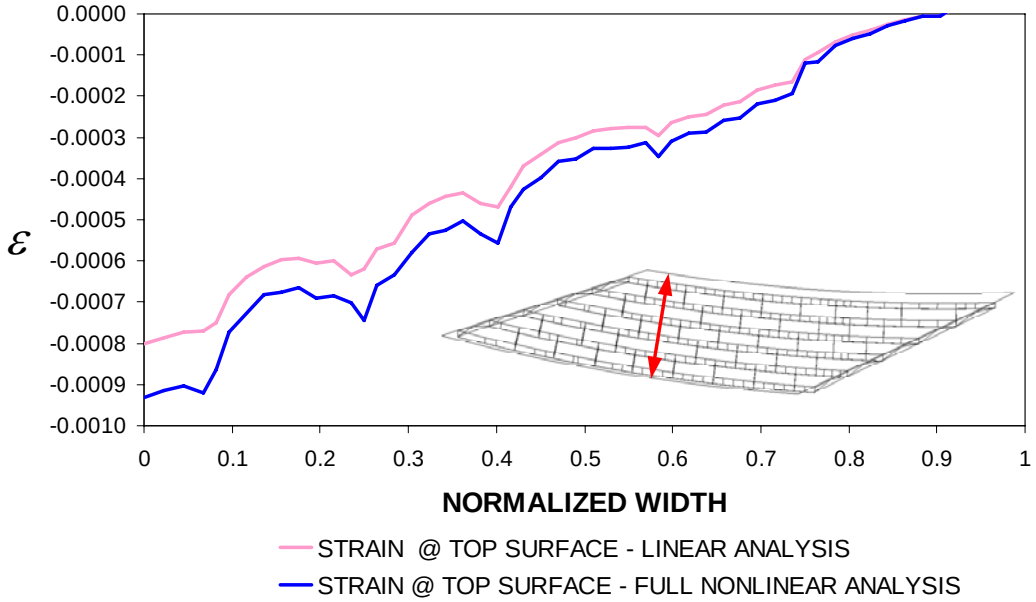

Figure 4.4.9. Longitudinal slab strains along the width of G1-S1 at M_p based 1/3 rule load level.

Figure 4.4.10 shows the normalized equivalent plastic strain variation along G1 at the M_p based 1/3 rule load level. Equivalent plastic strains are monitored at the outside, middle and inside fibers of the bottom flanges. The maximum equivalent plastic strain is 3.6 times the yield strain at the outside tip, 1.7 times the yield strain at the inside tip and 1.9 times the yield strain at the middle. All maximum strain values are observed at the bracing locations.

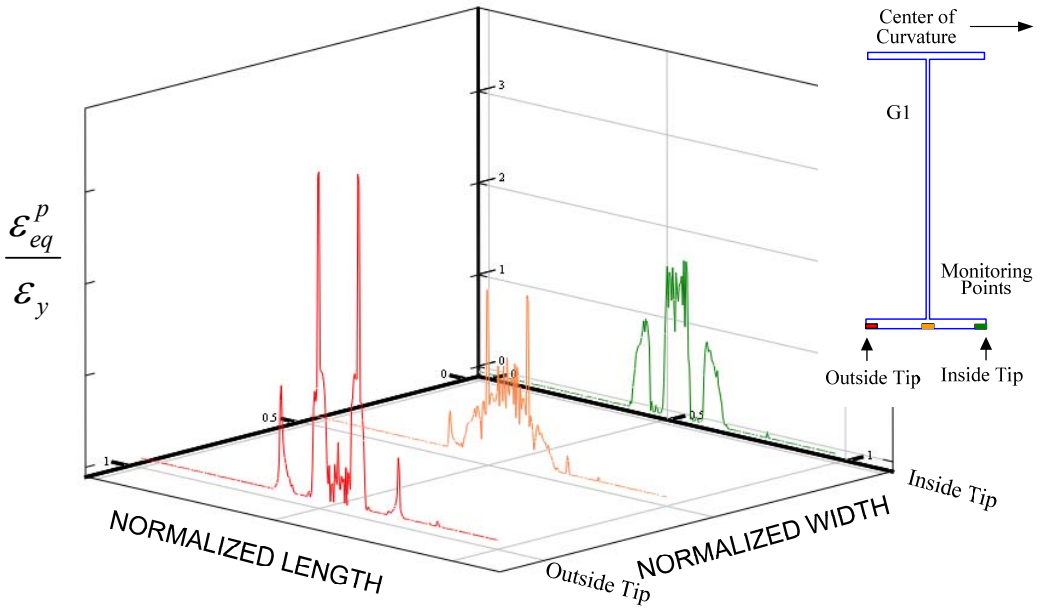

Figure 4.4.10. Normalized equivalent plastic strain along G1 at M_p based 1/3 rule load level.

Figure 4.4.11 shows the normalized strain variation at the bottom flange of section G1-S1 under different fractions of the factored live load. Again the strains are monitored at the outside, middle and inside fiber of the bottom flange. Also, Fig. 4.4.12 presents the normalized major-axis bending strain at the bottom flange of G1-S1 under different

fractions of the factored live load. Fig. 4.4.13 shows the normalized bottom flange lateral bending strain at G1-S1 under different fractions of the factored live load. The major-axis bending strain for G1-S1 at the M_p based 1/3 rule load level is 1.7 times the yield strain when the full nonlinear analysis is considered whereas it is 1.2 times the yield strain when the elastic analysis is considered. The flange lateral bending strain for G1-S1 at the M_p based 1/3 rule load level is 0.5 times the yield strain when the full nonlinear analysis is considered whereas it is 0.07 times the yield strain when the elastic analysis is considered.

Figures 4.4.14 and 4.4.15 show the vertical reactions under different fractions of the factored live load. Since the bridge is statically determinate, the radial reaction forces are found to be small or negligible. Thus they are not reported in this study.

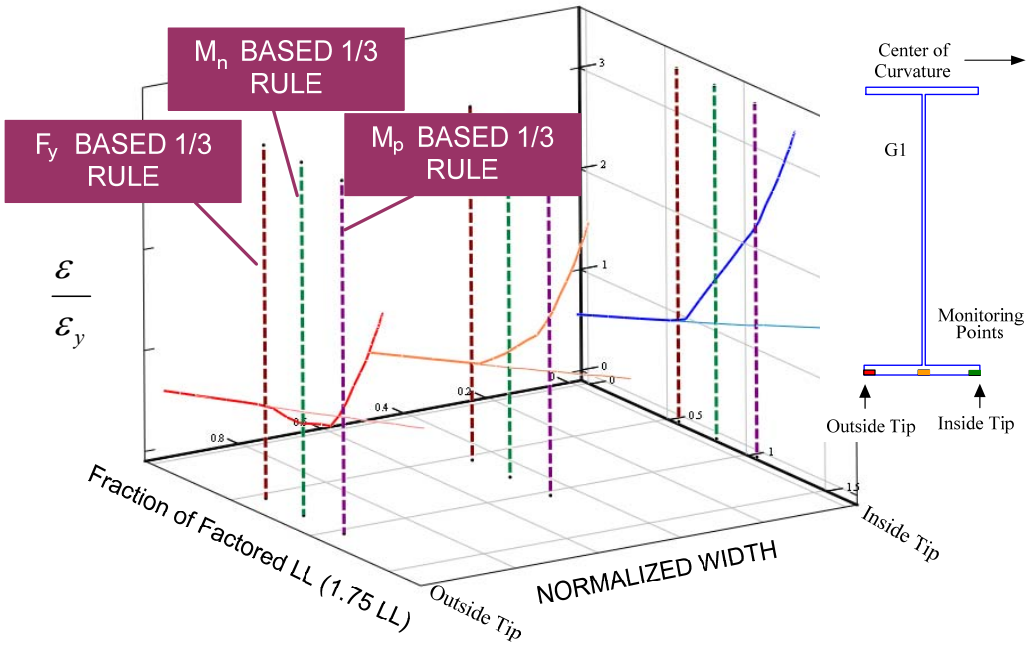

Figure 4.4.11. Normalized bottom flange strain at G1-S1.

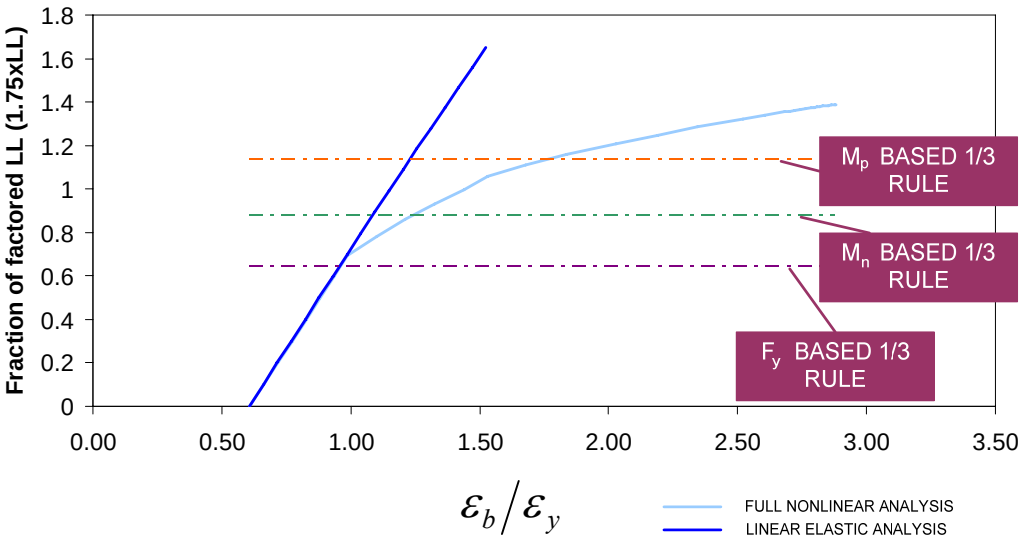

Figure 4.4.12. Normalized major-axis bending strain at bottom flange of G1-S1.

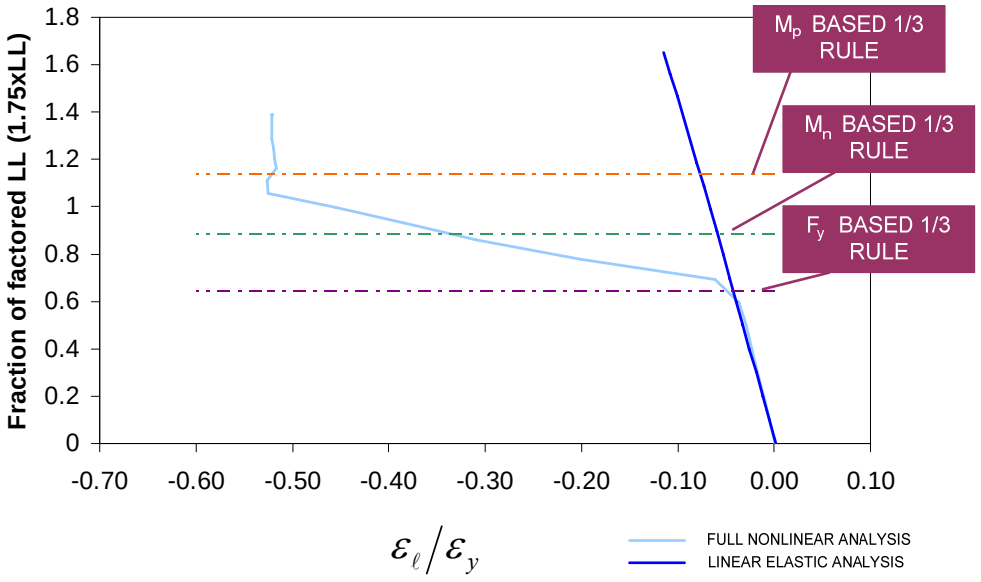

Figure 4.4.13. Normalized bottom flange lateral bending strain at G1-S1.

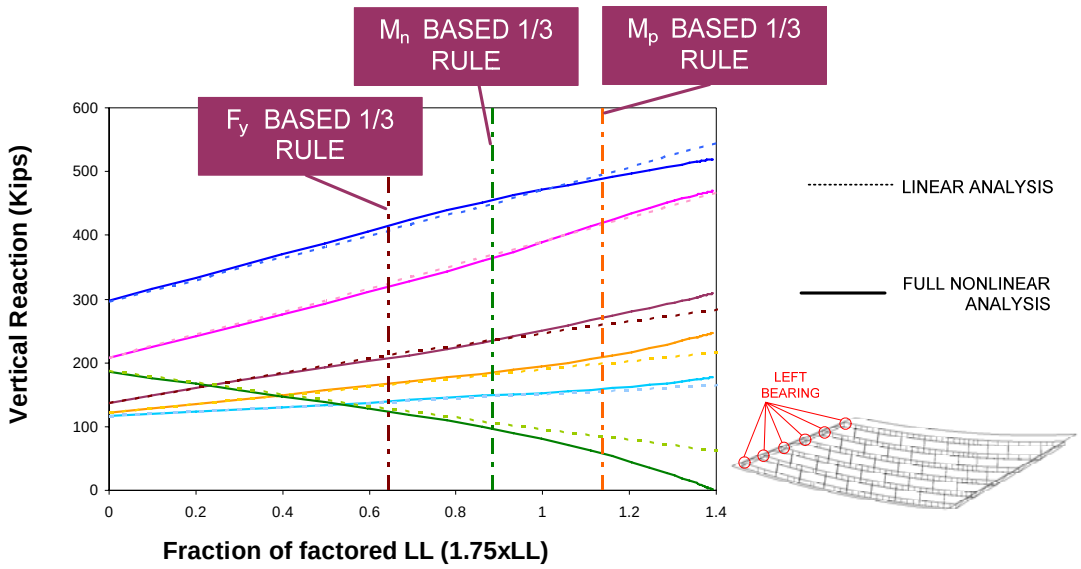

Figure 4.4.14. Vertical reactions at left bearing under different load levels.

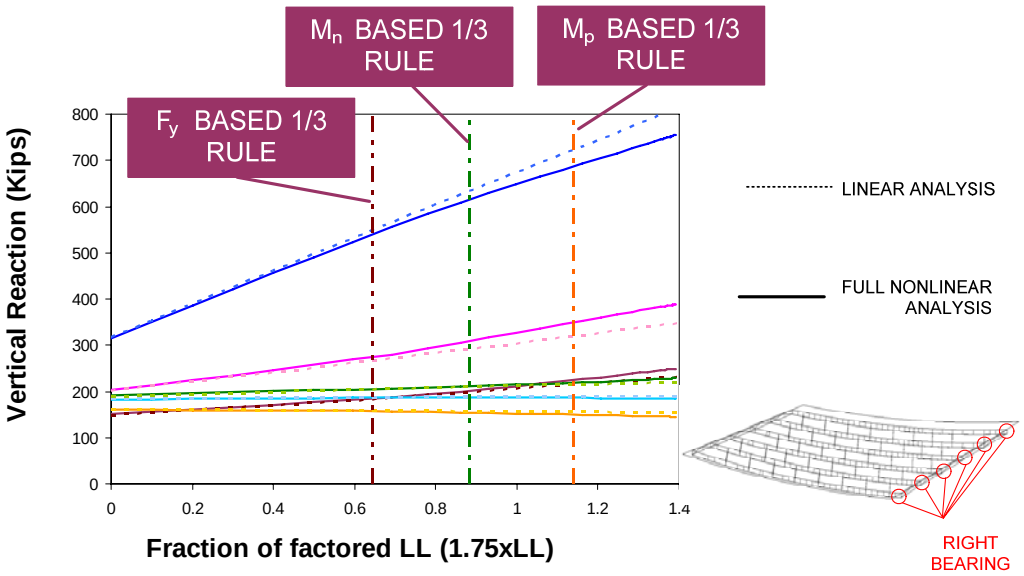

Figure 4.4.15. Vertical reactions at right bearing under different load levels.

The member forces of the selected cross-frames are monitored under the critical STRENGTH I load combination for G1-S1. It is found that the highest nonlinearity in the axial force is occurs in CF-203 under the different fractions of the factored live load. Therefore, the axial force variation at this cross-frame is investigated in a detailed fashion by conducting several types of analyses. Figure 4.4.16 shows the axial forces in the members of CF-203 obtained from the linear elastic analysis, geometric nonlinear analysis and full nonlinear analysis using the 3-D beam-shell FEA model. Furthermore, Fig. 4.4.17 compares the axial forces in the members of CF-203 determined using the geometrically nonlinear 3-D beam-shell and 3-D grid models.

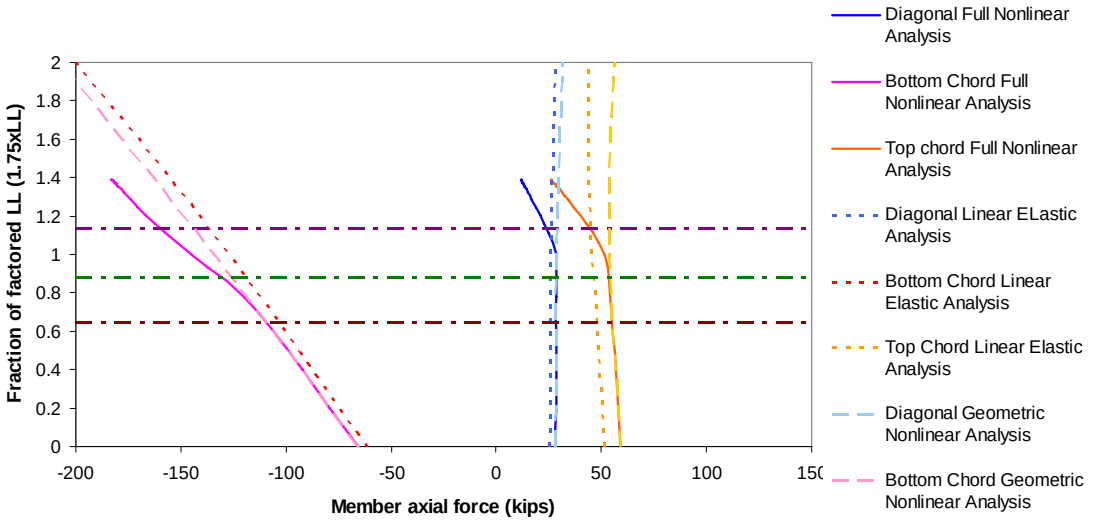

Figure 4.4.16. Axial force variation at CF-203 from 3-D beam-shell model.

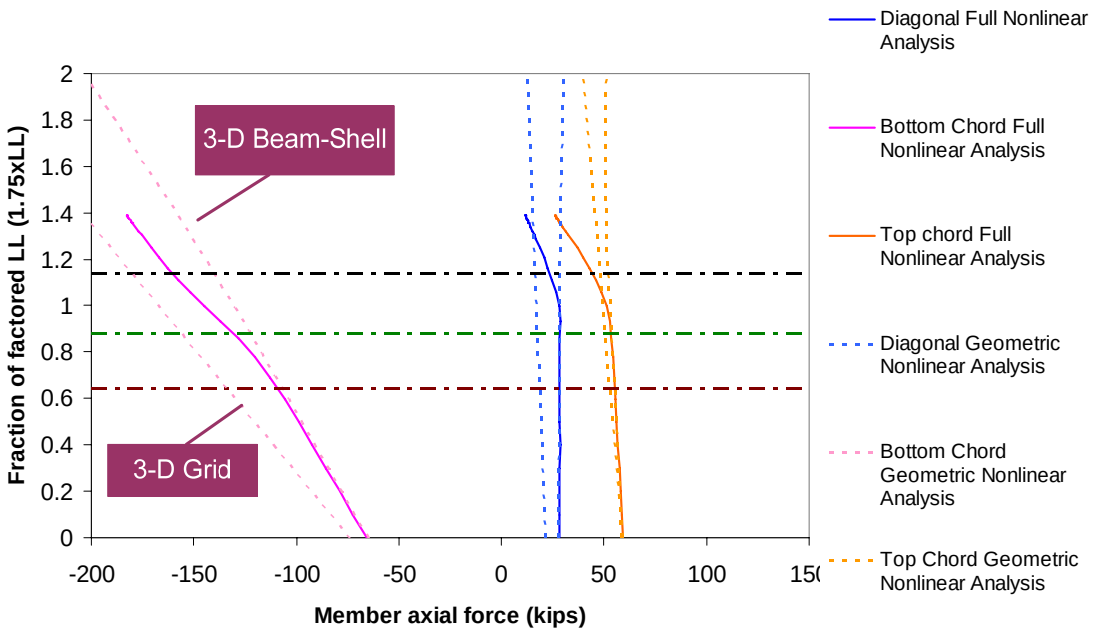

Figure 4.4.17. Axial force variation at CF-203 from 3-D beam-shell model and 3-D grid model.

4.5 Evaluation of G3

Although, the M_p based 1/3 rule load level is targeted for G3-S1, this level can not be achieved as the analysis halted before G3-S1 reaches its yield capacity. This is due to the critical live load position for G3-S1 which is positioned close to the outside girder (See Figs. 2.4.42 and 2.4.43). Outside girder reaches its capacity before G3 reaches its desired load level. Therefore, the internal moment at the mid-length of G1 is also monitored. Figure 4.5.1 shows the internal moments under different fractions of the factored live load at the mid-length of the outside girder and G3-S1. The F_y based 1/3 rule load level which is 1.98 times the factored live load, is shown for G3-S1 in Fig. 4.5.1. Additionally, the M_n based 1/3 rule load level is calculated as $1.25(DC1+DC2)+1.5DW$ plus 3.13 times the factored live load. The M_p based 1/3 rule load level is calculated as

$1.25(DC1+DC2)+1.5DW$ plus 3.54 times the factored live load. Figures 4.5.2 and 4.5.3 present the vertical reactions under different fractions of the factored live load.

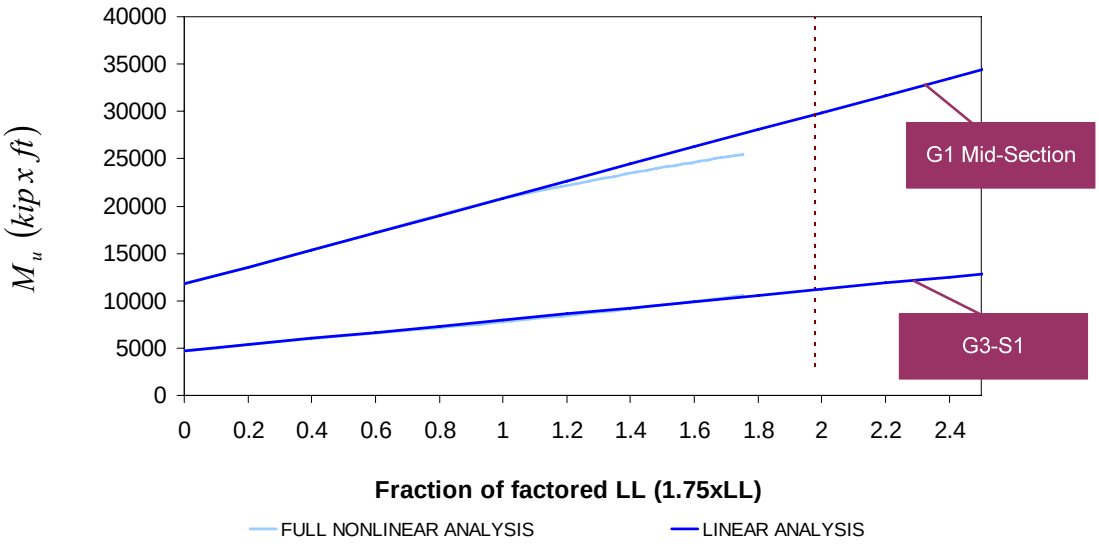

Figure 4.5.1. Internal Moment at the mid-section of the outside girder and G3-S1.

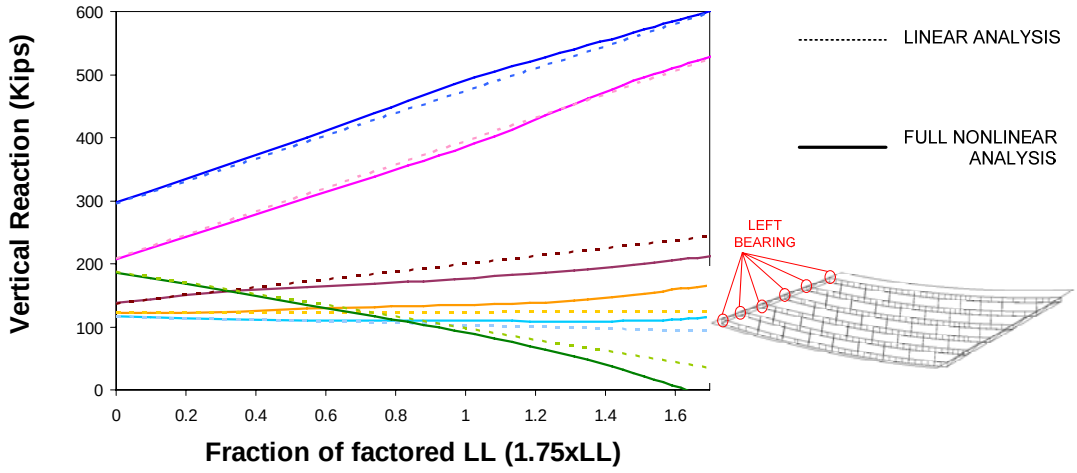

Figure 4.5.2. Vertical reactions at left bearing under different fractions of live load level.

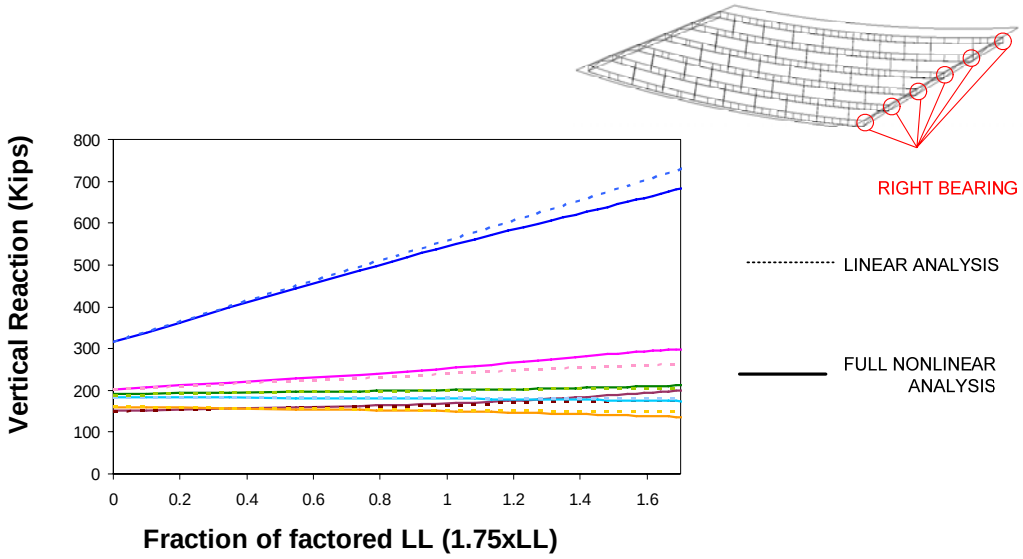

Figure 4.5.3. Vertical reactions at left bearing under different fractions of live load level.

The normalized major-axis bending strain and the normalized lateral bending strain at the mid-length of G1 are illustrated in Figs. 4.5.4 and 4.5.5. Also, the normalized major-axis bending strain and the normalized lateral bending strain at G3-S1 are illustrated in Figs. 4.5.6 and 4.5.7. Figure 4.5.8 shows the vertical displacements at G3-S1. Additionally, the radial displacements are presented in Fig. 4.5.9. Since the analysis is halted below desired load levels, the responses for G3-S1 are investigated at the load level which the analysis is ended. Figure 4.5.10 shows the theoretical fully-plastic strength curve, the M_p based one third rule, the F_y based one third rule for G3-S1 and the normalized flange lateral bending stress level at G3-S1. This stress level is obtained from the design checks which are presented in Section 2.5. Also, the theoretical fully-plastic strength curve for G3-S1 is determined based on Yoo et al. (1997). Additionally, Fig. 4.5.11 shows the normalized internal moment versus the normalized lateral bending strain at G3-S1.

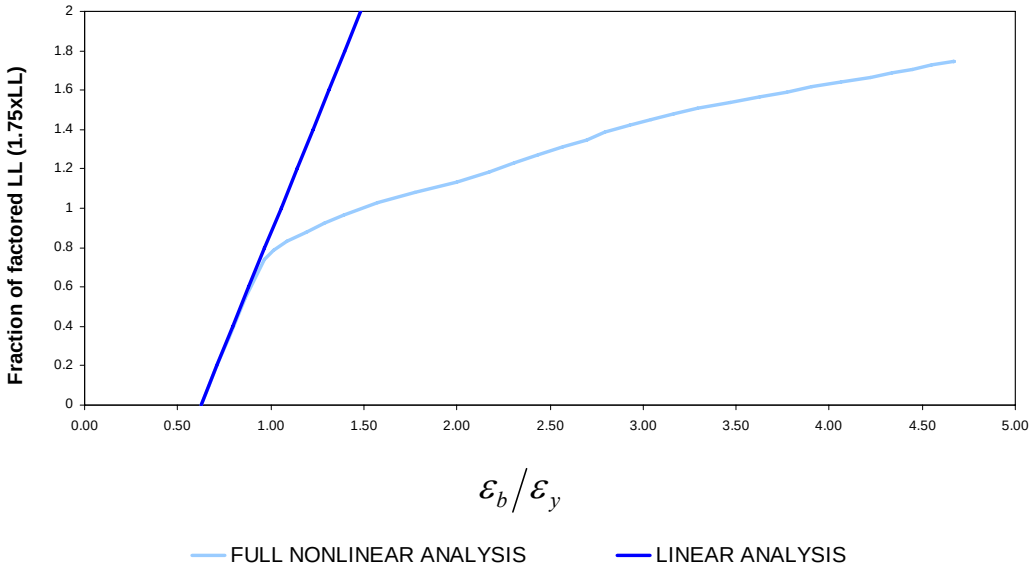

Figure 4.5.4. Normalized major-axis bending strain at bottom flange of mid-section of G1.

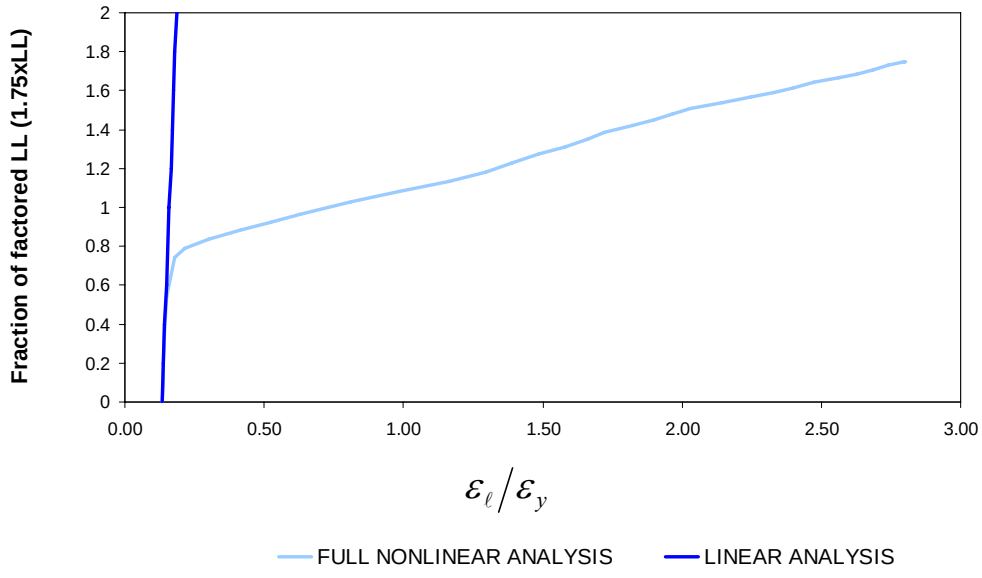

Figure 4.5.5. Normalized bottom flange normalized lateral bending strain at mid-section of G1.

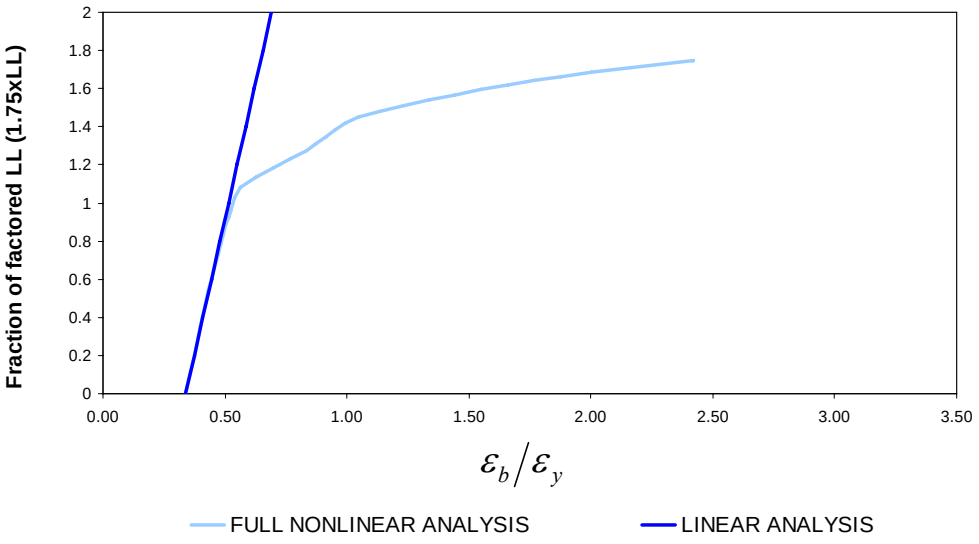

Figure 4.5.6. Normalized major-axis bending strain at bottom flanges of G3-S1.

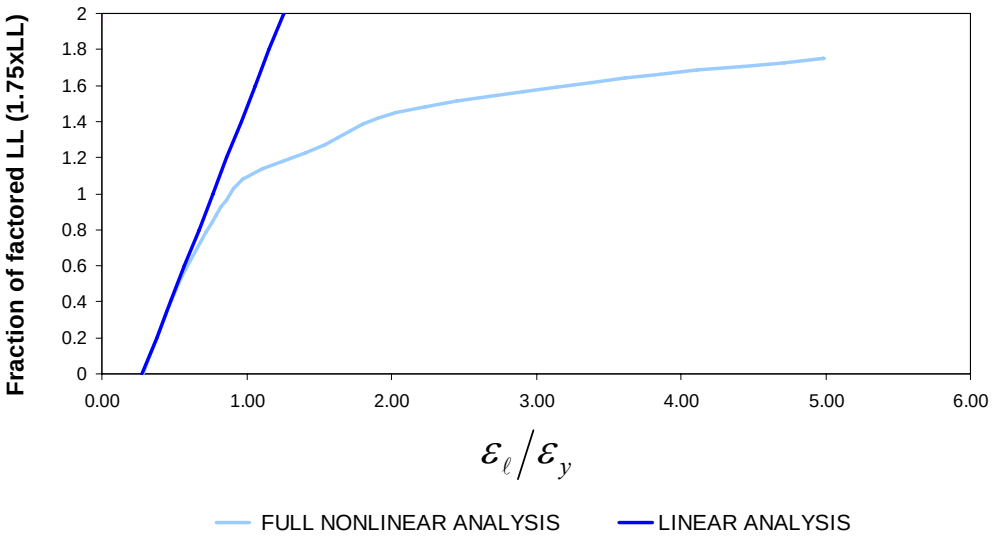

Figure 4.5.7. Normalized bottom flange lateral bending strain of G3-S1.

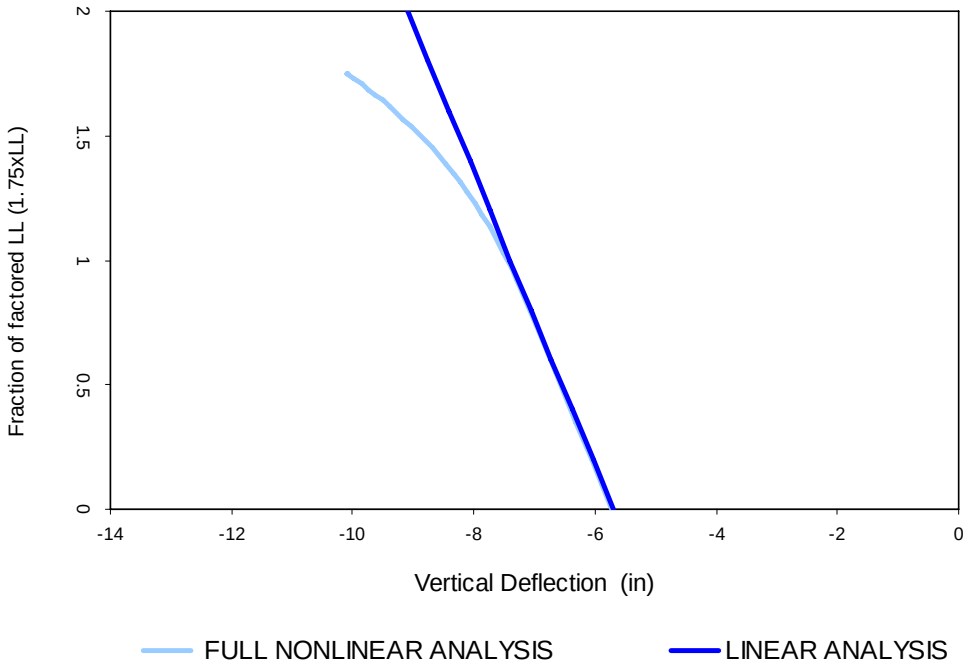

Figure 4.5.8. Vertical deflection at G3-S1 under different fractions of factored live load

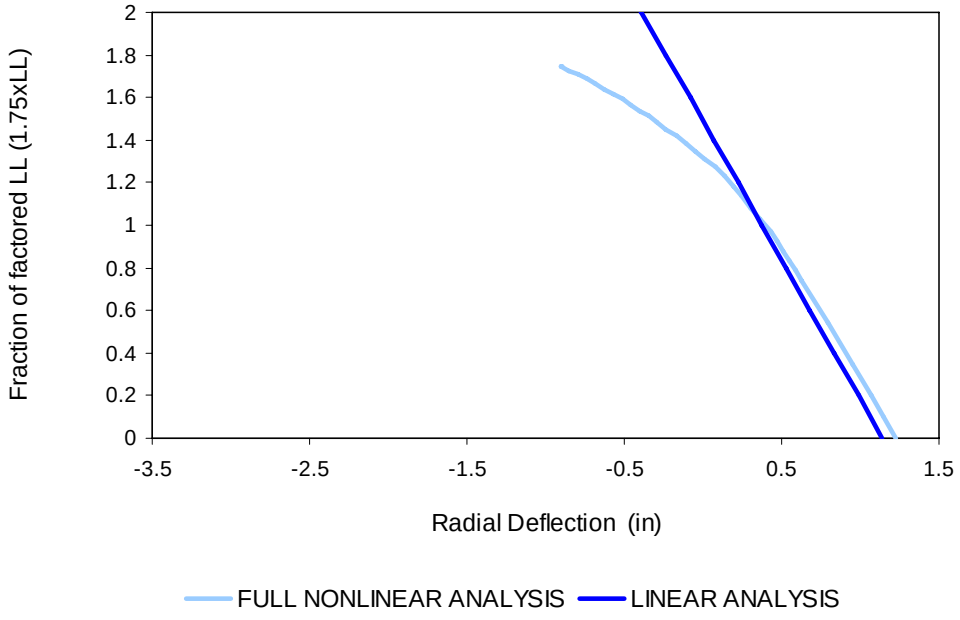

Figure 4.5.9. Radial deflection at G3-S1 under different fractions of factored live load

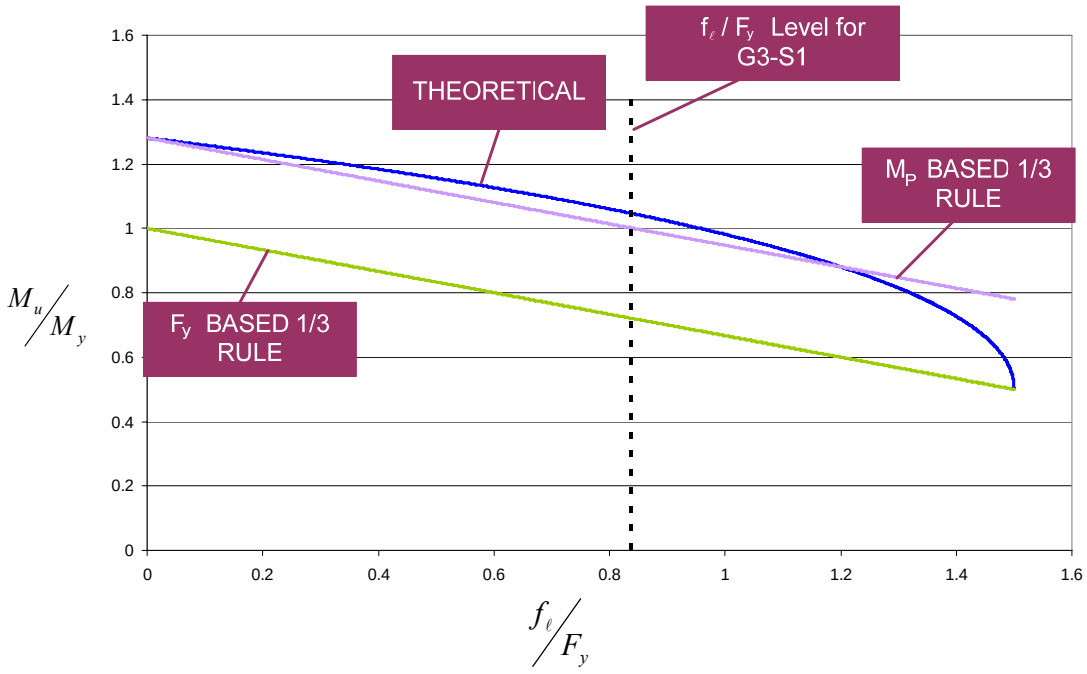

Figure 4.5.10. Comparison of theoretical fully-plastic strength, M_p based one third rule and F_y based one third rule for G3-S1.

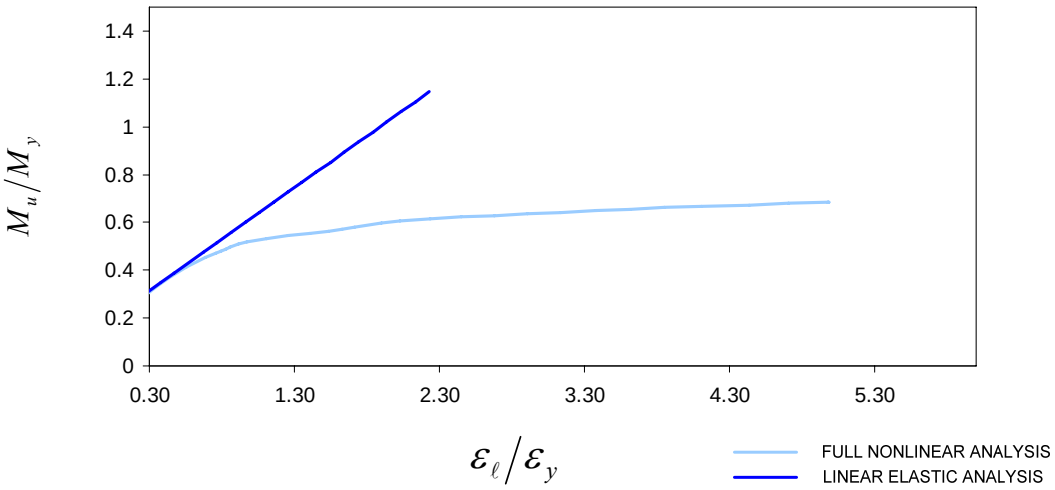

Figure 4.5.11. Normalized internal moment versus normalized bottom flange lateral bending strain at G3-S1.

4.6 Evaluation of G6

The strength behavior of G6 is investigated at section G6-S1 where the maximum strength unity check is observed under the critical STRENGTH I load combination for this girder. Figure 4.6.1 shows the vertical deflections and Fig. 4.6.2 shows the radial displacements at G6-S1 under different fractions of the factored live load. The vertical deflection of G6-S1 at the M_p based 1/3 rule load level is 18 inches when the full nonlinear analysis is considered whereas it is 16.3 inches based on the elastic analysis.

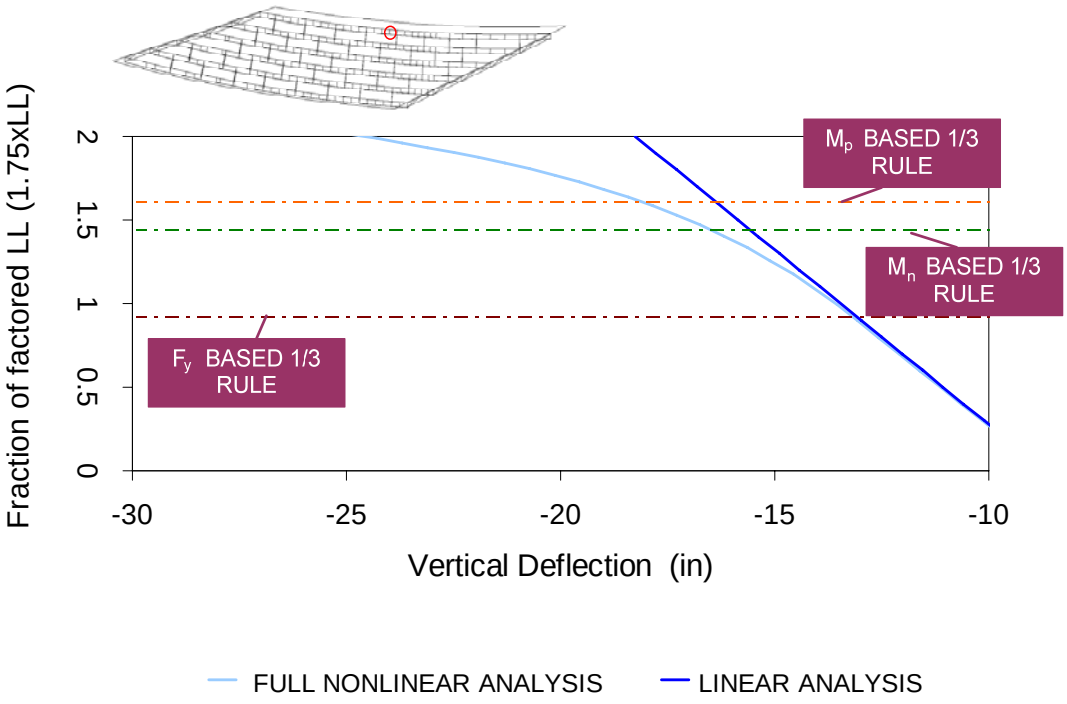

Figure 4.6.1. Vertical deflection at G6-S1 under different fractions of factored live load

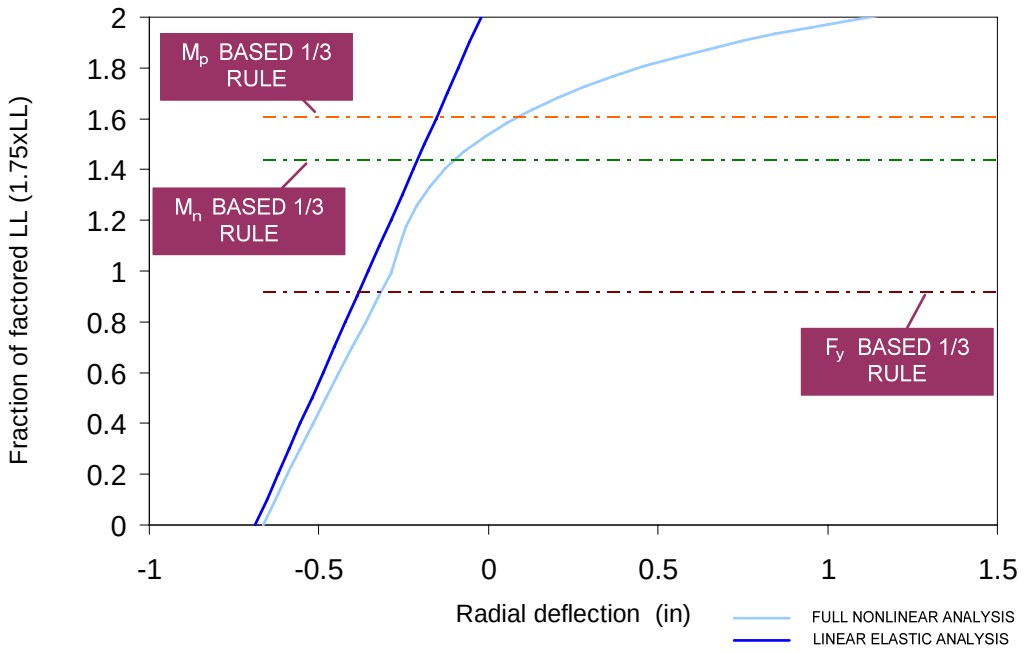

Figure 4.6.2. Radial deflection at G6-S1 under different fractions of factored live load.

Figure 4.6.3 illustrates the internal moments at G6-S1 for different load levels. Figures 4.6.4 and 4.6.5 present the normalized bottom flange major axis bending and flange lateral bending strains along the length of G6 at the M_p based 1/3 rule load level. The maximum bottom flange major-axis bending strain is 2.4 times the yield strain. The maximum flange lateral bending strain is 1.6 times the yield strain. Both maximums are observed at the bracing points. Figures 4.6.6 through 4.6.8 show the web out-of-plumbness of G1, G3 and G6 at the M_p based 1/3 rule load level. Also, the slab top surface strains are plotted along the radial line across the width of the bridge at G6-S1 at the M_p based 1/3 rule load level and are illustrated in Fig. 4.6.9.

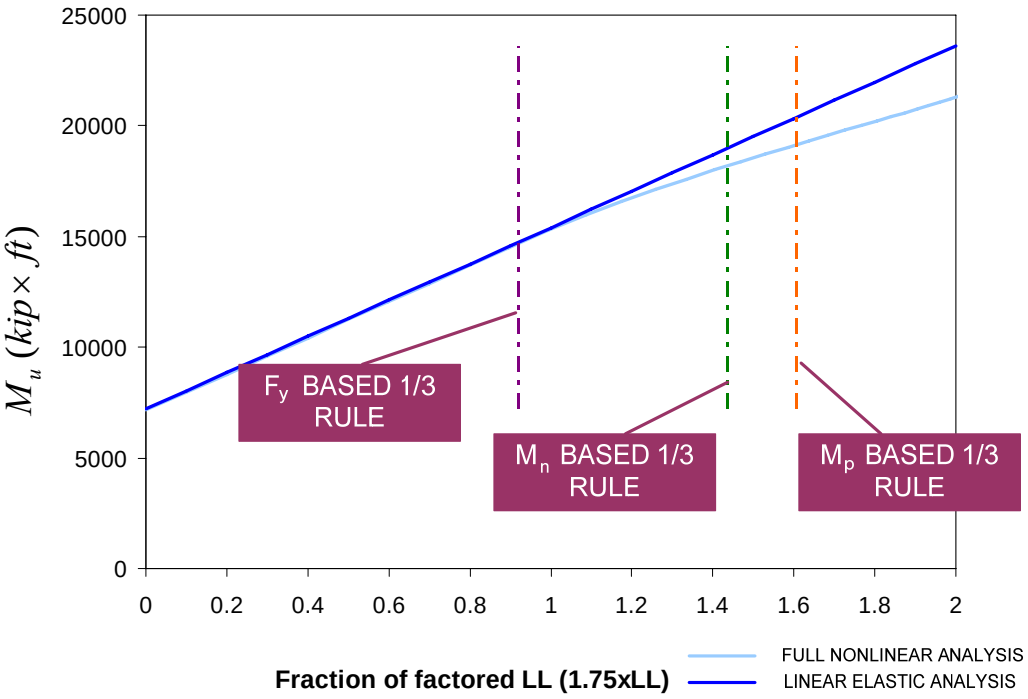

Figure 4.6.3. Internal moments at G6-S1 under different fractions of factored live load.

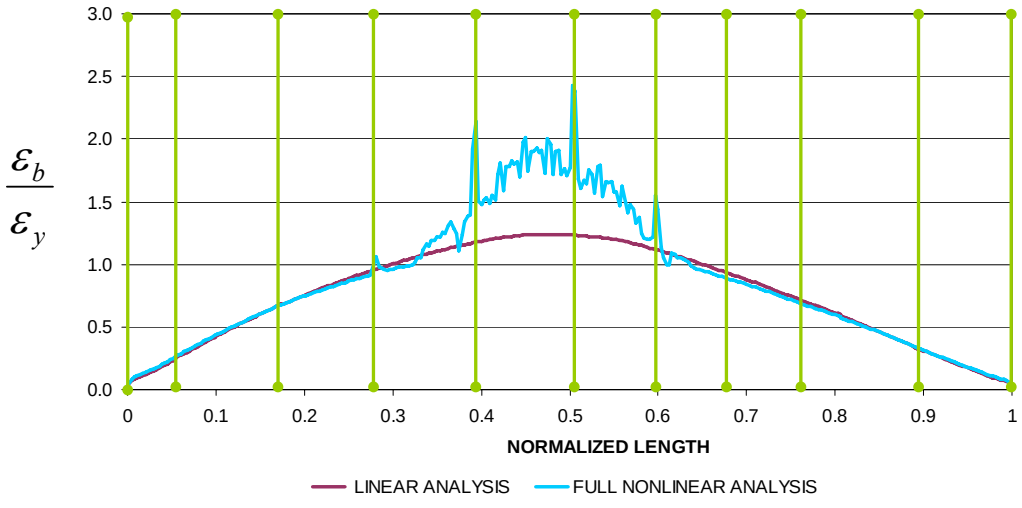

Figure 4.6.4. Normalized major-axis bending strain along G6 at M_p based 1/3 rule load level.

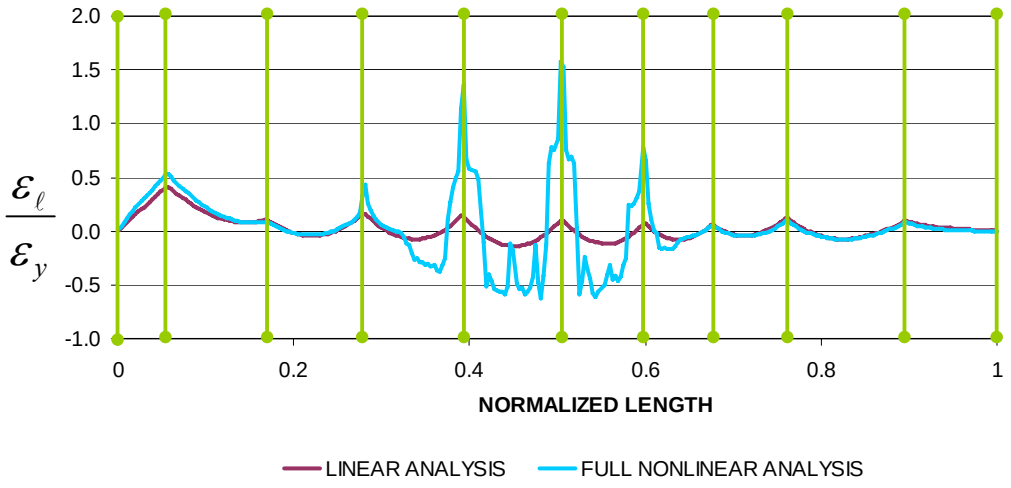

Figure 4.6.5. Normalized flange lateral bending strain along G6 at M_p based 1/3 rule load level.

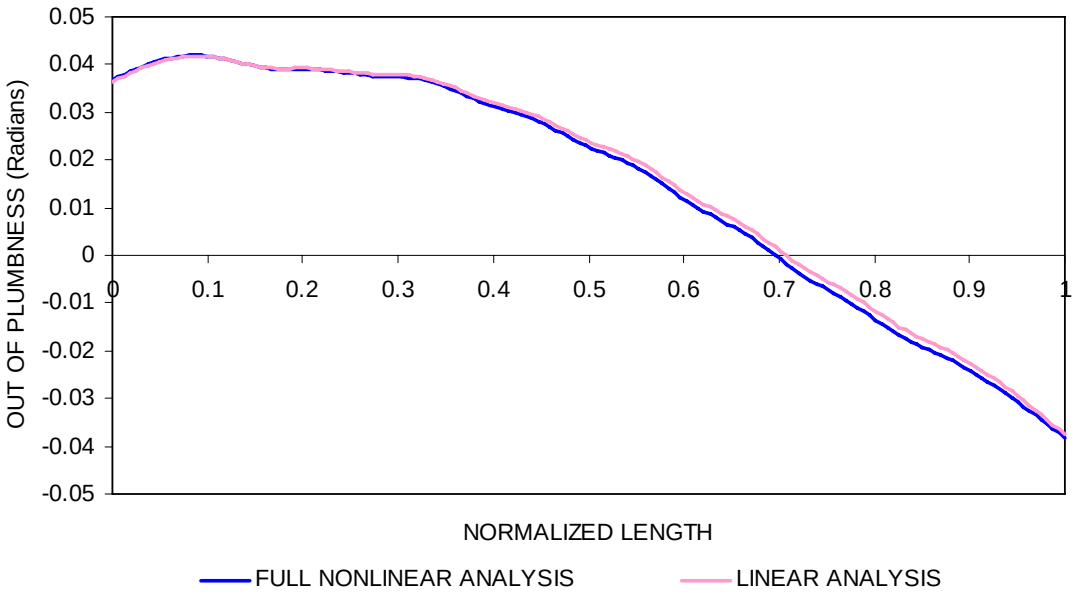

Figure 4.6.6. Out-of-plumbness along G1at M_p based 1/3 rule load level.

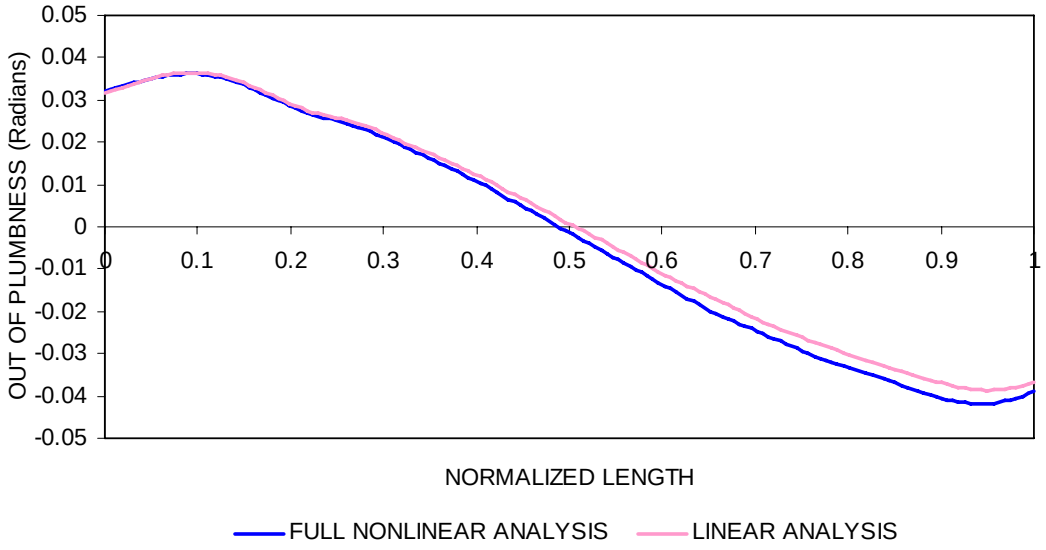

Figure 4.6.7. Out-of-plumbness along G3 at M_p based 1/3 rule load level.

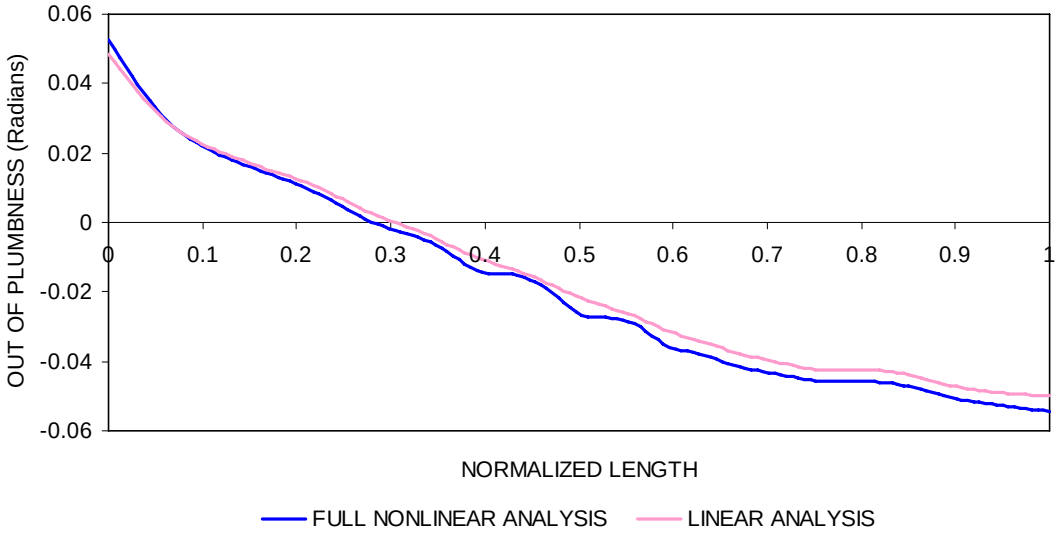

Figure 4.6.8. Out-of-plumbness along G6 at M_p based 1/3 rule load level.

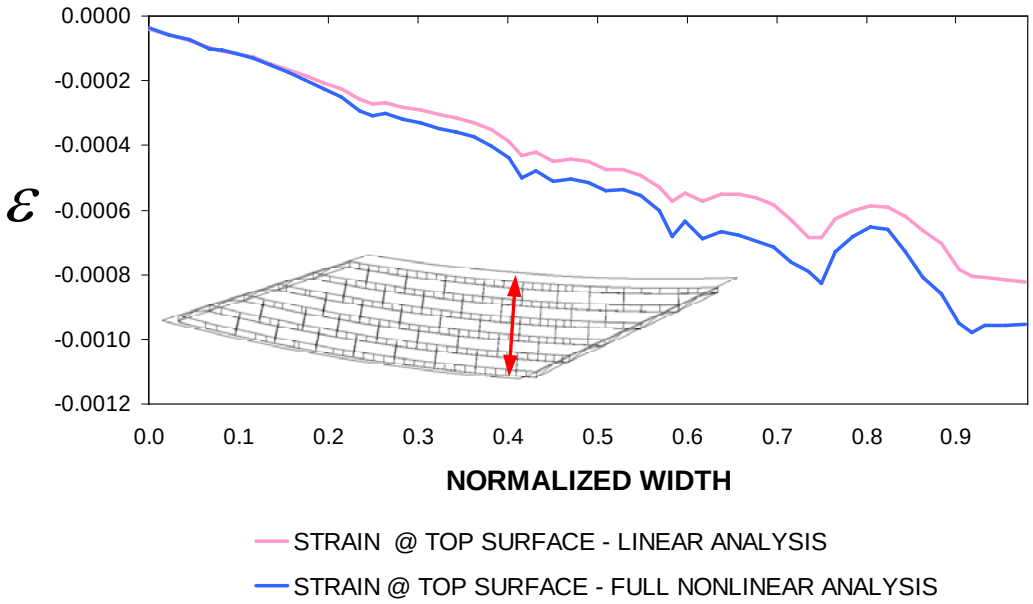

Figure 4.6.9. Slab strains along the width of G6-S1 at M_p based 1/3 rule load level.

The normalized equivalent plastic strain variation along G6 at the M_p based 1/3 rule load level is presented in Fig. 4.6.10. The maximum equivalent plastic strain is 3.3 times the yield strain at the outside tip, 1.6 times the yield strain at the inside tip and 1.7 times the yield strain at the middle. Moreover, Fig. 4.6.11 shows the normalized strain variation at the bottom flange of G6-S1 under different fractions of the factored live load. Figure 4.6.12 presents the normalized major-axis bending strain at the bottom flange of G6-S1 and Fig. 4.6.13 shows the normalized bottom flange lateral bending strain at G6-S1 under different fractions of the factored live load. The major-axis bending strain at G6-S1 is 2.1 times the yield strain at the M_p based 1/3 rule load level when the full nonlinear analysis is considered whereas it is 1.27 times the yield strain when the elastic analysis is considered. In addition, the flange lateral bending strain at G6-S1 is 0.5 times

the yield strain at the M_p based 1/3 rule load level when the full nonlinear analysis is considered whereas it is 0.07 times the yield strain when the elastic analysis is considered. Moreover, Figs. 4.6.14 and 4.6.15 show the vertical reactions under different fractions of the factored live load. The member forces of the selected cross-frames are monitored under the critical STRENGTH I load combination for G6-S1. It is found that the highest nonlinearity in the axial force occurs at CF-305 under different fractions of the factored live load. Figure 4.6.16 compares the axial forces in the members of CF-305 determined using the geometrically nonlinear 3-D beam-shell model.

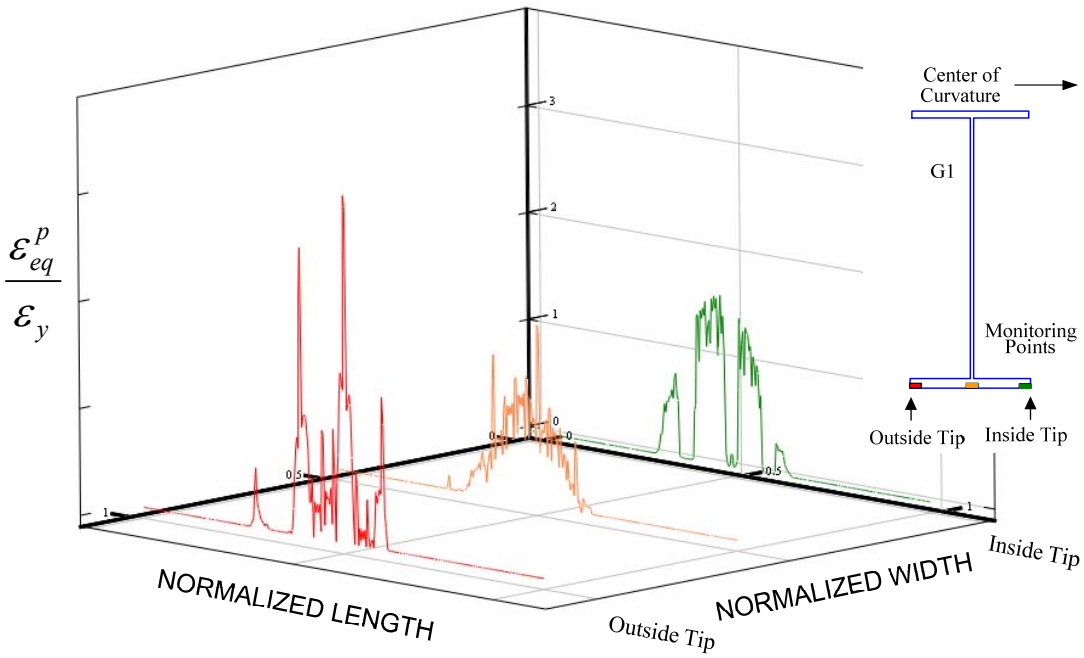

Figure 4.6.10. Normalized equivalent plastic strain along G6 at M_p based 1/3 rule load level.

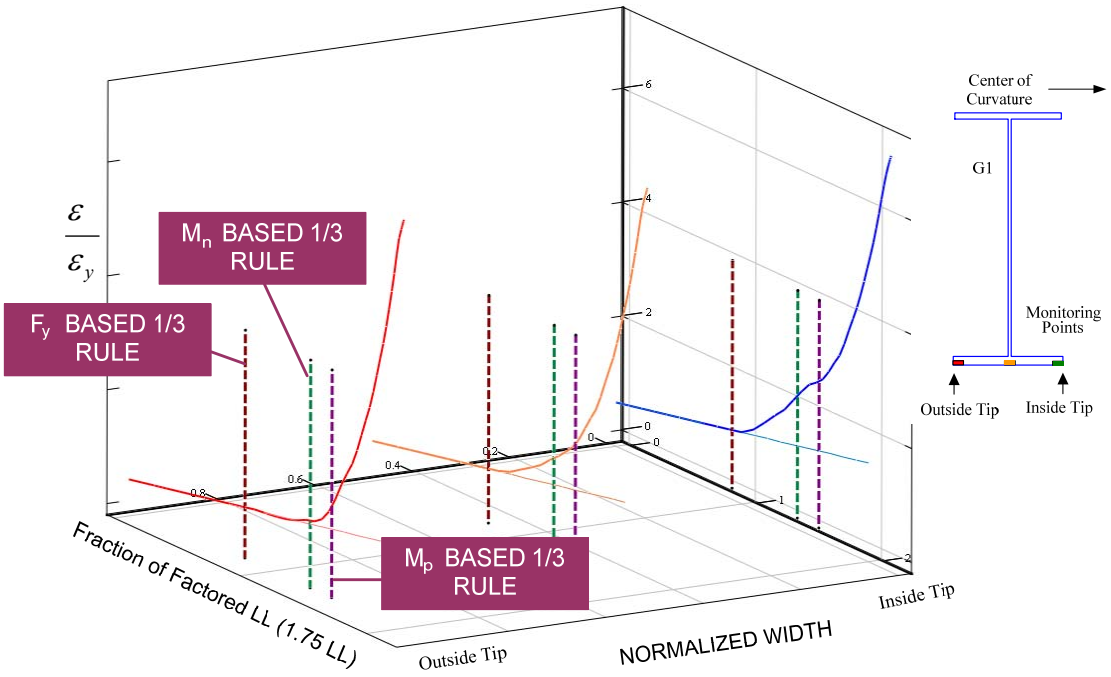

Figure 4.6.11. Normalized strain at the bottom flanges of G6-S1.

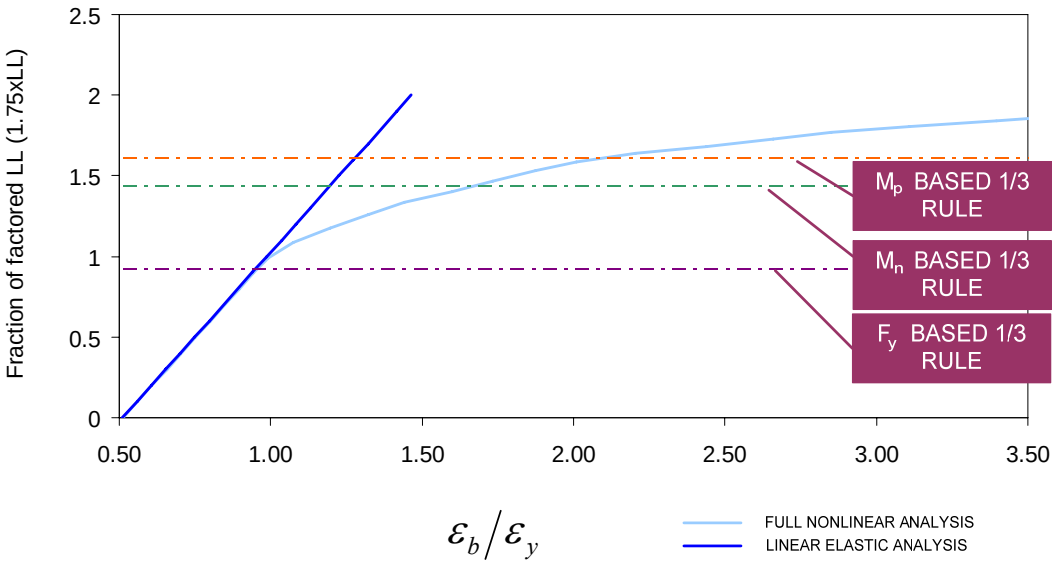

Figure 4.6.12. Normalized major-axis bending strain at the bottom flange of G6-S1.

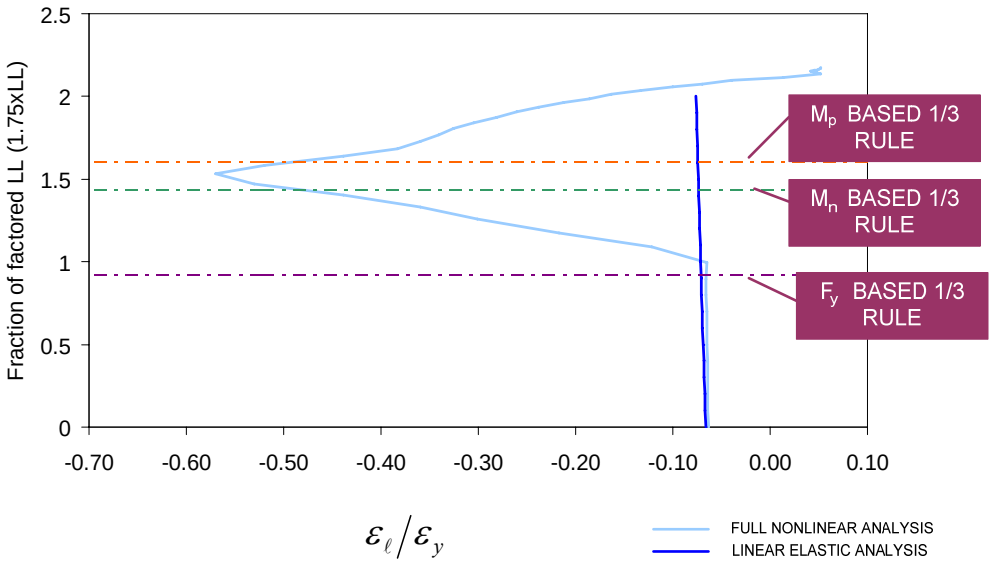

Figure 4.6.13. Normalized bottom flange lateral bending strain at G6-S1.

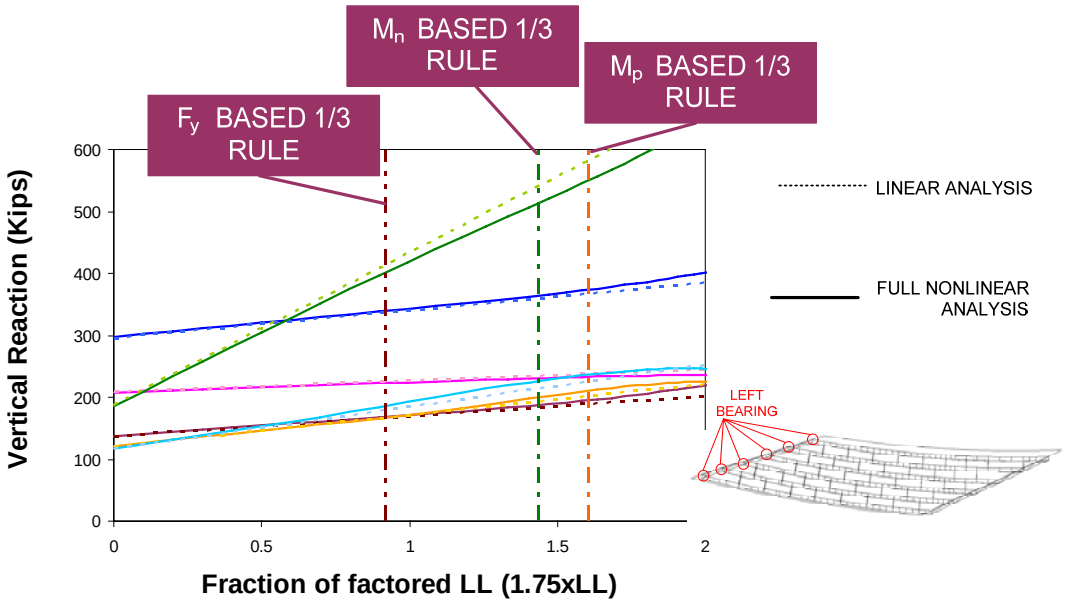

Figure 4.6.14. Vertical reactions at left bearing under different load levels.

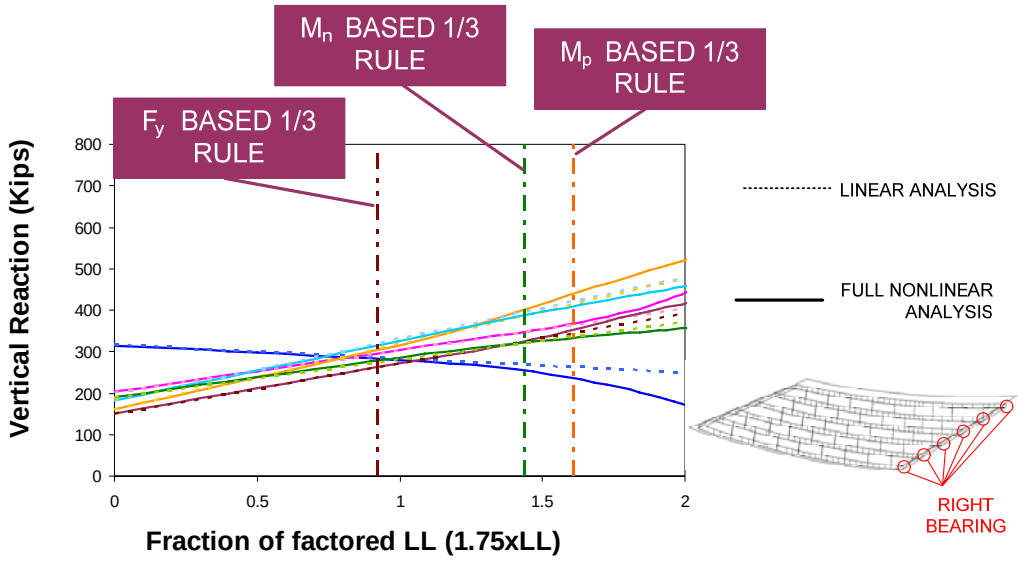

Figure 4.6.15. Vertical reactions at right bearing under different load levels.

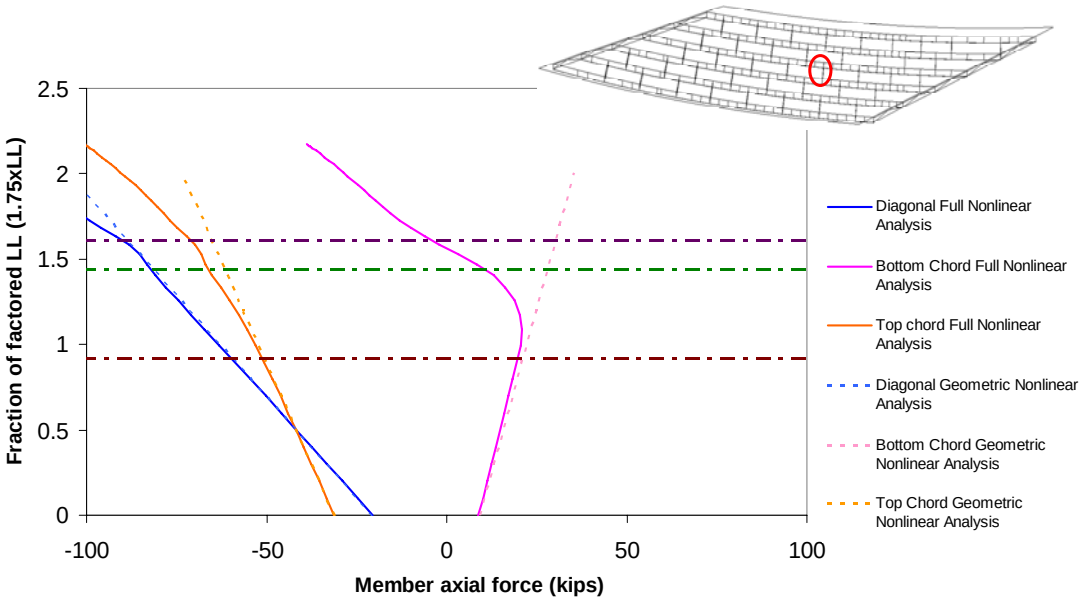

Figure 4.6.16. Axial force variation at CF-305 from 3-D beam-shell model.

4.7 Evaluation of CF-107 & CF-203

In this section critical STRENGTH I load combinations for CF-107 and CF-203 (See Figs. 2.4.49 through 2.4.52) are applied to the bridge and full nonlinear analyses are conducted. The full nonlinear analysis results are compared with the linear analysis results at the STRENGTH I load level for both cross-frames. Figure 4.7.1 shows the axial forces for the members of CF-107 from the full nonlinear and linear analyses. Additionally, Fig. 4.7.2 presents the axial forces for the members of CF-203 from the full nonlinear and linear analyses.

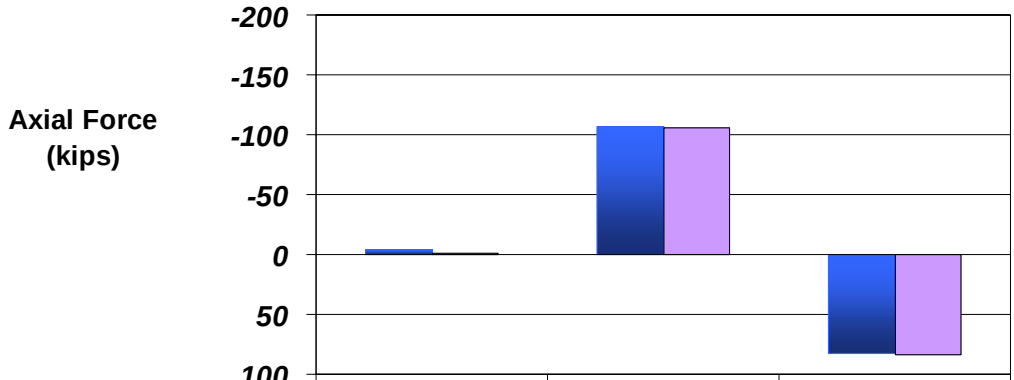

	Bottom Chord	Diagonal	Top Chord
Full Nonlinear Analysis	-3.5	-107.2	83.2
Linear Analysis	-0.6	-106.0	83.4

Figure 4.7.1. Axial forces for the members of CF-107 from full nonlinear and linear analyses (STRENGTH I load level).

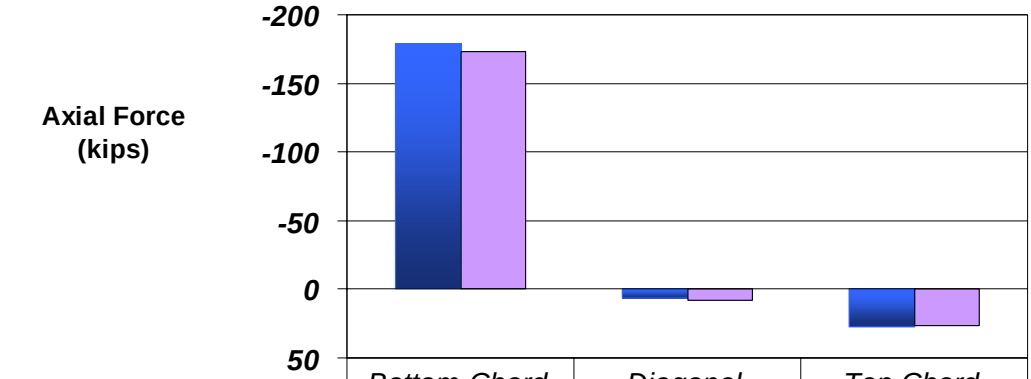

	Bottom Chord	Diagonal	Top Chord
Full Nonlinear Analysis	-179.3	6.5	27.5
Linear Analysis	-172.9	7.7	26.3

Figure 4.7.2. Axial forces for the members of CF-203 from full nonlinear and linear analyses (STRENGTH I load level).

4.8 Synthesis of Full Nonlinear Results

In this section, the full nonlinear analysis results are compared with the linear analysis results to understand the strength behavior of the bridge. To begin with the facia girders, significant yielding is observed near the mid-length of G1 and G6 at M_p based 1/3 rule load level. (See Figs. 4.4.4, 4.4.5, 4.6.4 and 4.6.5). Also, the major-axis bending and flange lateral bending strains peak at the cross-frame locations and mid cross-frame locations. Although the major-axis and lateral bending strain plots give useful understanding about the regions subjected to higher strains, they do not show the regions where the strains exceed the flange yield strain. Therefore, the equivalent plastic strains which are shown in Figs. 4.4.10 and 4.6.10 are included to illustrate the spread of yielding in the steel sections. It is clear that there is significant yielding near the mid-length of the bridge and the yielding is greatest at several cross-frame locations on the outside tips of the G1 and G6 bottom flanges at the M_p-based 1/3 rule load level. Additionally, it should be noted that the entire bottom flange is yielded near the mid-length. Moreover, it can be seen from Figs. 4.4.11 and 4.6.11 that the outside tip strains of the bottom flanges are smaller than the inside tip and middle strains of the bottom flanges at G1-S1 and G6-S1 under the same fraction of factored live load. This is due to the fact that flange lateral bending moments reduce the tensile strains in the outer part of the flanges at the sections that have the largest strains.

Figure 4.4.3 shows that internal moments at G1-S1 start to decrease at the load level of 0.78 times the factored live load plus $1.25(DC1+DC2)+1.5DW$ due to moment redistribution. Although, the moment redistribution increases with the increasing load, the nonlinearity of the moment redistribution is small relative to the linear predictions up

to the M_p based 1/3 rule load level. Similarly, Fig. 4.6.3 shows the internal moments at G6-S1. The internal moments predicted by the full nonlinear analysis start to deviate from the linear predictions at 1.04 times the factored live load plus $1.25(DC1+DC2)+1.5DW$. Nonetheless, the deviation which is due to redistribution of moments is small relative to the linear prediction at M_p based 1/3 rule load level.

The vertical displacement of the critical sections at G1 and G6 which can be seen at Figs. 4.4.1 and 4.6.1, differ 1.8 inches for the outside girder and 1.7 inches for the inside girder when full nonlinear and linear analyses are compared at the corresponding M_p based 1/3 rule load levels. This difference decreases to 0.59 inches for G1 and 0.86 inches for G6 when the corresponding M_n based 1/3 rule load level is considered. In the same manner, the radial deflections for G1-S1 and G6-S1 that can be seen at Figs. 4.4.2 and 4.6.2 vary 0.77 inches for G1 and 0.217 inches for G6 at the M_p based 1/3 rule load level. Again this difference decreases to 0.19 inches for G1 and 0.152 inches for G6 when the M_n based 1/3 rule load level is considered. Moreover, it is predicted from Figs. 4.4.6 through 4.4.8 and Figs. 4.6.6 through 4.6.8 that the web out-of-plumbness of G1, G3, G6 which are obtained from the full nonlinear and linear analyses match with each other. Most importantly, although the deflections become slightly nonlinear at the M_p based 1/3 rule load level, still there is a good match between the full nonlinear and linear analyses. Figures 4.4.9 and 4.6.9 show the top surface slab longitudinal strains across the width of the bridge at G1-S1 and G6-S1. Both results point out that accumulated strains are within the elastic limit of the defined concrete stress-strain response and are significantly less than the nominal concrete crushing strain of 0.003. Furthermore, it is obvious that these strains vary approximately in a linear fashion across the bridge width.

It should be noted that the major-axis and flange lateral bending strains at G1-S1 and G6-S1, which are illustrated in Figs. 4.4.12, 4.6.12, 4.4.13 and 4.6.13, deviate from the linear predictions at the M_p based 1/3 rule load level. However, this nonlinear variation is not significant relative to the linear predictions. Figures 4.4.14, 4.4.15, 4.6.14, 4.6.15 provide the vertical reactions at the bearings under different fractions of the factored live load. The vertical reactions show slight nonlinearity close to the M_p based 1/3 rule load level. Nonetheless, it is clear that the variation in the girder reactions are predominantly linear up to the M_p based 1/3 rule load level.

To continue with the cross-frames, Figs. 4.7.1 and 4.7.2 illustrate that the axial forces used for the cross-frame member design of CF-203 and CF-107 are not affected from the material and geometric nonlinearity when the critical STRENGTH I load configuration is applied at the M_p load level. Additionally, it is observed from Fig. 4.4.16 that the axial forces of CF-203 increase linearly up to up to the M_n based 1/3 rule load level. On the other hand, the deviation is greater between the full nonlinear and linear analyses up to the M_p based 1/3 rule load level. However, this nonlinearity is not high when compared with the linear results of different models. Figure 4.4.17 illustrates the range of the linear analysis results which is obtained by using different models. It should be noted that the full nonlinear analysis results are between the range of linear analysis results of the two elastic models up to the M_p based 1/3 rule load level. Most importantly, it is clear from Figs. 4.4.16, 4.4.17 and 4.6.16 that the axial forces deviate significantly from the linear predictions after the M_p based 1/3 rule load level is exceeded on G1 and G6. To sum up, the axial forces in the cross-frame members are increased by as much as 13.7 % due to the girder inelasticity in the subject bridge. However, the effect of using the 3D grid

versus the 3D FEA models is larger than the effect of the girder inelasticity in the 3D FEA solutions. The axial force predicted by the 3D grid model is 21.5% higher than those predicted by the 3D FEA model at the M_p-based 1/3 rule load level. Therefore cross-frames should be designed such that they should be capable of ensuring enough strength to resist forces within a range.

Lastly, the flange lateral response of G3-S1 is investigated. It can be seen from Fig. 4.5.1 that the internal moments are linear for G3 whereas they are linear for G1 up to 1.04 times the factored live load plus $1.25(DC1+DC2)+1.5DW$ and then it starts to deviate from the linear predictions. Additionally, Figs. 4.5.2 and 4.5.3 show that the deviations in the vertical forces are significant relative to the linear results at the end of the analysis which is due to significant inelastic moment redistribution. Figure 4.5.4 shows that the major-axis bending strain for the outside girder is 4.7 times the yield strain at the end of the analysis. It should be noted that this maximum major-axis bending strain is 3 times the yield strain when G1-S1 on G1 is evaluated. Therefore, the nonlinearity of the major-axis bending strain is significant relative to the linear predictions. As a conclusion, the critical loading for G3-S1 causes yielding of the outside girder and reaching its capacity at the end of the analysis before G3 reaches to the F_y based 1/3 rule load level.

The flange lateral bending results are investigated for G3-S1. The maximum major-axis bending strain for G3-S1 is 2.43 times the yield strain (See Fig. 4.5.6). Similarly, Fig. 4.5.7 illustrates the nonlinearity of the flange lateral bending strain at G3-S1. The flange lateral bending strains predicted from both analyses are linear up to 1.1 times the factored live load plus $1.25(DC1+DC2)+1.5DW$. Then the full nonlinear

analysis results start to deviate significantly after this point. Furthermore, the deflections are predominantly linear at G3-S1 (See Figs. 4.5.8 and 4.5.9).

Most importantly, Fig. 4.5.10 illustrates that the reduction in the major-axis bending resistance due to the flange lateral bending tends to be higher than the expected based on the $0.6 \times f_\ell$ limit. This is mainly due to the A_f / A_w ratio of the cross-section where A_f is the area of the flange and A_w is the area of the web. This ratio is 1.5 for G3-S1. In addition, the f_ℓ / F_y ratio which is also illustrated in Fig. 4.5.10 is 0.85 for G3-S1 where $0.6 \times f_\ell$ limit is violated slightly. Also, the maximum possible M_u / M_y ratio for G3-S1 is determined from the M_p based 1/3 rule strength curve as 1.01 and this level is investigated from Fig. 4.5.11. It is found that at that level the nonlinearity is predominantly linear. The M_u / M_y ratio is obtained as 0.6 at G3-S1 from the previous design checks (Presented in Section 2.5). It is obvious from Fig. 4.5.11 that if the M_u / M_y ratio equals to 0.6, the nonlinearity in the flange lateral bending strain is small relative to the linear analysis results. As a result, the AASHTO (2007) flange lateral bending stress limit of $0.6 \times F_y$ is a practical maximum lateral bending stress value in most cases; however, due to the more complex plastic strength interaction behavior of composite I-sections in positive bending, this limit is in general, a conservative restriction on the design of these types of sections.

CHAPTER 5

SUMMARY AND CONCLUSIONS

5.1 Summary

This thesis addresses the design procedures and the strength behavior of a representative highly skewed and horizontally curved bridge at and above a number of limits in the AASHTO (2007) Specifications.

A refined 3-D beam-shell FEA model is developed and used for the elastic-design analysis of the subject bridge. Both linear (first-order) and geometric nonlinear (second-order) analyses are conducted on the noncomposite structure during construction. The ABAQUS 6.5.1 software (HKS 2004) is used for these analyses. Stresses, moments and deflections at various sections are obtained throughout the bridge by superposing the DC1, DW, DC2 and LL analysis results. These solutions are checked against the constructability, strength and serviceability limit states required by AASHTO (2007). Single-angle cross-frame compression members are identified and checked using the AISC (2005) procedures as discussed by White (2007). Additionally, the elastic FEA results are compared with the elastic results from refined 3-D grid models implemented in the structural analysis program GT-SABRE (Chang 2006).

Refined full nonlinear analyses are conducted using the same finite element discretization employed in the above elastic FEA solutions. These models are used for investigating the strength behavior of the bridge. The full nonlinear analyses include the simulation of final construction dead load effects on the noncomposite structure followed by the effects of applied loads on the completed composite structure.

The results from these FEA studies are considered with the results of prior studies to arrive at recommendations for the design of horizontally curved and skewed I-girder bridges. Key observations and findings from FEA studies are presented in the following sections.

5.2 Elastic Analysis and Design

- The second-order amplifications are determined from the 3D FEA under the noncomposite dead and construction loadings and are compared with the AASHTO amplification factors. It is found that the second-order amplification of the lateral bending stresses is quite large in the subject bridge compared to the amplification predicted by the AASHTO amplification factors. This is due to the overall torsional deflections of the bridge structure. This effect can be captured only by conducting a second-order analysis of the bridge system. The AASHTO amplification factors are based only on the characteristics of the unbraced lengths between the cross-frame locations.
- It is observed that major-axis bending stresses and deflections are not affected significantly by the geometric nonlinearity whereas the influence of geometric nonlinearity is noticeably high for the flange lateral bending stresses. Since the influence of geometric nonlinearity is obviously important for the noncomposite dead and construction loadings, the responses from the geometric nonlinear (second-order) analysis for these loadings are combined with the responses from the geometrically linear (first-order) analysis for the composite loadings in the design checks.

- The layover of the girders at the bearing lines can be approximated as:

$$\Delta_x = \Delta_z \times Tan(\theta) \tag{5.1}$$

where;

Δ_x = layover

Δ_z = deflection of the top flange at the bearing due to the major-axis bending rotation

θ = skew angle of the considered bearing

If the girder end rotation can be determined accurately by a given type of analysis, the layover can be easily predicted by Eq. 5.1.

- Both stress and moment-based flexural resistance equations are used for checking the strength limit states. The reduction in the strength ratio by using the AASHTO moment-based flexural resistance equation is determined for a number of critical sections for the subject bridge. The reduction in the strength ratio is 15% for the section G1-S1. This section has the maximum unity check among the critical sections.
- The benefit of combining the maximum and concurrent major-axis and flange lateral bending values due to live load when checking the section resistances, compared to using the maximums due to different live loads, is investigated. It is found that no extra effort is needed, other than the bookkeeping, to calculate the maximum with their concurrent value for each of the major-axis bending and flange lateral bending from different live load positions for the considered section.
- The flange lateral bending in the subject bridge is predominantly due to the skew of the bearing lines and the use of the staggered cross-frames. It is expected that in bridges where the flange lateral bending is dominated more by the effect of horizontal

curvature, the maximum flange lateral bending will tend to be approximately concurrent with the maximum major-axis bending.

- It is noted that the variation in the girder responses between the FEA and the 3D grid models is quite small. However, the cross-frame member forces show significant differences between two models. This is believed to be due to the web distortional flexibility in the beam-shell FEA model.

5.3 Full Nonlinear FEA

- The load level at $M_n = M_p$ refer as M_p-based 1/3 rule load level. Eq. 1.1 is used with $M_n = M_p$ in order to assess the impact of the potential most liberal format of the AASHTO (2007) resistance equation. The vertical and radial displacements are found to be predominantly linear up to the M_p-based 1/3 rule load level. The results of linear elastic analysis can be used to obtain good estimates of girder moments and deflections at this load level.
- Although, inelastic moment redistribution increases with increasing load, the total internal moments at G1-S1 and G6-S1 deviate from the elastic predictions by only 7.6 % and 6.1 % at the M_p-based 1/3 rule load level.
- At the M_p-based 1/3 rule load level significant yielding is observed near the mid-length of the bridge. The yielding is greatest at several cross-frame locations on the outside tips of the G1 and G6 bottom flanges. However, the yielding is progressed on the other locations.

- The top surface slab longitudinal strains across the width of the bridge at G1-S1 and G6-S1 are within the elastic limit of the defined concrete stress-strain response and are significantly less than the nominal concrete crushing strain of 0.003. In addition, these strains vary approximately in a linear fashion across the bridge width.
- The vertical reactions deviate slightly from the elastic predictions (maximum of 5.2 % deviation). The variation in the girder reactions is predominantly linear up to the M_p-based 1/3 rule load level.
- The AASHTO (2007) flange lateral bending stress limit of 0.6 F_y is a practical maximum lateral bending stress value in most cases; however, due to the more complex plastic strength interaction behavior of composite I-sections in positive bending, this limit is in general a conservative restriction on the design of these types of sections.
- Cross-frames are critical load carrying elements in horizontally curved bridges. It is noted that the axial forces in the cross-frame members is increased by as much as 13.7 % due to the girder inelasticity in the subject bridge. However, the effect of using the 3D grid versus the 3D FEA models is larger than the effect of the girder inelasticity in the 3D FEA solutions. The axial force predicted by the 3D grid models is up to 21.5% higher than that predicted by 3D FEA models at the M_p-based 1/3 rule load level.
- Based on the comparisons to the inelastic FEA results, the AASHTO (2007) provisions are observed to give accurate and conservative elastic analysis and design limits.

5.4 Conclusions

The results of this study show that the overall system and component responses of the subject bridge are predominantly linear up to the M_p-based 1/3 rule resistance level. Based on this research as well as other supporting research (Jung 2006), the M_n-based 1/3 rule resistance is believed to be justified for curved composite I-sections in positive bending. This provides a substantial increase in the strength estimate for curved I-girder bridges since the current design provisions limit the flexural resistance in positive bending to a maximum of $\phi_f F_{yf}$ in terms of the flange stresses.

5.5 Recommendations for Further Research

This study provides a reasonably comprehensive assessment of the strength behavior of a representative simple-span curved and skewed I-bridge. Nevertheless, there are additional worthwhile areas for further study. These areas are as follows:

- The subject bridge has staggered cross-frames. Staggered cross-frames have the effect of decreasing the cross-frame forces and increasing the flange lateral bending stresses. The flange lateral moments and the cross-frame member axial forces may differ substantially in girders with continuous cross-frame lines. Therefore, it would be useful to redesign the subject bridge with continuous cross-frames and then to check its behavior by full nonlinear analysis.
- Cross-frames are major load transferring elements of the bridge. The influence of the analysis type (3D FEA versus 3D grid and elastic versus full nonlinear) on the member forces is investigated in this study. The elastic 3D FEA model predicted smaller axial forces in the critical cross-frame members compared to the 3D grid

model. However, the influence of inelasticity in the full nonlinear 3D FEA solutions increases these forces nearly to the values determined from the 3D grid solutions. One possibility that might be considered to account for the effect of girder inelasticity is to apply an "overstrength factor" of sorts to the cross-frame members to help decrease the likelihood that they are loaded beyond their strength limits. This approach would be akin to the application of overstrength factors to FR moment connections in building seismic design. Based on the results from the 3D FEA and 3D grid analysis studies conducted in this research, it would appear that such a factor may need to be related to the type of analysis (3D FEA versus 3D grid or other types of analysis models).

- It is observed in this study that theoretical nominal flexural resistance of compact composite sections in positive flexure can be reduced significantly by the equation $M_n = \left(1.07 - 0.7\left(D_p / D_t\right)\right) \times M_p$ in AASHTO (2007). This equation is intended to protect the concrete deck from premature crushing. It provides a larger margin of safety for girders where the plastic neutral axis of the cross-section is lower than 10 % of the total section depth below the top surface of the slab. Nevertheless, the longitudinal top surface slab strains of the study bridge are well within the elastic limit of the defined concrete stress-strain response and are significantly less than the nominal concrete crushing strain of 0.003 at the M_p-based 1/3 rule strength limit. Furthermore, equations such as the above do not exist for concrete girder design. Therefore, the implications of the above equation might be revisited and more liberal limits considered.

APPENDIX A

BRIDGE COMPONENT DESIGN

This appendix presents the detailed calculations for girder flexural design based on the AASHTO (2007) and for the design of single-angle cross-frame compression members using the procedures from the AISC (2005) Specification as discussed in White (2007). Standard design templates are generated for each of the above component design using the Mathcad (2005) program and are used repeatedly to the extent possible where the same or similar design rules are applied.

The critical sections for the constructability under the STRENGTH IV load combination are presented and labeled in Fig. A.1.1. Section G1-S2 on G1 has the maximum strength unity check on G1 under the STRENGTH IV load combination. Separated critical sections are identified as G1-S1 and G1-S4 on G1 for strength limit state check on the completed structure. Also, section G1-S3 on G1, has the maximum top flange lateral bending stress on G1 under the STRENGTH IV load combination. Moreover, section G1-S5 on G1, has the maximum bottom flange lateral bending stress on G1 under the STRENGTH IV load combination.

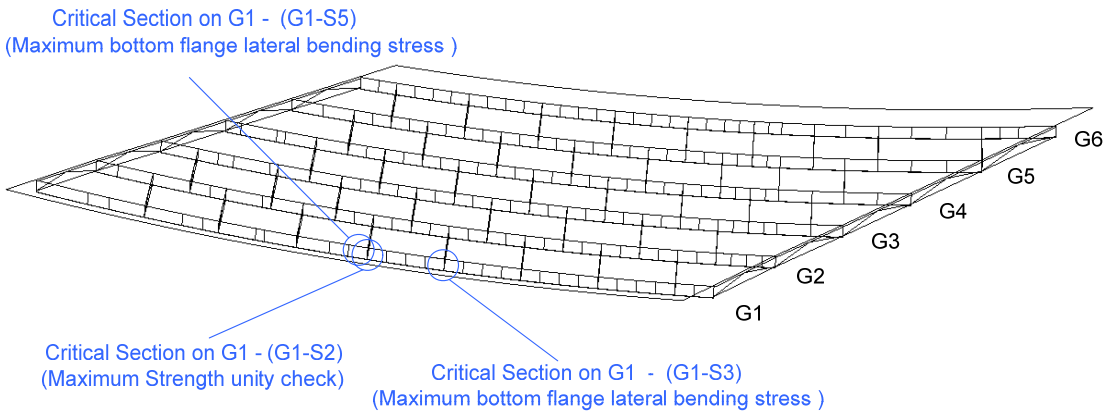

Figure A.1.1. Critical sections for checking constructability limit states under STRENGTH IV load combination (1.5 DC1).

Furthermore, two critical section for G1 are identified for the strength limit state under the STRENGTH I load combination on the completed structure. Section G1-S1 correspond to the maximum strength unity checks on G1. The vehicular live load configurations are determined to maximize this unity check. However, section G1-S4 is defined as the location that has the largest flange lateral bending stress (f_ℓ) under the STRENGTH I load combination on G1. In this case, the vehicular live loads are configured to maximize this largest f_ℓ value. The critical sections for the strength limit state under the STRENGTH I load combination are presented and labeled in Fig. A.1.2.

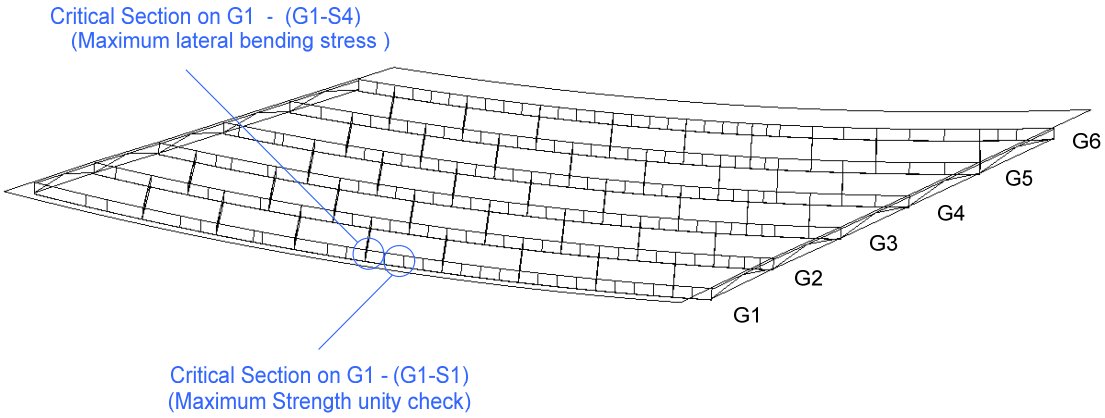

Figure A.1.2. Considered critical sections and their notations (STRENGTH I load level)

Section A.1 gives a set of the design worksheets for the flexural design of the outside girder including the determination of the lateral torsional buckling capacity of the noncomposite section from overall buckling of the system. Section A.2 presents a set of design worksheets concerning the design of cross-frame compression members.

A-1

POSITIVE MOMENT FLEXURAL DESIGN - G1 - Section 2 (G1-2)

$ksi := 10^3 \cdot psi$; $kips := 10^3 lbf$

Material Properties:

- Steel Properties:

$F_{yc} := 50ksi$; $F_{yw} := 50ksi$; $F_{yt} := 50ksi$; $E := 29000 \cdot ksi$

$F_{yr} := \max\left(\min\left(0.7 \cdot F_{yc}, F_{yw}\right), 0.5 \cdot F_{yc}\right)$ $F_{yr} = 35ksi$

- Concrete Properties:

$f_c := 4.0ksi$; $E_c := 3644.148ksi$; $n := \frac{E}{E_c}$; $n = 7.958$ $W_{conc} := 150 \frac{lbf}{ft^3}$

Plate Girder Dimensions:

G1-2

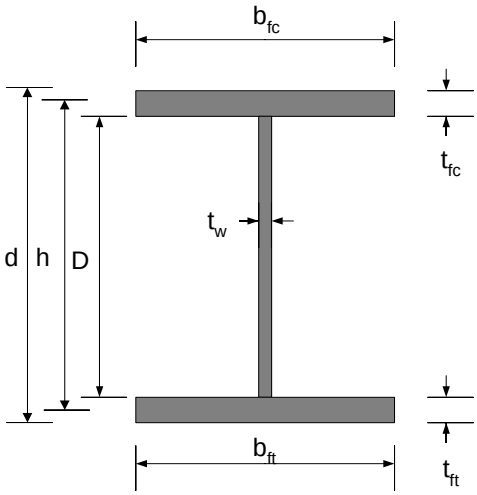

GIRDER LENGTH:

$L := 159.86ft$

TOP FLANGE:

$b_{fc} := 18in$

$t_{fc} := 2in$

$\frac{b_{fc}}{2t_{fc}} = 4.5$

BOTTOM FLANGE:

$b_{ft} := 20in$

$t_{ft} := 2.75in$

$\frac{b_{ft}}{2 \cdot t_{ft}} = 3.64$

WEB:

$D := 72in$ $t_w := 0.75in$ $\frac{D}{t_w} = 96$

$d := D + t_{ft} + t_{fc}$ $d = 76.75\,in$

$h := D + \frac{t_{ft} + t_{fc}}{2}$ $h = 74.375\,in$

Cross-section Proportion Limits :

- Web proportion checks for webs without longitudinal stiffeners

$$\text{Web\_Proportion\_Check} := \begin{cases} \text{"OK"} & \text{if } \frac{D}{t_w} \le 150 \\ \text{"NG"} & \text{otherwise} \end{cases}$$

$\text{Web\_Proportion\_Check} = \text{"OK"}$

- Flange proportion checks

$$I_{yc} := \frac{t_{fc} \cdot b_{fc}^{3}}{12} \qquad I_{yt} := \frac{t_{ft} \cdot b_{ft}^{3}}{12} \qquad \frac{I_{yc}}{I_{yt}} = 0.53$$

$$\text{Compression\_Flange\_Check} := \begin{cases} \text{"OK"} & \text{if } \frac{b_{fc}}{2 \cdot t_{fc}} \le 12.0 \wedge b_{fc} \ge \frac{D}{6} \wedge t_{fc} \ge 1.1 \cdot t_w \wedge 0.1 \le \frac{I_{yc}}{I_{yt}} \le 10 \\ \text{"NG"} & \text{otherwise} \end{cases}$$

$\text{Compression\_Flange\_Check} = \text{"OK"}$

$$\text{Tension\_Flange\_Check} := \begin{cases} \text{"OK"} & \text{if } \frac{b_{ft}}{2 \cdot t_{ft}} \le 12.0 \wedge b_{ft} \ge \frac{D}{6} \wedge t_{ft} \ge 1.1 \cdot t_w \\ \text{"NG"} & \text{otherwise} \end{cases}$$

$\text{Tension\_Flange\_Check} = \text{"OK"}$

Non-Composite Section Properties:

Top flange area :

$A_{fc} := b_{fc} \cdot t_{fc}$ $\quad A_{fc} = 36\,in^2$

Bottom flange area:

$A_{ft} := b_{ft} \cdot t_{ft}$ $\quad A_{ft} = 55\,in^2$

Web area:

$A_{web} := D \cdot t_w$ $\quad A_{web} = 54\,in^2$

Total section area :

$A_{girder} := A_{fc} + A_{ft} + A_{web}$ $\quad A_{girder} = 145\,in^2$

Neutral axis :

$$D_c := \frac{A_{fc} \cdot \left(\frac{t_{fc}}{2}\right) + A_{ft} \cdot \left(d - \frac{t_{ft}}{2}\right) + A_{web} \cdot \left(\frac{D}{2} + t_{fc}\right)}{A_{girder}} - t_{fc} \qquad D_c = 40.991\,in \qquad \frac{D_c}{D} = 0.569$$

<u>Note:</u> Neutral axis measured from the lower surface of the top flange.

Shear center : $h_u := D_c + \frac{t_{fc}}{2}$ $\quad h_l := D - D_c + \frac{t_{ft}}{2}$

$$e := \frac{I_{yc} \cdot h_u - I_{yt} \cdot h_l}{I_{yc} + I_{yt}} \qquad e = -6.615\,in$$ (offset distance from the neutral axis)

Moment of inertia with respect to a neutral axis :

$$I_{girder} := \frac{b_{fc} \cdot t_{fc}^3}{12} + \left[A_{fc} \cdot \left(D_c + t_{fc} - \frac{t_{fc}}{2}\right)^2\right] \ldots + \frac{b_{ft} \cdot t_{ft}^3}{12} + \left[A_{ft} \cdot \left[d - \left(D_c + t_{fc}\right) - \frac{t_{ft}}{2}\right]^2\right] \ldots + \frac{t_w \cdot D^3}{12} + A_{web} \cdot \left(D_c + t_{fc} - \frac{D}{2} - t_{fc}\right)^2$$

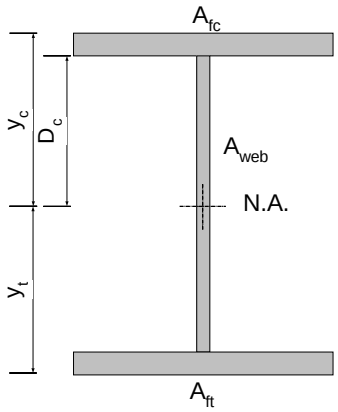

$I_{girder} = 145876.383\,in^4$

Section modulus to the compression flange :

$y_c := D_c + t_{fc}$ $\quad y_c = 42.991\,\text{in}$

$S_c := \frac{I_{girder}}{y_c}$ $\quad S_c = 3393.222\,\text{in}^3$

Section modulus of the tension flange :

$y_t := d - y_c$ $\quad y_t = 33.759\,\text{in}$

$S_t := \frac{I_{girder}}{y_t}$ $\quad S_t = 4321.049\,\text{in}^3$ $\quad \frac{A_{ft}}{A_{fc}} = 1.528$

- Web Bend-buckling Resistance

$\frac{D_c}{D} = 0.569$ $\quad \frac{2D_c}{t_w} = 109.308$

bend-buckling coeffient :

$k := \frac{9}{\left(\frac{D_c}{D}\right)^2}$ $\quad k = 27.768$

$F_{crw} := 0.9 \cdot E \cdot \frac{k}{\left(\frac{D}{t_w}\right)^2}$ $\quad F_{crw} = 78.64\,\text{ksi}$

- Yield Moment

$M_{yt\_noncomp} := S_t \cdot F_{yt}$ $\quad M_{yt\_noncomp} = 18004.371\,\text{kips}\cdot\text{ft}$

$M_{yc\_noncomp} := S_c \cdot F_{yc}$ $\quad M_{yc\_noncomp} = 14138.426\,\text{kips}\cdot\text{ft}$

$M_{y\_noncomp} := \begin{cases} M_{yt\_noncomp} & \text{if } M_{yt\_noncomp} \le M_{yc\_noncomp} \\ M_{yc\_noncomp} & \text{otherwise} \end{cases}$ $\quad M_{y\_noncomp} = 14138.426\,\text{kips}\cdot\text{ft}$

- Radius of Gyration for LTB Check

$r_t := \frac{b_{fc}}{\sqrt{12 \cdot \left(\frac{h}{d} + \frac{D_c \cdot t_w \cdot D^2}{3 \cdot b_{fc} \cdot t_{fc} \cdot h \cdot d}\right)}}$ $\quad r_t = 4.69\,\text{in}$

***Note:** The exact r_t equation is used in the above.*

- Flange-Strength Reduction Factors (Noncomposite Girder) :

Hybrid Factor :

$D_n := \max(D - D_c, D_c)$ $D_n = 40.991\,\text{in}$

$\text{First\_Yield\_at} := \begin{cases} \text{"Bottom Flange"} & \text{if } M_{yt\_noncomp} < M_{yc\_noncomp} \\ \text{"Top Flange"} & \text{otherwise} \end{cases}$

$\text{First\_Yield\_at} = \text{"Top Flange"}$

$f_n := \begin{cases} F_{yt} & \text{if } M_{yt\_noncomp} < M_{yc\_noncomp} \\ F_{yc} & \text{otherwise} \end{cases}$ $f_n = 50\,\text{ksi}$

$A_{fn} := \begin{cases} A_{ft} & \text{if } M_{yt\_noncomp} < M_{yc\_noncomp} \\ A_{fc} & \text{otherwise} \end{cases}$ $A_{fn} = 36\,\text{in}^2$

$\rho := \min\left(\frac{F_{yw}}{f_n}, 1.0\right)$ $\rho = 1$

$\beta := \frac{2 \cdot D_n \cdot t_w}{A_{fn}}$ $\beta = 1.708$

$R_{h\_noncomp} := \frac{12 + \beta \cdot (3 \cdot \rho - \rho^3)}{12 + 2 \cdot \beta}$ $R_{h\_noncomp} = 1$

Web Load-Shedding Factor :

$D_c = 40.991\,\text{in}$

$a_{wc} := \frac{2 \cdot D_c \cdot t_w}{A_{fc}}$ $a_{wc} = 1.708$

$\frac{D}{t_w} = 96$

$\lambda_{rw} := 5.7\sqrt{\frac{E}{F_{yc}}}$ $\lambda_{rw} = 137.274$

$0.95 \cdot \sqrt{\frac{E \cdot k}{F_{yc}}} = 120.561$

$R_{b\_noncomp} := \begin{cases} 1.0 & \text{if } \frac{2 \cdot D_c}{t_w} \le \lambda_{rw} \wedge \frac{D}{t_w} \le 0.95 \cdot \sqrt{\frac{E \cdot k}{F_{yc}}} \wedge \frac{D}{t_w} \le 150 \\ \text{otherwise} & \\ \quad \begin{cases} 1 - \left(\frac{a_{wc}}{1200 + 300 \cdot a_{wc}}\right) \cdot \left(\frac{2 \cdot D_c}{t_w} - \lambda_{rw}\right) & \text{if } 1 - \left(\frac{a_{wc}}{1200 + 300 \cdot a_{wc}}\right) \cdot \left(\frac{2 \cdot D_c}{t_w} - \lambda_{rw}\right) \le 1.0 \\ 1.0 & \text{otherwise} \end{cases} \end{cases}$

$R_{b\_noncomp} = 1$

Composite Section Properties :

Effective Width of Slab

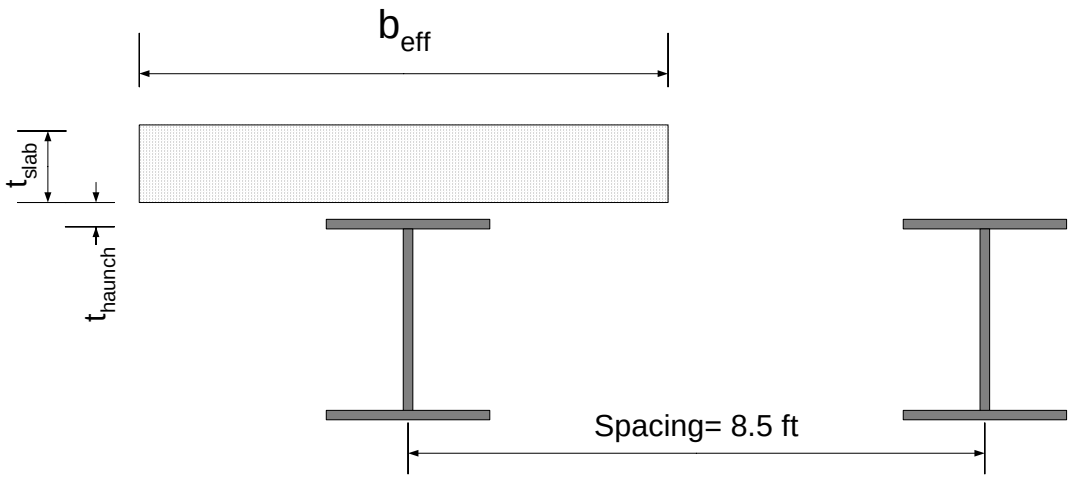

$t_{haunch} := 3.5in$ $b_{eff\_int} := 8.44ft$

$t_{slab} := 7.5in$

***NOTE**: the full tributary width for each girder is used in the design check.*

$b_{slab} := 8.44ft$

$b_{s\_3n} := \frac{b_{slab}}{3n}$

Reinforcement:

Average top reinforcing steel area : $A_{top\_rebar} := \frac{0.18\,in \cdot b_{slab}}{12}$ $A_{top\_rebar} = 1.519\,in^2$

Average bottom reinforcing steel area : $A_{bottom\_rebar} := \frac{0.27\,in \cdot b_{slab}}{12}$ $A_{bottom\_rebar} = 2.279\,in^2$

Location of top reinforcing steel : $y_{rt} := 2.75 \cdot in$

Location of bottom reinforcing steel : $y_{rb} := 5.75 \cdot in$

Long Term Composite Section Properties(3n) :

$A_{con\_3n} := b_{s\_3n} \cdot t_{slab}$ $A_{con\_3n} = 31.817\,in^2$

$A_{total\_3n} := A_{girder} + A_{con\_3n}$ $A_{total\_3n} = 176.817\,in^2$

$$NA_{3n} := \frac{A_{fc}\cdot\left(t_{slab} + t_{haunch} - \frac{t_{fc}}{2}\right) + A_{ft}\cdot\left(D + t_{slab} + t_{haunch} + \frac{t_{ft}}{2}\right) + A_{web}\cdot\left(\frac{D}{2} + t_{slab} + t_{haunch}\right) + A_{con\_3n}\cdot\frac{t_{slab}}{2}}{A_{total\_3n}}$$

$NA_{3n} = 43.31\,in$

***Note:** Neutral axis is measured from the top of concrete slab*

$$I_{3n} := \frac{b_{fc}\cdot t_{fc}^3}{12} + \left[A_{fc}\cdot\left(NA_{3n} - t_{slab} - t_{haunch} + \frac{t_{fc}}{2}\right)^2\right] \ldots + \frac{b_{ft}\cdot t_{ft}^3}{12} + \left[A_{ft}\cdot\left(t_{slab} + t_{haunch} + D + t_{ft} - NA_{3n} - \frac{t_{ft}}{2}\right)^2\right] \ldots + \frac{t_w\cdot D^3}{12} + A_{web}\cdot\left(NA_{3n} - t_{slab} - t_{haunch} - \frac{D}{2}\right)^2 + \frac{b_{s\_3n}\cdot t_{slab}^3}{12} + A_{con\_3n}\cdot\left(NA_{3n} - \frac{t_{slab}}{2}\right)^2$$

$I_{3n} = 206745.162\,in^4$

Section Moduli:

$S_{slab\_3n} := \frac{I_{3n}}{NA_{3n}}$ $S_{slab\_3n} = 4773.621\,in^3$

$y_{c\_3n} := NA_{3n} - t_{slab} - t_{haunch} + t_{fc}$ $y_{c\_3n} = 34.31\,in$

$S_{c\_3n} := \frac{I_{3n}}{y_{c\_3n}}$ $S_{c\_3n} = 6025.812\,in^3$

$y_{t\_3n} := d - y_{c\_3n}$ $y_{t\_3n} = 42.44\,in$

$S_{t\_3n} := \frac{I_{3n}}{y_{t\_3n}}$ $S_{t\_3n} = 4871.461\,in^3$

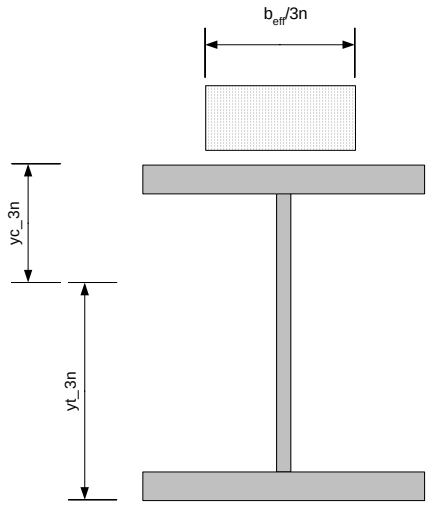

$D_{t\_3n} := D + t_{haunch} + t_{slab} + t_{ft}$ $D_{t\_3n} = 85.75\,in$

$D_{c\_3n} := y_{c\_3n} - t_{fc}$ $D_{c\_3n} = 32.31\,in$

$\frac{D_{c\_3n}}{D} = 0.449$ $\frac{2D_{c\_3n}}{t_w} = 86.16$

- Yield Moment (Long-term, Shored Construction) :

<u>Note:</u> Unshored Construction is used in the study

$M_{yt\_longterm} := S_{t\_3n} \cdot F_{yt}$ $M_{yt\_longterm} = 20297.755\,kips \cdot ft$

$M_{yc\_longterm} := S_{c\_3n} \cdot F_{yc}$ $M_{yc\_longterm} = 25107.548\,kips \cdot ft$

$$M_{y\_longterm} := \begin{cases} M_{yt\_longterm} & \text{if } M_{yt\_longterm} \le M_{yc\_longterm} \\ M_{yc\_longterm} & \text{otherwise} \end{cases}$$

$M_{y\_longterm} = 20297.755\,kips \cdot ft$

- Concrete Stress at $M_{y\text{-Long Term}}$ (shored construction)

$f_{c\_3n} := \frac{M_{y\_longterm} \cdot NA_{3n}}{I_{3n} \cdot 3n}$ $f_{c\_3n} = 2.137\,ksi$ $\frac{f_{c\_3n}}{f_c} = 0.534$

Web Load-Shedding Factor :

$D_{c\_3n} = 32.31\,in$

$a_{wc} := \frac{2 \cdot D_{c\_3n} \cdot t_w}{A_{fc}}$ $\quad a_{wc} = 1.346$ $\quad \frac{D}{t_w} = 96$

$\lambda_{rw} := 5.7\sqrt{\frac{E}{F_{yc}}}$ $\quad \lambda_{rw} = 137.274$ $\quad 0.95 \cdot \sqrt{\frac{E \cdot k}{F_{yc}}} = 120.561$

$$R_{b\_3n} := \begin{cases} 1.0 \text{ if } \frac{2 \cdot D_c}{t_w} \le \lambda_{rw} \wedge \frac{D}{t_w} \le 0.95 \cdot \sqrt{\frac{E \cdot k}{F_{yc}}} \wedge \frac{D}{t_w} \le 150 \\ \text{otherwise} \\ \quad \begin{cases} 1 - \left(\frac{a_{wc}}{1200 + 300 \cdot a_{wc}}\right) \cdot \left(\frac{2 \cdot D_c}{t_w} - \lambda_{rw}\right) \text{ if } 1 - \left(\frac{a_{wc}}{1200 + 300 \cdot a_{wc}}\right) \cdot \left(\frac{2 \cdot D_c}{t_w} - \lambda_{rw}\right) \le 1.0 \\ 1.0 \text{ otherwise} \end{cases} \end{cases}$$

$R_{b\_3n} = 1$

Short Term Composite Section Properties (n):

Effective Flange Width

$b_{s\_n} := \frac{b_{slab}}{n}$

$A_{con\_n} := b_{s\_n} \cdot t_{slab}$ $\quad A_{con\_n} = 95.452\,in^2$

$A_{total\_n} := A_{girder} + A_{con\_n}$ $\quad A_{total\_n} = 240.452\,in^2$

$$NA_n := \frac{A_{fc} \cdot \left(t_{slab} + t_{haunch} - \frac{t_{fc}}{2}\right) + A_{ft} \cdot \left(D + t_{slab} + t_{haunch} + \frac{t_{ft}}{2}\right) + A_{web} \cdot \left(\frac{D}{2} + t_{slab} + t_{haunch}\right) + A_{con\_n} \cdot \frac{t_{slab}}{2}}{A_{total\_n}}$$

$NA_n = 32.841\,in$

<u>Note:</u> Neutral is axis measured from the top of concrete slab

$$I_n := \frac{b_{fc}\cdot t_{fc}^3}{12} + \left[A_{fc}\cdot\left(NA_n - t_{slab} - t_{haunch} + \frac{t_{fc}}{2}\right)^2\right] \ldots$$
$$+ \frac{b_{ft}\cdot t_{ft}^3}{12} + \left[A_{ft}\cdot\left(t_{slab} + t_{haunch} + D + t_{ft} - NA_n - \frac{t_{ft}}{2}\right)^2\right] \ldots$$
$$+ \frac{t_w\cdot D^3}{12} + A_{web}\cdot\left(NA_n - t_{slab} - t_{haunch} - \frac{D}{2}\right)^2 + \frac{b_{s\_n}\cdot t_{slab}^3}{12} + A_{con\_n}\cdot\left(NA_n - \frac{t_{slab}}{2}\right)^2$$

$I_n = 280275.227\,in^4$

Section Moduli :

$S_{slab\_n} := \frac{I_n}{NA_n}$ $\quad S_{slab\_n} = 8534.418\,in^3$

$y_{c\_n} := NA_n - t_{slab} - t_{haunch} + t_{fc}$ $\quad y_{c\_n} = 23.841\,in$

$S_{c\_n} := \frac{I_n}{y_{c\_n}}$ $\quad S_{c\_n} = 11756.225\,in^3$

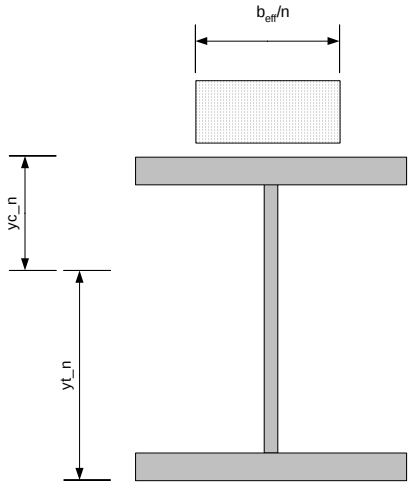

$y_{t\_n} := d - y_{c\_n}$ $\quad y_{t\_n} = 52.909\,in$

$S_{t\_n} := \frac{I_n}{y_{t\_n}}$ $\quad S_{t\_n} = 5297.265\,in^3$

$D_{c\_n} := y_{c\_n} - t_{fc}$ $\quad D_{c\_n} = 21.841\,in$

$\frac{D_{c\_n}}{D} = 0.303$ $\quad \frac{2D_{c\_n}}{t_w} = 58.242$

- Yield Moment (Short-term, Shored Construction) :

***Note:* Unshored Construction is used in the study**

$M_{yt\_shortterm} := S_{t\_n} \cdot F_{yt}$ $\quad M_{yt\_shortterm} = 22071.938\,\text{kips}\cdot\text{ft}$

$M_{yc\_shortterm} := S_{c\_n} \cdot F_{yc}$ $\quad M_{yc\_shortterm} = 48984.271\,\text{kips}\cdot\text{ft}$

$$M_{y\_shortterm} := \begin{cases} M_{yt\_shortterm} & \text{if } M_{yt\_shortterm} \le M_{yc\_shortterm} \\ M_{yc\_shortterm} & \text{otherwise} \end{cases}$$

$M_{y\_shortterm} = 22071.938\,\text{kips}\cdot\text{ft}$

- Concrete Stress at $M_{y\text{-Short Term}}$ (shored construction)

$f_{c\_n} := \dfrac{M_{y\_shortterm} \cdot NA_n}{I_n}$ $\quad f_{c\_n} = 3.9\,\text{ksi}$ $\quad \dfrac{f_{c\_n}}{f_c} = 0.975$

- Section Properties:

$\lambda_f := \dfrac{b_{fc}}{2 \cdot t_{fc}}$ $\quad \lambda_f = 4.5$ $\quad \lambda_{pf} := 0.38 \cdot \sqrt{\dfrac{E}{F_{yc}}}$ $\quad \lambda_{pf} = 9.152$ $\quad \lambda_{rf} := 0.56 \sqrt{\dfrac{E}{F_{yr}}}$ $\quad \lambda_{rf} = 16.12$

$$Flange\_compactness := \begin{cases} \text{"compact flange"} & \text{if } \lambda_f < \lambda_{pf} \\ \text{"noncompact flange"} & \text{if } \lambda_{pf} < \lambda_f < \lambda_{rf} \end{cases}$$

$Flange\_compactness = \text{"compact flange"}$

Web Load-Shedding Factor :

$D_{c\_n} = 21.841\,\text{in}$

$a_{wc} := \dfrac{2 \cdot D_{c\_n} \cdot t_w}{A_{fc}}$ $\quad a_{wc} = 0.91$ $\quad \dfrac{D}{t_w} = 96$

$\lambda_{rw} := 5.7 \sqrt{\dfrac{E}{F_{yc}}}$ $\quad \lambda_{rw} = 137.274$ $\quad 0.95 \cdot \sqrt{\dfrac{E \cdot k}{F_{yc}}} = 120.561$

$$R_{b\_n} := \begin{cases} 1.0 & \text{if } \dfrac{2 \cdot D_c}{t_w} \le \lambda_{rw} \wedge \dfrac{D}{t_w} \le 0.95 \cdot \sqrt{\dfrac{E \cdot k}{F_{yc}}} \wedge \dfrac{D}{t_w} \le 150 \\ \text{otherwise} & \\ \quad \begin{cases} 1 - \left(\dfrac{a_{wc}}{1200 + 300 \cdot a_{wc}}\right) \cdot \left(\dfrac{2 \cdot D_c}{t_w} - \lambda_{rw}\right) & \text{if } 1 - \left(\dfrac{a_{wc}}{1200 + 300 \cdot a_{wc}}\right) \cdot \left(\dfrac{2 \cdot D_c}{t_w} - \lambda_{rw}\right) \le 1.0 \\ 1.0 & \text{otherwise} \end{cases} & \end{cases}$$

$R_{b\_n} = 1$

Plastic Moment Capacity (Composite Section) :

$P_{rb} := F_{yr} \cdot A_{bottom\_rebar}$ $\quad P_{rb} = 79.758\,\text{kips}$

$P_{rt} := F_{yr} \cdot A_{top\_rebar}$ $\quad P_{rt} = 53.172\,\text{kips}$

$P_s := 0.85 \cdot f_c \cdot b_{slab} \cdot t_{slab}$ $\quad P_s = 2582.64\,\text{kips}$

$P_c := F_{yc} \cdot A_{fc}$ $\quad P_c = 1800\,\text{kips}$

$P_t := F_{yt} \cdot A_{ft}$ $\quad P_t = 2750\,\text{kips}$

$P_w := F_{yw} \cdot A_{web}$ $\quad P_w = 2700\,\text{kips}$

$A_{rs} := A_{bottom\_rebar} + A_{top\_rebar}$

$A_{rs} = 3.798\,\text{in}^2$

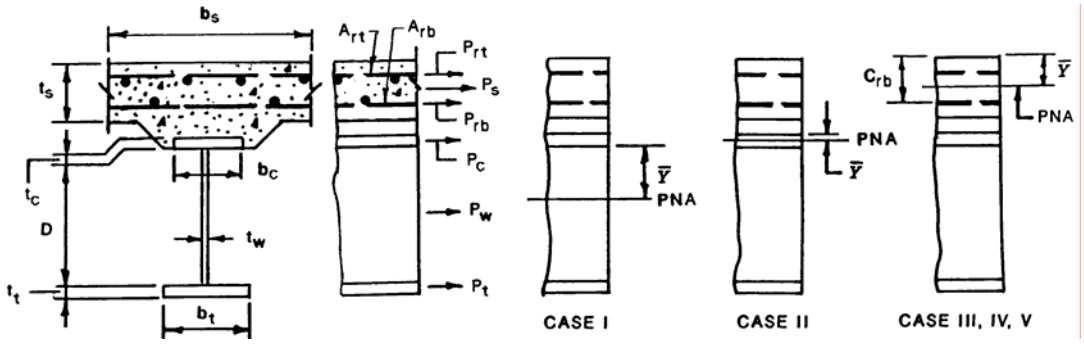

Computation of Plastic-Moment Capacity(Positive Flexure)

Location_of_PNA :=
- "In Web (Case I) " if $P_t + P_w \geq P_c + P_s + P_{rb} + P_{rt}$
- otherwise
  - "In Top Flange (Case II) " if $P_t + P_w + P_c \geq P_s + P_{rb} + P_{rt}$
  - otherwise
    - "Slab, Below Prb (Case III)" if $P_t + P_w + P_c \geq \frac{y_{rb}}{t_{slab}} \cdot P_s + P_{rb} + P_{rt}$
    - otherwise
      - "Slab,at Prb (Case IV)" if $P_t + P_w + P_c + P_{rb} \geq \frac{y_{rb}}{t_{slab}} \cdot P_s + P_{rt}$
      - "Slab, Above Prb (Case V) " otherwise

*** if it is case V check additional cases*

Location_of_PNA = "In Web (Case I) "

$$Y_{bar} := \begin{cases} \frac{D}{2}\cdot\left(\frac{P_t - P_c - P_s - P_{rt} - P_{rb}}{P_w} + 1\right) & \text{if } P_t + P_w \geq P_c + P_s + P_{rb} + P_{rt} \\ \text{otherwise} \\ \quad \begin{cases} \frac{t_{fc}}{2}\cdot\left(\frac{P_w + P_t - P_s - P_{rt} - P_{rb}}{P_c} + 1\right) & \text{if } P_t + P_w + P_c \geq P_s + P_{rb} + P_{rt} \\ \text{otherwise} \\ \quad \begin{cases} t_{slab}\cdot\frac{P_c + P_w + P_t - P_{rt} - P_{rb}}{P_s} & \text{if } P_t + P_w + P_c \geq \frac{y_{rb}}{t_{slab}}\cdot P_s + P_{rb} + P_{rt} \\ \text{otherwise} \\ \quad \begin{cases} y_{rb} & \text{if } P_t + P_w + P_c + P_{rb} \geq \frac{y_{rb}}{t_{slab}}\cdot P_s + P_{rt} \\ t_{slab}\cdot\frac{P_{rb} + P_c + P_w + P_t - P_{rt}}{P_s} & \text{otherwise} \end{cases} \end{cases} \end{cases} \end{cases}$$

$$Y_{bar} = 12.459\,\text{in}$$

$$d_s := \begin{cases} \frac{t_{slab}}{2} + t_{haunch} + Y_{bar} & \text{if } P_t + P_w \geq P_c + P_s + P_{rb} + P_{rt} \\ \text{otherwise} \\ \quad \begin{cases} \frac{t_{slab}}{2} + t_{haunch} - t_{fc} + Y_{bar} & \text{if } P_t + P_w + P_c \geq P_s + P_{rb} + P_{rt} \\ \text{"Not necessary for calculating Mp"} & \text{otherwise} \end{cases} \end{cases}$$

$$d_s = 19.709\,\text{in}$$

$$d_{rt} := \begin{cases} t_{slab} - y_{rt} + t_{haunch} + Y_{bar} & \text{if } P_t + P_w \geq P_c + P_s + P_{rb} + P_{rt} \\ \text{otherwise} \\ \quad \begin{cases} t_{slab} - y_{rt} + t_{haunch} - t_{fc} + Y_{bar} & \text{if } P_t + P_w + P_c \geq P_s + P_{rb} + P_{rt} \\ Y_{bar} - y_{rt} & \text{otherwise} \end{cases} \end{cases}$$

$$d_{rt} = 20.709\,\text{in}$$

$$d_{rb} := \begin{cases} t_{slab} - y_{rb} + t_{haunch} + Y_{bar} & \text{if } P_t + P_w \geq P_c + P_s + P_{rb} + P_{rt} \\ \text{otherwise} \\ \quad \begin{cases} t_{slab} - y_{rb} + t_{haunch} - t_{fc} + Y_{bar} & \text{if } P_t + P_w + P_c \geq P_s + P_{rb} + P_{rt} \\ \text{otherwise} \\ \quad \begin{cases} Y_{bar} - y_{rb} & \text{if } P_t + P_w + P_c \geq \frac{y_{rb}}{t_{slab}} \cdot P_s + P_{rb} + P_{rt} \\ \text{otherwise} \\ \quad \begin{cases} \text{"Not necessary for calculating Mp"} & \text{if } P_t + P_w + P_c + P_{rb} \geq \frac{y_{rb}}{t_{slab}} \cdot P_s + P_{rt} \\ y_{rb} - Y_{bar} & \text{otherwise} \end{cases} \end{cases} \end{cases} \end{cases}$$

$d_{rb} = 17.709\,\text{in}$

$$d_c := \begin{cases} Y_{bar} - \frac{t_{fc}}{2} & \text{if } P_t + P_w \geq P_c + P_s + P_{rb} + P_{rt} \\ \text{otherwise} \\ \quad \begin{cases} \text{"Not necessary for calculating Mp"} & \text{if } P_t + P_w + P_c \geq P_s + P_{rb} + P_{rt} \\ t_{slab} + t_{haunch} - \frac{t_{fc}}{2} - Y_{bar} & \text{otherwise} \end{cases} \end{cases}$$

$d_c = 0.291\ \text{m}$

$$d_w := \begin{cases} \text{"Not necessary for calculating Mp"} & \text{if } P_t + P_w \geq P_c + P_s + P_{rb} + P_{rt} \\ \text{otherwise} \\ \quad \begin{cases} \frac{D}{2} + t_{fc} - Y_{bar} & \text{if } P_t + P_w + P_c \geq P_s + P_{rb} + P_{rt} \\ t_{slab} + t_{haunch} - Y_{bar} + \frac{D}{2} & \text{otherwise} \end{cases} \end{cases}$$

$d_w = \text{"Not necessary for calculating Mp"}\ \text{in}$

$$d_t := \begin{cases} D - Y_{bar} + \frac{t_{ft}}{2} & \text{if } P_t + P_w \geq P_c + P_s + P_{rb} + P_{rt} \\ \text{otherwise} \\ \quad \begin{cases} D + t_{fc} - Y_{bar} + \frac{t_{ft}}{2} & \text{if } P_t + P_w + P_c \geq P_s + P_{rb} + P_{rt} \\ t_{slab} + t_{haunch} - Y_{bar} + D + \frac{t_{ft}}{2} & \text{otherwise} \end{cases} \end{cases}$$

$d_t = 60.916\,\text{in}$

$$M_p := \begin{cases} \frac{P_w}{2 \cdot D} \cdot \left[Y_{bar}^{\,2} + \left(D - Y_{bar}\right)^2 \right] + P_s \cdot d_s + P_{rt} \cdot d_{rt} + P_{rb} \cdot d_{rb} + P_c \cdot d_c + P_t \cdot d_t & \text{if } P_t + P_w \geq P_c + P_s + P_{rb} + P_{rt} \\ \text{otherwise} \\ \quad \begin{cases} \frac{P_c}{2 \cdot t_{fc}} \cdot \left[Y_{bar}^{\,2} + \left(t_{fc} - Y_{bar}\right)^2 \right] + P_s \cdot d_s + P_{rt} \cdot d_{rt} + P_{rb} \cdot d_{rb} + P_w \cdot d_w + P_t \cdot d_t & \text{if } P_t + P_w + P_c \geq P_s + P_{rb} + P_{rt} \\ \text{otherwise} \\ \quad \begin{cases} \frac{Y_{bar}^{\,2} \cdot P_s}{2 \cdot t_{slab}} + P_{rt} \cdot d_{rt} + P_{rb} \cdot d_{rb} + P_c \cdot d_c + P_w \cdot d_w + P_t \cdot d_t & \text{if } P_t + P_w + P_c \geq \frac{y_{rb}}{t_{slab}} \cdot P_s + P_{rb} + P_{rt} \\ \text{otherwise} \\ \quad \begin{cases} \frac{Y_{bar}^{\,2} \cdot P_s}{2 \cdot t_{slab}} + P_{rt} \cdot d_{rt} + P_c \cdot d_c + P_w \cdot d_w + P_t \cdot d_t & \text{if } P_t + P_w + P_c + P_{rb} \geq \frac{y_{rb}}{t_{slab}} \cdot P_s + P_{rt} \\ \frac{Y_{bar}^{\,2} \cdot P_s}{2 \cdot t_{slab}} + P_{rt} \cdot d_{rt} + P_{rb} \cdot d_{rb} + P_c \cdot d_c + P_w \cdot d_w + P_t \cdot d_t & \text{otherwise} \end{cases} \end{cases} \end{cases}$$

$$M_p = 25911.81\,\text{kips}\cdot\text{ft}$$

$$D_{cp} := \begin{cases} \frac{D}{2} \cdot \left[\frac{F_{yt} \cdot A_{ft} - F_{yc} \cdot A_{fc} - 0.85 \cdot f_c \cdot \left(b_{slab} \cdot t_{slab}\right) - F_{yr} \cdot A_{rs}}{F_{yw} \cdot A_{web}} + 1 \right] & \text{if } P_t + P_w \geq P_c + P_s + P_{rb} + P_{rt} \\ 0 & \text{otherwise} \end{cases}$$

$$D_{cp} = 12.459\,\text{in}$$

$$D_p := \left(Y_{bar} + t_{slab} + t_{haunch}\right)$$

$$D_p = 23.459\,\text{in}$$

$$\text{Section\_compactness} := \begin{cases} \text{"compact section"} & \text{if } F_{yt} < 70 \cdot \text{ksi} \wedge F_{yc} < 70 \cdot \text{ksi} \wedge \frac{D}{t_w} \leq 150 \wedge \frac{2 D_{cp}}{t_w} \leq 3.76 \cdot \sqrt{\frac{E}{F_{yc}}} \\ \text{"noncompact section"} & \text{otherwise} \end{cases}$$

$$\text{Section\_compactness} = \text{"compact section"}$$

Unshored Composite Section Properties :

Yield Moment (unshored) associated with STRENGTH I - G1-S1

$f_{D1t} := 24.489\,ksi$ $f_{D1c} := 30.55\,ksi$ $M_{DC2} := 1376.125\,kip\cdot ft$ $M_{DW} := 1124.808\,kip\cdot ft$

$M_{D1t} := f_{D1t}\cdot S_t$ $M_{D1c} := f_{D1c}\cdot S_c$ $M_{D2} := M_{DC2} + M_{DW}$

$M_{D1t} = 8818.181\,kips\cdot ft$ $M_{D1c} = 8638.578\,kips\cdot ft$ $M_{D2} = 2500.933\,kip\cdot ft$

Tension Flange :

$$M_{ADt} := \left(F_{yt} - \frac{M_{D1t}}{S_t} - \frac{M_{D2}}{S_{t\_3n}}\right)\cdot S_{t\_n} \qquad M_{ADt} = 8542.01\,kips\cdot ft$$

$$M_{yt} := M_{D1t} + M_{D2} + M_{ADt} \qquad M_{yt} = 19861.124\,kips\cdot ft$$

Compression Flange :

$$M_{ADc} := \left(F_{yc} - \frac{M_{D1c}}{S_c} - \frac{M_{D2}}{S_{c\_3n}}\right)\cdot S_{c\_n} \qquad M_{ADc} = 14175.616\,kips\cdot ft$$

$$M_{yc} := M_{D1c} + M_{D2} + M_{ADc} \qquad M_{yc} = 25315.128\,kips\cdot ft$$

$$M_{AD} := \min\left(M_{ADt}, M_{ADc}\right) \qquad M_{AD} = 8542.01\,kips\cdot ft$$

$$M_{y\_unshored} := \min\left(M_{yt}, M_{yc}\right) \qquad M_{y\_unshored} = 19861.124\,kips\cdot ft$$

$$S_{xt\_2.4} := \frac{M_{yt}}{F_{yt}} \qquad S_{xt\_2.4} = 4766.67\,in^3$$

Concrete Stress at First Yield (unshored)

$$f_{conc\_composite\_unshored\_at\_My} := \left(\frac{M_{D2}}{S_{slab\_3n}\cdot 3n} + \frac{M_{AD}}{S_{slab\_n}\cdot n}\right) \qquad f_{conc\_composite\_unshored\_at\_My} = 1.773\,ksi$$

$$\frac{f_{conc\_composite\_unshored\_at\_My}}{f_c} = 0.443$$

Shape Factor :

$$\frac{M_p}{M_{y\_unshored}} = 1.305 \qquad \frac{M_p}{M_{y\_shortterm}} = 1.174 \qquad \frac{M_p}{M_{y\_longterm}} = 1.277$$

Flange Hybrid Strength Reduction Factor (Composite Girder) :

NOTE: The NA is assumed to be located in the web and is assumed to be closest to the top flange

$$f_{c\_composite\_unshored\_at\_My} := \left(\frac{M_{D2}}{S_{c\_3n}} + \frac{M_{AD}}{S_{c\_n}} + \frac{M_{D1c}}{S_c} \right) \qquad f_{c\_composite\_unshored\_at\_My} = 44.25\,\text{ksi}$$

$$f_{t\_composite\_unshored\_at\_My} := \left(\frac{M_{D2}}{S_{t\_3n}} + \frac{M_{AD}}{S_{t\_n}} + \frac{M_{D1t}}{S_t} \right) \qquad f_{t\_composite\_unshored\_at\_My} = 50\,\text{ksi}$$

$$D_{c\_yield} := d \cdot \frac{f_{c\_composite\_unshored\_at\_My}}{f_{c\_composite\_unshored\_at\_My} + f_{t\_composite\_unshored\_at\_My}} - t_{fc} \qquad D_{c\_yield} = 34.034\,\text{in}$$

$$D_{n\_yield} := \max\left(D - D_{c\_yield}, D_{c\_yield}\right) \qquad D_{n\_yield} = 37.966\,\text{in} \qquad \frac{D_{c\_yield}}{D} = 0.473 \qquad \frac{2D_{c\_yield}}{t_w} = 90.756$$

$$\text{First\_Yield\_at} := \begin{cases} \text{"Bottom Flange"} & \text{if } M_{yt} < M_{yc} \\ \text{"Top Flange"} & \text{otherwise} \end{cases} \qquad \text{First\_Yield\_at} = \text{"Bottom Flange"}$$

$$f_n := F_{yt} \qquad f_n = 50\,\text{ksi}$$

$$\rho := \min\left(\frac{F_{yw}}{f_n}, 1.0 \right) \qquad \rho = 1$$

$$A_{fn} := A_{ft}$$

$$\beta := \frac{2 \cdot D_{n\_yield} \cdot t_w}{A_{fn}} \qquad \beta = 1.035$$

$$R_{h\_comp} := \frac{12 + \beta \cdot \left(3 \cdot \rho - \rho^3\right)}{12 + 2 \cdot \beta} \qquad R_{h\_comp} = 1$$

Unshored Composite Section Properties :

Yield Moment (unshored) associated with STRENGTH I - G1-S4

$f_{D1t} := 24.576\,ksi$ $f_{D1c} := 30.967\,ksi$ $M_{DC2} := 1375.06675\,kip\cdot ft$ $M_{DW} := 1127.325\,kip\cdot ft$

$M_{D1t} := f_{D1t}\cdot S_t$ $M_{D1c} := f_{D1c}\cdot S_c$ $M_{D2} := M_{DC2} + M_{DW}$

$M_{D1t} = 8849.509\,kips\cdot ft$ $M_{D1c} = 8756.493\,kips\cdot ft$ $M_{D2} = 2502.392\,kip\cdot ft$

Tension Flange :

$$M_{ADt} := \left(F_{yt} - \frac{M_{D1t}}{S_t} - \frac{M_{D2}}{S_{t\_3n}}\right)\cdot S_{t\_n} \qquad M_{ADt} = 8502.019\,kips\cdot ft$$

$M_{yt} := M_{D1t} + M_{D2} + M_{ADt}$ $M_{yt} = 19853.919\,kips\cdot ft$

Compression Flange :

$$M_{ADc} := \left(F_{yc} - \frac{M_{D1c}}{S_c} - \frac{M_{D2}}{S_{c\_3n}}\right)\cdot S_{c\_n} \qquad M_{ADc} = 13764.242\,kips\cdot ft$$

$M_{yc} := M_{D1c} + M_{D2} + M_{ADc}$ $M_{yc} = 25023.126\,kips\cdot ft$

$M_{AD} := \min\left(M_{ADt}, M_{ADc}\right)$ $M_{AD} = 8502.019\,kips\cdot ft$

$M_{y\_unshored} := \min\left(M_{yt}, M_{yc}\right)$ $M_{y\_unshored} = 19853.919\,kips\cdot ft$

$$S_{xt\_2.3} := \frac{M_{yt}}{F_{yt}} \qquad S_{xt\_2.3} = 4764.941\,in^3$$

Concrete Stress at First Yield (unshored)

$$f_{conc\_composite\_unshored\_at\_My} := \left(\frac{M_{D2}}{S_{slab\_3n}\cdot 3n} + \frac{M_{AD}}{S_{slab\_n}\cdot n}\right) \qquad f_{conc\_composite\_unshored\_at\_My} = 1.766\,ksi$$

$$\frac{f_{conc\_composite\_unshored\_at\_My}}{f_c} = 0.441$$

Shape Factor :

$\frac{M_p}{M_{y\_unshored}} = 1.305$ $\frac{M_p}{M_{y\_shortterm}} = 1.174$ $\frac{M_p}{M_{y\_longterm}} = 1.277$

Flange Hybrid Strength Reduction Factor (Composite Girder) :

NOTE: The NA is assumed to be located in the web and is assumed to be closest to the top flange

$$f_{c\_composite\_unshored\_at\_My} := \left(\frac{M_{D2}}{S_{c\_3n}} + \frac{M_{AD}}{S_{c\_n}} + \frac{M_{D1c}}{S_c} \right) \qquad f_{c\_composite\_unshored\_at\_My} = 44.63\,\text{ksi}$$

$$f_{t\_composite\_unshored\_at\_My} := \left(\frac{M_{D2}}{S_{t\_3n}} + \frac{M_{AD}}{S_{t\_n}} + \frac{M_{D1t}}{S_t} \right) \qquad f_{t\_composite\_unshored\_at\_My} = 50\,\text{ksi}$$

$$D_{c\_yield} := d \cdot \frac{f_{c\_composite\_unshored\_at\_My}}{f_{c\_composite\_unshored\_at\_My} + f_{t\_composite\_unshored\_at\_My}} - t_{fc} \qquad D_{c\_yield} = 34.197\,\text{in}$$

$$D_{n\_yield} := \max\left(D - D_{c\_yield}, D_{c\_yield}\right) \qquad D_{n\_yield} = 37.803\,\text{in} \qquad \frac{D_{c\_yield}}{D} = 0.475 \qquad \frac{2D_{c\_yield}}{t_w} = 91.191$$

$$First\_Yield\_at := \begin{cases} \text{"Bottom Flange"} & \text{if } M_{yt} < M_{yc} \\ \text{"Top Flange"} & \text{otherwise} \end{cases} \qquad First\_Yield\_at = \text{"Bottom Flange"}$$

$$f_n := F_{yt} \qquad f_n = 50\,\text{ksi}$$

$$\rho := \min\left(\frac{F_{yw}}{f_n}, 1.0 \right) \qquad \rho = 1$$

$$A_{fn} := A_{ft}$$

$$\beta := \frac{2 \cdot D_{n\_yield} \cdot t_w}{A_{fn}} \qquad \beta = 1.031$$

$$R_{h\_comp} := \frac{12 + \beta \cdot \left(3 \cdot \rho - \rho^3\right)}{12 + 2 \cdot \beta} \qquad R_{h\_comp} = 1$$

Unshored Composite Section Properties :

Yield Moment (unshored) associated with STRENGTH IV - G1-S5

$f_{D1t} := 24.576\,ksi$ $f_{D1c} := 30.967\,ksi$ $M_{DC2} := 0\cdot kip\cdot ft$ $M_{DW} := 1127.325\cdot kip\cdot ft$

$M_{D1t} := f_{D1t}\cdot S_t$ $M_{D1c} := f_{D1c}\cdot S_c$ $M_{D2} := M_{DC2} + M_{DW}$

$M_{D1t} = 8849.509\,kips\cdot ft$ $M_{D1c} = 8756.493\,kips\cdot ft$ $M_{D2} = 1127.325\,kip\cdot ft$

Tension Flange :

$$M_{ADt} := \left(F_{yt} - \frac{M_{D1t}}{S_t} - \frac{M_{D2}}{S_{t\_3n}}\right)\cdot S_{t\_n} \qquad M_{ADt} = 9997.277\,kips\cdot ft$$

$M_{yt} := M_{D1t} + M_{D2} + M_{ADt}$ $M_{yt} = 19974.111\,kips\cdot ft$

Compression Flange :

$$M_{ADc} := \left(F_{yc} - \frac{M_{D1c}}{S_c} - \frac{M_{D2}}{S_{c\_3n}}\right)\cdot S_{c\_n} \qquad M_{ADc} = 16446.966\,kips\cdot ft$$

$M_{yc} := M_{D1c} + M_{D2} + M_{ADc}$ $M_{yc} = 26330.784\,kips\cdot ft$

$M_{AD} := \min\left(M_{ADt}, M_{ADc}\right)$ $M_{AD} = 9997.277\,kips\cdot ft$

$M_{y\_unshored} := \min\left(M_{yt}, M_{yc}\right)$ $M_{y\_unshored} = 19974.111\,kips\cdot ft$

$$S_{xt\_2.3.1} := \frac{M_{yt}}{F_{yt}} \qquad S_{xt\_2.3.1} = 4793.787\,in^3$$

Concrete Stress at First Yield (unshored)

$$f_{conc\_composite\_unshored\_at\_My} := \left(\frac{M_{D2}}{S_{slab\_3n}\cdot 3n} + \frac{M_{AD}}{S_{slab\_n}\cdot n}\right)$$

$f_{conc\_composite\_unshored\_at\_My} = 1.885\,ksi$

$$\frac{f_{conc\_composite\_unshored\_at\_My}}{f_c} = 0.471$$

Shape Factor :

$\frac{M_p}{M_{y\_unshored}} = 1.297$ $\frac{M_p}{M_{y\_shortterm}} = 1.174$ $\frac{M_p}{M_{y\_longterm}} = 1.277$

Unshored Composite Section Properties :

Yield Moment (unshored) associated with STRENGTH IV - G1-S2

$f_{D1t} := 29.512\,ksi$ $f_{D1c} := 37.160\,ksi$ $M_{DC2} := 0\,kip\cdot ft$ $M_{DW} := 1128.584\,kip\cdot ft$

$M_{D1t} := f_{D1t}\cdot S_t$ $M_{D1c} := f_{D1c}\cdot S_c$ $M_{D2} := M_{DC2} + M_{DW}$

$M_{D1t} = 10626.9\,kips\cdot ft$ $M_{D1c} = 10507.678\,kips\cdot ft$ $M_{D2} = 1128.584\,kip\cdot ft$

Tension Flange :

$$M_{ADt} := \left(F_{yt} - \frac{M_{D1t}}{S_t} - \frac{M_{D2}}{S_{t\_3n}}\right)\cdot S_{t\_n} \qquad M_{ADt} = 7816.966\,kips\cdot ft$$

$M_{yt} := M_{D1t} + M_{D2} + M_{ADt}$ $M_{yt} = 19572.45\,kips\cdot ft$

Compression Flange :

$$M_{ADc} := \left(F_{yc} - \frac{M_{D1c}}{S_c} - \frac{M_{D2}}{S_{c\_3n}}\right)\cdot S_{c\_n} \qquad M_{ADc} = 10377.318\,kips\cdot ft$$

$M_{yc} := M_{D1c} + M_{D2} + M_{ADc}$ $M_{yc} = 22013.581\,kips\cdot ft$

$M_{AD} := \min\left(M_{ADt}, M_{ADc}\right)$ $M_{AD} = 7816.966\,kips\cdot ft$

$M_{y\_unshored} := \min\left(M_{yt}, M_{yc}\right)$ $M_{y\_unshored} = 19572.45\,kips\cdot ft$

$$S_{xt\_2.1} := \frac{M_{yt}}{F_{yt}} \qquad S_{xt\_2.1} = 4697.388\,in^3$$

Concrete Stress at First Yield (unshored)

$$f_{conc\_composite\_unshored\_at\_My} := \left(\frac{M_{D2}}{S_{slab\_3n}\cdot 3n} + \frac{M_{AD}}{S_{slab\_n}\cdot n}\right) \qquad f_{conc\_composite\_unshored\_at\_My} = 1.5\,ksi$$

$$\frac{f_{conc\_composite\_unshored\_at\_My}}{f_c} = 0.375$$

Shape Factor :

$\frac{M_p}{M_{y\_unshored}} = 1.324$ $\frac{M_p}{M_{y\_shortterm}} = 1.174$ $\frac{M_p}{M_{y\_longterm}} = 1.277$

Unshored Composite Section Properties :

Yield Moment (unshored) associated with STRENGTH IV - G1-S3

$f_{D1t} := 28.741\,ksi$ $f_{D1c} := 36.180\,ksi$ $M_{DC2} := 0\cdot kip\cdot ft$ $M_{DW} := 1112.221\cdot kip\cdot ft$

$M_{D1t} := f_{D1t}\cdot S_t$ $M_{D1c} := f_{D1c}\cdot S_c$ $M_{D2} := M_{DC2} + M_{DW}$

$M_{D1t} = 10349.273\,kips\cdot ft$ $M_{D1c} = 10230.565\,kips\cdot ft$ $M_{D2} = 1112.221\,kip\cdot ft$

Tension Flange :

$$M_{ADt} := \left(F_{yt} - \frac{M_{D1t}}{S_t} - \frac{M_{D2}}{S_{t\_3n}}\right)\cdot S_{t\_n} \qquad M_{ADt} = 8175.109\,kips\cdot ft$$

$M_{yt} := M_{D1t} + M_{D2} + M_{ADt}$ $M_{yt} = 19636.603\,kips\cdot ft$

Compression Flange :

$$M_{ADc} := \left(F_{yc} - \frac{M_{D1c}}{S_c} - \frac{M_{D2}}{S_{c\_3n}}\right)\cdot S_{c\_n} \qquad M_{ADc} = 11369.334\,kips\cdot ft$$

$M_{yc} := M_{D1c} + M_{D2} + M_{ADc}$ $M_{yc} = 22712.12\,kips\cdot ft$

$M_{AD} := \min\left(M_{ADt}, M_{ADc}\right)$ $M_{AD} = 8175.109\,kips\cdot ft$

$M_{y\_unshored} := \min\left(M_{yt}, M_{yc}\right)$ $M_{y\_unshored} = 19636.603\,kips\cdot ft$

$$S_{xt\_2.2} := \frac{M_{yt}}{F_{yt}} \qquad S_{xt\_2.2} = 4712.785\,in^3$$

Concrete Stress at First Yield (unshored)

$$f_{conc\_composite\_unshored\_at\_My} := \left(\frac{M_{D2}}{S_{slab\_3n}\cdot 3n} + \frac{M_{AD}}{S_{slab\_n}\cdot n}\right) \qquad f_{conc\_composite\_unshored\_at\_My} = 1.562\,ksi$$

$$\frac{f_{conc\_composite\_unshored\_at\_My}}{f_c} = 0.39$$

Shape Factor :

$$\frac{M_p}{M_{y\_unshored}} = 1.32 \qquad \frac{M_p}{M_{y\_shortterm}} = 1.174 \qquad \frac{M_p}{M_{y\_longterm}} = 1.277$$

Constructibility Check 1, STRENGTH IV

Construction load stresses are factored, load factor = 1.5

G1 top flange - G1-S2

$\phi_f := 1.0$ $L_b := 18.024 \cdot ft$ $L_b = 18.024\,ft$ $R_{b\_noncomp} = 1$ $R_b := R_{b\_noncomp}$

Moment Gradient Modifier for LTB(Cb) :

$f_0 := 35.340 ksi$ $f_2 := 36.150 ksi$ $f_{mid} := 35.780 \cdot ksi$

$f_1 := \max\left[\left(2 \cdot f_{mid} - f_2\right), f_0\right]$ $f_1 = 35.41\,ksi$

$$C_b := 1.75 - 1.05 \cdot \left(\frac{f_1}{f_2}\right) + 0.3 \cdot \left(\frac{f_1}{f_2}\right)^2 \qquad C_b = 1.01$$

Estimation of Flange Second Order Lateral Bending Stress:

$f_{b1} := 36.150 \cdot ksi$ $f_{l1} := 4.91 \cdot ksi$

i) Based on k=1.0 $k := 1.0$

$$\lambda := \frac{k \cdot L_b}{r_t} \qquad \lambda = 46.118$$

$$F_{cr} := \frac{C_b \cdot R_b \cdot \pi^2 \cdot E}{\lambda^2} \qquad F_{cr} = 135.83\,ksi$$

$$AF := \begin{cases} \dfrac{0.85}{1 - \dfrac{f_{b1}}{F_{cr}}} & \text{if } \dfrac{0.85}{1 - \dfrac{f_{b1}}{F_{cr}}} \geq 1 \\ 1 & \text{otherwise} \end{cases} \qquad AF = 1.158$$

ii) Based on k=0.875 $k := 0.875$

***Note: k = 0.875 is estimated based on the end restraint effects.**

$$\lambda := \frac{k \cdot L_b}{r_t} \qquad \lambda = 40.354$$

$$F_{cr0.875} := \frac{C_b \cdot R_b \cdot \pi^2 \cdot E}{\lambda^2} \qquad F_{cr0.875} = 177.41\,ksi$$

$$AF := \begin{cases} \dfrac{0.85}{1 - \dfrac{f_{b1}}{F_{cr0.875}}} & \text{if } \dfrac{0.85}{1 - \dfrac{f_{b1}}{F_{cr0.875}}} \geq 1 \\ 1 & \text{otherwise} \end{cases} \qquad AF = 1.068$$

$f_{b2} := 37.160 \cdot ksi$ $f_{l2} := 1.26 \cdot ksi$

Actual second-order amplification: $\dfrac{f_{l2}}{f_{l1}} = 0.257$

Maximum Lateral Bending Stress Limit

$f_{l2} = 1.26\,\text{ksi}$ $\qquad 0.6F_{yc} = 30\,\text{ksi}$

$$\text{Lateral\_bending\_stress\_limit\_Check} := \begin{cases} \text{"OK"} & \text{if } f_{l2} < 0.6F_{yc} \\ \text{"NG"} & \text{otherwise} \end{cases}$$

Lateral_bending_stress_limit_Check = "OK"

$$\text{Lateral\_bending\_stress\_ratio} := \frac{f_{l2}}{0.6F_{yc}}$$

Lateral_bending_stress_ratio = 0.042

Yielding Limit

$f_{b2} + f_{l2} = 38.42\,\text{ksi}$ $\qquad \phi_f R_{h\_noncomp} \cdot F_{yc} = 50\,\text{ksi}$

$$\text{Yielding\_Limit\_Check} := \begin{cases} \text{"OK"} & \text{if } f_{b2} + f_{l2} \le \phi_f R_{h\_noncomp} \cdot F_{yc} \\ \text{"NG"} & \text{otherwise} \end{cases}$$

Yielding_Limit_Check = "OK"

$$\text{Yielding\_ratio} := \frac{f_{b2} + f_{l2}}{\phi_f R_{h\_noncomp} \cdot F_{yc}}$$

Yielding_ratio = 0.768

Strength Limit

$f_{l2} := 10.030 \cdot \text{ksi}$ $\qquad$ **** Note that f_{l2} is the maximum stress within the unbraced length***

Local Buckling Resistance :

$F_{yr} := 0.7 \cdot F_{yc}$

$\lambda_f := \dfrac{b_{fc}}{2 \cdot t_{fc}}$ $\quad \lambda_f = 4.5$ $\quad \lambda_{pf} := 0.38 \cdot \sqrt{\dfrac{E}{F_{yc}}}$ $\quad \lambda_{pf} = 9.152$ $\quad \lambda_{rf} := 0.56 \cdot \sqrt{\dfrac{E}{F_{yr}}}$ $\quad \lambda_{rf} = 16.12$

$$F_{nc\_FLB} := \begin{cases} R_b \cdot R_{h\_noncomp} \cdot F_{yc} & \text{if } \lambda_f \le \lambda_{pf} \\ \left[1 - \left(1 - \dfrac{F_{yr}}{R_{h\_noncomp} \cdot F_{yc}}\right) \cdot \left(\dfrac{\lambda_f - \lambda_{pf}}{\lambda_{rf} - \lambda_{pf}}\right)\right] \cdot R_b \cdot R_{h\_noncomp} \cdot F_{yc} & \text{if } \lambda_{pf} < \lambda_f \le \lambda_{rf} \end{cases}$$

$F_{nc\_FLB} = 50\,\text{ksi}$

Lateral Torsional Buckling Resistance :

$L_b = 18.024\,\text{ft}$ $L_p := 1.0 \cdot r_t \cdot \sqrt{\frac{E}{F_{yc}}}$ $L_p = 9.412\,\text{ft}$ $L_r := \pi \cdot r_t \cdot \sqrt{\frac{E}{F_{yr}}}$ $L_r = 35.342\,\text{ft}$

$$F_{nc\_LTB} := \begin{cases} R_b \cdot R_{h\_noncomp} \cdot F_{yc} & \text{if } L_b \le L_p \\ \min\left[C_b \cdot \left[1 - \left(1 - \frac{F_{yr}}{R_{h\_noncomp} \cdot F_{yc}}\right) \cdot \left(\frac{L_b - L_p}{L_r - L_p}\right)\right] \cdot R_b \cdot R_{h\_noncomp} \cdot F_{yc}, R_b \cdot R_{h\_noncomp} \cdot F_{yc}\right] & \text{if } L_p < L_b \le L_r \\ \text{otherwise} \\ \quad \begin{cases} F_{cr} & \text{if } F_{cr} \le R_b \cdot R_{h\_noncomp} \cdot F_{yc} \\ R_b \cdot R_{h\_noncomp} \cdot F_{yc} & \text{otherwise} \end{cases} \end{cases}$$

$F_{nc\_LTB} = 45.439\,\text{ksi}$

$$\text{Controling\_Strength} := \begin{cases} \text{"Flange Local Buckling"} & \text{if } F_{nc\_FLB} \le F_{nc\_LTB} \\ \text{"Lateral Torsional Buckling"} & \text{otherwise} \end{cases}$$

Controling_Strength = "Lateral Torsional Buckling"

$f_{b2} + \frac{f_{l2}}{3} = 40.5\,\text{ksi}$ $F_{nc} := \min\left(F_{nc\_LTB}, F_{nc\_FLB}\right)$ $\phi_f F_{nc} = 45.44\,\text{ksi}$

$$\text{Strength\_Limit\_Check} := \begin{cases} \text{"OK"} & \text{if } f_{b2} + \frac{f_{l2}}{3} \le \phi_f F_{nc} \\ \text{"NG"} & \text{otherwise} \end{cases}$$

Strength_Limit_Check = "OK"

$$\text{Strength\_ratio} := \frac{f_{b2} + \frac{f_{l2}}{3}}{\phi_f F_{nc}}$$

Strength_ratio = 0.891

Web bend buckling limit

$k := \frac{9}{\left(\frac{D_c}{D}\right)^2}$ $k = 27.768$ $F_{crw} := 0.9 \cdot E \cdot \frac{k}{\left(\frac{D}{t_w}\right)^2}$ $\phi_f F_{crw} = 78.64\,\text{ksi}$ $f_{b2} = 37.16\,\text{ksi}$

$$\text{Strength\_Limit\_Check} := \begin{cases} \text{"OK"} & \text{if } f_{b2} \le \phi_f F_{crw} \\ \text{"NG"} & \text{otherwise} \end{cases}$$

Strength_Limit_Check = "OK"

$$\text{Web\_bend\_buckling\_ratio} := \frac{f_{b2}}{\phi_f F_{crw}}$$

Web_bend_buckling_ratio = 0.47

G1 bottom flange - G1-S2

$f_{b2} := 29.512 \cdot ksi$ $f_{l2} := 8.48 \cdot ksi$

Maximum Lateral Bending Stress Limit

$f_{l2} = 8.48\,ksi$ $0.6F_{yt} = 30\,ksi$

$$Lateral\_bending\_stress\_limit\_Check := \begin{cases} "OK" & \text{if } f_{l2} < 0.6F_{yt} \\ "NG" & \text{otherwise} \end{cases}$$

$Lateral\_bending\_stress\_limit\_Check = "OK"$

$$Lateral\_bending\_stress\_ratio := \frac{f_{l2}}{0.6F_{yt}}$$

$Lateral\_bending\_stress\_ratio = 0.283$

Yielding Limit

$f_{b2} + f_{l2} = 37.992\,ksi$ $\phi_f R_{h\_noncomp} \cdot F_{yt} = 50\,ksi$

$$Yielding\_Limit\_Check := \begin{cases} "OK" & \text{if } f_{b2} + f_{l2} \le \phi_f R_{h\_noncomp} \cdot F_{yt} \\ "NG" & \text{otherwise} \end{cases}$$

$Yielding\_Limit\_Check = "OK"$

$$Yielding\_ratio := \frac{f_{b2} + f_{l2}}{\phi_f R_{h\_noncomp} \cdot F_{yt}}$$

$Yielding\_ratio = 0.76$

ESTIMATION OF THE CAPACITY BASED ON THE OVERALL BUCKLING OF THE SYSTEM

For G1-S2

***Note that ρ_o is maximum at this location where ρ_o is the ratio of the factored compression flange stress to the section yield strength.*

$ksi := 10^3 \cdot psi$; $kips := 10^3 lbf$

$f_{b2} := 37.16 \cdot ksi$ $f_{l2} := 10.030 \cdot ksi$ $F_{yc} := 50 \cdot ksi$ $F_{yr} := 35 \cdot ksi$

$R_b := 1$ $R_h := 1$ $\phi_f := 1$

$$\rho_o := \frac{f_{b2}}{F_{yc}} \qquad \rho_o = 0.743$$

$\gamma_{e\_LTB} := 2.5406$

***Note that γ_{e_LTB} is the ratio of the load at buckling to the load of f_{b2}.*

$$\frac{F_{yc}}{FeLTB} = \rho_o \cdot \gamma_{e\_LTB} \qquad \rho_o \cdot \gamma_{e\_LTB} = 1.888$$

$$R_b \cdot R_h \cdot F_{yc} \cdot \left[1 - \left(1 - \frac{F_{yr}}{R_h \cdot F_{yc}} \right) \cdot \left(\frac{\pi \cdot \sqrt{\frac{1}{\rho_o \cdot \gamma_{e\_LTB}}} - 1}{\pi \cdot \sqrt{\frac{F_{yc}}{F_{yr}}} - 1} \right) \right] = 42.996\,ksi$$

$$F_{nc} := \min \left[R_b \cdot R_h \cdot F_{yc} \cdot \left[1 - \left(1 - \frac{F_{yr}}{R_h \cdot F_{yc}} \right) \cdot \left(\frac{\pi \cdot \sqrt{\frac{1}{\rho_o \cdot \gamma_{e\_LTB}}} - 1}{\pi \cdot \sqrt{\frac{F_{yc}}{F_{yr}}} - 1} \right) \right], R_b \cdot R_h \cdot F_{yc} \right]$$

$F_{nc} = 42.996\,ksi$

***F_{nc} was calculated as 45.439 ksi based on the resistance equation in terms of unbraced lengths of L_b.*

$$\text{LTB\_Check} := \begin{cases} \text{"OK"} & \text{if } f_{b2} \le \phi_f \cdot F_{nc} \\ \text{"NG"} & \text{otherwise} \end{cases}$$

LTB_Check = "OK"

$$\text{Strength\_Limit\_Check} := \begin{cases} \text{"OK"} & \text{if } f_{b2} + \frac{f_{l2}}{3} \le \phi_f \cdot F_{nc} \\ \text{"NG"} & \text{otherwise} \end{cases}$$

Strength_Limit_Check = "OK"

$$\text{Strength\_ratio} := \frac{f_{b2} + \frac{f_{l2}}{3}}{\phi_f \cdot F_{nc}}$$

Strength_ratio = 0.942

**** Strength ratio was calculated as 0.891 based on the resistance equation in terms of unbraced lengths of L_b.***

Constructibility Check 2, STRENGTH IV

Construction load stresses are factored, load factor = 1.5

G1 top flange - G1-S3

$\phi_f := 1.0$ $L_b := 18.024 \cdot ft$ $L_b = 18.024\,ft$ $R_{b\_noncomp} = 1$ $R_b := R_{b\_noncomp}$

Moment Gradient Modifier for LTB(Cb) :

$f_0 := 35.340 ksi$ $f_2 := 36.150 ksi$ $f_{mid} := 35.780 \cdot ksi$

$f_1 := \max\left[\left(2 \cdot f_{mid} - f_2\right), f_0\right]$ $f_1 = 35.41\,ksi$

$$C_b := 1.75 - 1.05 \cdot \left(\frac{f_1}{f_2}\right) + 0.3 \cdot \left(\frac{f_1}{f_2}\right)^2 \qquad C_b = 1.01$$

Estimation of Flange Second Order Lateral Bending Stress:

$f_{b1} := 35.340 \cdot ksi$ $f_{l1} := 5.56 \cdot ksi$

i) Based on k=1.0 $k := 1.0$

$$\lambda := \frac{k \cdot L_b}{r_t} \qquad \lambda = 46.118$$

$$F_{cr} := \frac{C_b \cdot R_b \cdot \pi^2 \cdot E}{\lambda^2} \qquad F_{cr} = 135.83\,ksi$$

$$AF := \begin{cases} \dfrac{0.85}{1 - \dfrac{f_{b1}}{F_{cr}}} & \text{if } \dfrac{0.85}{1 - \dfrac{f_{b1}}{F_{cr}}} \geq 1 \\ 1 & \text{otherwise} \end{cases} \qquad AF = 1.149$$

ii) Based on k=0.875 $k := 0.875$

***Note: k = 0.875 is estimated based on the end restraint effects.**

$$\lambda := \frac{k \cdot L_b}{r_t} \qquad \lambda = 40.354$$

$$F_{cr0.875} := \frac{C_b \cdot R_b \cdot \pi^2 \cdot E}{\lambda^2} \qquad F_{cr0.875} = 177.41\,ksi$$

$$AF := \begin{cases} \dfrac{0.85}{1 - \dfrac{f_{b1}}{F_{cr0.875}}} & \text{if } \dfrac{0.85}{1 - \dfrac{f_{b1}}{F_{cr0.875}}} \geq 1 \\ 1 & \text{otherwise} \end{cases} \qquad AF = 1.061$$

$f_{b2} := 36.180 \cdot ksi$ $f_{l2} := 3.13 \cdot ksi$

Actual second-order amplification: $\dfrac{f_{l2}}{f_{l1}} = 0.563$

Maximum Lateral Bending Stress Limit

$f_{l2} = 3.13\,\text{ksi}$ $\qquad 0.6F_{yc} = 30\,\text{ksi}$

$$\text{Lateral\_bending\_stress\_limit\_Check} := \begin{cases} \text{"OK"} & \text{if } f_{l2} < 0.6F_{yc} \\ \text{"NG"} & \text{otherwise} \end{cases}$$

Lateral_bending_stress_limit_Check = "OK"

$$\text{Lateral\_bending\_stress\_ratio} := \frac{f_{l2}}{0.6F_{yc}}$$

Lateral_bending_stress_ratio = 0.104

Yielding Limit

$f_{b2} + f_{l2} = 39.31\,\text{ksi}$ $\qquad \phi_f R_{h\_noncomp} \cdot F_{yc} = 50\,\text{ksi}$

$$\text{Yielding\_Limit\_Check} := \begin{cases} \text{"OK"} & \text{if } f_{b2} + f_{l2} \le \phi_f R_{h\_noncomp} \cdot F_{yc} \\ \text{"NG"} & \text{otherwise} \end{cases}$$

Yielding_Limit_Check = "OK"

$$\text{Yielding\_ratio} := \frac{f_{b2} + f_{l2}}{\phi_f R_{h\_noncomp} \cdot F_{yc}}$$

Yielding_ratio = 0.786

Strength Limit

$f_{l2} := 10.030 \cdot \text{ksi}$ **** Note that f_{l2} is the maximum stress within the unbraced length***

Local Buckling Resistance :

$F_{yr} := 0.7 \cdot F_{yc}$

$\lambda_f := \dfrac{b_{fc}}{2 \cdot t_{fc}}$ $\quad \lambda_f = 4.5$ $\quad \lambda_{pf} := 0.38 \cdot \sqrt{\dfrac{E}{F_{yc}}}$ $\quad \lambda_{pf} = 9.152$ $\quad \lambda_{rf} := 0.56 \sqrt{\dfrac{E}{F_{yr}}}$ $\quad \lambda_{rf} = 16.12$

$$F_{nc\_FLB} := \begin{cases} R_b \cdot R_{h\_noncomp} \cdot F_{yc} & \text{if } \lambda_f \le \lambda_{pf} \\ \left[1 - \left(1 - \dfrac{F_{yr}}{R_{h\_noncomp} \cdot F_{yc}}\right) \cdot \left(\dfrac{\lambda_f - \lambda_{pf}}{\lambda_{rf} - \lambda_{pf}}\right)\right] \cdot R_b \cdot R_{h\_noncomp} \cdot F_{yc} & \text{if } \lambda_{pf} < \lambda_f \le \lambda_{rf} \end{cases}$$

$F_{nc\_FLB} = 50\,\text{ksi}$

Lateral Torsional Buckling Resistance :

$L_b = 18.024\,\text{ft}$ $L_p := 1.0 \cdot r_t \cdot \sqrt{\frac{E}{F_{yc}}}$ $L_p = 9.412\,\text{ft}$ $L_r := \pi \cdot r_t \cdot \sqrt{\frac{E}{F_{yr}}}$ $L_r = 35.342\,\text{ft}$

$$F_{nc\_LTB} := \begin{cases} R_b \cdot R_{h\_noncomp} \cdot F_{yc} & \text{if } L_b \le L_p \\ \min\left[C_b \cdot \left[1 - \left(1 - \frac{F_{yr}}{R_{h\_noncomp} \cdot F_{yc}}\right) \cdot \left(\frac{L_b - L_p}{L_r - L_p}\right)\right] \cdot R_b \cdot R_{h\_noncomp} \cdot F_{yc},\ R_b \cdot R_{h\_noncomp} \cdot F_{yc}\right] & \text{if } L_p < L_b \le L_r \\ \text{otherwise} \\ \quad \begin{cases} F_{cr} & \text{if } F_{cr} \le R_b \cdot R_{h\_noncomp} \cdot F_{yc} \\ R_b \cdot R_{h\_noncomp} \cdot F_{yc} & \text{otherwise} \end{cases} \end{cases}$$

$F_{nc\_LTB} = 45.439\,\text{ksi}$

$$\text{Controling\_Strength} := \begin{cases} \text{"Flange Local Buckling"} & \text{if } F_{nc\_FLB} \le F_{nc\_LTB} \\ \text{"Lateral Torsional Buckling"} & \text{otherwise} \end{cases}$$

Controling_Strength = "Lateral Torsional Buckling"

$f_{b2} + \frac{f_{l2}}{3} = 39.52\,\text{ksi}$ $F_{nc} := \min\left(F_{nc\_LTB}, F_{nc\_FLB}\right)$ $\phi_f F_{nc} = 45.44\,\text{ksi}$

$$\text{Strength\_Limit\_Check} := \begin{cases} \text{"OK"} & \text{if } f_{b2} + \frac{f_{l2}}{3} \le \phi_f F_{nc} \\ \text{"NG"} & \text{otherwise} \end{cases}$$

Strength_Limit_Check = "OK"

$$\text{Strength\_ratio} := \frac{f_{b2} + \frac{f_{l2}}{3}}{\phi_f F_{nc}}$$

Strength_ratio = 0.87

Web bend buckling limit

$k := \frac{9}{\left(\frac{D_c}{D}\right)^2}$ $k = 27.768$ $F_{crw} := 0.9 \cdot E \cdot \frac{k}{\left(\frac{D}{t_w}\right)^2}$ $\phi_f F_{crw} = 78.64\,\text{ksi}$ $f_{b2} = 36.18\,\text{ksi}$

$$\text{Strength\_Limit\_Check} := \begin{cases} \text{"OK"} & \text{if } f_{b2} \le \phi_f F_{crw} \\ \text{"NG"} & \text{otherwise} \end{cases}$$

Strength_Limit_Check = "OK"

$$\text{Web\_bend\_buckling\_ratio} := \frac{f_{b2}}{\phi_f F_{crw}}$$

Web_bend_buckling_ratio = 0.46

G1 bottom flange - G1-S3

$f_{b2} := 28.741 \cdot ksi$ $f_{l2} := 7.65 \cdot ksi$

Maximum Lateral Bending Stress Limit

$f_{l2} = 7.65\,ksi$ $0.6F_{yt} = 30\,ksi$

$$Lateral\_bending\_stress\_limit\_Check := \begin{cases} "OK" & \text{if } f_{l2} < 0.6F_{yt} \\ "NG" & \text{otherwise} \end{cases}$$

$Lateral\_bending\_stress\_limit\_Check = "OK"$

$$Lateral\_bending\_stress\_ratio := \frac{f_{l2}}{0.6F_{yt}}$$

$Lateral\_bending\_stress\_ratio = 0.255$

Yielding Limit

$f_{b2} + f_{l2} = 36.391\,ksi$ $\phi_f R_{h\_noncomp} \cdot F_{yt} = 50\,ksi$

$$Yielding\_Limit\_Check := \begin{cases} "OK" & \text{if } f_{b2} + f_{l2} \le \phi_f R_{h\_noncomp} \cdot F_{yt} \\ "NG" & \text{otherwise} \end{cases}$$

$Yielding\_Limit\_Check = "OK"$

$$Yielding\_ratio := \frac{f_{b2} + f_{l2}}{\phi_f R_{h\_noncomp} \cdot F_{yt}}$$

$Yielding\_ratio = 0.728$

Constructibility Check 3, STRENGTH IV

Construction load stresses are factored, load factor = 1.5

G1 top flange - G1-S5

$\phi_f := 1.0$ $L_b := 18.024 \cdot ft$ $L_b = 18.024\,ft$ $R_{b\_noncomp} = 1$ $R_b := R_{b\_noncomp}$

Moment Gradient Modifier for LTB(Cb) :

$f_0 := 35.340 ksi$ $f_2 := 36.150 ksi$ $f_{mid} := 35.780 \cdot ksi$

$f_1 := \max\left[\left(2 \cdot f_{mid} - f_2\right), f_0\right]$ $f_1 = 35.41\,ksi$

$$C_b := 1.75 - 1.05 \cdot \left(\frac{f_1}{f_2}\right) + 0.3 \cdot \left(\frac{f_1}{f_2}\right)^2$$

$C_b = 1.01$

Estimation of Flange Second Order Lateral Bending Stress:

$f_{b1} := 36.150 \cdot ksi$ $f_{l1} := 4.91 \cdot ksi$

i) Based on k=1.0 $k := 1.0$

$$\lambda := \frac{k \cdot L_b}{r_t}$$ $\lambda = 46.118$

$$F_{cr} := \frac{C_b \cdot R_b \cdot \pi^2 \cdot E}{\lambda^2}$$ $F_{cr} = 135.83\,ksi$

$$AF := \begin{cases} \dfrac{0.85}{1 - \dfrac{f_{b1}}{F_{cr}}} & \text{if } \dfrac{0.85}{1 - \dfrac{f_{b1}}{F_{cr}}} \geq 1 \\ 1 & \text{otherwise} \end{cases}$$ $AF = 1.158$

ii) Based on k=0.875 $k := 0.875$

***Note: k = 0.875 is estimated based on the end restraint effects.**

$$\lambda := \frac{k \cdot L_b}{r_t}$$ $\lambda = 40.354$

$$F_{cr0.875} := \frac{C_b \cdot R_b \cdot \pi^2 \cdot E}{\lambda^2}$$ $F_{cr0.875} = 177.41\,ksi$

$$AF := \begin{cases} \dfrac{0.85}{1 - \dfrac{f_{b1}}{F_{cr0.875}}} & \text{if } \dfrac{0.85}{1 - \dfrac{f_{b1}}{F_{cr0.875}}} \geq 1 \\ 1 & \text{otherwise} \end{cases}$$ $AF = 1.068$

$f_{b2} := 37.160 \cdot ksi$ $f_{l2} := 1.26 \cdot ksi$

Actual second-order amplification: $\dfrac{f_{l2}}{f_{l1}} = 0.257$

Maximum Lateral Bending Stress Limit

$f_{l2} = 1.26\,ksi$ $\qquad 0.6F_{yc} = 30\,ksi$

$$Lateral\_bending\_stress\_limit\_Check := \begin{cases} "OK" & \text{if } f_{l2} < 0.6F_{yc} \\ "NG" & \text{otherwise} \end{cases}$$

Lateral_bending_stress_limit_Check = "OK"

$$Lateral\_bending\_stress\_ratio := \frac{f_{l2}}{0.6F_{yc}}$$

Lateral_bending_stress_ratio = 0.042

Yielding Limit

$f_{b2} + f_{l2} = 38.42\,ksi$ $\qquad \phi_f R_{h\_noncomp} \cdot F_{yc} = 50\,ksi$

$$Yielding\_Limit\_Check := \begin{cases} "OK" & \text{if } f_{b2} + f_{l2} \le \phi_f R_{h\_noncomp} \cdot F_{yc} \\ "NG" & \text{otherwise} \end{cases}$$

Yielding_Limit_Check = "OK"

$$Yielding\_ratio := \frac{f_{b2} + f_{l2}}{\phi_f R_{h\_noncomp} \cdot F_{yc}}$$

Yielding_ratio = 0.768

Strength Limit

$f_{l2} := 10.030 \cdot ksi$ **** Note that** f_{l2} **is the maximum stress within the unbraced length***

Local Buckling Resistance :

$F_{yr} := 0.7 \cdot F_{yc}$

$\lambda_f := \frac{b_{fc}}{2 \cdot t_{fc}}$ $\qquad \lambda_f = 4.5$ $\qquad \lambda_{pf} := 0.38 \cdot \sqrt{\frac{E}{F_{yc}}}$ $\qquad \lambda_{pf} = 9.152$ $\qquad \lambda_{rf} := 0.56 \sqrt{\frac{E}{F_{yr}}}$ $\qquad \lambda_{rf} = 16.12$

$$F_{nc\_FLB} := \begin{cases} R_b \cdot R_{h\_noncomp} \cdot F_{yc} & \text{if } \lambda_f \le \lambda_{pf} \\ \left[1 - \left(1 - \frac{F_{yr}}{R_{h\_noncomp} \cdot F_{yc}}\right) \cdot \left(\frac{\lambda_f - \lambda_{pf}}{\lambda_{rf} - \lambda_{pf}}\right)\right] \cdot R_b \cdot R_{h\_noncomp} \cdot F_{yc} & \text{if } \lambda_{pf} < \lambda_f \le \lambda_{rf} \end{cases}$$

$F_{nc\_FLB} = 50\,ksi$

Lateral Torsional Buckling Resistance :

$L_b = 18.024\,\text{ft}$ $\quad L_p := 1.0 \cdot r_t \cdot \sqrt{\frac{E}{F_{yc}}}$ $\quad L_p = 9.412\,\text{ft}$ $\quad L_r := \pi \cdot r_t \cdot \sqrt{\frac{E}{F_{yr}}}$ $\quad L_r = 35.342\,\text{ft}$

$$F_{nc\_LTB} := \begin{cases} R_b \cdot R_{h\_noncomp} \cdot F_{yc} & \text{if } L_b \le L_p \\ \min\left[C_b \cdot \left[1 - \left(1 - \frac{F_{yr}}{R_{h\_noncomp} \cdot F_{yc}} \right) \cdot \left(\frac{L_b - L_p}{L_r - L_p} \right) \right] \cdot R_b \cdot R_{h\_noncomp} \cdot F_{yc}, R_b \cdot R_{h\_noncomp} \cdot F_{yc} \right] & \text{if } L_p < L_b \le L_r \\ \text{otherwise} \\ \quad \begin{cases} F_{cr} & \text{if } F_{cr} \le R_b \cdot R_{h\_noncomp} \cdot F_{yc} \\ R_b \cdot R_{h\_noncomp} \cdot F_{yc} & \text{otherwise} \end{cases} \end{cases}$$

$F_{nc\_LTB} = 45.439\,\text{ksi}$

$$\text{Controling\_Strength} := \begin{cases} \text{"Flange Local Buckling"} & \text{if } F_{nc\_FLB} \le F_{nc\_LTB} \\ \text{"Lateral Torsional Buckling"} & \text{otherwise} \end{cases}$$

Controling_Strength = "Lateral Torsional Buckling"

$f_{b2} + \frac{f_{l2}}{3} = 40.5\,\text{ksi}$ $\quad F_{nc} := \min\left(F_{nc\_LTB}, F_{nc\_FLB}\right)$ $\quad \phi_f F_{nc} = 45.44\,\text{ksi}$

$$\text{Strength\_Limit\_Check} := \begin{cases} \text{"OK"} & \text{if } f_{b2} + \frac{f_{l2}}{3} \le \phi_f F_{nc} \\ \text{"NG"} & \text{otherwise} \end{cases}$$

Strength_Limit_Check = "OK"

$$\text{Strength\_ratio} := \frac{f_{b2} + \frac{f_{l2}}{3}}{\phi_f F_{nc}}$$

Strength_ratio = 0.891

Web bend buckling limit

$k := \frac{9}{\left(\frac{D_c}{D}\right)^2}$ $\quad k = 27.768$ $\quad F_{crw} := 0.9 \cdot E \cdot \frac{k}{\left(\frac{D}{t_w}\right)^2}$ $\quad \phi_f F_{crw} = 78.64\,\text{ksi}$ $\quad f_{b2} = 37.16\,\text{ksi}$

$$\text{Strength\_Limit\_Check} := \begin{cases} \text{"OK"} & \text{if } f_{b2} \le \phi_f F_{crw} \\ \text{"NG"} & \text{otherwise} \end{cases}$$

Strength_Limit_Check = "OK"

$$\text{Web\_bend\_buckling\_ratio} := \frac{f_{b2}}{\phi_f F_{crw}}$$

Web_bend_buckling_ratio = 0.47

G1 bottom flange - G1-S5

$f_{b2} := 29.491 \cdot ksi$ $f_{l2} := 8.51 \cdot ksi$

Maximum Lateral Bending Stress Limit

$f_{l2} = 8.51\,ksi$ $0.6F_{yt} = 30\,ksi$

$$Lateral\_bending\_stress\_limit\_Check := \begin{cases} "OK" & \text{if } f_{l2} < 0.6F_{yt} \\ "NG" & \text{otherwise} \end{cases}$$

$Lateral\_bending\_stress\_limit\_Check = "OK"$

$$Lateral\_bending\_stress\_ratio := \frac{f_{l2}}{0.6F_{yt}}$$

$Lateral\_bending\_stress\_ratio = 0.284$

Yielding Limit

$f_{b2} + f_{l2} = 38.001\,ksi$ $\phi_f R_{h\_noncomp} \cdot F_{yt} = 50\,ksi$

$$Yielding\_Limit\_Check := \begin{cases} "OK" & \text{if } f_{b2} + f_{l2} \le \phi_f R_{h\_noncomp} \cdot F_{yt} \\ "NG" & \text{otherwise} \end{cases}$$

$Yielding\_Limit\_Check = "OK"$

$$Yielding\_ratio := \frac{f_{b2} + f_{l2}}{\phi_f R_{h\_noncomp} \cdot F_{yt}}$$

$Yielding\_ratio = 0.76$

Strength Limit State Check 1-1, STRENGTH I

All stresses and moments are unfactored except construction load stresses are factored, load factor = 1.25. Also the dynamic allowance of 1.33 is included in the calcuation of the truck load stresses.

**** In this section, live loads is checked based on maximum major-axis bending values with concurrent flange lateral bending stress.***

G1 Bottom flange -G1-S1

$M_{u\_constr} := 8738.755 \cdot kips \cdot ft$ $M_{u\_DC2} := 1100.893 \cdot kips \cdot ft$ $M_{u\_DW} := 749.872 \cdot kips \cdot ft$ $M_{u\_LL} := 6822.992 \cdot kips \cdot ft$

$M_u := \left(M_{u\_constr} + 1.25 M_{u\_DC2}\right) + 1.5 \cdot \left(M_{u\_DW}\right) + 1.75 \cdot \left(M_{u\_LL}\right)$ $M_u = 23179.915\ kips \cdot ft$

$f_{b\_constr} := 24.268 \cdot ksi$ $f_{b\_DC2} := 2.712 \cdot ksi$ $f_{b\_DW} := 1.847 \cdot ksi$ $f_{b\_LL} := 15.456 \cdot ksi$

$f_b := \left(f_{b\_constr} + 1.25 f_{b\_DC2}\right) + 1.5 \cdot \left(f_{b\_DW}\right) + 1.75 \cdot \left(f_{b\_LL}\right)$ $f_b = 57.477\ ksi$

$f_{l\_constr} := -0.850 \cdot ksi$ $f_{l\_DC2} := 0.412 \cdot ksi$ $f_{l\_DW} := 0.177 \cdot ksi$ $f_{l\_LL} := 1.940 \cdot ksi$

$f_l := \left(f_{l\_constr} + 1.25 f_{l\_DC2}\right) + 1.5 \cdot \left(f_{l\_DW}\right) + 1.75 \cdot \left(f_{l\_LL}\right)$ $f_l = 3.325\ ksi$

Ductility Requirement:

$D_p = 23.459\ in$ $D_{t\_3n} = 85.75\ in$

$$Ductility\_Requirement\_Check := \begin{cases} \text{"OK"} & \text{if } D_p \le 0.42 \cdot D_{t\_3n} \\ \text{"NG"} & \text{otherwise} \end{cases}$$

$Ductility\_Requirement\_Check = \text{"OK"}$

$$Ductility\_ratio := \frac{D_p}{0.42 \cdot D_{t\_3n}}$$

$Ductility\_ratio = 0.651$

Maximum Lateral Bending Stress Limit

$f_l = 3.325\ ksi$ $0.6F_{yc} = 30\ ksi$

$$Lateral\_bending\_stress\_limit\_Check := \begin{cases} \text{"OK"} & \text{if } f_l < 0.6F_{yc} \\ \text{"NG"} & \text{otherwise} \end{cases}$$

$Lateral\_bending\_stress\_limit\_Check = \text{"OK"}$

$$Lateral\_bending\_stress\_ratio := \frac{f_l}{0.6F_{yc}}$$

$Lateral\_bending\_stress\_ratio = 0.111$

Strength Limit

** stress based equation considered as noncompact section*

$f_b + \frac{f_l}{3} = 58.59\,\text{ksi}$ $\qquad \phi_f \cdot R_{h\_comp} \cdot F_{yt} = 50\,\text{ksi}$

$$\text{Strength\_Limit\_Check} := \begin{cases} \text{"OK"} & \text{if } f_b + \frac{f_l}{3} \le \phi_f \cdot R_{h\_comp} \cdot F_{yt} \\ \text{"NG"} & \text{otherwise} \end{cases}$$

Strength_Limit_Check = "NG"

$$\text{Strength\_ratio} := \frac{f_b + \frac{f_l}{3}}{\phi_f \cdot R_{h\_comp} \cdot F_{yt}}$$

Strength_ratio = 1.172

** moment based equation considered as compact section*

Nominal Flexural resistance:

$$M_n := \begin{cases} M_p & \text{if } D_p \le 0.1 \cdot D_{t\_3n} \\ M_p \cdot \left(1.07 - 0.7 \cdot \frac{D_p}{D_{t\_3n}}\right) & \text{otherwise} \end{cases}$$

$\frac{D_p}{D_{t\_3n}} = 0.274$

$M_n = 22763.459\,\text{kips}\cdot\text{ft}$ $\qquad \phi_f \cdot M_n = 22763.459\,\text{kips}\cdot\text{ft}$

$M_u + \frac{f_l \cdot S_{xt\_2.4}}{3} = 23620.24\,\text{kips}\cdot\text{ft}$

$$\text{Strength\_Limit\_Check} := \begin{cases} \text{"OK"} & \text{if } M_u + \frac{f_l \cdot S_{xt\_2.4}}{3} \le \phi_f \cdot M_n \\ \text{"NG"} & \text{otherwise} \end{cases}$$

Strength_Limit_Check = "NG"

$$\text{Strength\_ratio} := \frac{M_u + \frac{f_l \cdot S_{xt\_2.4}}{3}}{\phi_f \cdot M_n}$$

Strength_ratio = 1.038

$$\text{Change\_in\_strength} := \frac{M_n - \frac{f_l \cdot S_{xt\_2.4}}{3}}{\left(F_{yt} - \frac{f_l}{3}\right) \cdot S_{xt\_2.4}}$$

Change_in_strength = 1.149

Strength Limit State Check 1-2, STRENGTH I

All stresses and moments are unfactored except construction load stresses are factored, load factor = 1.25. Also the dynamic allowance of 1.33 is included in the calcuation of the truck load stresses.

**** In this section, live loads is checked based on both maximums of major-axis bending values and flange lateral bending stress.***

G1 Bottom flange - G1-S1

$M_{u\_constr} := 8738.755 \cdot kips \cdot ft$ $M_{u\_DC2} := 1100.893 \cdot kips \cdot ft$ $M_{u\_DW} := 749.872 \cdot kips \cdot ft$ $M_{u\_LL} := 6822.992 \cdot kips \cdot ft$

$M_u := \left(M_{u\_constr} + 1.25 M_{u\_DC2}\right) + 1.5 \cdot \left(M_{u\_DW}\right) + 1.75 \cdot \left(M_{u\_LL}\right)$

$M_u = 23179.915\ kips \cdot ft$

$f_{b\_constr} := 24.268 \cdot ksi$ $f_{b\_DC2} := 2.712 \cdot ksi$ $f_{b\_DW} := 1.847 \cdot ksi$ $f_{b\_LL} := 15.456 \cdot ksi$

$f_b := \left(f_{b\_constr} + 1.25 f_{b\_DC2}\right) + 1.5 \cdot \left(f_{b\_DW}\right) + 1.75 \cdot \left(f_{b\_LL}\right)$

$f_b = 57.477\ ksi$

$f_{l\_constr} := -0.850 \cdot ksi$ $f_{l\_DC2} := 0.412 \cdot ksi$ $f_{l\_DW} := 0.177 \cdot ksi$ $f_{l\_LL} := 1.992 \cdot ksi$

$f_l := \left(f_{l\_constr} + 1.25 f_{l\_DC2}\right) + 1.5 \cdot \left(f_{l\_DW}\right) + 1.75 \cdot \left(f_{l\_LL}\right)$

$f_l = 3.416\ ksi$

Maximum Lateral Bending Stress Limit

$f_l = 3.416\ ksi$ $0.6F_{yc} = 30\ ksi$

$$Lateral\_bending\_stress\_limit\_Check := \begin{cases} \text{"OK"} & \text{if } f_l < 0.6F_{yc} \\ \text{"NG"} & \text{otherwise} \end{cases}$$

$Lateral\_bending\_stress\_limit\_Check = \text{"OK"}$

$$Lateral\_bending\_stress\_ratio := \frac{f_l}{0.6F_{yc}}$$

$Lateral\_bending\_stress\_ratio = 0.114$

Strength Limit

** stress based equation considered as noncompact section*

$f_b + \frac{f_l}{3} = 58.62\,\text{ksi}$ $\qquad \phi_f \cdot R_{h\_comp} \cdot F_{yt} = 50\,\text{ksi}$

$$\text{Strength\_Limit\_Check} := \begin{cases} \text{"OK"} & \text{if } f_b + \frac{f_l}{3} \le \phi_f \cdot R_{h\_comp} \cdot F_{yt} \\ \text{"NG"} & \text{otherwise} \end{cases}$$

Strength_Limit_Check = "NG"

$$\text{Strength\_ratio} := \frac{f_b + \frac{f_l}{3}}{\phi_f \cdot R_{h\_comp} \cdot F_{yt}}$$

Strength_ratio = 1.172

** moment based equation considered as compact section*

Nominal Flexural resistance:

$$M_n := \begin{cases} M_p & \text{if } D_p \le 0.1 \cdot D_{t\_3n} \\ M_p \cdot \left(1.07 - 0.7 \cdot \frac{D_p}{D_{t\_3n}}\right) & \text{otherwise} \end{cases}$$

$M_n = 22763.459\,\text{kips}\cdot\text{ft}$ $\qquad \phi_f M_n = 22763.459\,\text{kips}\cdot\text{ft}$

$M_u + \frac{f_l \cdot S_{xt\_2.4}}{3} = 23632.29\,\text{kips}\cdot\text{ft}$

$$\text{Strength\_Limit\_Check} := \begin{cases} \text{"OK"} & \text{if } M_u + \frac{f_l \cdot S_{xt\_2.4}}{3} \le \phi_f M_n \\ \text{"NG"} & \text{otherwise} \end{cases}$$

Strength_Limit_Check = "NG"

$$\text{Strength\_ratio} := \frac{M_u + \frac{f_l \cdot S_{xt\_2.4}}{3}}{\phi_f M_n}$$

Strength_ratio = 1.038

$$\text{Change\_in\_strength} := \frac{M_n - \frac{f_l \cdot S_{xt\_2.4}}{3}}{\left(F_{yt} - \frac{f_l}{3}\right) \cdot S_{xt\_2.4}}$$

Change_in_strength = 1.15

Strength Limit State Check 2-1, STRENGTH I

All stresses and moments are unfactored except construction load stresses are factored, load factor = 1.25. Also the dynamic allowance of 1.33 is included in the calcuation of the truck load stresses.

**** In this section. live loads is checked based on maximum flange lateral bending stress with concurrent major-axis bending values.***

G1 Bottom flange - G1-S4

$M_{u\_constr} := 8765.031 \cdot kips \cdot ft$ $M_{u\_DC2} := 1100.054 \cdot kips \cdot ft$ $M_{u\_DW} := 751.550 \cdot kips \cdot ft$ $M_{u\_LL} := 5934.907 \cdot kips \cdot ft$

$$M_u := \left(M_{u\_constr} + 1.25 M_{u\_DC2}\right) + 1.5 \cdot \left(M_{u\_DW}\right) + 1.75 \cdot \left(M_{u\_LL}\right)$$

$M_u = 21653.511\ kips \cdot ft$

$f_{b\_constr} := 24.341 \cdot ksi$ $f_{b\_DC2} := 2.710 \cdot ksi$ $f_{b\_DW} := 1.851 \cdot ksi$ $f_{b\_LL} := 13.444 \cdot ksi$

$$f_b := \left(f_{b\_constr} + 1.25 f_{b\_DC2}\right) + 1.5 \cdot \left(f_{b\_DW}\right) + 1.75 \cdot \left(f_{b\_LL}\right)$$

$f_b = 54.032\ ksi$

$f_{l\_constr} := 6.1 \cdot ksi$ $f_{l\_DC2} := 0.291 \cdot ksi$ $f_{l\_DW} := 0.147 \cdot ksi$ $f_{l\_LL} := 1.286 \cdot ksi$

$$f_l := \left(f_{l\_constr} + 1.25 f_{l\_DC2}\right) + 1.5 \cdot \left(f_{l\_DW}\right) + 1.75 \cdot \left(f_{l\_LL}\right)$$

$f_l = 8.935\ ksi$

Maximum Lateral Bending Stress Limit

$f_l = 8.935\ ksi$ $0.6F_{yc} = 30\ ksi$

$$Lateral\_bending\_stress\_limit\_Check := \begin{cases} "OK" & \text{if } f_l < 0.6F_{yc} \\ "NG" & \text{otherwise} \end{cases}$$

$Lateral\_bending\_stress\_limit\_Check = "OK"$

$$Lateral\_bending\_stress\_ratio := \frac{f_l}{0.6F_{yc}}$$

$Lateral\_bending\_stress\_ratio = 0.298$

Strength Limit

** stress based equation considered as noncompact section*

$f_b + \frac{f_l}{3} = 57.01\,\text{ksi}$ $\qquad \phi_f R_{h\_comp} \cdot F_{yt} = 50\,\text{ksi}$

$$\text{Strength\_Limit\_Check} := \begin{cases} \text{"OK"} & \text{if } f_b + \frac{f_l}{3} \le \phi_f R_{h\_comp} \cdot F_{yt} \\ \text{"NG"} & \text{otherwise} \end{cases}$$

Strength_Limit_Check = "NG"

$$\text{Strength\_ratio} := \frac{f_b + \frac{f_l}{3}}{\phi_f R_{h\_comp} \cdot F_{yt}}$$

Strength_ratio = 1.14

** moment based equation considered as compact section*

Nominal Flexural resistance:

$$M_n := \begin{cases} M_p & \text{if } D_p \le 0.1 \cdot D_{t\_3n} \\ M_p \cdot \left(1.07 - 0.7 \cdot \frac{D_p}{D_{t\_3n}}\right) & \text{otherwise} \end{cases}$$

$M_n = 22763.459\,\text{kips}\cdot\text{ft}$ $\qquad \phi_f M_n = 22763.459\,\text{kips}\cdot\text{ft}$

$M_u + \frac{f_l \cdot S_{xt\_2.3}}{3} = 22836.11\,\text{kips}\cdot\text{ft}$

$$\text{Strength\_Limit\_Check} := \begin{cases} \text{"OK"} & \text{if } M_u + \frac{f_l \cdot S_{xt\_2.3}}{3} \le \phi_f M_n \\ \text{"NG"} & \text{otherwise} \end{cases}$$

Strength_Limit_Check = "NG"

$$\text{Strength\_ratio} := \frac{M_u + \frac{f_l \cdot S_{xt\_2.3}}{3}}{\phi_f M_n}$$

Strength_ratio = 1.003

$$\text{Change\_in\_strength} := \frac{M_n - \frac{f_l \cdot S_{xt\_2.3}}{3}}{\left(F_{yt} - \frac{f_l}{3}\right) \cdot S_{xt\_2.3}}$$

Change_in_strength = 1.156

Strength Limit State Check 2-2, STRENGTH I

All stresses and moments are unfactored except construction load stresses are factored, load factor = 1.25. Also the dynamic allowance of 1.33 is included in the calcuation of the truck load stresses.

**** In this section, live loads is checked based on both maximums of major-axis bending values and flange lateral bending stress.***

G1 Bottom flange - G1-S4

$M_{u\_constr} := 8765.031 \cdot kips \cdot ft$ $M_{u\_DC2} := 1100.054 \cdot kips \cdot ft$ $M_{u\_DW} := 751.550 \cdot kips \cdot ft$ $M_{u\_LL} := 6752.699 \cdot kips \cdot ft$

$M_u := \left(M_{u\_constr} + 1.25 M_{u\_DC2}\right) + 1.5 \cdot \left(M_{u\_DW}\right) + 1.75 \cdot \left(M_{u\_LL}\right)$

$M_u = 23084.647\ kips \cdot ft$

$f_{b\_constr} := 24.341 \cdot ksi$ $f_{b\_DC2} := 2.710 \cdot ksi$ $f_{b\_DW} := 1.851 \cdot ksi$ $f_{b\_LL} := 15.297 \cdot ksi$

$f_b := \left(f_{b\_constr} + 1.25 f_{b\_DC2}\right) + 1.5 \cdot \left(f_{b\_DW}\right) + 1.75 \cdot \left(f_{b\_LL}\right)$

$f_b = 57.275\ ksi$

$f_{l\_constr} := 6.1 \cdot ksi$ $f_{l\_DC2} := 0.291 \cdot ksi$ $f_{l\_DW} := 0.147 \cdot ksi$ $f_{l\_LL} := 1.286 \cdot ksi$

$f_l := \left(f_{l\_constr} + 1.25 f_{l\_DC2}\right) + 1.5 \cdot \left(f_{l\_DW}\right) + 1.75 \cdot \left(f_{l\_LL}\right)$

$f_l = 8.935\ ksi$

Maximum Lateral Bending Stress Limit

$f_l = 8.935\ ksi$ $0.6F_{yc} = 30\ ksi$

$$Lateral\_bending\_stress\_limit\_Check := \begin{cases} \text{"OK"} & \text{if } f_l < 0.6F_{yc} \\ \text{"NG"} & \text{otherwise} \end{cases}$$

$Lateral\_bending\_stress\_limit\_Check = \text{"OK"}$

$$Lateral\_bending\_stress\_ratio := \frac{f_l}{0.6F_{yc}}$$

$Lateral\_bending\_stress\_ratio = 0.298$

Strength Limit

** stress based equation considered as noncompact section*

$$f_b + \frac{f_l}{3} = 60.25\,\text{ksi} \qquad \phi_f R_{h\_comp} \cdot F_{yt} = 50\,\text{ksi}$$

$$\text{Strength\_Limit\_Check} := \begin{cases} \text{"OK"} & \text{if } f_b + \frac{f_l}{3} \le \phi_f R_{h\_comp} \cdot F_{yt} \\ \text{"NG"} & \text{otherwise} \end{cases}$$

Strength_Limit_Check = "NG"

$$\text{Strength\_ratio} := \frac{f_b + \frac{f_l}{3}}{\phi_f R_{h\_comp} \cdot F_{yt}}$$

Strength_ratio = 1.205

** moment based equation considered as compact section*

Nominal Flexural resistance:

$$M_n := \begin{cases} M_p & \text{if } D_p \le 0.1 \cdot D_{t\_3n} \\ M_p \cdot \left(1.07 - 0.7 \cdot \frac{D_p}{D_{t\_3n}}\right) & \text{otherwise} \end{cases} \qquad M_n = 22763.459\,\text{kips·ft} \qquad \phi_f M_n = 22763.459\,\text{kips·ft}$$

$$M_u + \frac{f_l \cdot S_{xt\_2.3}}{3} = 24267.25\,\text{kips·ft}$$

$$\text{Strength\_Limit\_Check} := \begin{cases} \text{"OK"} & \text{if } M_u + \frac{f_l \cdot S_{xt\_2.3}}{3} \le \phi_f M_n \\ \text{"NG"} & \text{otherwise} \end{cases}$$

Strength_Limit_Check = "NG"

$$\text{Strength\_ratio} := \frac{M_u + \frac{f_l \cdot S_{xt\_2.3}}{3}}{\phi_f M_n}$$

Strength_ratio = 1.066

$$\text{Change\_in\_strength} := \frac{M_n - \frac{f_l \cdot S_{xt\_2.3}}{3}}{\left(F_{yt} - \frac{f_l}{3}\right) \cdot S_{xt\_2.3}}$$

Change_in_strength = 1.156

Service Limit State Check 1-1 SERVICE II

All stresses are unfactored, but the dynamic allowance of 1.33 is included in the calcuation of the truck load stresses

**** In this section, live loads is checked based on maximum major-axis bending stress with concurrent flange lateral bending stress.***

G1 Bottom flange - G1-S1

$f_{b\_constr} := 19.275 \cdot ksi$ $f_{b\_DC2} := 2.712 \cdot ksi$ $f_{b\_DW} := 1.847 \cdot ksi$ $f_{b\_LL} := 15.456 \cdot ksi$

$f_b := 1\left(f_{b\_constr} + f_{b\_DC2}\right) + 1 \cdot \left(f_{b\_DW}\right) + 1.33 \cdot \left(f_{b\_LL}\right)$ $f_b = 44.39\,ksi$

$f_{l\_constr} := -0.150 \cdot ksi$ $f_{l\_DC2} := 0.412 \cdot ksi$ $f_{l\_DW} := 0.177 \cdot ksi$ $f_{l\_LL} := 1.940 \cdot ksi$

$f_l := 1\left(f_{l\_constr} + f_{l\_DC2}\right) + 1 \cdot \left(f_{l\_DW}\right) + 1.33 \cdot \left(f_{l\_LL}\right)$ $f_l = 3.019\,ksi$

$f_b + \frac{f_l}{2} = 45.9\,ksi$ $0.95 \cdot R_{h\_comp} \cdot F_{yt} = 47.5\,ksi$

$$Permanent\_Deformation\_Check := \begin{cases} "OK" & \text{if } f_b + \frac{f_l}{2} \le 0.95 \cdot R_{h\_comp} \cdot F_{yt} \\ "NG" & \text{otherwise} \end{cases}$$

$Permanent\_Deformation\_Check = "OK"$

$$Permanent\_deformation\_ratio := \frac{f_b + \frac{f_l}{2}}{0.95 \cdot R_{h\_comp} \cdot F_{yt}}$$

$Permanent\_deformation\_ratio = 0.966$

Service Limit State Check 1-2 SERVICE II

All stresses are unfactored, but the dynamic allowance of 1.33 is included in the calcuation of the truck load stresses

**** In this section, live loads is checked based on both maximums of major-axis bending stress and flange lateral bending stress.***

G1 Bottom flange - G1-S1

$f_{b\_constr} := 19.275 \cdot ksi$ $f_{b\_DC2} := 2.712 \cdot ksi$ $f_{b\_DW} := 1.847 \cdot ksi$ $f_{b\_LL} := 15.456 \cdot ksi$

$f_b := 1\left(f_{b\_constr} + f_{b\_DC2}\right) + 1 \cdot \left(f_{b\_DW}\right) + 1.33 \cdot \left(f_{b\_LL}\right)$ $f_b = 44.39\,ksi$

$f_{l\_constr} := -0.150 \cdot ksi$ $f_{l\_DC2} := 0.412 \cdot ksi$ $f_{l\_DW} := 0.177 \cdot ksi$ $f_{l\_LL} := 1.992 \cdot ksi$

$f_l := 1\left(f_{l\_constr} + f_{l\_DC2}\right) + 1 \cdot \left(f_{l\_DW}\right) + 1.33 \cdot \left(f_{l\_LL}\right)$ $f_l = 3.088\,ksi$

$f_b + \frac{f_l}{2} = 45.93\,ksi$ $0.95 \cdot R_{h\_comp} \cdot F_{yt} = 47.5\,ksi$

$$Permanent\_Deformation\_Check := \begin{cases} "OK" & \text{if } f_b + \frac{f_l}{2} \le 0.95 \cdot R_{h\_comp} \cdot F_{yt} \\ "NG" & \text{otherwise} \end{cases}$$

Permanent_Deformation_Check = "OK"

$$Permanent\_deformation\_ratio := \frac{f_b + \frac{f_l}{2}}{0.95 \cdot R_{h\_comp} \cdot F_{yt}}$$

Permanent_deformation_ratio = 0.967

Service Limit State Check 2-1 SERVICE II

All stresses are unfactored, but the dynamic allowance of 1.33 is included in the calcuation of the truck load stresses

**** In this section. live loads is checked based on maximum flange lateral bending stress with concurrent major-axis bending stress.***

G1 Bottom flange - G1-S4

$f_{b\_constr} := 19.327 \cdot ksi$ $f_{b\_DC2} := 2.710 \cdot ksi$ $f_{b\_DW} := 1.851 \cdot ksi$ $f_{b\_LL} := 13.444 \cdot ksi$

$f_b := 1\left(f_{b\_constr} + f_{b\_DC2}\right) + 1 \cdot \left(f_{b\_DW}\right) + 1.33 \cdot \left(f_{b\_LL}\right)$ $f_b = 41.769\,ksi$

$f_{l\_constr} := 4.160 \cdot ksi$ $f_{l\_DC2} := 0.291 \cdot ksi$ $f_{l\_DW} := 0.147 \cdot ksi$ $f_{l\_LL} := 1.286 \cdot ksi$

$f_l := 1\left(f_{l\_constr} + f_{l\_DC2}\right) + 1 \cdot \left(f_{l\_DW}\right) + 1.33 \cdot \left(f_{l\_LL}\right)$ $f_l = 6.308\,ksi$

$f_b + \frac{f_l}{2} = 44.92\,ksi$ $0.95 \cdot R_{h\_comp} \cdot F_{yt} = 47.5\,ksi$

$$Permanent\_Deformation\_Check := \begin{cases} "OK" & \text{if } f_b + \frac{f_l}{2} \le 0.95 \cdot R_{h\_comp} \cdot F_{yt} \\ "NG" & \text{otherwise} \end{cases}$$

$Permanent\_Deformation\_Check = "OK"$

$$Permanent\_deformation\_ratio := \frac{f_b + \frac{f_l}{2}}{0.95 \cdot R_{h\_comp} \cdot F_{yt}}$$

$Permanent\_deformation\_ratio = 0.946$

Service Limit State Check 2-2 SERVICE II

All stresses are unfactored, but the dynamic allowance of 1.33 is included in the calcuation of the truck load stresses

**** In this section, live loads is checked based on both maximums of major-axis bending values and flange lateral bending stress.***

G1 Bottom flange - G1-S4

$f_{b\_constr} := 19.327 \cdot ksi$ $f_{b\_DC2} := 2.710 \cdot ksi$ $f_{b\_DW} := 1.851 \cdot ksi$ $f_{b\_LL} := 15.297 \cdot ksi$

$f_b := 1\left(f_{b\_constr} + f_{b\_DC2}\right) + 1 \cdot \left(f_{b\_DW}\right) + 1.33 \cdot \left(f_{b\_LL}\right)$ $f_b = 44.233\,ksi$

$f_{l\_constr} := 4.160 \cdot ksi$ $f_{l\_DC2} := 0.291 \cdot ksi$ $f_{l\_DW} := 0.147 \cdot ksi$ $f_{l\_LL} := 1.286 \cdot ksi$

$f_l := 1\left(f_{l\_constr} + f_{l\_DC2}\right) + 1 \cdot \left(f_{l\_DW}\right) + 1.33 \cdot \left(f_{l\_LL}\right)$ $f_l = 6.308\,ksi$

$f_b + \frac{f_l}{2} = 47.39\,ksi$ $0.95 \cdot R_{h\_comp} \cdot F_{yt} = 47.5\,ksi$

$$Permanent\_Deformation\_Check := \begin{cases} "OK" & \text{if } f_b + \frac{f_l}{2} \le 0.95 \cdot R_{h\_comp} \cdot F_{yt} \\ "NG" & \text{otherwise} \end{cases}$$

$Permanent\_Deformation\_Check = "OK"$

$$Permanent\_deformation\_ratio := \frac{f_b + \frac{f_l}{2}}{0.95 \cdot R_{h\_comp} \cdot F_{yt}}$$

$Permanent\_deformation\_ratio = 0.998$

A-2 SINGLE ANGLE CROSS-FRAME MEMBER DESIGN

$ksi := 10^3 \cdot psi$; $kips := 10^3 lbf$

Material Properties:

- Steel Properties:

$F_y := 50ksi$; $E := 29000 \cdot ksi$; $\phi_c := 0.9$

Cross-Frame 107-Diagonal Check

Cross- Sectional Properties L5x3x1/2 (interior cross-frames):

$A_g := 3.75 \cdot in^2$ $r_x := 0.824\,in$

Determination of the equivalent slenderness (KL/r)

Unequal-leg angle connected through the longer leg

$L_b := 18.024 \cdot ft$

$L := 6.59 \cdot ft$

$\frac{L}{r_x} = 95.971$

$$Equivalent\_Slenderness := \begin{cases} 72 + 0.75 \cdot \frac{L}{r_x} & \text{if } 0 \le \frac{L}{r_x} \le 80 \\ 32 + 1.25 \cdot \frac{L}{r_x} & \text{if } 32 + 1.25 \cdot \frac{L}{r_x} \le 200 \wedge \frac{L}{r_x} > 80 \end{cases}$$

$Equivalent\_Slenderness = 151.964$

Determination of the nominial resistance F_n

$$F_e := \frac{\pi^2 \cdot E}{Equivalent\_Slenderness^2}$$

$F_e = 12.394\,ksi$

$0.44 \cdot F_y = 22\,ksi$

$$F_n := \begin{cases} \left(0.658^{\frac{F_y}{F_e}}\right) \cdot F_y & \text{if } F_e \ge 0.44 \cdot F_y \\ 0.877 \cdot F_e & \text{otherwise} \end{cases}$$

$F_n = 10.87\,ksi$ $N_n := F_n \cdot A_g$ $N_n = 40.761\,kip$

Strength Limit State Check 1, STRENGTH I

The total axial force is factored with 1.25DC,1.5 DW, 1.75LL, Also the dynamic allowance of 1.33 is included in the calcuation of the truck loads

$N := 106 \cdot kips$

$\phi_c \cdot N_n = 36.685\ kips$

$$Strength\_Limit\_Check := \begin{cases} "OK" & \text{if } N \le \phi_c \cdot N_n \\ "NG" & \text{otherwise} \end{cases}$$

$Strength\_Limit\_Check = "NG"$

$$\frac{N}{\phi_c \cdot N_n} = 2.889$$

Cross-Frame 203-Bottom Chord Check

Cross- Sectional Properties L5x3x1/2 (interior cross-frames):

$A_g := 3.75 \cdot in^2$ $r_x := 0.824\,in$

Determination of the equivalent slenderness (KL/r)

Unequal-leg angle connected through the longer leg

$L_b := 17.836 \cdot ft$

$L := 8.5 \cdot ft$

$\frac{L}{r_x} = 123.786$

$$Equivalent\_Slenderness := \begin{cases} 72 + 0.75 \cdot \frac{L}{r_x} & \text{if } 0 \le \frac{L}{r_x} \le 80 \\ 32 + 1.25 \cdot \frac{L}{r_x} & \text{if } 32 + 1.25 \cdot \frac{L}{r_x} \le 200 \wedge \frac{L}{r_x} > 80 \end{cases}$$

$Equivalent\_Slenderness = 186.733$

Determination of the nominial resistance F_n

$$F_e := \frac{\pi^2 \cdot E}{Equivalent\_Slenderness^2}$$

Equivalent_Slenderness

$F_e = 8.208\,ksi$

$0.44 \cdot F_y = 22\,ksi$

$$F_n := \begin{cases} \left(0.658^{\left(\frac{F_y}{F_e}\right)}\right) \cdot F_y & \text{if } F_e \ge 0.44 \cdot F_y \\ 0.877 \cdot F_e & \text{otherwise} \end{cases}$$

$F_n = 7.199\,ksi$ $N_n := F_n \cdot A_g$ $N_n = 26.995\,kips$

Strength Limit State Check 1, STRENGTH I

The total axial force is factored with 1.25DC,1.5 DW, 1.75LL, Also the dynamic allowance of 1.33 is included in the calcuation of the truck loads

$N := 173 \cdot kips$

$\phi_c \cdot N_n = 24.296\ kips$

$$Strength\_Limit\_Check := \begin{cases} \text{"OK"} & \text{if } N \le \phi_c \cdot N_n \\ \text{"NG"} & \text{otherwise} \end{cases}$$

$Strength\_Limit\_Check = \text{"NG"}$

$$\frac{N}{\phi_c \cdot N_n} = 7.121$$

CROSS-FRAME MEMBER DESIGN- Required Members

$ksi := 10^3 \cdot psi$; $kips := 10^3 lbf$

Material Properties:

- Steel Properties:

$F_y := 50ksi$; $E := 29000 \cdot ksi$; $\phi_c := 0.9$

Cross-Frame 107-Diagonal Check

Cross- Sectional Properties L5x5x5/8 (interior cross-frames):

$A_g := 5.86 \cdot in^2$ $r_x := 1.52in$

Determination of the equivalent slenderness (KL/r)

Equal-leg angle

$L_b := 18.024 \cdot ft$

$L := 6.59 \cdot ft$

$\frac{L}{r_x} = 52.026$

$$Equivalent\_Slenderness := \begin{cases} 72 + 0.75 \cdot \frac{L}{r_x} & \text{if } 0 \le \frac{L}{r_x} \le 80 \\ 32 + 1.25 \cdot \frac{L}{r_x} & \text{if } 32 + 1.25 \cdot \frac{L}{r_x} \le 200 \wedge \frac{L}{r_x} > 80 \end{cases}$$

$Equivalent\_Slenderness = 111.02$

Determination of the nominial resistance F_n

$$F_e := \frac{\pi^2 \cdot E}{Equivalent\_Slenderness^2}$$

$F_e = 23.222\,ksi$

$0.44 \cdot F_y = 22\,ksi$

$$F_n := \begin{cases} \left(0.658^{\frac{F_y}{F_e}}\right) \cdot F_y & \text{if } F_e \ge 0.44 \cdot F_y \\ 0.877 \cdot F_e & \text{otherwise} \end{cases}$$

$F_n = 20.304\,ksi$

$N_n := F_n \cdot A_g$ $N_n = 118.982\,kip$

Strength Limit State Check 1, STRENGTH I

The total axial force is factored with 1.25DC,1.5 DW, 1.75LL, Also the dynamic allowance of 1.33 is included in the calcuation of the truck loads

$N := 106 \cdot kips$

$\phi_c \cdot N_n = 107.084\ kips$

$$Strength\_Limit\_Check := \begin{cases} \text{"OK"} & \text{if } N \le \phi_c \cdot N_n \\ \text{"NG"} & \text{otherwise} \end{cases}$$

Strength_Limit_Check = "OK"

$$\frac{N}{\phi_c \cdot N_n} = 0.99$$

Cross-Frame 203-Bottom Chord Check

Cross- Sectional Properties L8x8x9/16 (interior cross-frames):

$A_g := 8.68 \cdot in^2$

$r_x := 2.49in$

Determination of the equivalent slenderness (KL/r)

Equal-leg angle

$L_b := 17.836 \cdot ft$

$L := 8.5 \cdot ft$

$\frac{L}{r_x} = 40.964$

$$Equivalent\_Slenderness := \begin{cases} 72 + 0.75 \cdot \frac{L}{r_x} & \text{if } 0 \le \frac{L}{r_x} \le 80 \\ 32 + 1.25 \cdot \frac{L}{r_x} & \text{if } 32 + 1.25 \cdot \frac{L}{r_x} \le 200 \wedge \frac{L}{r_x} > 80 \end{cases}$$

$Equivalent\_Slenderness = 102.723$

Determination of the nominial resistance F_n

$$F_e := \frac{\pi^2 \cdot E}{Equivalent\_Slenderness^2}$$

Equivalent_Slenderness

$F_e = 27.125\,ksi$

$0.44 \cdot F_y = 22\,ksi$

$$F_n := \begin{cases} \left(0.658^{\frac{F_y}{F_e}}\right) \cdot F_y & \text{if } F_e \ge 0.44 \cdot F_y \\ 0.877 \cdot F_e & \text{otherwise} \end{cases}$$

$F_n = 23.115\,ksi$ $\quad N_n := F_n \cdot A_g \quad N_n = 200.64\,kips$

Strength Limit State Check 1, Strength I

The total axial force is factored with 1.25DC,1.5 DW, 1.75LL, Also the dynamic allowance of 1.33 is included in the calcuation of the truck loads

$N := 173 \cdot kips$

$\phi_c \cdot N_n = 180.576\ kips$

$$Strength\_Limit\_Check := \begin{cases} \text{"OK"} & \text{if } N \le \phi_c \cdot N_n \\ \text{"NG"} & \text{otherwise} \end{cases}$$

$Strength\_Limit\_Check = \text{"OK"}$

$$\frac{N}{\phi_c \cdot N_n} = 0.958$$

REFERENCES

AASHTO (1998). *AASHTO LRFD Bridge Design Specifications 2nd* Edition with 1999, 2000 and 2001 Interims, American Association of State and Highway Transportation Officials, Washington D.C.

AASHTO (2003). *Guide Specifications for Horizontally Curved Steel Girder Highway Bridges with Design Examples for I-Girder and Box-Girder Bridges*, American Association of State and Highway Transportation Officials, Washington D.C.

AASHTO (2004a). *AASHTO LRFD Bridge Design Specifications, 3rd Edition*, American Association of State and Highway Transportation Officials, Washington D.C.

AASHTO (2004b). *AASHTO LRFD Bridge Design Specifications, 3rd Edition* with 2005 Interims, American Association of State and Highway Transportation Officials, Washington D.C.

AASHTO (2004c). *A Policy on Geometric Design of Highways and Streets*, American Association of State and Highway Transportation Officials, Washington D.C.

AASHTO (2007). *AASHTO LRFD Bridge Design Specifications, 4th Edition*, American Association of State and Highway Transportation Officials, Washington D.C.

ACI 318 and 318R (2002). *Building Code Requirements for Structural Concrete(ACI 318) and Commentary (ACI-318R)*, American Concrete Institute, Farmington Hills, MI, 442 pp.

AISC (1999). *Load and Resistance Factor Design Specification for Structural Steel Buildings*, American Institute of Steel Construction, Chicago, IL, 292 pp

AISC (2005). *Specification for Structural Steel Buildings*, American Institute of Steel Construction, Chicago, IL.

Beshah, F. (2006). "Testing of Composite Bridge," Volume 9, Curved Steel Bridge Research Project, Federal Highway Administration, Nov. 2006

Chang, C.-J. (2006). "GT-SABRE Manual." Structural Engineering, Mechanics and Materials, School of Civil and Environmental Engineering, Georgia Institute of Technology, Atlanta, GA.

Chang C.-J. (2006) "Construction Simulation of Curved Steel I-Girder Bridges," PhD Thesis, School of Civil and Environmental Engineering, Georgia Institute of Technology, Atlanta

Cook R. D., Malkus D. S., Plesha M. E., Witt R. J. (2002), *Concepts and applications of Finite Element Analysis*, fourth edition, Willey & Sons Inc., 719pp.

Hall, D.H., Grubb, M.A. and Yoo, C.H. (1999). "Improved Design Specifications for Horizontally Curved Steel Girder Highway Bridges," Report No. 424, NCHRP Project 12-38 Final Report, Transportation Research Board, NRC, Washington, D.C.

HKS (2004), *ABAQUS/Standard Manual Version 6.5-1*, Hibbitt, Karlsson & Sorensen, Inc., Pawtucket, RI.

Jung S.K. (2006) "Inelastic Strength Behavior of Horizontally Curved Composite I-Girder Bridge Structural Systems," PhD Thesis, School of Civil and Environmental Engineering, Georgia Institute of Technology, Atlanta

Krzmarzick, D. P. and Hajjar, J. F. (2006). "Load Rating of Composite Steel Curved I-Girder Bridges Through Load Testing with Heavy Trucks," Report No. MN/RC-2006-40, Minnesota Department of Transportation, St. Paul, Minnesota

Lee, J. and Fenves, G.L. (1998). "Plastic-Damage Model for Cyclic Loading of Concrete Structures," Journal of Engineering Mechanics, ASCE, 124(8),892-900.

Mozer, J, R. Ohlson and C. Culver, " Stability of Curved Plate Girders – P2,"Prepared for the Department of Transportation, Federal Highway Administration, and Participating States under Contract Number FH-11-7389, Department of Civil Engineering, Carnegie-Mellon University, Pittsburg, PA, 1971, 121 pp.

NHI (2007), "Load and Resistance Factor Design (LRFD) For Highway Bridge Superstructures," NHI Course No. 130081A,U.S. Department of Transportation Federal Highway Administration, Publication No. FHWA-NHI-07-035.

White, D.W. and Grubb, M.A. (2005). "Unified Resistance for Design of Curved and Tangent Steel Bridge I-Girders," TRB 6th International Bridge Engineering Conference, Transportation Research Board, 20pp

White,D.W., Jung, S. K., and Chang, C. J. (2002)."Design of Curved Composite Test Bridge,"Report to PSI Inc. and FHWA,December.

White, D. W., Zureick, A. H., Phoawanich, N. P., and Jung, S. K. (2001). "Development of Unified Equations for Design of Curved and Straight Steel Bridge I Girders," Final Report to AISI, PSI, Inc. and FHWA, October.

White,D.W. (2007)."Structural Behavior of Steel," *Steel Bridge Design Handbook*, national Steel Bridge Alliance, Chapter 6

Wright, W. and Beshah, F. (2006). "Construction of Test Bridge," Volume 8, Curved Steel Bridge Research Project, Federal Highway Administration, Nov. 200

Yoo, C.H. and J.S. Davidson, "Yield-Interaction Equations for Nominal Bending Strength of Curved I-Girders," Journal of Bridge Engineering, American Society of Civil Engineers, Reston, VA, Vol.2, No.2, 1997, pp. 37-44.

Zureick, A.H., White, D.W., Phoawanich, N., and Park, J. (2002). "Shear Strength of Horizontally Curved Steel I-Girders – Experimental Tests, "Structural Engineering, Mechanics and Materials Report No. 02-4, Final Report to Professional Services Industries, Inc. and Federal Highway Administration, School of Civil and Environmental Engineering, Georgia Institute of Technology, Atlanta, Georgia, March, 157pp